THE UNIVERSITY OF CHICAGO

A NOVEL ANTIVIRAL MECHANISM OF INTERFERON GAMMA TARGETING VIRAL REPLICATION COMPLEXES

A DISSERTATION SUBMITTED TO

THE FACULTY OF THE DIVISION OF THE BIOLOICAL SCIENCES

AND THE PRITZKER SCHOOL OF MEDICINE

IN CANDIDACY FOR THE DEGREE OF

DOCTOR OF PHILOSOPHY

COMMITTEE ON MICROBIOLOGY

BY

SCOTT BENJAMIN BIERING

CHICAGO, ILLINOIS

JUNE 2018

TABLE OF CONTENTS

LIST OF FIGURES

LIST OF TABLES

ACKNOWLEDGEMENTS

There are many individuals whom I must acknowledge. First and foremost, I acknowledge my advisor, Dr. Seungmin Hwang. He taught me to be a meticulous, thorough, and efficient scientist; I consider Seungmin's way of doing science to be the gold standard. He has invested so much time into my training and for this I am eternally grateful. I hope that I can live up to his expectations and maintain these high standards throughout my scientific career. In the same light, I would like to acknowledge Dr. Jayoung Choi. She has been a strong scientific role model to me and she represents the scientist I would like to become. I must also acknowledge my previous mentor, Dr. Hector Aguilar-Carreno. Without him I don't think I would be in science today. Hector was my gateway into science and he instilled in me tremendous passion for the field of virology. I owe him my career.

Next, I would like to acknowledge my mother, Paula Harvey. She has pushed me since day 1 and the example she provided gave me a work ethic and an inquisitive attitude. Anything I have accomplished and will accomplish is because of her. I acknowledge my father, Stephen Biering, for constant love and support. Next I acknowledge my brother, Tom Biering, who is both my brother and best friend who understands me better than anybody. I acknowledge my grandmother, Peggie Biering, for her constant love and support. My lifelong best friends Jake Cregut and David Millet have meant the world to me. They are my family and their support has given me much needed strength in life, especially during graduate school. Lastly, I acknowledge the love of my life Brittany Nelson. She has taught me so much about myself, the world, and

who I want to become. She softens my shortcomings and amplifies my strengths. I am eternally grateful to her.

ABSTRACT

Replication complexes (RCs) of positive-strand RNA viruses [(+)RNA] are membranous structures built from membranes of host organelles. These structures are essential to the viral lifecycle for both promoting viral replication and protecting the virus from the host immune response. Though we understand much about how these structures are formed, we did not know if these conserved viral structures could be targeted by host antiviral defense systems. We recently found such a pathway by which interferon gamma (IFNG) mediates disruption of the murine norovirus (MNV) RC, in a manner dependent on the ATG12-ATG5-ATG16L1 complex but independent of degradative autophagy. However, the mechanism and potential effectors of this antiviral pathway were unknown.

In this dissertation, we show that the RC of MNV is detected via an interaction between the autophagy protein ATG16L1 and viral RNA-dependent RNA polymerase (RdRp), one of the most conserved viral proteins. Recruitment of ATG16L1 brings the entire LC3-conjugation system to the RC, marking it with LC3 and homologs. This LC3 localization to the RC demarcates the structure as a “non-self” target for this IFNG-mediated antiviral activity. Once marked, LC3 and homologs recruited a family of immune effectors known as the interferon (IFN)-inducible GTPases, which destroy the RC. These IFN-inducible GTPases are induced by IFNG and antagonize replication of MNV both *in vitro* and *in vivo*. The IFN-inducible GTPases are membranolytic effectors which also disrupt the membranous replication structures of protozoan parasites, bacteria, and fungi. Thus, we have determined that this antiviral activity against the RC of MNV is in fact an evolutionarily conserved anti-microbial pathway by which the host

detects “non-self” structures through demarcation with autophagy proteins, which in turn recruit membranolytic IFN-inducible GTPases.

CHAPTER I

Introduction

A portion of this chapter has been modified from a review article published in BioEssays: Demarcation of Viral Shelters Results in Destruction by Membranolytic GTPases: Antiviral Function of Autophagy Proteins and Interferon-Inducible GTPases (**https://doi.org/10.1002/bies.201700231**). The authors and affiliations are Hailey M. Brown[a], Scott B. Biering[b], Allen Zhu[c], Jayoung Choi[d], and Seungmin Hwang[a,b,c,d,*]

[a]Committee on Immunology,

[b]Committee on Microbiology,

[c]Committee on Cancer Biology,

[d]Department of Pathology, The University of Chicago, Chicago, IL 60637, USA

*Correspondence to: Seungmin Hwang; Email: shwang@bsd.uchicago.edu

Positive-Strand RNA Viruses

Viruses are obligate intracellular parasites that depend on the host's cellular machinery to replicate their genomes. Viruses are evolutionarily diverse, possessing different strategies to take command of host cells; in general viruses that are closely related share common replication strategies. One major divergent factor used to categorize viruses is their genetic makeup. Classification of viruses based on their genetic material is known as the Baltimore classification (Baltimore, 1971). The Baltimore classification differentiates viruses into classes based on whether they

possess a single- or double-stranded DNA or RNA genome. Further, the direction by which the genetic information flows during viral replication is also included in the Baltimore classification; an example for RNA viruses being whether RNA is first translated to protein or reverse-transcribed to DNA. In all, the Baltimore classification contains seven groups encompassing all known viruses.

Group IV hosts the positive-strand or positive-sense RNA [(+)RNA] viruses which make up ~1/3 of all known viruses and include many medically and economically relevant pathogens such as Zika virus, Dengue virus, Hepatitis C virus, Polio virus, SARS-coronavirus (SARS), MERS-coronavirus (MERS), and Norovirus (den Boon et al., 2010). (+)RNA viruses are unique in that their genomes can function directly as a messenger RNA, which is translated by host machinery immediately upon release into the cytosol following viral entry into the cell. This means (+)RNA viruses do not need to package an RNA-dependent RNA polymerase (RdRp) within the viral particle, in contrast to negative-strand RNA (-RNA) viruses [(-)RNA].

Like all viruses, (+)RNA viruses must replicate within host cells. This is a hostile environment because viral sensors capable of detecting double-stranded RNA (dsRNA), which is produced by viruses during replication, are present throughout the cytoplasm. Once activated, these host sensors trigger an antiviral state in the cell capable of antagonizing the viral lifecycle (Takeuchi and Akira, 2007, 2009). The success of a virus is dependent on its ability to circumvent or avoid these host defenses. One common strategy pathogens utilize is to sequester themselves in an immune privileged niche where they can safely replicate away from these host immune sensors (Kumar and Valdivia, 2009; Randow et al., 2013). A unique aspect of the (+)RNA virus lifecycle, that

exemplifies this sequestration strategy, is that upon translation of viral proteins, host organelle derived membranes are rearranged to form membranous replication complexes (RCs) where the virus localizes its replication machinery (den Boon et al., 2010; Harak and Lohmann, 2015; Novoa et al., 2005). The organelle membrane source as well as the sub-cellular localization of the RC varies by virus but overall it is believed these membranous viral structures play similar functions. These structures are also commonly referred to as replication organelles, replication compartments, virus factories, and membranous webs. Growing evidence suggests that these RCs shield the virus from the host immune response by sequestering viral pathogen associated molecular patterns (PAMPs) away from pattern recognition receptors (PRRs) lurking in the cytoplasm (Overby et al., 2010; Uchida et al., 2014; Weber et al., 2006). RCs also mediate the viral lifecycle by concentrating the replication machinery in a single location, enhancing interactions between viral and cellular components, and also providing a way for the virus to spatiotemporally regulate transition from early to late lifecycle (den Boon et al., 2010; Romero-Brey and Bartenschlager, 2014; Shulla and Randall, 2016). (+)RNA viruses construct their RCs by using viral proteins to either directly recruit membranes or by recruiting cellular components capable of manipulating and recruiting membranes (Shulla and Randall, 2016).

History and Structure of Viral Replication Complexes

Viral RCs were first described over half a century ago and as imaging technology has improved so has our insight into their biogenesis and structure (KALLMAN et al.,

1958). The development of EM tomography has resulted in many outstanding structural studies describing RCs of different viruses (den Boon et al., 2010; Harak and Lohmann, 2015; Kopek et al., 2007; Romero-Brey and Bartenschlager, 2014). Interestingly, these structural studies have only identified two RC classes, an intriguing finding considering the significant evolutionary distance between (+)RNA viruses and suggestive of convergent evolution. These two RC classes are spherule invaginations and double membrane vesicles (DMVs) (Harak and Lohmann, 2015; Shulla and Randall, 2016). The spherule invagination class is generated through negative curvature of a membrane into the lumen of an organelle away from the cytoplasm. These structures maintain a small neck that connects the RC interior to the cytoplasm, believed to selectively determine what can travel in and out of the structure (Harak and Lohmann, 2015; Quinkert et al., 2005). The DMV RC class is generated through the partial closure of an exvaginated single membrane vesicle, accompanied by further invaginations. In contrast to the spherule invagination class, only a minority of DMVs undergoing active replication (e.g.: presence of dsRNA), possess a visible open connection to the cytoplasm. One would expect an open connection to be required for trafficking of cytoplasmic material in and out of the RC, so if/ how DMVs can function without one is unclear. Several reports have shown that Hepatitis C virus (HCV) recruits nuclear pore complex machinery to their DMV RCs, suggesting a potential mechanism for selective RC entry and exit (Neufeldt et al., 2013; Neufeldt et al., 2016).

How (+)RNA Viruses Build Replication Complexes

Some RCs resemble double-membrane autophagosomes and in fact studies on the *Picornaviridae* have demonstrated that their RCs require the autophagic machinery for formation (Dreux and Chisari, 2010; Jackson et al., 2005; Schlegel et al., 1996; Suhy et al., 2000). In addition to utilizing autophagic proteins, such as microtubule-associated-protein-1-light-chain-3 (LC3), known to manipulate membranes (Carlsson and Simonsen, 2015), viral proteins are either directly or indirectly responsible for manipulating cellular membranes to build their RC. For many viruses, formation of the RC can be recapitulated through the expression of one or a few viral proteins (Harak and Lohmann, 2015). These proteins can interact directly with membranes to form the RC, interact with host proteins responsible for lipid manipulation, or both. A plethora of cellular factors that manipulate lipid composition and membrane curvature have been shown to interact with viral proteins, a few examples of these are reticulons, components of the endosomal sorting complexes required for transport (ESCRT) pathway, proteins involved in vesicle transport, cyclophilins, lipid transfer proteins, de novo lipid synthesis through components such as fatty acid synthase (FASN), phosphatidylinositol (PI)-4 kinases, and autophagy proteins (Harak and Lohmann, 2015; Shulla and Randall, 2016).

Role of the Replication Complex in the (+)RNA Virus Lifecycle

Once formed, the viral RC mediates efficient viral replication and coordinates the transition from RNA replication to genome packaging, all the while shielding the virus from innate immune detection (den Boon et al., 2010). Viral replication is a coordinated

and efficient process for which RCs are essential. RCs create an environment where viral components are in a relatively small place, ensuring maximal interaction between viral proteins, viral RNA, and coopted cellular components, pushing the lifecycle forward (den Boon et al., 2010; Harak and Lohmann, 2015; Shulla and Randall, 2016). Further, once the genome has been replicated the virus needs to package these genomes into capsids, forming new virions which then exit the cell. For many viruses, such as Dengue virus and SARS-COV, the viral genomes are packaged into capsids in close proximity to their RC (Knoops et al., 2008; Welsch et al., 2009). Although capsid proteins are not commonly observed to be localized within RCs, they are shown to target to proximal regions where efficient packaging of the viral genome can take place (den Boon et al., 2010; Shulla and Randall, 2016). Further, for enveloped viruses that bud from the cell via the secretory pathway, the RC is commonly localized in a proximal area to the appropriate organelle, allowing for efficient viral budding (Knoops et al., 2008).

When a (+)RNA virus replicates its genome, it must first produce a negative-stranded anti-sense RNA template, and in doing so produces a dsRNA intermediate which can be detected by pattern recognition receptors (PRR) in the cytoplasm and in endosomes (e.g. TLR3, MDA5, and RIG-I) (Weber et al., 2006; Yoneyama et al., 2015). Detection of viral RNA can result in host mediated degradation of viral RNA and/or production of interferons which will induce a general antiviral response (Yoneyama et al., 2015). (+)RNA viruses have evolved many strategies to solve this problem. One common approach is to directly antagonize the interferon signaling pathway (García-Sastre, 2017). Another is a strategy of general avoidance, which is what the RC is believed to adopt (Overby et al., 2010; Uchida et al., 2014). Data for HCV suggests that

cytoplasmic PRRs are excluded from the replication complex (Neufeldt et al., 2016). Further, RNA within RCs has been shown to be resistant to nuclease treatment, suggesting the material inside is protected from the external environment (Miyanari et al., 2003; Paul et al., 2013; Quinkert et al., 2005). This model implies that RCs of +RNA viruses sequester dsRNA intermediates where the immune system cannot detect them (Overby et al., 2010; Uchida et al., 2014).

Viral Replication Complexes: A Potential Target of Antiviral Activity

RCs of (+)RNA viruses are well conserved membranous structures built by viruses to both enhance viral replication and prevent detection by the innate immune response. We suspected that such a conserved “non-self” viral induced structure would provide a target to the antiviral innate immune response. When innate immune sensors are activated they induce expression of interferons. Interferons are cytokines that induce an antiviral state and signal through the Janus Kinase (JAK)/ Signal Transducer and Activator of Transcription (STAT) signaling pathway to upregulate hundreds of interferon stimulated genes (ISGs) which antagonize the viral lifecycle (Schneider et al., 2014; Schoggins and Rice, 2011). For (+)RNA viruses, nearly every stage of the viral lifecycle has been shown to be antagonized by ISGs, except one, the formation/ maintenance of the viral replication complex. As demonstrated above, we have learned a lot about how viruses build their RCs and what their function is, but we know little to nothing about how/ if the host can detect these membranous viral replication compartments and antagonize them. Given the high structural conservation of RCs, we hypothesized that

the host has evolved a mechanism to detect and antagonize these structures. However, if targeting the viral RC proved to be an effective antiviral strategy against (+)RNA viruses, and the host evolved an effective strategy to do this, then why has such a pathway not yet been identified? When considering how essential these structures are for the viral lifecycle, an antiviral pathway targeting them would apply a large selective pressure on the virus to evade such a pathway, providing an explanation to why such an antiviral pathway has not yet been identified.

Murine Norovirus as a Model (+)RNA Virus

MNV is a (+)RNA virus with a genome around 7.5 kilobase pairs large, belonging to the *Caliciviridae* family and the sole member of the norovirus (NV) genogroup V (Glass et al., 2009; Karst et al., 2003; Thackray et al., 2007). MNV is currently the primary model to study Human Norovirus (HNV), which occupies the norovirus genogroups I, II, and IV. HNV is the primary cause of non-bacterial acute gastroenteritis worldwide, lacks a robust animal model for *in vivo* study, and is difficult to culture *in vitro (Duizer et al., 2004)*. Further, there is currently no vaccine or therapeutics available to treat patients with HNV, so understanding the viral lifecycle and basis for disease is critical. Though some studies have been published reporting *in vitro* conditions in which HNV can be cultivated, they are labor intensive and difficult to manipulate, thus MNV is currently one of the most robust systems to study norovirus biology (Ettayebi et al., 2016; Jones et al., 2014; Wobus et al., 2006). In addition to being closely related to HNV, MNV is easy to study in mice, simple to cultivate in cell culture, and straight

forward to genetically manipulate (Hwang et al., 2014). Thanks to the MNV model, we have learned a lot about norovirus basic biology as well as complex host-pathogen interactions between mice and MNV (Baldridge et al., 2016; Thorne and Goodfellow, 2014).

MNV is an enteric virus which replicates in the mouse gut. MNV was initially isolated from immune-deficient STAT1$^{-/-}$ mice (Karst et al., 2003). These mice cannot control MNV replication and the virus spreads systemically, eventually killing infected mice. This overt pathology in STAT1$^{-/-}$ mice was what allowed the detection and isolation of MNV, but MNV is not pathogenic in WT C57BL/6 mice, and may even act as something of a beneficial commensal microbe; MNV was shown to substitute a positive role of the gut microbiota in germ free mice (Kernbauer et al., 2014). Further, after the initial isolation of MNV, many mouse facilities spanning different institutions tested their colonies and isolated numerous different strains of MNV (Barron et al., 2011; Kim et al., 2010; Smith et al., 2012). To date, many strains of MNV have been isolated with two of the best studied *in vivo* being the acute strain CW3 and the persistent strain CR6. CW3, the strain primarily studied *in vitro*, replicates in the small intestine and spreads systemically to the spleen and other organs before being cleared from the mouse about seven days post infection. CW3 induces a strong inflammatory T-helper 1 CD4^{+} T cell response (T_H1) in the host, potentially explaining why this MNV strain is cleared (Nice et al., 2013). CR6, on the other hand, remains localized to the intestine and colon, is shed from the feces, and persists for the life of the mouse (Nice et al., 2013). The reason CR6 persists and CW3 does not, is not fully understood and an area of active investigation. Genetically, the ability of CR6 to persist is dependent on the viral non-

structural polyprotein 1 and 2 (NS1/2); glutamic acid 94 of CR6 allows it to persist and making a D94E substitution in CW3 results in a persistent mutant virus (Nice et al., 2013). A recent study suggests that mechanistically, NS1/2 allows CR6 to establish a persistent reservoir of infection in epithelial cells of the gut (Lee et al., 2017). Treating mice with exogenous interferon lambda (IFNL) clears this persistent reservoir in the gut, effectively curing mice of MNV infection (Baldridge et al., 2015; Nice et al., 2015). How CR6 infects epithelial cells is still unknown because MNV has been shown to have an *in vivo* and *in vitro* cellular tropism for cells of the myeloid lineage (specifically macrophages and dendritic cells expressing the MNV receptor CD300lf). In contrast, CD300lf is not expressed on epithelial cells, and thus cannot be infected *in vitr*o (Lee et al., 2017). Other studies have shown that MNV can also infect B cells and T cells in a CD300lf dependent manner (Grau et al., 2017; Haga et al., 2016; Jones et al., 2014; Orchard et al., 2016; Wobus et al., 2004). The other major phenotypic difference between CW3 and CR6 is their virulence in immunocompromised mice. $STAT1^{-/-}$ mice cannot control replication of CW3 and quickly succumb to infection, while CR6 persists at high viral titer but does not kill these mice. The gene responsible for this phenotype is the major viral capsid protein, viral protein 1 (VP1). Swapping the VP1 capsid from CR6 into CW3 (CW3-$VP1^{CR6}$) results in a mutant CW3 virus that is no longer virulent in $STAT1^{-/-}$ mice (Strong et al., 2012).

In cells, the viral lifecycle of MNV follows the major steps of all (+)RNA viruses. MNV enters the cell by utilizing the proteinaceous receptor CD300lf (Haga et al., 2016; Orchard et al., 2016), and internalizes into endosomes in a manner dependent on dynamin and cholesterol, but independently of clathrin and caveolae (Gerondopoulos et

al., 2010). Further, ganglioside-linked terminal sialic acid moieties were shown to play a role as attachment factors for MNV (Taube et al., 2009). After internalization, the MNV genome is released into the cytoplasm by an unknown mechanism, and the open reading frame 1 (ORF1) of the (+)RNA genome is immediately translated into a large polyprotein. The (+)RNA genome of MNV is covalently linked to the MNV non-structural protein 5 (NS5), also known as VPg, which assists in translation of the viral genome through recruitment of host translation machinery (Chung et al., 2014; Daughenbaugh et al., 2006; Thorne and Goodfellow, 2014). Upon translation of the ORF1 polyprotein, it is subsequently cleaved proteolytically (Sosnovtsev et al., 2006) by the viral protease NS6 as well as other host proteases, into six non-structural proteins: NS1/2, NS3, NS4, NS5, NS6, and NS7 (Thorne and Goodfellow, 2014).

Once processed, the MNV non-structural viral proteins begin to build the MNV RC in a perinuclear region, recruiting lipids and proteins from the endoplasmic reticulum (ER), golgi apparatus, and endosomes (Hyde and Mackenzie, 2010; Hyde et al., 2009). Further, the proper perinuclear localization of the MNV RC has been shown to be important for optimal viral replication and depends on the cytoskeleton network (Hyde et al., 2012). MNV nonstructural proteins 1/2, 3, and 4 have been implicated in contributing to building the RC and localizing to/ manipulating membranes (Cotton et al., 2017; Hyde and Mackenzie, 2010; Hyde et al., 2009; Thorne and Goodfellow, 2014), and these observations seem to extend to the homologous non-structural proteins of HNV as well (Doerflinger et al., 2017). Overall, these studies suggest that all three of these MNV nonstructural proteins are required to produce a native MNV RC, but NS4 expression alone induces both single- and double-membrane vesicles that look similar to the native

RC induced by MNV infection, suggesting that it is the major player in the dramatic membrane rearrangements and RC formation observed during infection.

Following formation of the RC, all non-structural proteins localize to the RC (Hyde and Mackenzie, 2010), including the RdRp NS7, which replicates the MNV genome; replication is further enhanced via interactions between VPg and NS7 (Subba-Reddy et al., 2011, 2018). Replication of the MNV genome produces dsRNA replication intermediates which can be used as markers for active replicating MNV RCs. The MNV genome contains 4 ORFs. ORF1 is translated from the positive-strand MNV genome and encodes all non-structural proteins (NS1/2-NS7). ORF2 and ORF3 encode the major and minor capsid proteins, respectively (VP1 and VP2), and are translated from the MNV subgenomic RNA. The MNV subgenomic RNA is only produced from the negative strand, thus the late lifecycle capsid proteins, which are required for packaging the genome, are only produced after viral replication has started; this represents a potential mechanism by which MNV separates early lifecycle from late lifecycle (i.e. genome replication from genome packaging) (Thorne and Goodfellow, 2014). Following production of the subgenomic RNA, MNV begins producing the ORF2 and ORF3 encoded products, the major and minor capsid proteins which begin to assemble spontaneously into viral capsids containing the MNV genome (Bertolotti-Ciarlet et al., 2002). It is believed that VP2, the minor capsid protein, serves to bridge the VP1 major capsid protein with the (+)RNA MNV genome, but a direct interaction between the MNV genome and VP2 has not yet been demonstrated (Sosnovtsev et al., 2005; Vongpunsawad et al., 2013). Lastly, how the assembled and mature viral progeny escape from the cell is not well understood. Because MNV is a lytic virus that induces

apoptosis of infected cells *in vitro*, this viral triggered cell death is believed to be a possible escape mechanism utilized by MNV (Bok et al., 2009; Furman et al., 2009). Further supporting this hypothesis is the observation that inhibiting apoptosis of MNV infected cells in culture decreases the amount of infectious MNV produced compared to control cells (Furman et al., 2009; Thorne and Goodfellow, 2014).

All viruses in the *Caliciviridae* family possess these first three ORFs, but MNV is unique in the fact that it possess a fourth ORF encoding a protein known as virulence factor 1 (VF1); ORF4 is translated from the MNV subgenomic RNA and VF1 has been shown to be important in suppressing the host innate immune response. Mutant viruses not expressing VF1 trigger increased expression of type I interferons and induce apoptosis more quickly compared to WT MNV in cell culture. Even though MNV VF1 null mutants can replicate normally *in vitro*, continuous passage of these mutant virus in cell culture results in spontaneous restoration of VF1 expression. Lastly, MNV not expressing VF1 is less able to cause pathology in $STAT1^{-/-}$ mice compared to WT MNV (McFadden et al., 2011; Thorne and Goodfellow, 2014).

In conclusion, MNV is a small (+)RNA virus from the *Caliciviridae* family which has been heavily studied as the primary model for human norovirus (Wobus et al., 2006). Many methods and techniques have been developed to genetically manipulate and study the virus *in vitro* and *in vivo (Hwang et al., 2014)*. MNV readily replicates in permissible cells and transiently expressing the MNV entry receptor, CD300lf, in non-permissible cells renders them permissible (Haga et al., 2016; Orchard et al., 2016; Wobus et al., 2004). Further, the RC of MNV forms a concentrated perinuclear puncta, making this structure easy to visualize by both immunofluorescent and electron

microscopy. The MNV RC can be visualized by staining for the NS7 RdRp or dsRNA. Because the MNV non-structural proteins localize to the RC, the membrane rearrangements characterizing the RC can be visualized by simply overexpressing the MNV ORF1, and looking for localization of NS7 (Hwang et al., 2012; Hyde and Mackenzie, 2010). For technical ease and relevance to understanding infectious disease, MNV is a good model to study (+)RNA viruses, including investigation of potential antiviral mechanisms targeting viral RCs. An interferon-mediated antiviral pathway targeting the RC of MNV was previously identified when investigating the role autophagy proteins play in the MNV lifecycle (Hwang et al., 2012).

Autophagy as a Proviral and Antiviral Pathway

Autophagy is a catabolic process, conserved from yeast to humans, by which cytoplasmic materials are sequestered in a double-membrane bound vesicle, termed the autophagosome, and delivered to the lysosome for degradation. Autophagy plays a role in maintaining cell homeostasis, recycling cellular material, degrading damaged organelles, and clearing invading intracellular pathogens. Canonical degradative autophagy is mediated by many cellular proteins encompassing several large protein complexes (Feng et al., 2014; He and Klionsky, 2009); these autophagy related proteins (ATGs) were identified originally in yeast by screening for mutants that were defective in their ability to form autophagic bodies in conditions of starvation or lysosomal inhibition (Takeshige et al., 1992; Tsukada and Ohsumi, 1993). Under basil conditions, the molecular target of rapamycin (mTOR) keeps the upstream autophagy machinery in an

inactive state. However, under activating conditions such as starvation, mTOR is inhibited, which allows the uncoordinated 51-like-kinase (ULK) initiation complex of autophagy to activate the phosphatidylinositol 3-kinase (PI3K) nucleation complex on a membrane where the autophagosome will form. The growing autophagosome (the omegasome) begins to form with the help of this Atg14 containing PI3K nucleation complex which converts phosphatidylinositol into phosphatidylinositol 3-phosphate (PtdIns3P) at the initiation site. Then the WD repeat domain phosphoinositide-interacting protein 2b (WIPI2b) binds to PtdIns3P on the growing autophagosome. WIPI2b acts to recruit two ubiquitin-like conjugation systems, together known as the LC3-conjugation complex, to the autophagosome. It does so through a direct interaction with Atg16L1, which subsequently recruits other components of the Atg12-Atg5-Atg16L1 complex which acts to extend and elongate the autophagic membrane structure. In addition, ubiquitin-like molecule LC3 (Atg8) is processed by Atg4, activated by Atg7 E1 enzyme, conjugated with Atg3 E2 enzyme, and finally conjugated to phosphatidylethanolamine (PE) residues on autophagosomes by the Atg12-Atg5-Atg16L1 complex which acts as an E3-like ligase. Atg8/LC3 works to extend and close the structure, mediating the maturation of the autophagosome. Atg8 has several homologs in humans and mice encompassing the LC3 homolog family members (LC3a and b) and Gamma-aminobutyric acid receptor-associated proteins (GABARAPs) (GABARAP, GABARAPL1, and GABARAPL2). Both families of Atg8 homologs are essential for canonical degradative autophagy but are shown to play different roles in autophagosome maturation (Weidberg et al., 2010). Finally, syntaxin 17 on the autophagosome acts as a soluble N-ethylmaleimide-sensitive factor attachment protein

receptor (SNARE) to bind to the lysosomal SNARE VAMP8 to mediate autophagosome and lysosomal fusion, resulting in an autolysosome (Itakura et al., 2012). In summary, a growing autophagosome is formed by the initiation and nucleation complexes of autophagy and subsequently two ubiquitin-like-conjugation systems, together known as the LC3-conjugation complex, act in concert to conjugate LC3 to the autophagosome which promotes closure and maturation of the globular membranous structure, which then fuses with the lysosome (Feng et al., 2014; He and Klionsky, 2009; Levine et al., 2011).

Besides maintaining cellular homeostasis, autophagy has been demonstrated to be critical for host defense against various pathogens (Levine et al., 2011). Xenophagy is a subset of autophagy by which a microbe or microbial components are recognized and sequestered in a double-membrane bound autophagosome and subsequently delivered to the lysosome for degradation. Xenophagy has been shown to function against intracellular bacteria, protozoan parasites, and even viruses (virophagy) such as Sindbis virus (SINV), a (+)RNA virus from the *Togaviridae* family (Jordan and Randall, 2012; Liang et al., 1998; Orvedahl et al., 2010). Autophagy plays other antiviral roles in addition to xenophagy/ virophagy which include mediating the interferon response by bringing viral pathogen associated molecular patterns (PAMPs) to innate immune sensors in endosomes to trigger production of antiviral interferons and cytokines (Lee et al., 2007). In addition, autophagy has been shown to mediate the adaptive immune response to viruses through enhancement of viral peptide processing and presentation on major histocompatibility complex class I and II (MHC I and MHC II) (English et al., 2009; Lee et al., 2010; Paludan et al., 2005; Schmid et al., 2007). As would be expected

with the high mutation rates of viruses, the antiviral properties of autophagy apply a strong selective pressure on viruses and thus many have evolved mechanisms to antagonize the antiviral activity of autophagy (Dong and Levine, 2013; Gannagé et al., 2009; Jordan and Randall, 2012; Orvedahl and Levine, 2008).

Though autophagy can play an antiviral role against some viruses, other viruses require autophagy to complete their lifecycle. This is the case for many (+)RNA viruses that need to rearrange host membranes to set up their RC. Because autophagy is in essence a pathway that rearranges host membranes in response to an environmental trigger (e.g. starvation or cellular stress) and because many autophagy proteins are able to manipulate membranes, some viruses can commandeer the autophagy pathway or specific autophagy proteins to build their RC. A good example of this is poliovirus, a (+)RNA virus from the *Picornaviridae* family. Poliovirus builds a DMV class RC which resembles a double-membrane autophagosome, leading to the hypothesis that poliovirus and other viruses in the *Picronaviridae* family utilize autophagy proteins to build their RC (Suhy et al., 2000). Indeed, it was shown that the autophagy pathway is important for both replication and release of poliovirus from infected cells; further, the autophagy protein LC3 localizes to the RC of poliovirus (Jackson et al., 2005). Though it is still unclear mechanistically how autophagy is benefitting poliovirus, there are several potential mechanisms that have been proposed. Autophagy could be mediating formation of the RC, promoting cellular homeostasis to keep virally infected cells alive longer to maximize viral production, recycling cellular components to make nutrients available for viral replication, or even mediating viral exit from the cell (Corona et al., 2018; Dong and Levine, 2013). Whether autophagy is required for building the RC of

picornaviruses may be difficult to determine because it is reported that RCs utilized by these viruses are heterogeneous, meaning the virus may utilize multiple and potentially redundant pathways to build their RCs, therefore even if autophagy is absent, a picorna virus RC can still be built (Jordan and Randall, 2012). Further studies are required to determine definitively what proviral role autophagy is playing in the picornavirus lifecycle.

Autophagy has also been reported to play a proviral role for (+)RNA viruses of the *Coronaviridae* and *Flaviviridae* families (Jordan and Randall, 2012). For coronaviruses, it was originally proposed that their RCs may be autophagosomes (Prentice et al., 2004). However, further studies reported contradictory results indicating that the requirement of autophagy may be cell type dependent; in some cases what is required instead of degradative autophagy is the cytosolic version of LC3 (LC3-I), which was localized to the RC (Knoops et al., 2008; Reggiori et al., 2010). So for the coronaviruses, while autophagy seems to play a proviral role, it is not mechanistically clear what that role is (Jordan and Randall, 2012). For the flaviviruses, both Dengue virus (DENV) and Hepatitis C virus (HCV) require autophagy for optimal viral replication. The proviral mechanism for HCV is unclear but it clearly promotes viral replication. Further, the HCV RdRp has been shown to interact with the autophagy protein Atg5 early in infection, suggesting a possible point of interaction between HCV and autophagy (Dreux et al., 2009; Guévin et al., 2010). For DENV, excellent mechanistic studies have shown that this virus induces a form of autophagy known as lipophagy, where lipid droplets are digested through an autophagic pathway which releases free fatty acids and other nutrients that help the dengue virus lifecycle. For dengue virus,

LC3 does not localize to the RC and it is not believed that lipohagy plays a direct role in building the RC (Heaton and Randall, 2010; Jordan and Randall, 2017; Welsch et al., 2009). Clearly many (+)RNA viruses use components of the autophagy pathway for their own benefit. Other viruses outside the (+)RNA virus class can utilize autophagy to their advantage, including Herpes viruses, Human Immunodeficiency Virus (HIV), Hepatitis B Virus (HBV), and many more (Choi et al., 2018; Dong and Levine, 2013; Jordan and Randall, 2012). The field of virology has now documented numerous examples of both proviral and antiviral functions of the autophagy pathway in addition to individual autophagy components. Naturally, upon discovery of MNV, the pressing question was what relationship, if any, does autophagy have with MNV and in extension human norovirus (Karst et al., 2003; Wobus et al., 2006)?

An Antiviral Pathway of Interferon Gamma Targets the Replication Complex of Murine Norovirus and Requires Autophagy Proteins

Upon discovery of MNV and the adoption of this virus as the primary model for HNV, virologists asked what role the autophagy pathway plays in norovirus biology. This question was addressed *in vitro* using bone marrow derived macrophages (BMDMs), a biologically relevant cell type for MNV infection, extracted from mice with a conditional knock out of Atg5 in cells with lysozyme-M (LysM) driven expression of cre-recombinase (*Atg5*$^{f/f}$+LysMcre), thus macrophages will be the major cell type deficient for Atg5 (DeSelm et al., 2011; Zhao et al., 2008). As MNV was able to replicate comparably in both the KO and control cells, this experiment revealed that MNV did not

require Atg5 to replicate (Hwang et al., 2012). In addition to understanding the role autophagy plays in the lifecycle of MNV, it was also of interest to understand if autophagy proteins could play an antiviral role against MNV. Since the type II interferon, interferon gamma (IFNG), had previously been implicated in host defense against bacterial and protozoan pathogens in a manner dependent on autophagy proteins, it was tested if the antiviral activity of IFNG against MNV was dependent on autophagy proteins (Levine et al., 2011; Zhao et al., 2008). The resulting experiment tested whether IFNG was able to control MNV in Atg5 WT and KO BMDMs pretreated with IFNG (Hwang et al., 2012). In addition to the finding that autophagy was dispensable for replication of the virus in BMDMs, this experiment revealed that Atg5 was essential for the IFNG meditated antiviral activity against MNV (Hwang et al., 2012). This suggested that in the case of MNV, autophagy played an antiviral role which is initiated by IFNG treatment. This study suggested that autophagy was dispensable for replication of MNV, but a more recent study suggests that MNV does indeed utilize autophagy proteins for its lifecycle, but does not need them for formation of its RC (O'Donnell et al., 2016). This study suggests that MNV triggers early stages of autophagy, allowing LC3 to localize to autophagosomes, but doesn't allow these autophagosomes to fuse with the lysosome. The proviral mechanism for MNV is unclear but it was suggested that MNV sequesters proteins essential for autophagy to the MNV RC, thus utilizing these components in its lifecycle while also blocking degradative lysosomal fusion of autophagosomes (O'Donnell et al., 2016). These contradictory results are most likely due to differences in cell types used, i.e.: primary BMDMs vs. immortalized macrophage like RAW264.7 cells which are actually from a different strain of mouse; RAW264.7 cells are derived from a

BALB/c mouse while the BMDMs from the earlier studies are derived from C57BL/6 mice (Hwang et al., 2012; O'Donnell et al., 2016).

It was then investigated if canonical degradative autophagy was essential for this IFNG mediated antiviral activity against MNV. Using chemical modulators of the autophagy pathway it was demonstrated that, surprisingly, while autophagy proteins from the Atg12-Atg5-Atg16L1 complex were required for this IFNG mediated antiviral activity, degradative autophagy was completely dispensable. This suggested that this antiviral activity of IFNG was not a form of virophagy, and instead components of the autophagy pathway possessed a non-canonical antiviral activity against MNV able to function in a cassette-like manner independently from the whole pathway (Hwang et al., 2012).

At this point, little was known mechanistically about how these autophagy proteins were functioning in an antiviral manner against MNV in response to IFNG signaling. To learn more about the nature of this antiviral pathway, the stage of the MNV lifecycle that was antagonized/ blocked was then investigated. Experiments demonstrating that IFNG did not block pioneer translation of viral proteins, upon release of the viral genome into the cytoplasm, but blocked formation of the MNV RC suggested that the stage of the MNV lifecycle that IFNG antagonized was at the stage of RC formation. These experiments provided the first example that the RC of a (+)RNA virus could be the target of an interferon-mediated antiviral pathway (Hwang et al., 2012). This study also demonstrated that the autophagy protein Atg16L1, a component of the Atg12-Atg5-Atg16L1 complex and vital for this antiviral pathway, localized to the RC of MNV, suggesting that the autophagy proteins may target to the RC of MNV (Hwang et

al., 2012). Because Atg16L1 localized to the MNV RC independently of IFNG signaling, the autophagy proteins were not believed to play a direct antiviral role themselves against the RC, but instead were hypothesized to play a role in concert with one or multiple ISGs that are upregulated by IFNG.

In an effort to identify these ISGs, a follow up study determined that the IFNG mediated antiviral activity against MNV was dependent upon the signal transducer and activator of transcription 1 (STAT1) and the interferon regulatory factor 1 (IRF1) (Maloney et al., 2012). Both STAT1 and IRF1 regulate expression of many different cytokines, chemokines, and ISGs in response to IFNG (Kimura et al., 1994; Liu et al., 2003; Liu et al., 2005). Using this information, this study then identified a list of candidate ISGs that were upregulated in a STAT1 and IRF1 dependent manner (Maloney et al., 2012). Among this list of candidates was the guanylate binding proteins 1 and 2 (GBP1 and GBP2), proteins of the dynamin-like GTPase superfamily with known anti-microbial function (Yamamoto et al., 2012). It was hypothesized that one or several of these candidates would be involved in the IFNG mediated antiviral activity against MNV. Despite the fact that potential IFNG induced antiviral ISG candidates had been identified, none of the candidates appeared to be involved when tested individually. Thus, despite understanding more about the signaling pathway required for IFNG to upregulate potential ISGs acting against the MNV RC, we still did not know which ISGs, if any, worked in concert with the autophagy proteins to antagonize the RC of MNV (Hwang et al., 2012; Maloney et al., 2012).

An Antimicrobial Pathway of Interferon Gamma Disrupts the Parasitophorous Vacuole of *Toxoplasma gondii*

It was previously shown that the Atg12-Atg5-Atg16L1 complex of autophagy, but not degradative autophagy, was required for the IFNG mediated antiviral activity against the MNV RC, but the antiviral mechanism of the autophagy proteins and required ISGs were unknown (Hwang et al., 2012). An approach to identify individual candidate genes did not definitively show a role for of an ISG in this antiviral pathway (Maloney et al., 2012). A strategy to look into known IFNG mediated antiviral mechanisms against other viruses, with the hope of applying this knowledge to the IFNG mediated control of MNV, was not effective because few mechanistic details are known, so little insight can be gathered from the literature on the antiviral mechanisms against other viruses. In contrast, a cell autonomous mechanism of IFNG in controlling the intracellular parasite, *Toxoplasma gondii*, has been well studied, potentially offering insight into the antiviral pathway against MNV. *T. gondii*, the causative agent of toxoplasmosis, is a zoonotic protozoan parasite that infects a broad range of host species (Sibley, 2011). Toxoplasmosis is a major cause of foodborne illness in the United States and is primarily acquired from consuming undercooked meat (Jones et al., 2010). *T. gondii* infection can lead to complications in immunocompromised individuals, such as congenital diseases; however, healthy individuals can usually control the acute infection without manifesting serious symptoms. Most infected individuals fail to clear the pathogen entirely and *T. gondii* persists in a dormant state for the life of the host. It is estimated that approximately 1 out of 3 people are persistently infected globally (Jones et al., 2010; Pappas et al., 2009). For these reasons, many groups have studied the

mechanisms by which the host controls *T. gondii* infection. *T. gondii* actively invades cells and maintains itself in a plasma membrane derived vacuolar structure termed the parasitophorous vacuole (PV) that resides in the cytoplasm (Sibley, 2011). *T. gondii* removes most host proteins from the PV to exclude the vacuole from the endocytic pathway, ensuring it does not fuse with the lysosome (Sibley, 2011). This customization makes the PV a perfect niche for *T. gondii* to replicate, sequestered away from the hostile cytoplasm. Naïve cells are permissive to *T. gondii* infection and replication, but IFNG activated cells are a different situation.

When *T. gondii* infected cell are activated by IFNG, a group of interferon-inducible immune effectors are targeted to the parasitophorous vacuole membrane (PVM) and disrupt membrane integrity; this results in *T. gondii* exposure to the cytoplasm and parasite death (Howard et al., 2011; Kim et al., 2012; Martens et al., 2005). These immune effectors are known as the interferon (IFN)-inducible GTPases and are members of the dynamin-like GTPase superfamily. Dynamin is a GTPase protein which mediates budding off of membranous vesicles into the cytoplasm of eukaryotic cells, like during clathrin-mediated endocytosis. Dynamin does this by forming oligomers around the neck of a vesicle undergoing invagination and uses mechanical force from GTP hydrolysis to apply pressure to the neck, eventually causing it to break away from the plasma membrane or vesiculate (Roux et al., 2006; Urrutia et al., 1997). It is speculated that the IFN-inducible GTPases oligomerize on the PVM of *T. gondii* and vesiculate this membrane through GTP hydrolysis in a similar manner to dynamin, this is supported by structural studies but has not been demonstrated

biochemically (Howard et al., 2011; Kim et al., 2016; Kim et al., 2012; Zhao et al., 2008). At this point, it was not clear how these immune effectors target to the PVM of *T. gondii*.

Immunity Related GTPases and Guanylate Binding Proteins: Interferon-Inducible GTPases of the Dynamin-like GTPase Superfamily

The dynamin-like GTPase superfamily encompasses four sub-families of IFN-inducible GTPases including the immunity related GTPases (IRGs), guanylate binding proteins (GBPs), myxovirus resistance proteins (MXs), and the very large interferon-inducible GTPases (VLIGs) (Kim et al., 2012; Pilla-Moffett et al., 2016). The MX proteins have been well studied for their antiviral mechanisms against major human pathogens like influenza A virus (IAV) and HIV but are largely type I IFN-inducible and not reported to block RC formation/ maintenance of (+)RNA viruses; further these proteins are not reported to play a role in the IFNG mediated disruption of the *T. gondii* PV (Haller et al., 2015; Matzinger et al., 2013; Staeheli et al., 1986). The VLIGs are believed to be present in humans only as pseudogenes and not well studied for their role in the immune defense against *T. gondii* or other pathogens (Li et al., 2009; Pilla-Moffett et al., 2016). The IRGs and GBPs are both strongly induced by IFNG and target to the PVM of *T. gondii* (Howard et al., 2011; Kim et al., 2012; Martens et al., 2005; Yamamoto et al., 2012). Further, these IFN-inducible GTPases have also been reported to target and disrupt the replication vacuoles of other intracellular pathogens such as the intracellular bacterium *Chlamydia trachomatis* and the intracellular fungus microsporidian

Encephalitozoon cuniculi (Bernstein-Hanley et al., 2006; Ferreira-da-Silva et al., 2014; Pilla-Moffett et al., 2016).

Guanylate Binding Protein 1 (GBP1) was one of the first IFN-inducible genes discovered, about 35 years ago, but it's function in host immunity was not clear and so was not heavily studied (Cheng et al., 1983). Many years later, the IRGs were shown to be essential for control of several intracellular pathogens, including *T. gondii*, which led to the emergence of a field dedicated to the study these IFN-inducible GTPases and the roles they play in host immune defense against intracellular pathogens (Bernstein-Hanley et al., 2006; MacMicking et al., 2003; Singh et al., 2006; Taylor et al., 2000). Soon, the GBPs were also shown to play a similar protective role against intracellular pathogens such as *T. gondii* (Degrandi et al., 2007; Kim et al., 2011; Selleck et al., 2013; Yamamoto et al., 2012). Both the IRGs and GBPs were believed to have originated in a common ancestor of chordates but different species harbor very different repertoires of these immune effectors, which is especially true for the IRGs (Li et al., 2009).

In vertebrates, the *IRG* gene family has been subject to large episodes of gene loss and duplication, suggesting application or removal of selective pressures (Li et al., 2009). This is particularly apparent when comparing the *IRG* gene repertoire in mice and humans. Rodents have a large *IRG* gene repertoire expressing approximately 20 IRG proteins while humans express only 2, IRGM and IRGC, which are expressed at resting state and not IFN-inducible (Bekpen et al., 2005; Bekpen et al., 2009). This expansion and retraction of the IRGs in mice vs. humans is a great example of the red queen hypothesis in action, which describes the molecular-arms race between a host

and pathogen that adds a selective pressure to both, leading to the continuous and rapid evolution of new strategies to overcome the other (Brockhurst, 2011; Daugherty and Malik, 2012). From the perspective of the host, it must evolve new immune pathways and effectors to antagonize the pathogen as quickly as possible or else be overtaken by the pathogen. From the perspective of the pathogen, it must evolve new ways to counteract the host's immune system so it can continue to propagate in this host or else be cleared by the host. This process results in the accelerated expansion, duplication, and mutation of genes of both the host and pathogen. In the case of mice, an intimate evolutionary relationship has existed with *T. gondii* for a long time. This is because *T. gondii* can only complete its sexual lifecycle in feline species, which are definitive hosts. To gain access to this definitive host, the parasite commonly goes through an intermediate host, a role often played by rodents that are hunted and consumed by domestic house cats (Gazzinelli et al., 2014). It is believed this selective pressure is why mice have such an expanded repertoire of IRG proteins compared to humans who are lacking this selective pressure and thus have a collapsed repertoire of IRG proteins (Gazzinelli et al., 2014). Further, maintaining a large repertoire of these membranolytic effectors may come with a fitness cost, so without the positive pressure of an intracellular pathogen to maintain these effectors, the host may deplete these IRG proteins (Gazzinelli et al., 2014). In contrast, the GBPs are more highly conserved between mice and humans. Humans encode seven *GBP* genes and one pseudogene while mice encode 11 *GBP* genes and two pseudogenes (Kresse et al., 2008; Olszewski et al., 2006). In addition to their role in targeting to the replication vacuoles of intracellular pathogens, GBPs are shown to be important in the inflammasome pathway,

in regulating cellular proliferation, and regulating angiogenesis (Guenzi et al., 2001; Guenzi et al., 2003). These broad cellular functions suggest that these GBPs are essential to the host, offering an evolutionary explanation for the greater level of conservation in mammals compared to the IRGs.

The IRGs in mice share a similar structure, for example, they all contain a highly conserved GTPase domain and similar molecular size of 47,000 daltons. Because of this the IRGs have been believed to play similar redundant functions in host defense. However, it appears distinct IRGs possess diverse roles in response to microbial infection. Knock out analysis of various mouse IRG proteins showed different susceptibilities to various intracellular pathogens, suggesting that IRGs play different roles for different pathogens (Collazo et al., 2001; Taylor et al., 2000). These studies led to the discovery that the IRG proteins come in two categories, GKS effector IRGs and GMS regulator IRGs. The GKS effectors are characterized by a GxxxxGKS motif in the P-loop of the GTP-binding site while the GMS regulators are characterized by a GxxxxGMS motif in the P-loop of the GTP-binding site (Bekpen et al., 2005; Hunn et al., 2008). When cells are activated by IFNG but uninfected, the GKS effector IRGs reside in their inactive GDP bound form in the cytoplasm and associate only transiently with cellular organelles. The GMS regulator IRGs associate with membranes of cellular organelles and serve as guanine dissociation inhibitors (GDIs) to prevent the GTP mediated oligomerization of the GKS effectors on these “self” organelles, and thus prevent IRG mediated destruction of the host cell. These regulator proteins are believed to act as “guard” proteins that mark “self” membranes (Coers, 2013; Haldar et al., 2013; Maric-Biresev et al., 2016). Upon infection of an IFNG activated cell with *T.* gondii, the

GKS IRGs begin accumulating on the largely GMS devoid PVM in their GTP bound active state (Coers et al., 2008; Haldar et al., 2013; Hunn et al., 2008; Martens et al., 2005). The GBPs are believed to function in a similar fashion to the GKS effector IRGs. They target to the PVM of *T. gondii* in a GTP dependent fashion, and are also sensitive to regulation by the GMS regulator IRG proteins (Traver et al., 2011). In addition, murine GBP2 has been shown to have the ability to enter the ruptured PV and associate directly with the membrane of *T. gondii*, suggesting a direct anti-parasitic attack (Kravets et al., 2016). The nature of the relationship between the IRGs and GBPs is not completely understood. It is believed these systems overlap, early evidence came from the observation that in a mouse model with two key regulator GMS IRGs deleted ($Irgm1^{-/-}Irgm3^{-/-}$ or Irgm1/3 DKO) that GKS effector proteins became dysregulated and formed cytoplasmic aggregates of GTP bound active IRGs that colocalized with murine GBP2 (Traver et al., 2011). The current model describes a hierarchy by which the IRGs are recruited to the PVM first followed by recruitment of E3-ubiquitin ligases which ubuitinate targets at the PVM, which in turn recruit the autophagy adaptor protein p62, which finally directly recruits the GBPs (Haldar et al., 2015). Another study has demonstrated a direct protein-protein interaction between the GKS effector Irgb6 and the GBPs (Yamamoto et al., 2012). This hierarchy suggests an order to which the IFN-inducible GTPases are targeted to the PVM of *T. gondii*, but they do not reveal what the differential role of these two classes of immune effectors are on vesiculation and disruption of the PVM. Further, it was not understood how the IFN-inducible GTPases were targeted to the PVM of *T. gondii*. The “missing-self” model, described above, provides a potential explanation, however, it was later discovered that the essential

autophagy protein, Atg5, was required for targeting of the IRG proteins to the PVM of *T. gondii*, an observation that the “missing-self” model cannot fully explain (Zhao et al., 2008).

The Role of Autophagy Proteins in the Interferon Gamma Mediated Control of Protozoan Parasite *Toxoplasma gondii*

The mechanism by which the IRGs and GBPs target to the PVM of *T. gondii* was unclear, with the predominant theory being “non-self” by which GKS IRGs can target to a membrane devoid of GMS regulator IRG proteins (Coers, 2013). However, the regulation of IRG and GBP targeting to the PVM of *T. gondii* was shown to be more complex when it was determined that targeting was dependent on the essential autophagy protein Atg5 (Zhao et al., 2008). In Atg5 KO cells, IFNG failed to control replication of *T. gondii*. In these cells the IRGs and GBPs were still upregulated but now failed to target to the PV of *T. gondii*, and instead formed cytoplasmic aggregates, reminiscent of the dysregulated state seen in Irgm1/3 double KO cells. Further, this phenotype was not believed to be dependent on degradative autophagy because *T. gon*dii was not observed to be engulfed by a double-membrane bound autophagosome in any step of the Atg5-mediated targeting of the IRGs/GBPs to the PVM or disruption of this structure (Zhao et al., 2008). We provided further evidence for this hypothesis by showing that autophagy proteins involved in the initiation or nucleation complexes of degradative autophagy, ULK1, ULK2, and Atg14L, were not required for the IFNG mediated control of *T. gondii in vitro* and *in vivo*; these phenotypes correlated with

targeting of the IRGs and GBPs (Choi et al., 2014). Further, chemical modulation of the autophagy pathway did not affect the ability of IFNG to control *T. gondii* infection (Choi et al., 2014). We and others followed up and defined the cassette of autophagy proteins required for the targeting of the IRGs and GBPs to the PVM and the IFNG mediated control of *T. gondii*. Our results showed that components of the LC3-conjugation system, functioning independently from degradative autophagy, are required for this IFNG mediated control of *T. gondii*; this is reminiscent of the IFNG mediated control of MNV, which requires the Atg12-Atg5-Atg16L1 complex, a core component of the LC3-conjugation system (Choi et al., 2014; Haldar et al., 2014; Hwang et al., 2012; Ohshima et al., 2014). Further, because the LC3-conjugation system was required for this phenotype, we speculated that the mechanism may involve targeting of LC3 directly to the PVM of *T. gondii*, and indeed immunofluorescent microscopy revealed this to be the case, leading to the possibility that LC3 on the PVM may be mediating recruitment of the IFN-inducible GTPase effector proteins (Choi et al., 2014).

Focusing on this LC3-conjugation dependent targeting of the IFN-inducible GTPases to the PV of *T. gondii*, we hypothesized that LC3 recruitment to the PV was acting as a molecular beacon to mark the PV of *T. gondii* as a target for the IRGs and GBPs. We showed the sufficiency of the LC3-conjugation system to recruit the IFN-inducible GTPases by relocating Atg16L1, a key component of LC3-conjugation complex and the protein first recruited to the growing autophagosome, to either the mitochondrial outer membrane or the plasma membrane, places we did not observe Atg16L1 localization under basil conditions. Relocating Atg16L1 recruited the IFN-inducible GTPases to these new locations, rather than to the PV of *T. gondii* (Park et al.,

2016). This suggests that indeed the LC3-conjugation complex is sufficient to recruit the IFN-inducible GTPases to a target location, but was this dependent on LC3 itself as we hypothesize? Deletion of LC3b, the major LC3 homolog, did not affect the ability of the IFN-inducible GTPases to target to the PV or IFNG from controlling *T. gondii* replication, suggesting no role (Choi et al., 2014). However, LC3 is the mammalian homolog of Atg8 from yeast, and in mice several homologs of Atg8 exist, encompassing the LC3 family (LC3a and LC3b) and the GABARAP family (GABARAP, GABARPL1, and GABARAPL2). We found that indeed all homologs localized to the PVM of *T. gondii*, suggesting potential redundant roles of these Atg8 homologs (Choi et al., 2014). Indeed, when we knocked out or knocked down all Atg8 homologs, IFNG was no longer able to control *T. gondii* replication and the PVM was no longer targeted by the IFN-inducible GTPases (Choi et al., 2014). This study provided evidence that LC3 and homologs act as redundant molecular beacons on the PVM of *T. gondii*, marking the structure as a "non-self" target for the IFN-inducible GTPases. Further, another study also showed a role for an LC3 homolog in recruiting the IFN-inducible GTPases to the PV of *T. gondii*, but their data suggests a specific role for GABARAPL2 but not the LC3 homologs, which is contrary to our data and can potentially be explained by differences in methodology and system (Sasai et al., 2017). Having shown that the LC3-conjugation system of autophagy plays a novel role in targeting IFN-inducible GTPases to pathogen containing membranous structures, a pathway independent of canonical degradative autophagy, we termed this non-canonical targeting pathway: Targeting by AutophaGy proteins (TAG) (Choi et al., 2016; Park et al., 2016). Many questions remain on this TAG pathway against *T. gondii,* such as how is the PV designated as a target for TAG

and how do the LC3 homologs recruit the IFN-inducible GTPases? These are ongoing questions currently under investigation.

Parallels between TAG against *Toxoplasma gondii* and the IFNG Mediated Antiviral Pathway Targeting the Replication Complex of Murine Norovirus

An antiviral mechanism of IFNG which targets the MNV RC was previously discovered and shown to require the Atg12-Atg5-Atg16L1 complex, but not degradative autophagy (Hwang et al., 2012). To understand the mechanism by which IFNG exerts its antiviral activity against the RC of MNV in an autophagy dependent mechanism, we compared what we know about this understudied antiviral mechanism to the established field studying the disruption of the PV of *T. gondii* by IFN-inducible GTPases and autophagy proteins, TAG. At this point, many pressing questions on this antiviral mechanism against the RC of MNV remained. First, how does the Atg12-Atg5-Atg16L1 complex synergize with IFNG to antagonize the MNV RC? Second, is it just the Atg12-Atg5-Atg16L1 complex, or are other autophagy proteins also required for this IFNG-mediated antiviral activity targeting the MNV RC? Third, what ISGs are being upregulated by IFNG which are essential for this antiviral pathway? Lastly, how does the host determine the MNV RC as a target for this putative antiviral pathway? TAG against the PV of *T. gondii* involves the targeting of a “non-self” pathogen containing membranous vacuole (the PV) with the autophagy protein LC3 and homologs, which mark this structure as a target for recruitment of the membranolytic IFN-inducible GTPases, the IRGs and GBPs, which vesiculate and disrupt the structure. The putative

antiviral pathway against the MNV RC involves the IFNG-mediated disruption of a pathogen containing membranous vacuole (the RC) which involves an autophagy complex essential for LC3-conjugation but not degradative autophagy. The parallels we observed led us to speculate that TAG, which targets the PV of *T. gondii* and other intracellular pathogens, may be functioning in a similar fashion against the RC of MNV. Thus we hypothesized that the LC3-conjugation complex of autophagy was marking the MNV RC as a “non-self” membranous structure to recruit the IFN-inducible GTPases, destroying the RC.

It was unprecedented to propose that a viral RC was a target of TAG for several reasons. First, other targets of TAG such as the replication vacuoles of *T. gondii*, *C. trachomatis*, and *E. cuniculi*, are all constructed from the plasma membrane while the MNV RC is constructed from components of the ER, golgi-apparatus, and endosomes (Hyde and Mackenzie, 2010; Hyde et al., 2009). Further, the unicellular pathogens strip the majority of the host proteins from their replication compartments while the MNV RC is actually enriched in host proteins. The field speculated that targets of TAG present a host-protein devoid membranous structure, which is clearly not the case for the MNV RC (Coers, 2013). Further, though some early studies of the GBPs suggest some antiviral activity, the phenotype either has no proposed mechanism or a mechanism that antagonizes a lifecycle stage other than the RC, or functions on a virus not belonging to the (+)RNA class (Pilla-Moffett et al., 2016). Further, the IRG class of IFN-inducible GTPases had no clear evidence of antiviral activity. This led to the field speculating that the IRG and GBP classes were specific to large pathogens such as parasites and bacteria, while the MX proteins were the antiviral class of IFN-inducible GTPases (Pilla-

Moffett et al., 2016). This dissertation aims to challenge these conceptions and proposes that in fact these IRG and GBP IFN-inducible GTPases have robust antiviral activity targeting the RCs of (+)RNA viruses. We speculate that the host has evolved the TAG pathway in order to detect “non-self” pathogen containing membranous structures in the cytoplasm and mark them as targets for the membranolytic IFN-inducible GTPases, regardless of whether these be the membranous replication structures of protozoan parasites, intracellular bacteria, intracellular fungi, or even viruses. In attempts to provide answers to these questions this dissertation will focus on the following specific aims:

1. Define the role of the autophagy proteins in the interferon gamma mediated antiviral activity against the replication complex of Murine Norovirus. (Chapter II)

2. Identify the interferon stimulated gene(s) required for the interferon gamma mediated antiviral activity against the replication complex of Murine Norovirus. (Chapter II)

3. Determine a mechanism by which the host identifies the replication complex of Murine Norovirus as a target for this interferon gamma mediated antiviral activity. (Chapter III)

CHAPTER II

Viral replication complexes are targeted by LC3-guided interferon-inducible GTPases

The work presented in this chapter has been published as a manuscript in the Cell Press Journal, Cell Host and Microbe: Viral replication complexes are targeted by LC3-guided interferon-inducible GTPases (DOI: 10.1016/j.chom.2017.06.005). The authors and affiliations of this manuscript are Scott B. Biering,[1,10] Jayoung Choi,[2,10] Rachel A. Halstrom,[2] Hailey M. Brown,[3] Wandy L. Beatty,[5] Sanghyun Lee,[6] Broc T. McCune,[6] Erin Dominici,[2] Lelia E. Williams,[4] Robert C. Orchard,[6] Craig B. Wilen,[6] Masahiro Yamamoto,[7] Jörn Coers,[8] Gregory A. Taylor,[8,9] and Seungmin Hwang[1,2,3]*

[1]Committee on Microbiology,

[2]Department of Pathology,

[3]Committee on Immunology,

[4]Biological Sciences Collegiate Division,

The University of Chicago, Chicago, IL 60637, USA

[5]Department of Molecular Microbiology,

[6]Department of Pathology and Immunology,

Washington University School of Medicine, St. Louis, MO 63110, USA

[7]Laboratory of Immunoparasitology, World Premier International Research Center Immunology Frontier Research Center, Osaka University, Osaka 565-0871, Japan

[8]Departments of Medicine, Molecular Genetics and Microbiology, and Immunology, Duke University Medical Center, Durham, NC 27710, USA

[9]GRECC, Durham VA Health Care System, Durham, NC 27705, USA

[10]These authors contributed equally.

*Correspondence to and Lead Contact:

Seungmin Hwang; Email: shwang@bsd.uchicago.edu

SUMMARY

All viruses with positive-sense RNA genomes replicate on membranous structures in the cytoplasm, called replication complexes (RCs). RCs provide an advantageous microenvironment for viral replication, but it is unknown how the host immune system counteracts these structures. Here we show that interferon-gamma (IFNG) disrupts the RC of murine norovirus (MNV) via evolutionarily conserved autophagy proteins and the induction of IFN-inducible GTPases, which are known to destroy the membrane of vacuoles containing bacteria, protists, or fungi. The MNV RC was marked by the microtubule-associated-protein-1-light-chain-3 (LC3) conjugation system of autophagy and then targeted by immunity-related GTPases (IRGs) and guanylate binding proteins (GBPs) upon their induction by IFNG. Further, the LC3 conjugation system and the IFN-inducible GTPases were necessary to inhibit MNV replication in mice and human cells. These data suggest that viral RCs can be marked and antagonized by a universal immune defense mechanism targeting diverse pathogens replicating in cytosolic membrane structures.

Keywords

autophagy; ATG; LC3; targeting by autophagy proteins; interferon; IFN; interferon-inducible GTPase; immunity-related GTPase; IRG; guanylate binding protein; GBP; positive-sense RNA virus; replication complex; norovirus; vacuolar pathogen

INTRODUCTION

Positive-sense RNA (+RNA) viruses encompass about one-third of all known viruses, including many clinically relevant viruses (den Boon et al., 2010). A hallmark of all known +RNA viruses is to rearrange host endomembranes to form vacuole-like structures in the cytoplasm for their replication, termed the replication complex (RC) (den Boon and Ahlquist, 2010; den Boon et al., 2010). The RC provides +RNA viruses a base to exploit the cell and a shelter from the host immune system (Neufeldt et al., 2016; Shulla and Randall, 2016). However, it has been unclear how the host immune system counteracts viral RCs.

Recently, we found that the replication of murine norovirus (MNV) is inhibited by type II interferon (IFN), IFN-gamma (IFNG), at the stage of RC formation (Hwang et al., 2012) in contrast to type I IFNs that primarily inhibit the translation of MNV proteins (Changotra et al., 2009). Intriguingly, this antiviral activity of IFNG against the MNV RC depends on a protein complex involved in autophagy (Hwang et al., 2012). Autophagy is an evolutionarily conserved cellular pathway that delivers cytoplasmic material to lysosomes for degradation (Levine et al., 2011). Among the multiple types of autophagy, macroautophagy (henceforth, autophagy) is the major process that sequesters and transports cytosolic material inside double-membraned autophagosomes (Noda and Inagaki, 2015). For efficient formation of autophagosomes

and selective capture of cargo, ubiquitin-like microtubule-associated-protein-1-light-chain-3 (LC3) and its homologs must be conjugated to the membrane-embedded lipid phosphatidylethanolamine (PE). Similar to the conjugation of ubiquitin to a target amino acid residue, an E1-like activating enzyme, ATG7, and an E2-like conjugating enzyme, ATG3, function together with an E3-like ligase, the ATG12-ATG5-ATG16L1 complex to conjugate LC3 to PE (Noda and Inagaki, 2015). We found that IFNG requires this E3-like ATG12-ATG5-ATG16L1 ligase complex but not lysosomal degradation through autophagy to inhibit MNV RC formation and viral replication (Hwang et al., 2012). However, it remains unknown how IFNG utilizes this E3-like ligase complex to inhibit the MNV RC.

Intriguingly, *Atg5* is also required for IFNG to inhibit the replication of a protist parasite *Toxoplasma gondii* (Zhao et al., 2008). *T. gondii* invades and replicates within a parasitophorus vacuole (PV); when cells are primed with IFNG, the PV membrane (PVM) is disrupted by IFN-inducible GTPases, immunity-related GTPases (IRGs) and guanylate binding proteins (GBPs) (Pilla-Moffett et al., 2016). IRGs and GBPs are dynamin-like GTPases that are targeted to the membrane of cytoplasmic vacuoles containing bacteria, protists, or fungi (Ferreira-da-Silva et al., 2014; Pilla-Moffett et al., 2016). The targeted membranes are vesiculated, which leads to eventual rupture of the vacuoles and ultimately the death of exposed pathogens (Hunter and Sibley, 2012). Unexpectedly, *Atg5* was required for targeting the IRGs and GBPs to the PVM of *T. gondii* (Selleck et al., 2013; Zhao et al., 2008). We further found that only the LC3 conjugation system of autophagy but not lysosomal degradation is required to target these immune effectors to the PVM of *T. gondii* (Choi et al., 2014). Consequently,

control of *T. gondii* infections by IFNG *in vitro* and *in vivo* depends on the LC3 conjugation system (Choi et al., 2014; Haldar et al., 2014; Ohshima et al., 2014). Furthermore, we found that the LC3 conjugation system is necessary and sufficient to target the IFN-inducible GTPases to membranes; upon relocation of the LC3 conjugation system to the plasma membrane or the mitochondria outer membrane, IRGs and GBPs were redirected to these endomembranes (Park et al., 2016).

Based on this similar genetic requirement for IFNG to function against the membranous structures of MNV and *T. gondii*, we speculated that the same effector mechanism of the IFN-inducible GTPases might be used by IFNG to inhibit the MNV RC. Here we show that the MNV RC was indeed marked with LC3 and targeted by the IFN-inducible GTPases upon their induction by IFNG. Consequently, the LC3 conjugation system and the IFN-inducible GTPases were required for IFNG to inhibit MNV replication in both mice and humans. These data suggest that IFNG inhibits the replication of +RNA viruses via LC3 dependent targeting of IFN-inducible GTPases to the RC. Moreover, it implies that IFNG utilizes the same effector mechanism to inhibit various pathogens replicating in cytosolic membranous shelters, including +RNA viruses as well as bacteria, protists, and fungi.

RESULTS

The LC3 Conjugation System of Autophagy Is Required for IFNG to Inhibit MNV Replication Pharmacological modulation of canonical autophagy or lysosomal degradation has no substantial effect on the IFNG-mediated inhibition of MNV

replication (Hwang et al., 2012). To genetically define the role of the canonical autophagy pathway in this antiviral activity of IFNG, we examined *Ulk* (uncoordinated 51-like kinase) and *Atg14*. ULK1 and ULK2 are serine/threonine-protein kinases of the autophagy initiation complex that induces autophagy upon various signals (Chan et al., 2007). ATG14 is an essential component of the phosphatidylinositol 3-kinase (PI3K) complex that nucleates the formation of isolation membrane (Diao et al., 2015). In primary bone marrow derived macrophages (BMDMs) from *Ulk1*$^{-/-}$, *Ulk2*$^{-/-}$, or littermate control mice, there was no significant difference in viral replication or inhibition by IFNG (Figure 2.1A). To rule out the possibility of phenotype masking due to the redundancy of *Ulk1* and *Ulk2*, we also tested mouse embryonic fibroblasts (MEFs) from *Ulk1*$^{-/-}$*Ulk2*$^{-/-}$ mice (McAlpine et al., 2013). To overcome the barrier of entry, the limiting step in infection (Orchard et al., 2016), transfection of MNV viral RNA (vRNA) is frequently used to analyze MNV replication in non-infectable cell types (Hwang et al., 2014). Upon transfection of MNV vRNA into *Ulk1*$^{-/-}$*Ulk2*$^{-/-}$ and control MEFs, infectious MNV were produced and inhibited by IFNG comparably in both cell lines (Figures 2.1B and 2.1C). Similarly, MNV replication in control (*Atg14*$^{flox/flox}$) and *Atg14*-deficient (*Atg14*$^{flox/flox}$*+LysMcre*) BMDMs was comparable and similarly inhibited by IFNG (Figures 2.1D and 2.1E). These data affirmed our previous findings that the antiviral activity of IFNG requires a specific function of the ATG12-ATG5-ATG16L1 complex rather than the canonical autophagy pathway (Hwang et al., 2012).

Thus far, the only known function of the ATG12-ATG5-ATG16L1 complex is its E3-like ligase function to conjugate LC3 homologs to PE (Noda and Inagaki, 2015). LC3 conjugation also requires the proteolytic processing of LC3 by ATG4; we had previously

ruled out a role of ATG4B, the major isoform of ATG4, in the IFNG-mediated control of MNV replication (Hwang et al., 2012). This suggested an LC3-conjugation independent function of the ATG12-ATG5-ATG16L1 complex, but the existence of other ATG4 isoforms undermined such a conclusion. In order to definitively examine the necessity of LC3 conjugation, we investigated the role of E2-like ATG3 in the IFNG-mediated inhibition of MNV replication. MNV replication was considerably less inhibited by IFNG in the *Atg3*-deficient (*Atg3*$^{flox/flox}$+*LysMcre*) BMDMs compared to the control (*Atg3*$^{flox/flox}$) (Figure 2.1F). Since LC3 was still substantially conjugated to PE due to suboptimal deletion of *Atg3* (Figure 2.1G), we further examined *Atg3*-deficient MEFs (*Atg3*$^{-/-}$) (Choi et al., 2014). We confirmed functional knock-out of ATG3 and consequent obstruction of autophagy in *Atg3*$^{-/-}$ MEF, as manifested by lack of conversion of cytosolic LC3-I to membrane-bound LC3-II and accumulation of autophagy adaptor/cargo p62 (Figure 2.1H). MNV replication was not significantly controlled by IFNG in these *Atg3*$^{-/-}$ MEFs (Figure 2.1I), but lentiviral expression of ATG3 back into the *Atg3*$^{-/-}$ MEFs restored the control of MNV replication by IFNG (Figures 2.1H and 2.1I). Collectively, these data show that the IFNG-mediated inhibition of MNV replication requires the E2-like ATG3 as well as the E1-like ATG7 and the E3-like ATG12-ATG5-ATG16L1 complex (Hwang et al., 2012).

The requirement of the entire LC3 conjugation system for IFNG to inhibit MNV replication further suggested that the LC3 homologs might be involved in such control. Although we previously did not observe any significant role of LC3B (Hwang et al., 2012), the existence of multiple LC3 homologs (i.e. LC3A, LC3B, gamma-aminobutyric acid type A receptor-associated protein (GABARAP), GABARAP-like 1 (GABARAPL1),

and GABARAPL2 in the murine system) suggests a potential functional compensation among the homologs. In fact, we recently found that LC3 homologs fulfill redundant functions in the IFNG-mediated control of *T. gondii*; only with the knock-out/down of all LC3 homologs is the IFNG-mediated control of *T. gondii* lost (Park et al., 2016). Thus, to test the role of all LC3 homologs, we used the clustered regularly interspaced short palindromic repeat (CRISPR)/Cas9 system to knockout all remaining LC3 homologs, except one allele of *Gabarap,* in *Lc3b*$^{-/-}$ MEFs (Hwang et al., 2012) (Figures 2.2A and 2.2B). In the resultant MEFs and intermediate MEFs with wild type *Lc3a*, MNV replication was significantly less inhibited by IFNG, proportional to the knock-out of the LC3 homologs (Figure 2.1J). Collectively, these data demonstrated that LC3 homologs as well as the LC3 conjugation system were necessary for IFNG to inhibit MNV replication.

IFN-Inducible GTPases Are Targeted to the MNV RC via the LC3 Conjugation System

The parallel requirements of the LC3 conjugation system and the LC3 homologs in control of both MNV and *T. gondii* led us to speculate that the IFN-inducible GTPases might also be targeted by the LC3 conjugation system to the RC of MNV as they are targeted to the PVM of *T. gondii* (Park et al., 2016). In fact, LC3 localized on the MNV RC without IFNG activation (Figure 2.4A) in an *Atg5*-dependent manner (Figure 2.4B) and the localization of LC3 to the MNV RC requires the conjugation capability of LC3 (Figure 2.4C), just as it localizes on the PVM of *T. gondii* (Choi et al., 2016; Park et al., 2016). Thus, we further examined the potential targeting of IFN-inducible GTPases,

IRGs and GBPs to the MNV RC. Because we cannot detect MNV RCs in cells pre-activated with IFNG (Hwang et al., 2012), we delayed IFNG treatment to allow MNV to form detectable RCs before being counteracted by IFNG. At 10-12 hours of MNV infection and simultaneous IFNG treatment, we detected formation of MNV RCs as well as expression of IFN-inducible GTPases (Figures 2.3 and 2.4D). Under these experimental conditions, both LC3 and IRGA6 (a representative effector of the IRG protein family) localized to a portion of the RCs (Figures 2.3A and 2.3B); we reasoned that such colocalization might be limited and transient due to inhibition of the RC by the recruited IFN-inducible GTPases. In a similar experimental condition, we also confirmed the localization of LC3 and IRGA6 to the RC of another +RNA virus, encephalomyocarditis virus (EMCV) (Figures 2.4E and 2.4F).

Although IFNG treatment and/or MNV infection did not substantially affect the total conjugation level of LC3 (Figure 2.5A), the localization of LC3 onto the MNV RC was enhanced upon IFNG activation (Figure 2.5B), reminiscent of the events that happened on the PVM of *T. gondii* (Park et al., 2016). Importantly, both LC3 and IRGA6 localization to the MNV RC were dependent on the functional LC3 conjugation system, as their localizations were substantially reduced upon *Atg5* deletion (Figures 2.3A and 2.3B). In contrast, the deletion of *Atg14*, which does not disturb LC3 conjugation (Choi et al., 2014), did not affect their localizations to the MNV RC (Figures 2.3C and 2.3D). These data demonstrated that both LC3 and the IFN-inducible GTPases were indeed recruited to the MNV RC, dependent on the functional LC3 conjugation system but independent of the canonical autophagy pathway.

Compared to the cooperative targeting and overlapping function of effector IRGs on target membranes, individual GBPs can stimulate distinct defense mechanisms (Pilla-Moffett et al., 2016). To identify specific GBPs associated with the MNV RC, we expressed individual epitope-tagged GBPs (GBP1, -2, -3, -5, and -7; deleted in *Gbp*$^{chr3-/-}$ mice as described below) in both WT and *Gbp*$^{chr3-/-}$ BMDMs via lentiviral transduction. Only GBP1 and GBP2 significantly localized to the MNV RC upon IFNG activation in WT BMDMs (Figures 2.3E and 2.3F), but GBP2 was the only one that localized to the MNV RC in the absence of the other GBPs (Figures 2.5C and 2.5D). Interestingly, even GBP2 did not localize to the RC in the absence of IFNG activation (Figure 2.5E), suggesting that correct targeting requires an IFN-inducible co-factor(s) (e.g. a functional IRG system as described below). Like the effector IRGs, the localization of GBP2 to the MNV RC was dependent on *Atg5* but not on *Atg14* (Figures 2.6A-E). The IFN-inducible GTPases are known to be targeted only to vacuoles containing bacteria, protists, or fungi (Ferreira-da-Silva et al., 2014; Pilla-Moffett et al., 2016). The data shown here establishes the membranous RCs of +RNA viruses, MNV and EMCV, as a destination of these IFN-inducible GTPases.

LC3 and IFN-Inducible GTPases Localize on the Membrane of the MNV RC

To examine the recruitment of IRGs and GBPs to the MNV RC at an ultrastructural level, we performed electron microscopy (EM) of the MNV RC. To ensure a high infection rate for efficient EM analysis, we utilized the BV-2 cell line (Hwang et al., 2014). We first confirmed that a representative IRG (i.e. IRGA6) and GBPs (using a pan-GBP antibody detecting GBP1, -2, -3, -4, -5) localized to the MNV RC upon the

simultaneous MNV infection and IFNG treatment in BV-2 cells (Figure 2.6F). Under the same experimental condition, EM analysis revealed abundant vesicular structures around the nucleus only in MNV-infected cells (Figure 2.7A). We further found anti-ProPol (detecting both protease and polymerase of MNV) staining in these vesiculated areas (Figure 2.7B). Most anti-ProPol staining was associated with membranes and was significantly detectable only in infected cells (Figure 2.7B), suggesting that the vesicular structures are the MNV RC. Anti-LC3 staining was also detected around these anti-ProPol-positive structures in both untreated and IFNG-treated conditions (Figure 2.7B). Although simultaneous activation of the cells with IFNG did not significantly affect these structures, we detected both anti-IRGA6 and anti-GBP1-5 stainings on the vesicle membranes around anti-ProPol-positive structures in IFNG-treated cells (Figures 2.7C and 2.7D). While we could not definitively conclude the 3D topology of the proteins through these images, the majority of LC3, IRGA6, and GBP1-5 localized on the inner side of these vacuole-like structures together with ProPol, which is topologically the cytoplasmic side of the RC. These data suggest that LC3 and the IFN-inducible GTPases are recruited onto the cytoplasmic face of the MNV RC membrane and may exert their antiviral effect directly onto the membrane structure of the MNV RC.

IFNG Requires the IFN-Inducible GTPases to Inhibit MNV Replication *in vitro* and *in vivo*

To investigate the role of the IFN-inducible GTPases in the IFNG-mediated control of MNV, we obtained *Irgm1*$^{-/-}$*Irgm3*$^{-/-}$ mice (missing regulatory IRGs, *Irgm1 and Irgm3*; a non-functional IRG system) (Henry et al., 2009) and *Gbp* chromosome 3 deletion

(*Gbp*$^{chr3-/-}$, with the deletion of *Gbp1, -2, -3, -5, -7*; a non-functional GBP system) mice (Yamamoto et al., 2012) (Figures 2.10A and 2.10B). MNV RC formation is inhibited in WT BMDMs pre-activated with IFNG, but not in *Atg5*-deficient BMDMs (Hwang et al., 2012) (Figure 2.8A). Similarly, MNV RC formation was not inhibited by IFNG in BMDMs lacking either a functional IRG or GBP system (Figures 2.8A and 2.10C). These data suggest that both IRGs and GBPs are required for IFNG to inhibit the MNV RC. We further investigated the control of MNV replication by IFNG in BMDMs from *Irgm1*$^{+/+}$*Irgm3*$^{+/+}$ *(WT)*, *Irgm1*$^{+/-}$*Irgm3*$^{+/-}$ *(HET)*, and *Irgm1*$^{-/-}$*Irgm3*$^{-/-}$ *(KO)* mice. In *Irgm1* and *Irgm3* WT and HET BMDMs, MNV replication was completely inhibited upon pre-activation of the cells with IFNG (Figure 2.8B). In KO BMDMs, however, MNV replication was not substantially controlled by IFNG. To confirm the specificity of the phenotype, we restored individual and dual expression of IRGM1 and IRGM3 in the KO BMDMs via lentiviral transduction and could restore the IFNG-mediated control of MNV replication in *Irgm1*$^{-/-}$*Irgm3*$^{-/-}$ BMDMs expressing IRGM3 at a functional level (Figures 2.8C and 2.8D). We further confirmed that MNV replication is controlled normally by IFNG in *Irgm1*$^{-/-}$ BMDMs (Figure 2.10D). In BMDMs with *Gbp*^{chr3} deletion, MNV replication was substantially less inhibited by IFNG pre-treatment, compared to BMDMs with *Gbp*^{chr3} WT and HET (Figure 2.8E). When we restored the expression of GBP1 and GBP2 in *Gbp*$^{chr3-/-}$ BMDMs, only GBP2 was able to restore the IFNG-mediated control of MNV replication back to the level of WT BMDMs (Figures 2.8F and 2.8G). We further confirmed that MNV replication was substantially less inhibited by IFNG in *Gbp2*$^{-/-}$ BMDMs (Figure 2.11D). Although GBP2 did not localize onto the MNV RC in *Irgm1*$^{-/-}$ *Irgm3*$^{-/-}$ BMDMs, IRGA6 localized onto the MNV RC in *Gbp*$^{chr3-/-}$ BMDMs (Figures

2.11A-C). These data corroborate a sequential recruitment model of the IFN-inducible GTPases onto their target membranes, i.e., IRGs prior to GBPs (Haldar et al., 2015), and further suggest a two-stage inhibitory mechanism of the GTPases against the MNV RC: the IRGs alone and in collaboration with the GBP system. Taken together, these data suggest that the IFN-inducible GTPases not only localize on the MNV RC but also play an antiviral role against MNV replication *in vitro*.

We previously showed that MNV infection in mice can be controlled by either type I or type II IFN signaling (Hwang et al., 2012). Although the IFN-inducible GTPases can be induced by both types of IFNs (Degrandi et al., 2007; Sorace et al., 1995), IRGs and GBPs are required for IFNG but not for type I IFNs to inhibit MNV replication *in vitro* (Figure 2.11E). In order to definitively show the crucial role of the LC3 conjugation system (i.e. *Atg5*) in type II IFNG mediated control of MNV infection *in vivo*, the absence of type I IFN signaling is required (Hwang et al., 2012). Therefore, after breeding the *Irgm1*$^{-/-}$*Irgm3*$^{-/-}$ and *Gbp*$^{chr3-/-}$ mice to type I IFN receptor deficient mice (*Ifnar*$^{-/-}$), we examined the survival of MNV infected mice and MNV replication in various organs as previously reported (Hwang et al., 2012). The control mice were significantly susceptible to MNV infection, implying a key role of type I IFN signaling in controlling the *in vivo* infection of MNV (Figures 2.9A and 2.9C). Nevertheless, consistent with the *in vitro* BMDM data, the KO mice of IFN-inducible GTPases (*Ifnar*$^{-/-}$*Irgm1*$^{-/-}$*Irgm3*$^{-/-}$ and *Ifnar*$^{-/-}$ *Gbp*$^{chr3-/-}$) were more susceptible to MNV infection than their littermate control mice (Figures 2.9A and 2.9C); there was also substantially more viral replication in infected organs from KO mice than in organs from control mice (Figures 2.9B and 2.9D). Collectively, these data corroborate the importance of both type I IFN and type II IFN

signaling in controlling MNV infection *in vivo* (Hwang et al., 2012) and further demonstrate that both IRG and GBP systems play crucial roles in the IFNG-mediated control of MNV replication *in vivo* as well as *in vitro*.

The LC3 Conjugation System and IFN-Inducible GTPases Are Required for IFNG to Inhibit MNV Replication in the Human System

The LC3 conjugation system and GBPs are well conserved in both mice and humans. In contrast, the IRG protein family is smaller in humans, with only two proteins, IRGM and IRGC, identified (Bekpen et al., 2009). Previous work has shown that the LC3 conjugation system and the GBPs counteract pathogens in humans, although the functional mechanisms vary considerably (Al-Zeer et al., 2013; Johnston et al., 2016; Ohshima et al., 2014; Selleck et al., 2015). To examine the role of the LC3 conjugation system in controlling norovirus replication in human cells, we obtained HeLa cells with *Atg7* or *Atg16l1* knocked-out by the CRISPR/Cas9 system (Selleck et al., 2015). Consistent with our results in mouse macrophages, both LC3 and GBPs localized on the RC of MNV that resulted from the expression of MNV non-structural proteins (Hwang et al., 2012) (Figure 2.12A); the HeLa cell clones without functional *Atg7* or *Atg16l1* (Figure 2.12B) had substantially decreased localizations of LC3 and GBPs on the RCs (Figure 2.12C). In contrast, we did not detect any sign of IRGM localization on the MNV RC (Figure 2.11F). Using the vRNA transfection system, we further confirmed that the LC3 conjugation system was required for IFNG to inhibit MNV replication in HeLa cells (Figure 2.12D). Comparably, in human HAP1 cells with *Atg16l1*$^{-/-}$ or *Gbp*$^{1\text{-}7\text{-}/\text{-}}$ (complete human GBP knock-out) (Ohshima et al., 2014), MNV replication was

substantially less inhibited by IFNG than in the control cells (Figures 2.12E and 2.12F). Taken together, these data demonstrated that both the LC3 conjugation system and GBP system were required for IFNG to inhibit MNV replication in both humans and mice.

DISCUSSION

Viral RCs provide a shelter for +RNA viruses to efficiently replicate, yet if and how the host immune defense system counteracts these structures have been poorly understood. We previously discovered an antiviral activity of IFNG functioning against the RC of MNV, which requires a nondegradative function of the E3-like ligase ATG12-ATG5-ATG16L1 complex (Hwang et al., 2012). However, its functional mechanism and pertinent effector proteins were unknown (Maloney et al., 2012). Using the *T. gondii* model, we found that the E3-like ligase complex can determine the target membrane of the IRGs and GBPs (Choi et al., 2016; Park et al., 2016). Based on these similar genetic requirements, here we identify the IFN-inducible GTPases, IRGs and GBPs, as the immune effectors functioning against the RC of MNV. Our data demonstrate that the membranous replication compartment of +RNA viruses can be controlled by the same immune mechanism used to target vacuoles containing bacteria, protists, or fungi, suggesting a universal immune defense mechanism against multiple intracellular pathogens that lurk in endomembrane structures.

LC3 localizes on the RCs of many +RNA viruses (Jackson et al., 2005; Panyasrivanit et al., 2009; Prentice et al., 2004; Sir et al., 2012; Zhang et al., 2011). This can result from the viruses hijacking the autophagy machinery or simply using LC3

for their own benefit (Reggiori et al., 2010; Sharma et al., 2014). In fact, it was recently shown that MNV infection induces autophagy, leading to the localization of LC3 on the RC and facilitation of viral replication (O'Donnell et al., 2016). Regardless of LC3's potential proviral roles, LC3 could simultaneously play an antiviral function by recruiting the IFN-inducible GTPases to RCs as shown in this study. While IFNG requires *Atg5* to inhibit MNV replication, it can also act in the absence of *Atg5* to inhibit the replication of other +RNA viruses, such as EMCV, murine hepatitis virus, and West Nile virus (Hwang et al., 2012). This suggests that IFNG has an additional antiviral function independent of *Atg5*, and thus independent of the LC3 conjugation system and the IFN-inducible GTPases, to inhibit the replication of these viruses. Therefore, the crucial antiviral role of the IFN-inducible GTPases against the RC of other +RNA viruses may only be revealed in the absence of this '*Atg5*-independent' antiviral activity of IFNG.

The crucial role of IRGs and GBPs in controlling intracellular pathogens, especially those hiding within vacuole-like structures, are well documented (Pilla-Moffett et al., 2016). In recent years, GBPs have also been recognized for their role in regulating canonical and noncanonical inflammasome activation (Pilla-Moffett et al., 2016). In contrast, an antiviral function of the IRGs and GBPs has been poorly understood. For instance, the resistance of mice to Ebola virus, herpes simplex virus, and murine cytomegalovirus (Collazo et al., 2001; Taylor et al., 2000) was unaffected despite knockout of a regulatory IRG, while human IRGM has even been suggested to play a proviral role for hepatitis C virus, measles virus, and human immune deficiency virus type 1 (HIV-1) (Grégoire et al., 2011). Human GBPs have been reported to play antiviral roles against dengue virus, EMCV, vesicular stomatitis virus, and influenza

virus, but the underlying mechanisms are unknown (Anderson et al., 1999; Nordmann et al., 2012; Pan et al., 2012). Overall, there has been no clear functional mechanism determined for any anti- or proviral activities of IRGs and GBPs, with the exception of the recent report of GBP5 targeting the HIV-1 envelope glycoprotein independent of its GTPase activity (Krapp et al., 2016). Given this, the data shown here presents the definitive antiviral mechanism of both IRGs and GBPs against viral RCs, reflecting their general function against vacuolar pathogens.

IRGs and GBPs are known to oligomerize in a GTP-dependent manner on the membrane of pathogen-containing vacuoles, leading to vesiculation and subsequent disruption of the vacuole structures (Pilla-Moffett et al., 2016). The consequent exposure of the resident pathogens to the host cytoplasm leads to inhibition of the pathogen replication, activation of cytosolic pathogen sensors, and/or subsequent death of the pathogens and/or the host cells (Pilla-Moffett et al., 2016). Similarly, IRGs and GBPs may disrupt the structural integrity of the MNV RC and trigger additional antiviral responses by the host. However, translating the previously proposed membranolytic mechanism of the GTPases to the MNV RC has a major caveat: the size of the MNV RC. The MNV RC is roughly the same size as vesicles (ca. 50-300 nm in diameter) created from the PVM of *T. gondii* (ca. 5 um in length) during the process of IRG and GBP-mediated vacuole disruption (Wobus et al., 2004; Zhao et al., 2008). Thus, the dimensions of the MNV RC may be too small to be vesiculated by the IFN-inducible GTPases. If the IRGs and GBPs behave similarly on the membranes of the MNV RC as they do on the PVM of *T. gondii*, they may deform the structure and subsequently inhibit the function of the MNV RC, for example inhibiting viral genome replication and

transcription, rather than demolishing the structure. It is also possible that the GTPases may even block the formation of the MNV RC as well as disrupt the formed RCs. How the IRGs and GBPs exert their antiviral function against the MNV RC will be a subject of future mechanistic investigation.

It has been proposed that IRG targeting of vacuolar pathogens is limited to a select but disparate group, i.e., the protist *T. gondii*, the bacterium *Chlamydia trachomatis*, and the fungus *Encephalitozoon cuniculi* (Ferreira-da-Silva et al., 2014; Springer et al., 2013; Tiwari et al., 2009). It is suggested that the cytosolic face of these plasma membrane-derived vacuoles containing these target organisms may be distinct from host endomembrane-bound intracellular compartments, because the organisms enter host cells via non-endocytic/phagocytic mechanisms (Ferreira-da-Silva et al., 2014). Since MNV enters cells through a host endocytic process (Perry and Wobus, 2010) and its RC is known to be composed of membranes derived from the ER, Golgi, and endosome (Hyde et al., 2009), our study does not support this hypothesis. Independent of the mechanism of entry, the membrane structures may share common patterns allowing the IRG system to be activated and targeted. The control of MNV by IFNG is dependent on *Atg5*, because the putative *Atg5*-independent antiviral activity of IFNG cannot control MNV (Hwang et al., 2012). Likewise, the control of the disparate group of pathogens by IFNG might be dependent on the IRG system also because this is the only effective immune mechanism against these intracellular parasites. Further work is necessary to determine if there are any common pathogen-associated molecular patterns among this group of pathogens controlled by IRGs and how the IRG system is activated on these vacuole structures (Choi et al., 2016).

In summary, our study demonstrates that the LC3-conjugation system of autophagy has evolved to target the RC of the +RNA virus which in turn recruits the IFN-inducible GTPases for the inhibition of the RC. This provides a unifying working model in which the same effector mechanism is used against diverse intracellular pathogens that replicate inside cytosolic membrane structures. Importantly, this system is conserved in humans with a smaller set of the IFN-inducible GTPases. Further studies will determine how the cell-autonomous immune system utilizes the LC3 conjugation system to detect and destroy the membranous shelters of pathogens.

AUTHOR CONTRIBUTION

Conceptualization, S.B.B., J.C., and S.H.; Methodology, S.B.B., J.C., W.L.B., S.L., B.T.M., and S.H.; Investigation, S.B.B., J.C., R.A.H., H.M.B., W.L.B., S.L., B.T.M., E.D., L.E.W., and S.H.; Resources, R.C.O., C.B.W., M.Y., J.C., and G.A.T.; Writing – Original Draft, S.B.B. and S.H.; Writing – Review & Editing, S.B.B., J.C., G.A.T., S.H.; Visualization, S.B.B., J.C., and S.H.; Supervision, S.H.; Funding Acquisition, S.H.

ACKNOWLEDGMENTS

We thank Drs. Herbert W. Virgin (Washington University School of Medicine in St. Louis), Thirumala-Devi Kanneganti (St. Jude Children's Research Hospital), and Feng Zhang (Broad Institute) for sharing valuable research reagents for this study. This work was supported by startup fund to S.H., and in part by the Brinson Foundation Junior Investigator Grant, Cancer Research Foundation, an Institutional Research Grant (IRG-58-004-53-IRG) from the American Cancer Society, the University of Chicago Digestive Diseases Research Core Center (NIDDK P30DK42086), the University of Chicago Comprehensive Cancer Center Support Grant (P30 CA14599), the Cancer Center Core facilities (DNA sequencing and genotyping, flow cytometry, integrated microscopy, and monoclonal antibody), and the National Center for Advancing Translational Sciences of the National Institutes of Health (UL1 TR000430). S.B.B. was supported (in part) by NIH T32 GM007183 and H.M.B. was supported (in part) by NIH T32 AI007090. B.T.M. was supported by NCI-NIH award F31CA177194-01. G.A.T. was supported by VA grant I01 BX002369. All authors declare no conflict of interest.

CHAPTER III

Viral replication complexes are detected by ATG16L1 via interaction with viral polymerase

Major Experimental Contributors to data presented in this chapter include: Scott B. Biering, Dr. Jayoung Choi, Dr. Kyung Hyun Kim, and Dr. Seungmin Hwang

SUMMARY

Positive-Strand RNA [(+)RNA] viruses replicate in the host cytoplasm associated with a replication complex (RC). RCs are conserved membranous structures constructed by (+)RNA viruses from host orgranelle derived membranes. These membranous structures are believed to mediate efficient viral replication while shielding the virus from host immune sensors. We previously showed that this conserved viral structure served as an antiviral target of interferon gamma (IFNG). The RC is detected and marked with the autophagy protein LC3, independently of degradative autophagy, which enables the targeting of a membranolytic family of interferon (IFN)-inducible genes, known as the IFN-inducible GTPases, which antagonize the structure. This membranolytic pathway also targets and disrupts the membranous replication vacuoles of other intracellular pathogens such as protozoan parasites, bacteria, and fungi. However, it is still unclear how these pathogen associated replication structures are initially detected as “non-self” targets. Here we show that the conserved RNA-dependent RNA polymerase (RdRp) of Murine Norovirus (MNV) is sufficient to recruit the autophagy proteins via a direct

interaction with ATG16L1. We further show that the RdRps from several viruses interact with ATG16L1, suggesting this virus specific protein acts as a conserved “non-self” signal to recruit the autophagy proteins that demarcate the RC as a target for the antiviral pathway of IFNG. However, our data also reveals that RCs formed in the absence of an RdRp are still targeted by the IFN-inducible GTPases. These data suggest that the immune system may possess multiple detection mechanisms in order to demarcate a membrane structure as “non-self”, but once marked by autophagy proteins, follows the same membranolytic pathway.

INTRODUCTION

Positive-Sense RNA [(+)RNA] viruses are the largest virus class encompassing about 1/3 of all known viruses and include many medically relevent human pathogens such as Dengue virus, Zika virus, Poliovirus, SARS-coronavirus, and Norovirus (den Boon and Ahlquist, 2010; den Boon et al., 2010). (+)RNA have a conserved viral lifecycle, replicating in the cytoplasm associated with a virus induced modified host membrane structure known as the replication complex (RC) (den Boon and Ahlquist, 2010). The organelle membrane source and subcellar localization of these virally induced RCs vary by virus, but are believed to play a conserved function in the viral lifecycle.

Viral RCs benefit (+)RNA viruses in a few ways. First, it provides a homebase within which to concentrate viral and cellular components required for viral replication, this allows maximal interaction of the viral replication machinery. Also, the RC is

suggested to be important for viral packaging and egress from the cell, providing a location for capsid proteins and newly synthesized genomes to interact. For situations where the viral RC is implicated in egress, the virus usually builds its RC near an egress point, for example if a virus utilized the secretory pathway for egress, then a virus could build its RC near the endoplasmic reticulum, assemble, and then egress from this location (Novoa et al., 2005; Romero-Brey and Bartenschlager, 2014; Shulla and Randall, 2016). Finally, viral replication complexes are believed to shield the virus from the innate immune response. Specifically, when a (+)RNA virus replicates its genome, it must synthesize an anti-sense negative strand and in doing so a double-stranded RNA (dsRNA) intermediate is produced, serving as a potent activator of innate immune sensors. Viral RCs are believed to sequester viral RNA replication to a sheltered location away from the innate immune response (Biering et al., 2017a; Neufeldt et al., 2016; Shulla and Randall, 2016).

Intriguingly, despite the signifigant evolutionary distance between many (+)RNA viruses, only two sturcutural classes of replication complexes have been observed. These are spheruole invaginations and double-membrane vessicles (DMVs). The conservation of form and function of these viral RCs, despite the evolutionary distance between the diverse (+)RNA class, suggests convergent evolution of these critical viral structures. Since these structures are conserved and essential for the virus, they represent a target for antiviral activity. We recently identidified such a pathway by which IFNG mediates an antiviral pathway against Murine Norovirus (MNV), antagonizing the MNV RC. This antiviral pathway involves a non-degradative targeting mechanism of the LC3-conjugation complex of autophagy. We previously showed that LC3 and its

homologs are targted to the RC of MNV, which demarcates this viral structure as a target for a family of interferon stiumulated genes (ISGs) that are upregulated by IFNG. These ISGs are the membranolytic IFN-inducible GTPases encompassing the immunity related gtpase (IRGs) and guanylate binding protein (GBP) subfamilies, which both belong to the larger dynamin-like GTPases superfamily (Biering et al., 2017a; Biering et al., 2017b; Pilla-Moffett et al., 2016). This antiviral pathway of IFNG, which utilizes the LC3-conjugation complex of autophagy to target the IFN-inducible GTPases to the viral RC of MNV, is also able to target the membranous replication vacuoles of other disparate intracellular pathogens such as protozoan parasites, bacteria, and fungi (Bernstein-Hanley et al., 2006; Choi et al., 2016; Choi et al., 2014; Ferreira-da-Silva et al., 2014; Haldar et al., 2014). We have termed this pathway by which the autophagy proteins demarcate a membranous "non-self" target where the IFN-inducible GTPases are recruited, as Targeting by AutophaGy proteins (TAG) (Choi et al., 2016; Park et al., 2016). Our current working model suggests that the host has evolved TAG as a system to identify and mark "non-self" pathogen containing vacuoles for destruction by the IFN-inducible GTPases. Many questions remain on how this pathway functions and determines its targets.

The membranous replication structures of these disparate pathogens vary structurally, looking immensley different to the host. For example, the parasitophorous vauole (PV) of the protozoan parasite *Toxoplasma gondii* is dervived from the plasma membrane and *T. gondii* removes the majority of the host proteins from this vacuole in order to form its replication niche (Sibley, 2011). In contrast, MNV forms its replication complex in a perinuclear location using membranes derived from the endoplasmic

reticulum (ER), golgi-apparatus, and endosomes; the MNV RC contains cellular host proteins from each of these organelles (Hyde and Mackenzie, 2010; Hyde et al., 2009). Further, the MNV RC has been visualized as a heterogenous structure which most closely ressembles the DMV RC class (Romero-Brey and Bartenschlager, 2014). This comparison demonstrates that the RC of MNV and the PV of *T. gondii* are structurally different, originating from a different membrane source, possessing a distinct set of pathogen proteins, and being either rich or poor in host proteins, thus how TAG is able to identify both of these structures as targets for the autophagy proteins is unclear. The TAG pathway either functions through recognition of one redundant “non-self” pattern, which is possessed by each of these disparate membranous structures, or it can potentially use distinct upstream pathways that recognize a unique marker on these disparate replication structures, to target the autophagy proteins; but once marked as a “non-self” membranous target by LC3, the same downstream targeting of the membranoyltic IFN-inducible GTPases is initiated to destroy the structure. Though these two possibilities are not mutually exclusive, due to the immense differences in the known TAG targets, we favor a model by which distinct pathogen specific upstream signals serve to recruit the autophagy proteins to different targets of TAG.

In this study we decided to first determine the extent to which RCs of other (+)RNA viruses are targets for TAG as well as determine how TAG determines the RC of MNV as a target. Here we show that the non-structural protein 7 (NS7) of MNV, a virus specific protein also know as the viral RNA-dependent RNA polymerase (RdRp), interacts with the autophagy protein ATG16L1. In addition, the NS7-RdRp is sufficient to recruit the autophagy proteins to a given sub-cellular location. Further, we show an

interaction between Atg16L1 and the RdRps of several other viruses, which suggests this interaction may be one conserved pathway by which TAG recognizes a broad range of viral RCs as targets. Finally, while NS7 appears sufficient to recruit Atg16L1 to a given site, the RC is still targeted by TAG even when NS7 is absent, which suggests multiple and potentially redundant mechanisms by which the host identifies viral RCs as targets for TAG.

RESULTS

Not all Viral Replication Complexes are Targeted by the IFN-inducible GTPases

We previously established that the replication complex (RC) of Murine Norovirus (MNV), a (+)RNA virus from the *Caliciviridae* family, was antagonized by IFNG via targeting of membranolytic IFN-inducible GTPases to LC3-marked RCs (Biering et al., 2017b). We further established that the RC of encephalomyocarditis virus (EMCV), a (+)RNA virus from the *Picronaviridae* family, was also targeted by LC3 and the IFN-inducible GTPase, IRGA6. This established that IFNG mediated RC targeting was not specific to MNV and instead a general antiviral strategy. Though we showed the targeting of the EMCV RC by LC3 and IRGA6 in WT cells, we did not show that this targeting was dependent on the functional LC3-conjugation system. To test this possibility, we utilized bone marrow derived macrophages (BMDMs) from mice with a macrophage specific deletion of Atg5, an essential component of LC3-conjugation (*Atg5*$^{f/f}$+*LysMcre*) (Biering et al., 2017b; Hwang et al., 2012; Zhao et al., 2008). *Atg5*$^{f/f}$+*LysMcre* BMDMs or control *Atg5*$^{f/f}$ BMDMs were treated with IFNG, infected with

EMCV, then analyzed by immunofluorescnet microscopy (IFA) for colocalization of LC3 and the representative IFN-inducible GTPase, IRGA6. We observed that *Atg5*$^{f/f}$*+LysMcre* BMDMs were severely defective in their ability to target LC3 and IRGA6 to the RC of EMCV when compared to the control BMDMs, suggesting that the EMCV RC is indeed a bonafide target of TAG, dependent on demarcation of the structure by LC3, similair to MNV (Figure 3.1A and 3.1B).

In an attempt to extend this observation further, we tested other (+)RNA viruses to determine if their RCs were also targets for the IFN-inducible GTPases. We first utilized Zika virus (ZIKV), a human pathogen which poses a serious public health threat and a member of the *Flaviviridae* family. IFA did not reveal significant localization of either LC3 or the GBPs to the ZIKV RC, suggesting that in our specific condition, the ZIKV RC is not a target for the IFN-inducible GTPases (Figure 3.2A). In addition, we also tested Murine Hepatitis Virus (MHV), a (+)RNA virus and member of the *Coronaviridae* family, and determined that similair to ZIKV, the MHV RC was not a major target for the Interferon-inducible GTPases (Figure 3.2B). These data suggest that while some viral RCs are sentivie to TAG, others are not. Three possibilities exist which could explain these observations. First, differences in RC composition and structure may innately render some RCs sensitive to TAG while others are resistent. Second, as suggested by a constant molecular arms race, some viruses may have evolved strategies to evade and/ or antagonize the TAG pathway. Finally, our observation could also be explained by us simply having looked for the wrong immune effectors at the wrong time. Further investigation is required to understand why some RCs but not others are targets for the Interferon-inducible GTPases via TAG.

The Replication Compartments of Murine Norovirus and *Toxoplasma Gondii* are Detected through Distinct Pathways

Having determined that the RC of MNV is sensitive to TAG, we wanted to determine how the host is able identify the MNV RC as a target. To answer this question we first needed to know if the RC of MNV and the PV of *T. gondii* are recognized through common or distinct pathways. Knowing that signaling pathways can vary greatly in immortalized laboratory cell lines, we tested the ability of IFNG to control both MNV and *T. gondii* in different cell types. We found that the cell line J774A.1 was sensitive to infection by both of these pathogens and could control MNV replication upon IFNG treatment, but suprisingly, IFNG could not control *T. gondii* replication in this cell line (Figure 3.3A and 3.3B). Further, even though degradative autophagy and expression of the IFN-inducible GTPases were unnaffected in J774A.1 cells as determined by transcript analysis and protein expression, the IFN-inducible GTPases could not target to the PV of *T. gondii* (Figure 3.3C-D). Because we have previously determined that TAG against both the PV of *T. gondii* and the RC of MNV have similiair downstream functional requirements for the LC3-conjugation system to mark the structure in order to recruit the IFN-inducible GTPases, we can conclude that this difference in RC vs. PV targeting is most likely due to an upstream recognition step. Thus, these data suggest that in J774A.1 cells, the pathway by which the PV of *T. gondii* is intially detected is either absent or dysfunctional while the mechanism by which the MNV RC is detected remains intact. This observation provides evidence for the

hypothesis that the RC of MNV and the PV of *T. gondii* are detected as “non-self” via distinct upstream pathways.

ATG16L1 Detects the Replication Complex of Murine Norovirus through an Interaction with the Viral RNA-dependent RNA Polymerase

Our data suggests that TAG determines its target through distinct upstream pathways. Thus, we decided to determine the mechanism by which TAG recognizes the MNV RC as a target for the autophagy proteins. The immune systen functions through mechanisms that differentiate “self” from “non-self”. Three well accepted strategies that are utilized by our host immune system include the recognition of “missing-self”, “altered-self”, or “non-self” (Coers, 2013). In the case of the MNV RC, TAG could be utilizing any or all of these strategies to identify and localize the autophagy proteins to this membranous structure. For “missing-self”, MNV could potentially remove a host protein needed to inhibit indirect or direct recruitment of the autophagy proteins. For “altered-self”, the membrane curvature and rearrangements associated with RC formation may present structures and compounds in a context that is foreign to the host, and this may be a signal that is sufficient to indirectly or directly recruit the autophagy proteins. Lastly, in the case of “non-self” for MNV, viral proteins that are foreign to the host could localize to the RC membrane, which can serve to directly recruit the autophagy proteins or recruit upstream factors that then recruit the autophagy proteins. Again, these possibilities are not mutually exclusive and this essential RC detection pathway may utilize overlapping and redundant pathways to target the autophagy proteins to the MNV RC.

Because the MNV genome only encodes for 9 proteins which can be readily cloned and expressed in trans for biochemical analysis, we decided to first test the "non-self" hypothesis (Thorne and Goodfellow, 2014). To test the possibility that an MNV protein, present at the RC, interacts with a component of the LC3-conjugation system, we conducted a non-biased pulldown screen of each MNV protein individually, and tested their ability to coimmunoprecipitate (COIP) with autophagy proteins or the IFN-inducible GTPases. Our results identified two interactions. The first was between non-structural protein 5 (NS5) of MNV and both classes of the IFN-inducible GTPases (the IRGs and GBPs). The second interaction was between the non-structural protein 7 (NS7) of MNV and the essential component of the LC3 conjugation system, ATG16L1 (Figure 3.4). MNV-NS5 is also known as VPg, a viral protein which is covalently linked to the 5' end of the MNV genome and essential for translation and replication of the viral genome (Thorne and Goodfellow, 2014). NS5 is an essential mediator in both MNV genome replication and translation because it recruits cellular translation factors and the RdRp to the MNV genome through direct protein-protein interactions. This broad reactivity associated with NS5 has led this protein to be considered "sticky" which could potentially result in many non-specific or indirect interactions in pulldown assays (Thorne and Goodfellow, 2014). This means that our data revealing the pulldown of the IFN-inducible GTPases by MNV-NS5 may be a real interaction or it may be a result of non-specific and sticky interactions that do not play biologically relevent roles in TAG against the MNV RC. Due to this possibility we decided not to immediately follow up on this potential interaction and instead to focus on the putative interaction between NS7 and ATG16L1. NS7 serves as the RdRp for MNV. All (+)RNA viruses have RdRps that

are present at their RCs which directly mediate replication of the viral genome. RdRps are one of the most conserved (+)RNA viral proteins because of their essential role in the viral lifecycle (Koonin and Dolja, 1993; te Velthuis, 2014). For this reason, we considered the RdRp of MNV to be a strong “non-self” candidate that can potentially recruit the autophagy proteins that demarcate this structure for destruction by the membranolytic Interferon-inducible GTPases. Further, the conserved nature of this viral protein amonsgt all (+)RNA viruses suggests a possible pan-antiviral mechanism by which all RCs containing an RdRp can be targeted by the autopagy proteins and IFN-inducible GTPases.

We next validated the putative interaction between NS7 and ATG16L1 suggested by COIP. We utilized bimolecular fluorescence complementation (BiFC) to further test this interaction (Kodama and Hu, 2012). The BiFC system confirmed the putative interaction between ATG16L1 and NS7; also, using the well characterized interaction between ATG16L1 and Atg5 or an Atg5 mutant (Atg5-DM) which no longer interacts with ATG16L1 despite normal levels of protein expression, we could show that our system was functioning properly (Choi et al., 2014; Hwang et al., 2012) (Figure 3.5A and B). We were able to further validate this interaction by utilizing a yeast-two-hybrid assay which suggested the interaction between NS7 and ATG16L1 was weak, but specific compared to the vector controls (Bajaj Pahuja et al., 2015) (Figure 3.6). We further validated this putative interaction by using a glutathione S-transferase (GST) fusion pulldown assay which also suggested a direct interaction between ATG16L1 and NS7 and involved amino acids 79-249 of ATG16L1, this region is known as the coiled-coil domain (Fujita et al., 2013) (Figure 3.7).

Having demonstrated a direct protein-protein interaction between ATG16L1 and MNV-NS7, we wanted to investigate the biological relevence of this interaction in the recruitment of the autophagy proteins and the IFN-inducible GTPases to the MNV RC. To do this, we first asked if an MNV RC that was devoid of MNV-NS7 could be targeted by autophagy proteins or the IFN-inducible GTPases. If the NS7-RdRp of MNV is the only “non-self” signal that the host uses to target the MNV RC, then we would expect no targeting of an MNV RC that is devoid of the NS7-RdRp. We utilized a reverse genetics plasmid containing a clone of the MNV-ORF1, driven by a CMV promoter, which is sufficient to induce an RC-like structure (Biering et al., 2017b; Hwang et al., 2014; Hwang et al., 2012). The caveat to this experiment is the fact that these ORF1 induced structures are not bonafide MNV RCs because they are devoid of dsRNA, however, host proteins and viral proteins all localize to these structures like they do in conditions of WT MNV infection (Biering et al., 2017b; Cotton et al., 2017; Hyde and Mackenzie, 2010). We first asked if this reverse genetics clone could form RCs, visible by IFA, without NS7. When we transfected cells with the WT ORF1 or delta-NS7 (dNS7) ORF1 constructs, we could detect visible RCs produced from both constructs (Figure 3.8a). It should be noted that there were signifigantly fewer RCs detected from the dNS7 construct, and moreover, the signal from dNS7 was heterogeneous in that staining did not always reveal defined RC puncta, but sometimes resulted in cytoplasmic dispersal of viral proteins. Despite these differences we could still quantify IFN-inducible GTPases localization by only counting cells which had fully formed RCs that appeared comparable to the WT control. When cells were transfected with these constructs and treated with IFNG, we found no difference in targeting of the IFN-inducible GTPases to

RCs formed from WT ORF1 compared to RCs formed from dNS7 ORF1, suggesting that NS7 is not essential for RC targeting (Figure 3.8b). This data could be interpreted in two ways. First, it is possible that the interaction between NS7 and ATG16L1 is one of many mechanisms in which the MNV RC is recognized as a “non-self” target for the autophagy proteins and the IFN-inducible GTPases, and simply removing the NS7 “non-self” signal is not sufficient to prevent targeting of the RC. The second possibility is that the interaction between NS7 and ATG16L1 is simply an artififact that does not have any biological signifigance in TAG against the MNV RC.

To test these possibilities, we wanted to determine if MNV-NS7 was sufficient to recruit the autophagy proteins to a target membrane. This would suggest that the NS7 “non-self” signal is but one of multiple pathways the host uses to detect the MNV RC. To test sufficiency, we utilized the anchor away system which relocalizes a bait protein to the mitochondrial outer membrane, then it can be assessed, by IFA, which proteins also relocalize to the mitochondrial outer membrane, demonstrating sufficiency to relocate the target proteins (Park et al., 2016). We used NS7 as our bait protein and relocalized it to the mitochondrial outer membrane; interstingly enough we found this was sufficient to also relocalize ATG16L1, which is not normally localized to the mitochondrial outer membrane under basil conditions (Figure 3.9A and B). This data provide evidence that this interaction between NS7 and ATG16L1 may have biological signifigance in that it can define a membrane target for the LC3-conjugation system. This implies that NS7 at the replication complex may also be sufficient for recruitment of the LC3-conjugation complex and thus the IFN-inducible GTPases. These data support the hypotheis that NS7 acts as a “non-self” signal which identifies the RC of MNV as a

target for TAG. However, our data also suggests that even when NS7 is absent, the MNV RC is still targted, which implies the host may utilize multiple mechansisms to detect this structure, and an interaction between NS7 and ATG16L1 is only one mechanism.

The RNA-dependent RNA Polymerases of Multiple (+)RNA Viruses Interact with ATG16L1

We hypothesized that due to the high level of conservation between the RdRps of all (+)RNA viruses, that this viral protein may serve as a conserved universal “non-self” marker the host utilizes to target the RCs of many different viruses via a conserved interaction between ATG16L1. To test this hypothesis we asked if the RdRps of other viruses also interacted with ATG16L1. We utilized the RdRps of two strains of human norovirus from genogroup I-South Hampton and II.4-Sydney, as well as the RdRp from EMCV (3D-pol) from the EC9 strain. Utilizing BiFC as before, we determined that all three of these RdRps were able to interact with ATG16L1 (Figure 3.10). This observation supports our hypothesis, suggesting that the interaction between the MNV-NS7 RdRp and ATG16L1 may be utilizing a conserved motif that is present in the RdRps of all (+)RNA viruses, such as human norovirus and EMCV. To extend this idea further, it will be necessary to map this interaction domain, as well as test many more RdRps from even more distantly related (+)RNA viruses.

A Region in the C-terminus of the Coiled-Coil Domain of ATG16L1 is Required for the Interferon Gamma Mediated Control of MNV Replication

Our previous work shows that ATG16L1 can be visualized at the RC of MNV even when the LC3-conjugation system has been rendered dyfunctional through Atg5 deletion (Hwang et al., 2012). This suggests that ATG16L1 is the first autophagy protein to be recruited to the MNV RC and is thus responsible for the recruitment of the LC3-conjugation system. So we reason, for at least one potential mechanism of MNV RC TAG, that ATG16L1 determines a TAG target. This is supported by evidence that ATG16L1 desiginates the site for autophagosome elongation (Fujita et al., 2008). So for TAG against the MNV RC, we reasoned that if we can determine which residues of ATG16L1 are required for the IFNG mediated control of MNV, we can potentially identify one or multiple pathways by which it is recruited, such as recruitment by NS7. To better understand the mechanism by which ATG16L1 is recruited the MNV RC we sought to define the minimal region required for ATG16L1 to reconstitute IFNG mediated control of MNV in ATG16L1 KO BMDMs (*Atg16L1f/f + LysMcre*). ATG16L1 can be divided into three distinct domains including the N-terminal Atg5-binding region, the coiled-coil domain, and the C-terminal WD-40 repeat domain (Figure 3.11A). Our previous studies on TAG against the PV of *T. gondii* reveal that IFNG mediated control requires both the Atg5-binding region as well as the coiled-coil domain of ATG16L1 (Park et al., 2016). When we reconstituted ATG16L1 KO BMDMs with the different functional domains of ATG16L1, our data confirms that both the Atg5-binding region and the coiled-coil domains of ATG16L1 are required for the IFNG mediated control of MNV (Figure 3.11B-C). We know that the Atg5-binding domain of ATG16L1 is required in order to recruit the LC3-conjugation complex, demcarcating the RC as a target for TAG through LC3 localization followed by recruitment of the membranolytic IFN-inducible GTPases.

However, we do not understand why the coiled-coil region region is required for the IFNG mediated control of MNV. We speculate that an interaction between the ATG16L1 coiled-coil domain and NS7 is sufficient to recruit ATG16L1 to the MNV RC. The ATG16L1 coiled-coil region is known to mediate interactions that recruit ATG16L1 to the autophagosome or recruit cargo to be degraded in an autophagosome through binding to ubiquitin (Dooley et al., 2014; Fujita et al., 2008; Fujita et al., 2013; Nishimura et al., 2013). Because of this, we hypothesized that this coiled-coil region of ATG16L1 may also be mediating recruitment of ATG16L1 to the MNV RC. To define the region of the ATG16L1 coiled-coil domain (amino acids 80-249) required, we created truncation mutants of this region, based off of previously mapped domains (Figure 3.12A). When we reconstitued ATG16L1 KO BMDMs with these truncation mutants we determined that a region at the C-terminus of the ATG16L1 coiled-coil domain (amino acids 230-249) was essential for the IFNG mediated control of MNV (Figure 3.12B-C). This suggests that a protein-protein interaction between this region of the ATG16L1 coiled-coil fomain and NS7, or a yet unkown factor, may mediate the initial recruitment of ATG16L1 to the MNV RC, providing a mechanism of how the host recognizes the MNV RC as “non-self” and a target for TAG.

GTP Hydrolysis as well as Membrane Binding are Essential for GBP2 to Target to the Murine Norovirus Replication Complex

Having elucidated a potential pathway by which the MNV RC is detected by the host, we asked how the IFN-inducible GTPases mediated their antiviral activity against the MNV RC? For *T. gondii*, it is believed that these IFN-inducible GTPases possess

membranolytic properties which allow them to directly vesiculate and disrupt their target membrane (Pilla-Moffett et al., 2016). However, it is unclear if this is the same mechanism that is utlized to antagonize the MNV RC. We previously determined that murine GBP2 is the major GBP homolog that targets to the MNV RC, and in fact, removal of this IFN-inducible GTPases alone results in diminished IFNG mediated inhibition of MNV replication (Biering et al., 2017b). Because of this we decided to investigate the functional domains within murine GBP2 which determine targeting to the MNV RC. Murine GBP2 possess a G-domain at its N-terminus which mediates GTP binding and hydrolysis, followed by a middle helical region, then an effector domain, and finally a C-terminal CAAX domain which is important for direct membrane binding. It was previously determined, using mutants of murine GBP2, that GBP2 which was defective for nucleotide binding (D182N), GTP hydrolysis (K51A and E99A), as well as membrane binding (C586S) were less able to target to the PVM of *T. gondii* when compared to WT GBP2 (Kravets et al., 2012). We decided to test these same mutants for their ability to target to the MNV RC. When we reconstituted BMDMs from WT or GBP chromosome 3 knock out mice (lacking GBPs 1, 2, 3, 5, and 7), we determined that in the absense of other GBPs only WT GBP2 could target to the MNV RC. In WT BMDMs, we found that WT GBP2 as well as the E99A mutant could target to the MNV RC (Figure 3.13A-B). The GBP2-E99A mutant, which binds GTP but cannot hydrolyze it, is most likely recruited to the MNV RC via endogenous GBP2 that is targeted to the MNV RC, this is because GBPs can be recruited onto membranes through self-oligomerization in their GTP bound state (Pilla-Moffett et al., 2016). These data suggest that each of these domains are essential for MNV RC targeting, suggesting a similair

anti-microbial function of the GBPs against the MNV RC as well as the PV of *T. gondii*. Whether GBP2 functions in a membranolytic fashion against the MNV RC, as it is believed to do against *T. gondii*, is still unknown and will require further investigation.

DISCUSSION

We previously determined that the RCs of (+)RNA viruses can be targeted by a cell-autonomous detection pathway and antagonized by TAG, utilizing the autophagy proteins and IFN-inducible GTPases. The MNV RC is marked as “non-self” through localization of the autophagy protein LC3 and homologs, which in turn recruits the membranolytic IFN-inducible GTPases, which are essential for inhibiting the MNV RC (Biering et al., 2017a; Biering et al., 2017b). This antiviral pathway is also able to target the membranous replication vacuoles of other disparate pathogens, including protozoan parasites, bacteria, and fungi. We termed this evolutionary conserved pathway Targeting by AutophaGy proteins (TAG); an antimicrobial defense mechanism capable of antagonizing membranous pathogen containing replication vacuoles using the LC3-conjugation system of autophagy to designate the target membrane and recruit the membranolytic IFN-inducible GTPases to antagonize the structure (Choi et al., 2016; Park et al., 2016). Here we investigated how the host is able to identify these “non-self” pathogen containing membranous structures as targets for TAG. We hypothesized that due to the large structural differences between the replication vacuoles of these disparate pathogens, that the host may have evolved distinct upstream pathways to recruit the autophagy proteins to these replication structures. However, once the

membranous replication structures have been targeted by the autophagy proteins, the same recruitment and disruption by the IFN-inducible GTPases occurs.

We inititally made an observation which supported the notion that TAG may possess multiple upstream targeting pathways. Simply, we noticed a differential ability of IFNG to control MNV and *T. gondii* in the J774A.1 immortalized macrophage type cell line. When activated by IFNG, J774A.1 cells were able to control MNV infection but not *T. gondii* infection, which correlated with targeting of the IFN-inducible GTPases to the RC and PV, respectively. These data suggest that TAG identifies the RC of MNV and the PV of *T. gondii* in distinct manners, and that in this cell line the mechanism by which the PV of *T. gondii* is detected is not functioning properly while the MNV RC detection mechanism is intact. The potentail mechanism of *T. gondii* PV detection in J774A.1 cells is currently unknown, and an area of active investigation. However, a known defect of J774A.1 cells is cholesterol synthesis, making cholesterol and the cholesterol synthesis pathway potential candidates for further investigation in upstream detection of the *T. gondii* PV (Rodríguez-Acebes et al., 2009).

We decided to fous our efforts on identifying a mechanism by which the host identifies the MNV RC as “non-self” and reasoned that the host would utilize at least one of three strategies to do this. First, the construction of the MNV RC could remove key host proteins able to innactivate the TAG system, this fits the “missing-self” model which is exemplified by natural killer (NK) cells targeting host cells missing the major histocampatiblilty complex I (MHC-I) (Borrego, 2006; Coers, 2013). Potential candidates include the the IFN-inducible GTPase regulator proteins Irgm1 and Irgm3 which serve as guanine-dissociation inhibitors (GDIs) that keep the IRG effector proteins from

targeting “self-membranes”. However, the presence of Irgm1 and Irgm3 at the MNV RC has not yet been investigated, and is currently an area of active investigation. A second model is one of “altered-self” by which the foreign membrane curvature or host proteins recruited in a non-native context leads to the recognition of the MNV RC (Coers, 2013). Lastly, it is possible that MNV proteins, which are non-native to the host, could act as a “non-self” pathogen-associated molecular patterns (PAMPs) to mediate direct or indirect recruitment of the autophagy proteins (Coers, 2013). Our study identifies a direct protein-protein interaction between ATG16L1 and the MNV RdRp (NS7). Further, this interaction is sufficient to designate the target membrane of ATG16L1, suggesting that this interaction between ATG16L1 and NS7 can function as one pathway of MNV RC detection. However, our data also suggests that this may not be the only mechanism of RC detection, because even MNV RCs formed which are devoid of NS7 are targeted by the autophagy proteins and IFN-inducible GTPases, suggesting multiple pathways with redundant purpose.

A major appeal to the model by which the MNV RC is detected through the RdRp NS7 protein, is the highly conserved nature of this viral protein amongst all (+)RNA viruses, which suggests that this antiviral pathway may be able to detect and antagonize the RCs of many (+)RNA viruses through a conserved RdRp and ATG16L1 interaction. We extend our findings and support this model by showing an interaction between the RdRps of two strains of human norovirus and EMCV, suggesting that a conserved region of the RdRp may be important for this interaction. Another reason why the RdRp “non-self” PAMP model fits nicely, is due to prevoius studies which have demonstrated that the RdRps of (+)RNA viruses can act as PAMPs to induce activation

of RIG-I-like receptors (RLRs) and the inflamasome, providing a precedent of the immunogenic nature of the RdRps of (+)RNA viruses (Nikonov et al., 2013; Wang et al., 2017, 2018). Thus our data supports an attractive model which suggest that the autophagy protein ATG16L1 may act as direct immune sensors against (+)RNA viruses. Invading (+)RNA viruses must produce an RdRp to replicate and in doing so opens itself up to immune detection through binding to inflammasome components, RLRs, or even autophay proteins which initate TAG. Further, many viruses may have no choice but to recruit the autophagy proteins to their RC, as it has been reported that many viruses require the autophagy machinery for optimal replication (Choi et al., 2018; Jackson et al., 2005; Jordan and Randall, 2012). The autophagy proteins may then serve as something of a “double-egded sword” by which they are required for optimal viral replication but can also recruit the IFN-inducible GTPases which destroy the RC.

The outlook for viruses in this situation may seem bleak, but many examples have shown that (+)RNA viruses are able to evolve mechanisms to evade or antagonize antiviral pathways which target critical stages of their lifecycle (García-Sastre, 2017). Why should TAG against viral RCs be any different? Indeed, while we could show that TAG targets the RCs of MNV and EMCV, under the conditions we tested it does not target to the RCs of ZIKV or MHV. It is possible that ZIKV and MHV have evolved mechanisms to antagonize TAG. A precedent for TAG evasion exists, as virulent strains of *T. gondii* produce effector proteins which selectively innactivate the IRG proteins and certain strains of *C. trachomatis* can also evade TAG (Fentress et al., 2010; Haldar et al., 2016). Further, when comparing the TAG sensitive viruses to the TAG resistant viruses we have studied, the sensitive viruses have a smaller coding

capacity with less known immune evasion mechanisms while the *Flaviviridae* and *Coronaviridae* both have relatively larger coding capacity with more well characterized immune evasion strategies, suggesting that these viruses have likely evolved a way to antagonize TAG (Asif et al., 2017; Deng et al., 2017; Ye et al., 2013). Further study is needed to determine why the RCs of ZIKV and MHV are not targeted by TAG, is it indeed a direct evasion mechanism or is it simply due to differences in RC morphology and proteins? We consider this question to be of paramount importance in understanding the nature of antiviral TAG.

Another major question our model does not address has to do with the kinetics of TAG, namely, when during the viral lifecycle does the interaction between ATG16L1 and NS7 occur? The possibilities are that NS7 interacts with ATG16L1 in the cytoplasm, even before the RC has formed, and thus brings the autophagy proteins to the forming/ newly formed MNV RC as itself is recruited. Another possibility is that ATG16L1 may require some sort of lipid conext to bind to NS7, and thus would be recruited to the fully formed MNV RC where NS7 is associated with the MNV genome and membrane. These possibilites are not mutually exclusive and raise questions about the cytoplasmic permeability of the MNV RC. To test this, one could ask if ATG16L1 can target to viral RCs that are fully formed using live-cell imaging of fluorescently tagged autophagy proteins and viral proteins/ molecuoles. This would better our understanding of the nature of antiviral TAG, namely, does it simply prevent the formation of new RCs by antagonizing the process before it is completed or does it target and disrupt fully formed RC structures. Again, these possibilities are not mutually exclusive and are important

questions to which answers could lead to potential theraputic utility of the IFN-inducible GTPases.

Finally, we have mapped the region responsible for the IFNG mediated antiviral activity against MNV to the Atg5-binding domain and coiled-coil regions of ATG16L1. Atg5-binding is essential for recruitment of the LC3-conjugation system, but the purpose of the coiled-coil domain is not clear. We speculate that this region mediates an interaction with a component of the MNV RC, potentially NS7, which determines specificity of TAG. In fact, the ATG16L1 coiled-coil domain designates the site of LC3 lipidation during degradative autophagy, through interactions with autophagy proteins such as FIP200, WIPI2b, and ubiquitin, mediating degradative autophagy (Dooley et al., 2014; Fujita et al., 2008; Fujita et al., 2013; Nishimura et al., 2013). We determined that amino acids 230-249 of the coiled-coil domain of ATG16L1 are essential for the IFNG mediated control of MNV. Thus we speculate that this 19 amino acid region may be mediating the interaction with NS7, as well as still unknown factors, at the MNV RC to recruit the autophagy proteins and initiate TAG against the MNV RC. Studies on this region are ongoing, with the primary objective to determine if this 19 amino acid region mediates the interaction between ATG16L1 and NS7.

Chapter IV

Conclusions

This work describes an antiviral mechanism, mediated by interferon gamma (IFNG), targeting the replication complexes (RCs) of (+)RNA viruses. This antiviral pathway was known to require the ATG12-ATG5-ATG16L1 complex of autophagy, but not degradative autophagy. The autophagy proteins were not believed to play a direct antiviral role themselves, because they localized to the murine norovirus (MNV) RC independently of IFNG treatment, thus the role of the autophagy proteins in this antiviral pathway were unknown. Beyond this, it was believed that these autophagy proteins worked in concert with one or many interferon stiumlated genes to mediate this antiviral activty, but the identity of these immune effectors were unknown. To understand how this antiviral immune pathway functioned to antagonize the RC of (+) RNA viruses, I proposed to address three specific aims. First, to identify the repertoire and define the role of the autophagy proteins in the IFNG mediated antiviral activity against the replication complex of Murine Norovirus, which is discussed in chapter II. Next, to identify the interferon stimulated gene(s) required for this IFNG mediated antiviral activity against the RC of MNV, which is discussed in chapter II. Finally, to determine the mechanism by which the host identifies the RC of MNV as a target for this IFNG mediated antiviral activity, which is discussed in chapter III.

Other than the ATG12-ATG5-ATG16L1 complex of autophagy and proteins important for its formation, we were not sure what other autophagy proteins were needed and what their function was in this antiviral pathway. Here we were able to

determine that all components of the LC3-conjugation system of autophagy were required for this IFNG mediated antiviral activity against MNV. We showed that ATG3 (an E2-like enzyme for LC3) as well as the LC3 homologs were essential for this antiviral activity (Biering et al., 2017b). This is in contrast to our previous conclusions that LC3 was not involved due to the observation that IFNG was able to control MNV replication in LC3B KO cells, suggesting that the ATG12-ATG5-ATG16L1 complex but not the entire LC3-conjugation was required for this antiviral activity (Hwang et al., 2012). Our current data suggests this difference is because all LC3 homologs, which include both the LC3 and GABARAP families, are required for this antiviral activity, and removal of one homlog is not sufficient to see a phenotype. Further, another study investigating the role of the LC3-conjugation system in the IFNG mediated control of *T. gondii*, suggests that only the GABARAP proteins, specifically GABARAPL2, contributes to this antimicrobial pathway (Sasai et al., 2017). This is in contrast to our findings which suggest redundant roles of all homologs (Biering et al., 2017b). These discrepencies can be explained by the difference in pathogen (MNV vs. *T. gondii*), difference in strategy utilized to delete LC3 homologs, or other variations in experimental condition. Regardless, from our data we hypothesize that LC3 and homolgs mark the target membrane and recruit the IFN-inducible GTPases to this membrane. To fully elucidate the role of the LC3-homologs in this antiviral activity, we will need to test the sufficiency of the LC3 homologs to designate the target membrane for the IFN-inducible GTPases. Utilizing the anchor away system to test this is currently under investigation (Park et al., 2016).

In addition to defining the cassette and role of the autophagy proteins in this RC targeting antiviral activity, work presented in this dissertation also identified a family of IFN-inducible immune effectors which targeted to the RC and were essential for the IFNG mediated antiviral activity. These immune effectors include the IFN-inducible GTPase subfamilies IRGs and GBPs (Biering et al., 2017b). Uncovering the players of this antiviral pathway being the LC3-conjugation system and the IFN-inducible GTPases has allowed us to conclude that TAG is able to target viral RCs. Thus a membranous structure and pathogen class is added to the list of IFN-inducible GTPase sensitive strcutures which unifies the IFN-inducible GTPase field. The targets of these membranolytic immune effectors has been steadily growing, having been shown to target replication vacuoles of multiple protozoan parasites, bacteria, and even fungi (Pilla-Moffett et al., 2016). These pathogens all build their replication vacuole from the plasma membrane. With the addition of viral replication complexes to the list of targets for TAG, we can conclude that the membrane source of the structure is not important for targeting, as the MNV RC is not constructed from membranes from the plasma membrane but instead from the ER, golgi apparatus, and endosomes. Further, the TAG sensitive membrane can also be rich in host proteins like the MNV RC but in contrast to the replication vacuoles of the other pathogens which are appreciated to remove a large number of host proteins from the membrane to avoid lysosomal fusion (Coers, 2013; Pilla-Moffett et al., 2016). Because the MNV RC breaks away from these previously established patterns, the IFN-inducbile GTPase field can now speculate that these immune effectors have evolved to target diverse pathogen containing “non-self” membranous structures, and not only a special select class of pathogen. This may shift

the thinking of the field to ask quesitons such as “Why are some pathogens not targeted by TAG?”. How the TAG system acheieves specificity remains a pressing question for the field to address.

We attempt to answer such a question in chapter III of this work by asking how the viral RC of MNV is determined as a target for TAG? Since TAG targets the membranous replication vacuoles of a number of disparate pathogens, we wondered if TAG utilized the same or distinct upstream pathways for target identifiation. Both are valid possibilities but we favored a model by which distinct upstream detection pathways operate to recruit the autophagy proteins to the membranous replication structure, but then converge on a similair mechanism by which the LC3 marked structure recruits the IFN-inducible GTPases, mediating membrane disruption. Similarities can be seen between this TAG model and observations which demonstrate that viruses can be detected by the host through distinct upstream sensors and pathways (e.g. STING, RIG-I, and MDA5) but ultimately trigger a similair antiviral pathway involving interferons and proinflammatory cytokines (Jensen and Thomsen, 2012; Loo et al., 2008; Radoshevich and Dussurget, 2016). In support of this hypothesis we find that the J774A.1 cell line, which is deficient in cholesterol synthesis, can mediate TAG against MNV but not against *T. gondii*. This suggests that the host possess distinct pathways to detect these different structures and simply the pathway for MNV RC detection is intact while the pathway to detect the PV of *T. gondii* is dysfuncitonal. The caveat to this observation is the fact that J774A.1 cells are immortalized and thus may have many confounding mutations compared to primary cells, making observations from these cells biologically suspect. Further, we do not currently understand the mechanism at play

which blocks the detection of the PV of *T. gondii* in J774A.1 cells. These cells have a known defect in their ability to produce cholesterol because they are missing a functional *Dhcr24* gene, a terminal enzyme in cholesterol biosynthesis (Rodríguez-Acebes et al., 2009). Because of this we speculate that either cholesterol enriched at the PV of *T. gondii,* or a non-canonical function of the *Dhcr24* gene product, may serve as a "non-self" signal mediating the recognition of the PV as a target for TAG. This implies that the MNV RC is recognized by another pathway independently of the *Dhcr24* gene product. However, it is still possible that this pathway is also able to detect the MNV RC, but simply a redundant pathway exists in this cell type which functions redundantly for MNV RC targeting by TAG. Further studies are essential to elucidate this potential PV targeting mechanism in J774A.1 cells, as it is certainly possible that this detection pathway is mediated through a mutation functioning entirely independently of the *Dhcr24* gene product. Regardless, this observation sets a precedent that indeed, two structures that are TAG targets can be identified through distinct mechanisms.

This led us to investigate a mechanism by which the MNV RC was uniquely targeted by TAG. Invesigating the hypothesis that a viral protein may serve as a pathogen associated molecular pattern (PAMP) that directly recruits the autophagy proteins to the MNV RC, we found the RdRp of MNV (NS7) interacted with the coiled-coil region of ATG16L1. This observation makes biological sense because ATG16L1 is the autophagy protein known to define the target membrane for LC3, so direct recruitment of ATG16L1 to the RC suggests a protein-protein interaction mediating RC recognition by TAG (Fujita et al., 2008). In addition, some viruses benefit from

recruitment of autophagy machinery to their RCs, leading to the speculation that autophagy proteins play a role in RC biogenesis (Choi et al., 2018; Jackson et al., 2005; Jordan and Randall, 2012). Due to the high levels of conservation amongst RdRps of (+)RNA viruses, this ATG16L1 and RdRp interaction may be a conserved mechanism utilized by the virus to promote it's lifcycle. Indeed, we observe that the RdRps of several (+)RNA viruses interact with ATG16L1. However, this recruitment may serve as a "double-edged sword" because even though the autophagy machinery may be beneficial for the viral lifecycle, our data suggest that it also demarcates the RC as a target for TAG (Biering et al., 2017a; Choi et al., 2018).

Though our data demonstrates that NS7 is sufficient to recruit ATG16L1 to a target membrane, we observe that RCs that are missing NS7 can still recruit the autophagy proteins and the interferon-inducible GTPases. This suggests that a direct interaction between ATG16L1 and NS7 may simply be one of many redundant mechanisms by which the MNV RC is identified as a target for TAG. This makes sense given our hypothesis that the host targets distinct structures via different mechanisms. So in other words, there may be many different "non-self" membranous detection mechanisms utilized by the host and one structure may be identified by more than one, thus when we make an MNV RC missing one detection mechanism (e.g. NS7) other mechanisms such as lipid composition or membrane structure may be serving as redundant "non-self" signals to directly or indirectly recruit the autophagy proteins. An interesting experiment to conduct would be to take advantage of the high mutation rate of (+)RNA viruses, and passage MNV in the presence of low levels of IFNG, applying a selective pressure, but not enough to completely block viral replication. This way if MNV

were able to evolve a mechanism to evade IFNG mediated TAG, we could isolate an IFNG resistant mutant and work backwards to determine what mutations confer resistance. We speculate one such evasion strategy could be to mutate the RdRp in such a way that does not drastically alter the polymerase function, but breaks the protein-protein interaction with ATG16L1. This of course may not be possible, as the ATG16L1 interacting domain of the NS7 RdRp is probably in a highly conserved motif essential for the polymerase to function.

This raises the question, are all viral RCs sentitive to TAG? Indeed, our data suggests this is not the case. We find that though the RCs of MNV and EMCV are targeted by the autophagy proteins and the IFN-inducible GTPases, the RCs of ZIKV and MHV are not targeted. This could be explained as a technical issue, suggesting that the time points we examined were wrong and thus not sufficient to see targeting to ZIKV and MHV RCs. Alternatively, these viruses may be evading TAG through some virally evolved mechanism(s). Potentially, differences in RC structure could result in naturally TAG sensitive vs. naturally TAG resistant RCs. Since the RCs of MNV, EMCV, as well as MHV have all been characterized as closeley resembling the DMV class, the differences may not be as simple as spherule invagination vs. DMV. Instead, other factors such as lipid composition and origin, host proteins present (e.g. GMS regulator IRGs), exposure of viral PAMPS to the cytoplasm, viral active recruitment of autophagy proteins, as well as levels of heterogenitiy of observed RCs may all be factors which determine an RCs sentivity to TAG. These can be considered as passive strategies, and are more a result of the biology of the virus. However, can viruses actively antagonize the TAG pathway using virally encoded proteins? There is indeed precedent

for this with *T. gondii*. TAG resistant strains of *T. gondii* (considered virulent strains), encode proteins which inactivate the IRGs specifically (Fentress et al., 2010; Fleckenstein et al., 2012; Gazzinelli et al., 2014). Further, another intracellular pathogen, *Plasmodium berghei*, has been reported to be able to remove host autophagy proteins from its PVM, suggesting a potential mechanism to evade TAG (Agop-Nersesian et al., 2017). Considering the essential nature of the RC in the lifecycle of (+)RNA viruses, we speculate that viruses have evolved active mechanisms to antagonize TAG. Our work investigates four (+)RNA viruses, the two with smaller genomes are TAG sensitive (MNV and EMCV) and the two with larger genomes are TAG resistant (ZIKV and MHV). This suggests that viruses of the *Flaviviridae* and *Coronaviridae* families have more genetic economy with which to evolve such an evasion strategy, and further, plenty of previous studies describe mechanisms by which viruses from these families evade and antagonize the interferon signaling pathway (Deng et al., 2017; Ye et al., 2013). It would be interesting to test if the RdRps of ZIKV and MHV can interact with ATG16L1, which would suggest that these structures are capable of being targeted but simply are not. An excellent follow up study to further test this theory of viruses actively antagonizing TAG, would be to identify an attenuated strain of a virus that is TAG sensitive which originates from a TAG resistant parent, and ask what mutation made this virus sensitive to TAG. A candidate for such a study comes from Yellow Fever Virus (YFV), a (+)RNA virus from the *Flaviviridae* family. A recent study reports that a vaccine strain of YFV, known as 17D-204, is antagonized by IFNG at the stage of viral replication in a cell-autonomous manner, while the WT YFV is resistant to this IFNG mediated antiviral activity (Lam et al., 2018; Theiler and Smith,

1937). This IFNG sensitive YFV-17D-204 vaccine strain presents clear parallels with our work on the IFNG mediated control of MNV via RC targeting. It would facinating to determine if RCs from YFV-17D but not from WT YFV are targets of TAG. If so, this suggests that the genome of 17D has been mutated in some way that either the RC looks different from WT and thus is targeted (passive sensitivity), or that a protein essential for antagonizing TAG has been mutated. Many proteins are mutated between 17D and the WT parental strain, and no single mutation has been implicated in the attenuation of 17D, instead it is hypothesized that the attenutation of 17D is a combinatorial effect (Engel et al., 2006). So it would be necessary to revert the sequence of the mutant strain back to the WT sequence, one gene at a time to determine if indeed one viral gene was sufficient to antagonize TAG. Interestingly, the RdRp of 17D is highly mutated compared to the RdRP of WT YFW, potentially implicating this viral gene (Lam et al., 2018). If these experiments suggest that indeed 17D but not WT YFV are targeted by TAG, then a coinfection study investigating how cells infected with both viruses behaves would be interesting. Being able to visualize RCs from both viruses in a single cell could tell us whether the active evasion function of WT YFV rescues 17D from TAG or not. In other words, is the the ability of WT YFV to antagonize TAG specific to only a single RC or is the entire cell affected by the antagonisitc mechanism. Going one step further, one could coinfect with low MOIs of both viruses to ask if a potential TAG evasion mechanism of WT YFV is cell intrinsic or cell extrinsic. This would tell us a great deal about the antiviral nature of TAG against viruses and whether reistance is active, passive, or both.

Another exciting idea our work pushes forward comes again from the NS7 and ATG16L1 interaction. Our data suggests a direct interaction of a “non-self” viral protein acting as a PAMP which is detected by ATG16L1, mediating the host recognition of the MNV RC as a target for TAG. This suggests, in the context of antiviral TAG, that ATG16L1 acts as a pattern reognition receptor (PRR) directly detecting the RdRp of MNV and potentially other viruses. The RdRps of (+)RNA viruses are known to act as viral PAMPs, potentally due to their high level of conservation and specificity to RNA viruses (Nikonov et al., 2013; te Velthuis, 2014; Wang et al., 2017, 2018). This paints a picture for MNV that upon translation of the RdRp, it can activate an antiviral state by binding PRRs of the inflamasome, the RIG-I like receptors, and now the autophagy protein ATG16L1. This brings up the question, when does the ATG16L1 and NS7 interaction take place in a biologically relevent situation? Does the interaction occur in the cyotplasm before and during RC formation which results in recruitment of ATG16L1 to the RC along with the viral recruitment of NS7. Alternatively, the interaction may require or be enhanced by association of NS7 with a membrane or other co-factors present at the MNV RC, which would suggest that ATG16L1 recruits to NS7 in the replication complex. These possibilities are not mutually exclusive, but how ATG16L1 would be able to traffic into the RC, which is believed to restrict access of cytoplasmic proteins such as PRRs found in the cytoplasm would be unknown (Neufeldt et al., 2016; Overby et al., 2010). If NS7 brings ATG16L1 into the replication complex, then Atg16L1 would be utilizing NS7 as something of a “trojan horse” to gain access to a location it normally would not be able to go. If ATG16L1 specificially traffics into the mature RC, this would be an example of a cellular PRR having the ability to traffic into a viral RC,

which raises a lot of additional immunological questions. Further, as discussed briefly above, MNV may be actively recruiting ATG16L1 into the MNV RC to benefit viral replication, but in doing so, marking itself as a target for TAG (Biering et al., 2017a; O'Donnell et al., 2016). Our work has revealed a region within the coiled-coil domain of ATG16L1 that is essential for the antiviral activity of IFNG, this region may be mediating an interaction with NS7 as well as some potential other unknown factors. Conducting futher interaction studies of ATG16L1 truncation mutants under different conditions such as IFN treatment or with lipids, may further reveal what role ATG16L1 plays in detection of viral RCs.

This work also addresses a long standing question in the IFN-inducible GTPase field, namely, is this system conserved and functional in humans? As mentioned above, while the GBP IFN-inducible subfamily is well conserved between mice and humans, the IRG subfamily is not. The GBPs are known to play essential roles in additional cellular functions, which explains their conservation. It is hypothesized that the IRGs were expanded in mice due to a long evolutionary relationship with *T. gondii*, but without this selective pressure, human ancestors collapsed the IRG repertoire (Gazzinelli et al., 2014). Two IRGs are conserved in humans, human IRGM and IRGC, both of which are no longer interferon inducible (Bekpen et al., 2009; Bekpen et al., 2010; Pilla-Moffett et al., 2016). Though human IRGM is believed to play a role in the immune control of intracellular pathogens, this is believed to function through the promotion of degradative autophagy and not through the membranolytic disruption of replication vacuoles (Chauhan et al., 2015; Singh et al., 2006; Singh et al., 2010). Further, our data shows no role for human IRGM in the IFNG mediated control of MNV in human cells. Though it

should be noted that human IRGM appears to be criticial in the lifecycle of many viruses, as it is shown that the function of human IRGM correlates with the function of the autophagy pathway in human cells, which is beneficial for many viruses (Grégoire et al., 2011). How and if this relates to TAG in humans is unknown.

The IFN-inducible GTPases are most heavily studied for their activity against *T. gondii*, and many studies suggest that while the mebranolytic role of the IRGs and GBPs may play a major role in the host defense against *T. gondii* in mice, this pathway may not be conserved in humans. The main observations come from finding no GBP or LC3 targeting to the PVM of *T. gondii* in human cells. Instead, IFNG is reported to control *T. gondii* in human cells using alternative antimicrobial mechanisms such as tryptophan depletion, triggering cell death, and a new non-canonical pathway of autophagy which “suffocates” the PV of *T. gondii* in cellular membranes (Niedelman et al., 2013; Ohshima et al., 2014; Pfefferkorn, 1984; Selleck et al., 2015). So at this point it was unclear if TAG was conserved in the human system without a functional IRG system. Our data suggests that it is conserved and that the RC of MNV is targeted by LC3 and GBPs in human cell lines. This can be explained through difference in methods and pathogens, but overall our data clearly suggests that TAG functions in human cells, which calls on the IFN-inducible GTPase field to ask why we do not see TAG working against *T. gondii* in human cells. Simply the regulation of the TAG system may be different in human cells, with MNV once again detected through a different mechanism, resulting in loss of targeting for *T. gondii* but not for the MNV RC, which is similair to our observations in the mouse cell line J774A.1. Differences between cell lines and hosts will affect how these systems are regulated, and the absence of the IRG regulator

proteins, which also were shown to affect GBP localization, would imply that the system may be differentially regulated in humans (Traver et al., 2011). Further, all studies which have failed to find TAG functioning against *T. gondii* in human cells, have utilized immortalized cell lines which are less biologically relevent than primary cells. Clearly, further investigation into human TAG is needed to determine how to best use this conserved anti-microbial system for theraputic purposes.

Our work demonstrates that the conserved and essential RCs of (+)RNA viruses can be identified as “non-self” and targeted by the innate immune system. Our work elucidates a pathway by which these structures are identified via an interaction between the conserved viral RdRp and the autophagy protein ATG16L1, which then targets LC3 and homologs to the RC. Once targeted, LC3 demarcates these structures as “non-self” targets for the IFN-inducible GTPases which destroy the structures through a yet unclear mechanism. Though not biochemically demonstrated, it is believed that the IFN-inducible GTPases exert a membranolytic function against the replication vacuoles of *T. gondii* and others. A major question left unanswered in antiviral TAG, is about the nature of the antiviral mechanism of the IRGs and GBPs against the RC? Is this antiviral activity also through a membranolytic function which vesiculates the RC? It may not be biophysically possible for the RCs of MNV to be vesiculated by the IFN-inducible GTPases due to their small size, about the size of the vacuoles which are “blebbed” from the PV of *T. gondii*. We can think of three potential mechanism by which the IFN-inducible GTPases exert their antiviral activity upon the MNV RC. First, a traditional membranolytic blebbing mechanism may be utilized, as is hypothesized for the *T. gondii* PV. This would involve the targeting of the IRGs and GBPs to the RC membrane

interior, our data suggests the effectors bind to the same side as the MNV proteins (continuous with the cytoplasm), and vesiculate away membrane until the structural integrity of the RC is lost. Another possibility would involve, rather than loss of integrity from vesiculation, a massive membrane deformation induced by the IFN-inducible GTPases which no longer allows the viral replication machinery to associate with or utilize the RC membrane. Lastly, a final potential mechanism could be oligomerization of the IFN-inducible GTPases within the RC structure which would leave the membrane itself intact, but instead interfere with the interaction of MNV proteins, preventing recruitment and concentration of viral proteins, and a loss of ability for the virus to replicate. Indeed, an anti-bacterial mechanism has been recently described by which the intracellular bacteria, *Shigella flexneri,* is directly targeted by the GBPs, which prevent it from recruiting the cellular factors it requires for actin-mediated motility. WT *S. flexneri* encodes an effector protein which ubiquitinates the GBPs, sending them to the proteosome for degradation, yet another example of a pathogen actively evading the IFN-inducible GTPases (Wandel et al., 2017). Ongoing studies will attempt to understand the mechachanism by which the IFN-inducible GTPases exert their antiviral activity of the MNV RC. Strategies that will be employed include live-cell imaging, further ultrasturcutral studies, and *in vitro* isolation of the membranous RC followed by the addition of cocktails of recombinant IFN-inducbile GTPases.

Our work elucidates an antiviral pathway (TAG) by which the RCs of two (+)RNA viruses are targeted and antagonized. Considering the level of conservation of these membranous structures, and considering the potential for viruses to evade TAG, it is possible that the host is able to antagonize these membranous RCs through further

potentially redundant antiviral mechanisms. Indeed, a recent report showed that the RC of the (+)RNA virus, Equine Arteritis Virus (EAV) of the *Arteriviridae* family, was antagonized through an antiviral mechanism mediated by the type I IFN, interferon beta (IFNB) (Oudshoorn et al., 2016). Immune effectors required for this antiviral pathway were not identified, but the DMV RC of EAV was shown to be signifigantly deformed in IFNB activated cells (Oudshoorn et al., 2016). This antiviral pathway may certainly be TAG, as the IFN-inducible GTPases are also upregulated, though to a lesser extent, by IFNB. However, it is exciting to speculate that this antiviral activity of IFNB against EAV may be a completely novel RC targeting mechanism the host has evolved as a redundant RC targeting antiviral pathway. It will be essential to show whether this IFNB mediated antiviral activity against the EAV RC is mediated by the LC3-conjugation system as well as the IFN-inducible GTPases (Scutigliani and Kikkert, 2017).

TAG is essential to protect mice from MNV infection when the redundant antiviral activity of type I interferons are absent. Antiviral TAG is also functional against viruses in the human system. Further, TAG functions to identify and antagonize the replication compartments of a diverse list of intracellular pathogens, suggesting this pathway is a conserved and important way the host detects and destroys unfriendly membranes. Such a conserved membrane manipulating and attacking pathway must have functions in other areas of immunity as well. Future studies will expand our knowledge of how the autophagy proteins work in concert with the IFN-inducible GTPases to target membranes, and allow us to develop theraputics against many intracellular pathogens. Further, we can learn what the downstream effects of TAG are in immunity to intracellular pathogens, providing potential new avenues of study that connect the

innate and adaptive immune responses. Our work here showing that the RCs of (+)RNA viruses are targets of TAG serves to unify the field of IFN-inducible GTPases, opening doors to understand how two distinct antimicrobial pathways, interferons and autophagy, come together in one broadly conserved membranolytic antimicrobial pathway. In time, we can perhaps even develop drugs that target dormant intracellular parasites, such as *Mycobacterium tuberculosis* and *Plasmodium species*, and mark them in such a way to become targets of TAG.

Chapter V

Materials and Methods

The methods presented in this chapter have been modified from a manuscript published in the Cell Press Journal, Cell Host and Microbe: Viral replication complexes are targeted by LC3-guided interferon-inducible GTPases (DOI: 10.1016/j.chom.2017.06.005). The authors and affiliations of this manuscript are Scott B. Biering,[1,10] Jayoung Choi,[2,10] Rachel A. Halstrom,[2] Hailey M. Brown,[3] Wandy L. Beatty,[5] Sanghyun Lee,[6] Broc T. McCune,[6] Erin Dominici,[2] Lelia E. Williams,[4] Robert C. Orchard,[6] Craig B. Wilen,[6] Masahiro Yamamoto,[7] Jörn Coers,[8] Gregory A. Taylor,[8,9] and Seungmin Hwang[1,2,3]*

[1]Committee on Microbiology,

[2]Department of Pathology,

[3]Committee on Immunology,

[4]Biological Sciences Collegiate Division,

The University of Chicago, Chicago, IL 60637, USA

[5]Department of Molecular Microbiology,

[6]Department of Pathology and Immunology,

Washington University School of Medicine, St. Louis, MO 63110, USA

[7]Laboratory of Immunoparasitology, World Premier International Research Center Immunology Frontier Research Center, Osaka University, Osaka 565-0871, Japan

[8]Departments of Medicine, Molecular Genetics and Microbiology, and Immunology, Duke University Medical Center, Durham, NC 27710, USA

[9]GRECC, Durham VA Health Care System, Durham, NC 27705, USA

[10]These authors contributed equally.

*Correspondence to and Lead Contact:

Seungmin Hwang; Email: shwang@bsd.uchicago.edu

STAR Methods

CONTACT FOR REAGENT AND RESOURCE SHARING

Further information and requests for resources and reagents should be directed to and will be fulfilled by the Lead Contact, Seungmin Hwang (shwang@bsd.uchicago.edu).

EXPERIMENTAL MODEL AND SUBJECT DETAILS

Mice

All mice used in this study were from a C57BL/6 background. In all experiments, control and experimental mice were 6-8 week old littermates of both genders. Littermates of the same sex were housed together regardless of genotype. The following mice, including littermate controls, were used for bone marrow extraction: *Atg3*$^{flox/flox}$*+/-LysMcre*, *Atg5*$^{flox/flox}$*+/-LysMcre*, *Atg14*$^{flox/flox}$*+/-LysMcre, Irgm1*$^{-/-}$*Irgm3*$^{-/-}$, and *Gbp*$^{chr3-/-}$. *Atg3*$^{flox/flox}$*+/-LysMcre* mice were derived from *Atg3*$^{flox/flox}$ mice that were provided by Dr. You-Wen He, Duke University, USA (Jia and He, 2011). *Atg5*$^{flox/flox}$*+/-LysMcre* mice were provided by Dr. Herbert W. Virgin, Washington University in St. Louis, USA (Hwang et al., 2012).

Atg14$^{flox/flox}$*+/-LysMcre* mice were provided by Dr. Shizuo Akira, Osaka University, Japan. *Irgm1*$^{-/-}$*Irgm3*$^{-/-}$ mice were provided by Dr. Gregory Taylor, Duke University, USA (Henry et al., 2009). *Gbp*$^{chr3-/-}$ mice were provided by Dr. Masahiro Yamamoto, Osaka University, Japan (Yamamoto et al., 2012). The following mice, including littermate controls, were used for *in vivo* MNV infection: *Irgm1*$^{-/-}$*Irgm3*$^{-/-}$*Ifnar*$^{-/-}$ and *Gbp*$^{chr3-/-}$*Ifnar*$^{-/-}$. To generate these mice, either *Irgm1*$^{-/-}$*Irgm3*$^{-/-}$ or *Gbp*$^{chr3-/-}$ mice were crossed with *Ifnar*$^{-/-}$ mice. *Ifnar*$^{-/-}$ mice were provided by Dr. Herbert W. Virgin (Hwang et al., 2012). All mice were housed and bred at the University of Chicago under specific-pathogen-free conditions in a biosafety level 2 facility in accordance with federal and university guidelines. All experimental procedures were approved by the Animal Care and Use Committee of the University of Chicago. For *in vivo* MNV infection experiments, mice were assigned randomly to experimental groups and were housed by matching genotype and gender. The day after group assignment, the mice were transferred from the breeding facility to the infection facility; both are specific-pathogen-free and biosafety level 2 facilities. One week after transfer, the mice were infected with MNV. Mice were excluded from an experiment if they were noticeably sick or significantly smaller or weighed less than littermates on the day of infection. All *in vivo* experiments were conducted at least three times.

Primary Cells

The primary cells utilized in this study were murine bone marrow derived macrophages (BMDMs) and human foreskin fibroblasts (HFFs). Bone marrows were isolated from the

femurs and tibias of 6-8 week old mice of both genders listed above, and plated in non-tissue culture treated 10-cm dishes in 10 mls of BMDM media. On day 4, 10 mls of fresh BMDM media was added. On day 7, BMDMs were detached from the dish using ice-cold 0.02% EDTA in DPBS (Sigma-Aldrich, E8008), and seeded in tissue culture treated plates or on coverslips for subsequent experiments. Remaining D7 BMDMs were frozen in BMDM media containing 10 % DMSO and used later to set up replicate experiments if necessary. BMDMs were rested for three days after seeding, and used for experiments as described in METHOD DETAILS and figure legends. BMDMs of the following mice were prepared in Washington University in St. Louis, USA and brought to the University of Chicago: *Ulk1*$^{-/-}$, *Ulk2*$^{-/-}$ and *Irgm1*$^{-/-}$. *Ulk1*$^{-/-}$ and *Ulk2*$^{-/-}$ BMDMs were derived from the mice provided by Dr. Sharon Tooze, London Research Institute, U.K. (McAlpine et al., 2013). *Irgm1*$^{-/-}$ BMDMs were derived from the mice provided by Dr. Gregory Taylor, Duke University, USA (Henry et al., 2009). The composition of BMDM media was Dulbeco's Modified Eagle Medium (Mediatech, 10–013), 10% fetal bovine serum (Biowest, US1520), 5% horse serum (Life Technology, 16050), 1x MEM nonessential amino acids (Mediatech, 25-025-CI), 1 mM sodium pyruvate (Mediatech, 25-000-CI), 2 mM L-glutamine (Mediatech, 25-005-CI) and macrophage colony-stimulating factor (M-CSF). The source of the M-CSF was 10% CMG14-12 conditioned medium (Takeshita et al., 2000) for MNV infection, and 10% L929 conditioned media (Stanley and Heard, 1977) for EMCV infection. HFF cells were provided by Dr. Herbert W. Virgin and used for *T. gondii* maintenance. All cells were cultured at 37°C in 5% CO_2.

Cell Lines

Male *Ulk1*$^{-/-}$*Ulk2*$^{-/-}$ and female *Atg3*$^{-/-}$ murine embryonic fibroblasts (MEFs) were provided by Dr. Sharon Tooze, London Research Institute, U.K. (McAlpine et al., 2013) and Dr. Masaaki Komatsu, Tokyo Metropolitan Institute of Medical Science, Japan (Sou et al., 2008), respectively. Female *Lc3b*$^{-/-}$ MEFs were used to generate the CRISPR-KO cell lines of LC3 homologs and derived from *Lc3b*$^{-/-}$ mice that were obtained from Dr. Marlene Rabinovitch, Stanford University, USA (Cann et al., 2008). Female HeLa WT, *Atg7*$^{-/-}$, and *Atg16l1*$^{-/-}$ cells were previously described (Selleck et al., 2015) and provided by Drs. Herbert W. Virgin and Ramnik Xavier. Male HAP1 WT, *Atg16l1*$^{-/-}$, and *Gbp*$^{1\text{-}7\text{-}/\text{-}}$ cells were previously described (Ohshima et al., 2014) and provided by Dr. Masahiro Yamamoto. Female BV-2 cells were provided by Dr. Yuanan Lu, University of Hawaii at Manoa, USA (Cox et al., 2009) and used to titer infectious virus. Male RAW264.7 cells were provided by Dr. Herbert W. Virgin and used to titer infectious virus. Female 293T cells, obtained previously from Dr. Herbert W. Virgin, were used to produce lentivirus. J774A.1 cells were provided by Dr. Herbert W. Virgin and used for MNV and *T. gondii* infection. All cell lines were cultured at 37°C in 5% CO_2 in standard media: Dulbeco's Modified Eagle Medium (Mediatech, 10–013), 10% fetal bovine serum (Biowest, US1520), 1x MEM nonessential amino acids (Mediatech, 25-025-CI), 10 mM HEPES (Mediatech, 25-060-CI), and 100 U/ml each of penicillin and streptomycin (Mediatech, 30-002-CI). All experiments were conducted within no more than 5 passages upon thawing of cell stocks. Protein/gene deletion for mutant cells were confirmed by western blot, PCR and/or qPCR as indicated in METHOD DETAILS and figure legends.

Viruses

All MNV infections were conducted using the MNV-1.CW3 strain (Thackray et al., 2007). All EMCV infections were conducted using EMCV strain K which was obtained from Dr. Marco Colonna, Washington University in St. Louis, USA (Hwang et al., 2012). All Zika virus (ZIKV) infections were conducted using the Zika-Fortaleza/2015 strain which was obtained from Dr. Michaela Gack, University of Chicago, USA. All Murine Hepatitis Virus (MHV) infections were conducted using the A59 strain which was obtained from Dr. Susan Baker, Loyola University Chicago, USA (Deng et al., 2017). MNV-1.CW3 viruses were prepared from a CDNA clone containing the genome of MNV-1.CW3. $1x10^6$ 293T cells were seeded in 6-well plates and transfected with 4 ug of the MNV-1.CW3 plasmid for 48 hours to produce virus. MNV and EMCV were further amplified in BV-2 cells. Infected cells were incubated until the cells showed >90% cytopathic effect, usually for 48 hours. Infected cells were then frozen and thawed, and the cell lysates containing viral particles were centrifuged for 20 minutes at 3000 rpm to remove the cell debris. Supernatants were further centrifuged for 3 hours at 26,250 rpm at 4^oC to produce a concentrated virus stock. The viral stocks were frozen in small aliquots, and the titers of the stocks were determined by $TCID_{50}$. All viral infections were conducted with a viral stock aliquot having undergone only one cycle of freeze and thaw.

Protozoan Parasites

All infections with *T. gondii* were conducted using tachyzoites from the avirulent type II strain expressing green fluorescent protein (PTG). PTG tachyzoites were maintained

through continuous passage in human foreskin fibroblasts (HFFs) as previously described (Choi et al., 2014; Zhao et al., 2008).

METHOD DETAILS

Viral Infection and Viral RNA Transfection

Viral infections were performed as previously described (Hwang et al., 2012; Nice et al., 2013). $1x10^5$ cells (BMDM, BV-2, and HAP1) or $2x10^4$ cells (MEF, J774A.1, and HeLa) were seeded per well in 24-well plates. At 24 hours after seeding, cells were treated with mouse or human IFNG (Peprotech, 315-05 or 12410-1) or mouse IFN Beta (PBL Assay Science, 12410-1) for the time and at the doses indicated in the figures. At the time of infection, the media of cell was replaced with inoculum containing viruses at the MOI indicated in figure legends, and cells were infected for 30 minutes at room temperature. After incubation, the viral inoculum was removed, and cells were washed twice with PBS followed by addition of fresh media. In the case of simultaneous IFNG treatment with MNV infection for immunofluorescence assays, IFNG was added along with fresh media after infection. Transfection of MNV viral RNA (vRNA) is frequently used to overcome the barrier of entry, the limiting step of MNV infection (Orchard et al., 2016) when analyzing MNV replication in non-infectable cell types (MEFs, HAP1, and HeLa cells) (Hwang et al., 2014). MNV vRNA was isolated from the concentrated MNV stocks using TRI reagent (Sigma-Aldrich, T9424) according to the manufacturer's instruction. The amount of vRNA indicated in figure legends was transfected to cells using Lipofectamine 2000 (Invitrogen, 11668) according to the manufacturer's

instruction. The infected or transfected cells were harvested at the time indicated in figure legends by fixation with 2% formaldehyde (Ted Pella, 18505) in PBS for 10 minutes at room temperature (for flow cytometry and immunofluorescence assays), by freezing at negative 80 (for replication analysis by 50% Tissue Culture Infectious Dose [$TCID_{50}$] or Plaque Assay [PA]), or by lysis with protein sample buffer (for western blot).

MNV Replication Analysis *in vivo*

For *in vivo* MNV infections, 6-8 week old littermate mice of both genders were infected perorally with $1x10^5$ PFU of MNV in 25 ul of standard media. Mouse weight was recorded upon infection and monitored every 12 hours. For survival experiments, mice were euthanized and recorded as dead, according to approved IACUC protocols for >30% weight loss or if they became significantly moribund. For tissue viral burden analysis, infected mice were euthanized at 3 days post infection and organs were harvested and analyzed as previously described (Hwang et al., 2012). Organs were collected in standard media, subjected to a freeze-and-thaw cycle, and then homogenized in a bead beater using 1.0 mm zirconia/silica beads (BioSpec Products, 11079110z). After debris was removed by centrifugation, MNV titers in the homogenates were measured by $TCID_{50}$. Survival experiments were conducted 3 times using total 10 males and 6 females of *Irgm1*$^{+/-}$*Irgm3*$^{+/-}$*Ifnar*$^{-/-}$, 13 males and 7 females of *Irgm1*$^{-/-}$*Irgm3*$^{-/-}$*Ifnar*$^{-/-}$, 15 males and 11 females of *G*bp$^{+/-}$*Ifnar*$^{-/-}$, and 14 males and 12 females of *Gbp*$^{-/-}$*Ifnar*$^{-/-}$ mice. The tissue viral burden experiments were conducted 3 times using total 15 males and 5 females of *Irgm1*$^{+/-}$*Irgm3*$^{+/-}$*Ifnar*$^{-/-}$, 9 males and 5

females of *Irgm1*$^{-/-}$*Irgm3*$^{-/-}$*Ifnar*$^{-/-}$, 9 males and 10 females of *G*bp$^{+/-}$*Ifnar*$^{-/-}$, and 9 males and 5 females of *Gbp*$^{-/-}$*Ifnar*$^{-/-}$ mice.

$TCID_{50}$ and Plaque Assay

To quantitate infectious MNV, the infected cells with media were harvested by freezing at negative 80 and the infected cells were lysed through a freeze-and-thaw cycle. For Plaque Assay, the lysates were 10-fold serially diluted in standard media and added to RAW264.7 in 6-well plates. The cells were incubated for one hour with constant rocking at room temperature, and then the inoculums were replaced with overlay media containing 1% methylcellulose (Sigma-Aldrich, M0387). After incubation for four days, the overlay media was discarded and the cells were stained with 1% crystal violet (Fisher Chemical, C581) solution containing 20% ethanol for plaque counting. The limit of detection was calculated as the least number of infectious unit that can be detected at the lowest dilution (Hwang et al., 2012). For $TCID_{50}$ assay, the viral lysates were 10-fold serially diluted in standard media and added to BV-2 cells seeded in 96-well plates. 8-wells were infected for each dilution and further incubated for 5 days. $TCID_{50}$ was calculated by determining the dilution factor needed to show cytopathic effect (CPE) in 4 out of 8 (50%) wells. The limit of detection was calculated as the amount of virus that causes CPE in 4 out of 8 wells at the lowest dilution.

Toxoplasma gondii Infection *In Vitro*

$2x10^4$ J774A.1 cells were seeded in 24-well plates. The next day cells were treated with 100 U/ml of IFNG or not. 24 hours post IFNG treatment, cells were infected with PTG

tachyzoites at the MOI indicated in the figures. The infection protocol used was described previously (Choi et al., 2014). In brief, the PTG strain of the type II *T. gondii* strain was maintained in HFF cells. A flask of HFF cells showing ~70% lysis from PTG infection was selected for infection. A cell scraper was used to remove cells from the flask and then the total media, including cells, was disrupted by passage through a 26G needle and syringe to liberate the tachyzoites from the cells. The disrupted lysate was centrifuged at 400 x g for 10 minutes, and then resuspended in regular culture media before being added to cells. 24 hours post infection cells were fixed in 2% formaldehyde (Ted Pella; 18505) and then analyzed by flow cytometry as described below.

Co-Immunoprecipitation Assay

$1x10^6$ BV-2 cells, stably expressing the individual MNV genes in a pHNHF- lentivirus construct, were seeded in 10-cm plates and treated the next day with 100 U/ml IFNG. 24 hours post IFNG treatment, cells were washed once with 1x PBS and lysed in lysis buffer (50 mM Tris-HCl, 150 mM NaCl, 1% Triton X-100, protease inhibitor cocktail) for 10 mins at 4° C. The lysates were then subjected to one round of freeze and thaw, before being transferred to separate tubes and vortexed to ensure complete lysis. The lysate was then spun down in a microcentrifuge at max speed for 15 minutes to pellet the cell debris. The lysate was then transferred to a new tube. A sample of the lysate was removed and mixed with WB sample buffer to serve as the input control. The remaining lysate was transferred to 20 ul of lysis buffer washed M2 FLAG beads (Sigma A2220) and incubated at 4° C overnight (12 hours) and rotating. Then the beads were washed 4x with lysis buffer and WB sample buffer was added directly to the beads to

elute bound protein. The proteins eluted in WB sample buffer as well as the input controls were then subjected to WB analysis as described below.

Bimolecular Fluorescence Complementation Assay

$1x10^5$ 293T cells were seeded in 24-well plates. The next day cells were co-transfected with 250 ng of pCAGGS-EYN and 250 ng of pCAGGS-EYC (500 ng total) using lipofectamine 3000 according to the manufacturer's instruction, the combinations of genes used is indicated in the figures. Transfected cells were incubated for 36 hours at 37° C and then moved to 30° C for 12 hours to allow the reconstituted YFP to mature for optimal signal. Cells were then fixed in 1X PBS/ 2% formaldehyde and imaged in 24-well plates using a fluorescent microscope on the GFP channel.

Yeast-Two-Hybrid Analysis

The *Saccharomyces cerevisiae* yeast strain PJ69-4A was transformed with the plasmid combinations indicated in the figures (pGAD and pGBDU). The lithium acetate (LiAc) transformation strategy was used as previously described (Bajaj Pahuja et al., 2015). Transformants were plated on solid-agar selection plates containing -LEU-URA media and incubated at 30° C. 72 hours post plating, colonies were picked and grown up overnight in -LEU-URA liquid media at 30° C in a shaker. When the culture had grown up to an OD600 of 0.5-1.0, the culture was serially diluted, as indicated in the figures, and 10 ul was spotted onto solid agar plates containing selective media (-LEU-URA; -LEU-URA-HIS; -LEU-URA-HIS-ADE) and incubated at 30° C. Growth of colonies was examined 3 days post plating.

GST Pulldown Binding Assay

This experiment was conducted in Dr. Kyung Hyun Kim's lab at Korea University. In brief, recombinant MNV NS7 and fusion protein GST-Atg16L1-dN79-N249 (amino acids 79-249) were produced using an *E. coli* based protein expression system. These proteins were purified and utilized for analysis of direct protein-protein interaction. Proteins were mixed in a buffer containing 20 mM HEPES (pH 8.0) and 75 mM NaCl, and incubated for 30 minutes at room temperature. 200 ul of an anti-GST resin was then added and allowed to incubate for an additional 10 minutes at room temperature. The resin was then pelleted, and the unbound protein fraction was collected (FT or flow through). The pelleted resin was then washed with 5 ml of wash buffer and pelleted again; the wash buffer was then collected (W or wash). To elute proteins bound to the anti-GST resin 100 ul of elution buffer was added to the resin (elution buffer is 1 ml of wash buffer + 10 mM glutathione). The resin was pelleted and the elution fraction was collected (E or proteins eluted from the beads). Finally, SDS-PAGE sample buffer was added to the resin and boiled to remove any protein that remained bound to the beads and this fraction was collected (SDS or proteins remaining bound to the beads post elution). These four fractions were then analyzed by SDS-PAGE and Coomassie Blue staining.

Anchor-Away Assay

Anchor-Away analysis was conducted as previously described (Park et al., 2016). $2x10^4$ WT MEFs were seeded in 24-well plates containing coverslips. 24 hours post

seeding, cells were cotransfected with a plasmid containing the mitochondrial outer membrane protein TOMM20 fused to EGFP and a 2xFRB domain (the anchor) (pEGFP-N1-TOMM20-2xFRP) in addition to a plasmid containing MNV-NS7 fused to RFP and a 4xFKBP domain (the bait) (pDRFP-MNV-NS7-4xFKBP). 24 hours post transfection cells were treated with 100 U/ml IFNG. 48 hours post transfection, cells were treated with 50 nM rapamycin (LC laboratories, R5000) or a DMSO vehicle control, for 2 hours then fixed with 1X PBS/ 2% formaldehyde before being analyzed by immunofluorescence microscopy.

Western Blot

Cells were left untreated, or treated with IFNG (Peprotech, 315-05) or IFNB (PBL Assay Science, 12410-1), and/or treated with chloroquine (Sigma-Aldrich, **C6628, 50** μM**)** as indicated in the figures. Total cell lysates were harvested in the protein sample buffer (0.1 M Tris [pH 6.8], 4% SDS, 4 mM EDTA, 286 mM 2-mercaptoethanol, 3.2 M glycerol, 0.05% bromophenol blue) and proteins were resolved by SDS-PAGE. Proteins were then transferred onto PVDF membranes and probed with primary antibody diluted in PBS/0.1% TWEEN 20 (PBST) containing 5% skim milk for overnight at 4°C and secondary antibody diluted in PBST with 5% skim milk for 1 hour at room temperature, on a side-to-side rocker. After each antibody incubation, the membranes were washed with PBST for three times of ten-minute-cycle. Probed proteins were detected using ECL reagents on a ChemiDoc system with Image Lab software (Bio-Rad). All antibodies were probed by the method described above except for LC3a (Cell Signaling), which was probed in TBS/0.1% TWEEN 20 with 5% BSA according to the manufacturer's

instruction. The following antibodies were used: MNV ProPol (Hwang et al., 2012); IRGA6 and IRGB6 from Dr. Jonathan Howard, University of Cologne (Martens et al., 2004); IRGM1 and IRGM3 from Dr. Gregory Taylor, Duke University; ATG7, ATG16L1, LC3B, and p62 (Sigma-Aldrich); ATG5 (Novus Biologicals); ATG3 (MBL International); GBP1-5, GBP2, and Actin-HRP (Santa Cruz Biotechnology); HA (the Frank W. Fitch Monoclonal Antibody Facility, The University of Chicago); 2A (EMD Millipore); LC3A (Cell Signaling Technology); GABARAP (Abcam); HRP Goat anti-mouse and HRP Donkey anti-rabbit (BioLegend); and HRP Donkey anti-goat (Jackson ImmunoResearch).

Immunofluorescence Analysis

For immunofluorescence analysis, cells were seeded on coverslips in 24-well plates and then infected with MNV or transfected with a plasmid expressing either WT MNV open reading frame 1 (ORF1) or MNV ORF1 missing NS7 (dNS7) (Hwang et al., 2012) with or without treatment of IFNG as indicated in figure legends. Upon fixation with 2% formaldehyde (Ted Pella, 18505), cells were permeabilized with 0.05% Saponin (Acros, 41923) in PBS, and blocked and probed in PBS containing 0.05% Saponin and 5% normal donkey serum (Jackson ImmunoResearch, 017-000-121). Fixation, permeabilization and 2 rounds of blocking were conducted for 10 minutes each at room temperature, and staining with primary and secondary antibodies was conducted for 1 hour each at room temperature. Samples were washed 5 times with PBS/0.01% Saponin for 5 min after each antibody incubation. Nuclei were stained with Hoechst 33342 (Invitrogen, H1399). Coverslips were mounted on glass slides with ProLong

Diamond Antifade Mountant (Invitrogen, P36961). The images were acquired using the EVOS FL Cell Imaging System or Olympus FV1000 Laser Scanning Confocal Microscope (Integrated Light Microscopy Core Facility, The University of Chicago). Images from each channel were merged using ImageJ/Fiji. Primary antibodies detecting the following proteins were used: MNV ProPol (Hwang et al., 2012); IRGA6 from Dr. Jonathan Howard, University of Cologne (Martens et al., 2004); FLAG (Sigma-Aldrich); LC3B (MBL International); GBP1-5 (Santa Cruz Biotechnology); HA (The Frank W. Fitch Monoclonal Antibody Facility, The University of Chicago); double-strand RNA (J2; SCICONS); and IRGM (Abcam). The following secondary antibodies were used: Alexa Fluor 488 Donkey anti-Guinea Pig, Alexa Fluor 647 Donkey anti-Guinea Pig and Alexa Fluor 488 Donkey anti-Rabbit (Jackson ImmunoResearch); DyLight 649-Donkey anti-Rabbit, Alexa Fluor 555 Donkey anti-Rabbit, DyLight 649 Goat anti-Mouse, Alexa Fluor 555 Goat anti-Mouse and DyLight 488 Goat anti-Mouse (BioLegend). To quantitate the localization of proteins on the viral RC, a minimum of 3 independent experiments were performed and at least 50 RC-positive cells were counted per each condition in each experiment.

Flow Cytometry

For flow cytometric analysis of MNV replication, infected cells were stained with anti-ProPol and analyzed with a BD LSR Fortessa cell analyzer (Hwang et al., 2012). After fixation with PBS/2% formaldehyde, cells were permeabilized with PBS/0.2% TritionX-100. Cells were then blocked and probed in PBS/0.2% TritonX-100/1% normal goat serum/1% normal mouse serum with rabbit anti-ProPol (Hwang et al., 2012) and

DyLight 649-Donkey anti-Rabbit (Biolegend) for one hour each at room temperature. After each antibody incubation, cells were washed with PBS/0.2% TritionX-100. Uninfected and stained samples served as gating controls. Flow data were analyzed using FlowJo (FlowJo, LLC). For flow cytometric analysis of *T. gondii* infection, a green fluorescent protein expressing type II strain of *T. gondii* (PTG) was used, so cells were simply fixed in PBS/2% formaldehyde then permeabilized with PBS/0.1% TritionX-100 overnight before being assessed by flow cytometry using the FITC channel, and analyzed the same as above (Zhao et al., 2008).

Quantitative PCR (qPCR)

Cells were lysed with TRI reagent (Sigma-Aldrich, T9424) and total RNA was extracted according to the manufacturer's instruction. CDNA was reverse transcribed from 1 ug of total RNA using IMPROM-II reverse transcriptase (Promega, A3803) with random hexamer according to the manufacturer's instruction. qPCR was conducted using SYBR-green reagents on an Applied Biosystems StepOnePlus Real-Time PCR system. The qPCR primers used in this study are shown in **Table S1**.

Knock-out of *Lc3* Homologs

CRISPR/Cas9 technique was applied to knock-out *Lc3* homologs according to the published protocol (Ran et al., 2013). px458 (#48138) and px459 (#48139) plasmids were obtained from Addgene and the guide RNA sequences as shown in **Table S2** were cloned into the plasmids to delete genomic DNA between the two double-strand-breaks. Cells were transfected with the plasmids using Lipofectamine 2000. After 48

hours, transfected cells were enriched through one passage of puromycin (Sigma-Aldrich, P9620) treatment (3 ug/ml). Enriched cells were diluted and seeded in 96-well plates, aiming for 0.5 cell/well, and the monoclonal colonies of cells were picked at 7 days after the set-up and further amplified. Genomic DNAs were extracted from the amplified cells and screened for deletion by PCR. Positive colonies containing desired deletion were further verified through sequencing and western blot analysis for the targeted protein. A monoclonal cell line harboring a desired deletion of a targeted *Lc3* homolog were then subjected to the next round of knock out of another *Lc3* homolog until all *Lc3* homologs were deleted. The primers used to screen the deletion of targeted DNA (Fig S1A) are shown in **Table S2**.

Lentiviral Transduction

pHAGE-N-Flag-HA (pHNHF) (Behrends et al., 2010) lentiviral vectors were used to express genes of interest in BV-2 cells, *Atg16L1*$^{flox/flox}$*+/-LysMcre* BMDMs, *Atg5*$^{flox/flox}$*+/-LysMcre* BMDMs, *Atg14*$^{flox/flox}$*+/-LysMcre* BMDMs*, Irgm1/Irgm3* WT/KO BMDMs, *Atg3* WT/KO MEFs and *Gbp*^{chr3} WT/KO BMDMs. The pHNHF vector is a Gateway destination vector that expresses proteins of interest with N-terminal FLAG-HA-tag and allows for puromycin selection of transduced cells. Modified lentiviral vector, pCDH-MCS-T2A-copGFP-MSCV (C274) (System Biosciences, Mountain View, CA; CD523A-1) (Hwang et al., 2012), was used to produce lentivirus for transduction of *Irgm1/Irgm3* WT/KO BMDMs. The T2A sequence in C274 is an 18 amino acid sequence which allows simultaneous expression of the protein of interest and copGFP during translation through self-cleavage. It also leaves 2A tag at the C-terminus of the expressed protein.

All lentiviruses were generated in 293T cells as previously described (Choi et al., 2014; Hwang et al., 2012). The lentiviral vectors were transfected with the packaging vector (psPAX2) and the pseudotyping vector (pMD2.G). At 12 hours-post-transfection, the media was replaced with fresh media for target cells. Lentivirus released in media was collected at 24, 36, and 48 hours-post-transfection and filtered through 0.45 μm syringe filters (Millipore, MA). For MEF and BV-2 transduction, the cells were incubated with lentivirus for 48 hours and then selected with 3 ug/ml of puromycin (Sigma-Aldrich, P9620) for 3 passages. For BMDM transduction, lentiviruses were added to bone marrows on the day 4 of differentiation. On day 5, lentiviruses were replaced with fresh ones and the differentiating bone marrows were further incubated until the day 7. BMDMs transduced with pHNHF lentiviruses were then selected with 1 ug/ml of puromycin (Sigma-Aldrich, P9620) for three days. BMDMs transduced with C274 lentiviruses were analyzed for transduction efficiency based on copGFP expression. The transduced cells were seeded for the experiments described in figure legends and the expression of transduced genes were validated by western blot analysis.

Electron Microscopy

BV-2 cells were left uninfected or infected with MNV at MOI=25 and simultaneously left untreated or treated with 100 U/ml IFNG. At 10 hpi, the cells were fixed, processed, and examined as previously described (Selleck et al., 2015). For ultrastructural analyses, cells were fixed in 2% paraformaldehyde (Polysciences, 00380)/2.5% glutaraldehyde (Polysciences, 18426) in 100 mM sodium cacodylate buffer (Sigma-Aldrich, C0250), pH 7.2 for 1 hr at room temperature. Samples were washed in sodium cacodylate buffer

and post-fixed in 1% osmium tetroxide (Polysciences, 0972A) for 1 hour. Samples were then rinsed extensively in dH_20 prior to *en bloc* staining with 1% aqueous uranyl acetate (Ted Pella, 19481) for 1 hour. Following several rinses in dH_20, samples were dehydrated in a graded series 30%, 50%, 70%, 90%, 95% ethanol for 20 minutes each. Samples were further dehydrated in three changes of 100% ethanol for 20 minutes each followed by two changes in propylene oxide (Ted Pella, 18601) for 30 minutes each. Samples were then infiltrated with 1:1 propylene oxide:Eponate 12 resin (Ted Pella, 18012) for 30 minutes followed by 1:3 propylene oxide:Eponate 12 resin overnight at room temperature. Samples were infiltrated with freshly made Eponate 12 resin for eight hours, and then polymerized in the resin at 70°C overnight. Sections of 95 nm were cut with a Leica Ultracut UCT ultramicrotome (Leica Microsystems), stained with 1% uranyl acetate for 30 min and 3% lead citrate (Ted Pella, 19314) for 5 min, and viewed on a JEOL 1200 EX transmission electron microscope (JEOL USA) equipped with an AMT 8 megapixel digital camera and AMT Image Capture Engine V602 software (Advanced Microscopy Techniques). For immunolocalization, cells were fixed in 4% paraformaldehyde/0.05% glutaraldehyde in 100 mM piperazine-N,N[prime]-bis(2-ethanesulfonic acid) (PIPES)(Sigma-Aldrich, P6757)/0.5 mM $MgCl_2$ (Sigma-Aldrich, M8266), pH 7.2 for 1 hour at 4°C. Samples were then embedded in 10% gelatin and infiltrated overnight with 2.3 M sucrose (Sigma-Aldrich, S9378)/20% polyvinyl pyrrolidone (Sigma, PVP10) in PIPES/$MgCl_2$ at 4°C. Samples were trimmed, frozen in liquid nitrogen, and sectioned with a cryo-ultramicrotome. Sections of 50 nm were blocked with 5% FBS and 5% normal goat serum for 30 min and subsequently incubated with the indicated primary antibodies for 1 hour, followed by secondary

antibodies: donkey anti-guinea pig conjugated to 12 nm colloidal gold (Jackson ImmunoResearch, 706-205-148), donkey anti-mouse conjugated to 18 nm colloidal gold (Jackson ImmunoResearch, 715-215-150) and goat anti-rabbit conjugated to 18 nm colloidal gold (Jackson ImmunoResearch, 111-215-144) for 1 hour. Sections were washed in PIPES buffer followed by a water rinse, and stained with 0.3% uranyl acetate/2% methyl cellulose (Sigma, M6385) and analyzed by transmission electron microscopy. All labeling experiments were conducted in parallel with controls omitting the primary antibody. These controls were consistently negative at the concentration of colloidal gold conjugated secondary antibodies used in these studies. Primary antibodies detecting the following proteins were used: MNV ProPol (Hwang et al., 2012), IRGA6 from Dr. Jonathan Howard, University of Cologne (Martens et al., 2004), GBP1-5 (Santa Cruz Biotechology), and LC3B (MBL International).

QUANTITATION AND STATISTICAL ANALYSIS

All data were analyzed with Prism software (GraphPad) using one-way analysis of variation (One-way ANOVA) with multiple comparisons (for multiple samples), Student's t-test (for two samples), or Log-rank (Mantel-Cox) test (for *in vivo* survival) as indicated in figure legends. No specific method was used to determine whether the data met assumptions of the statistical approach. Unless otherwise stated, all experiments were performed at least three times and the data were combined for presentation as mean ± SEM. All differences not specifically indicated as significant were not significant (n.s., $p>0.05$). Significant value was indicated as; *, $p<0.05$; **, $p<0.01$; ***, $p<0.001$; ****, $p<0.0001$. Statistical parameters, including the statistical tests used, value of N (also

what N represents, if necessary), definition of center, and dispersion and precision measures, are reported in the Figures and Figure Legends.

References

Abadie, V., Sollid, L.M., Barreiro, L.B., and Jabri, B. (2011). Integration of genetic and immunological insights into a model of celiac disease pathogenesis. Annu Rev Immunol. 29, 493-525. DOI: 10.1146/annurev-immunol-040210-092915.

Agop-Nersesian, C., De Niz, M., Niklaus, L., Prado, M., Eickel, N., and Heussler, V.T. (2017). Shedding of host autophagic proteins from the parasitophorous vacuolar membrane of Plasmodium berghei. Sci Rep. 7(1), 2191. Published online 2017/05/19 DOI: 10.1038/s41598-017-02156-7.

Al-Zeer, M.A., Al-Younes, H.M., Lauster, D., Abu Lubad, M., and Meyer, T.F. (2013). Autophagy restricts Chlamydia trachomatis growth in human macrophages via IFNG-inducible guanylate binding proteins. Autophagy. 9(1), 50-62. Published online 2012/10/19 DOI: 10.4161/auto.22482.

Anderson, S.L., Carton, J.M., Lou, J., Xing, L., and Rubin, B.Y. (1999). Interferon-induced guanylate binding protein-1 (GBP-1) mediates an antiviral effect against vesicular stomatitis virus and encephalomyocarditis virus. Virology. 256(1), 8-14. DOI: 10.1006/viro.1999.9614.

Asif, A., Manzoor, S., Tuz-Zahra, F., Saalim, M., Ashraf, M., Ishtiyaq, J., and Khalid, M. (2017). Zika Virus: Immune Evasion Mechanisms, Currently Available Therapeutic Regimens, and Vaccines. Viral Immunol. 30(10), 682-690. Published online 2017/10/13 DOI: 10.1089/vim.2017.0046.

Bajaj Pahuja, K., Wang, J., Blagoveshchenskaya, A., Lim, L., Madhusudhan, M.S., Mayinger, P., and Schekman, R. (2015). Phosphoregulatory protein 14-3-3 facilitates SAC1 transport from the endoplasmic reticulum. Proc Natl Acad Sci U S A. 112(25), E3199-3206. Published online 2015/06/08 DOI: 10.1073/pnas.1509119112.

Baldridge, M.T., Nice, T.J., McCune, B.T., Yokoyama, C.C., Kambal, A., Wheadon, M., Diamond, M.S., Ivanova, Y., Artyomov, M., and Virgin, H.W. (2015). Commensal microbes and interferon-λ determine persistence of enteric murine norovirus infection. Science. 347(6219), 266-269. Published online 2014/11/27 DOI: 10.1126/science.1258025.

Baldridge, M.T., Turula, H., and Wobus, C.E. (2016). Norovirus Regulation by Host and Microbe. Trends Mol Med. 22(12), 1047-1059. Published online 2016/11/22 DOI: 10.1016/j.molmed.2016.10.003.

Baltimore, D. (1971). Expression of animal virus genomes. Bacteriol Rev. 35(3), 235-241.

Barron, E.L., Sosnovtsev, S.V., Bok, K., Prikhodko, V., Sandoval-Jaime, C., Rhodes, C.R., Hasenkrug, K., Carmody, A.B., Ward, J.M., Perdue, K., et al. (2011). Diversity of murine norovirus strains isolated from asymptomatic mice of different genetic backgrounds within a single U.S. research institute. PLoS One. 6(6), e21435. Published online 2011/06/28 DOI: 10.1371/journal.pone.0021435.

Behrends, C., Sowa, M.E., Gygi, S.P., and Harper, J.W. (2010). Network organization of the human autophagy system. Nature. 466(7302), 68-76. Published online 2010/06/20 DOI: 10.1038/nature09204.

Bekpen, C., Hunn, J.P., Rohde, C., Parvanova, I., Guethlein, L., Dunn, D.M., Glowalla, E., Leptin, M., and Howard, J.C. (2005). The interferon-inducible p47 (IRG) GTPases in vertebrates: loss of the cell autonomous resistance mechanism in the human lineage. Genome Biol. 6(11), R92. DOI: 10.1186/gb-2005-6-11-r92.

Bekpen, C., Marques-Bonet, T., Alkan, C., Antonacci, F., Leogrande, M.B., Ventura, M., Kidd, J.M., Siswara, P., Howard, J.C., and Eichler, E.E. (2009). Death and resurrection of the human IRGM gene. PLoS Genet. 5(3), e1000403. DOI: 10.1371/journal.pgen.1000403.

Bekpen, C., Xavier, R.J., and Eichler, E.E. (2010). Human IRGM gene "to be or not to be". Semin Immunopathol. 32(4), 437-444. DOI: 10.1007/s00281-010-0224-x.

Bernstein-Hanley, I., Coers, J., Balsara, Z.R., Taylor, G.A., Starnbach, M.N., and Dietrich, W.F. (2006). The p47 GTPases Igtp and Irgb10 map to the Chlamydia trachomatis susceptibility locus Ctrq-3 and mediate cellular resistance in mice. Proc Natl Acad Sci U S A. 103(38), 14092-14097. Published online 2006/09/07 DOI: 10.1073/pnas.0603338103.

Bertolotti-Ciarlet, A., White, L.J., Chen, R., Prasad, B.V., and Estes, M.K. (2002). Structural requirements for the assembly of Norwalk virus-like particles. J Virol. 76(8), 4044-4055.

Biering, S.B., Choi, J., Brown, H.M., and Hwang, S. (2017a). LC3s hire membrane breakers to attack viral shelters. Autophagy. 1-3. Published online 2017/09/26 DOI: 10.1080/15548627.2017.1371396.

Biering, S.B., Choi, J., Halstrom, R.A., Brown, H.M., Beatty, W.L., Lee, S., McCune, B.T., Dominici, E., Williams, L.E., Orchard, R.C., et al. (2017b). Viral Replication Complexes Are Targeted by LC3-Guided Interferon-Inducible GTPases. Cell Host Microbe. 22(1), 74-85.e77. Published online 2017/06/29 DOI: 10.1016/j.chom.2017.06.005.

Bok, K., Prikhodko, V.G., Green, K.Y., and Sosnovtsev, S.V. (2009). Apoptosis in murine norovirus-infected RAW264.7 cells is associated with downregulation of survivin. J Virol. 83(8), 3647-3656. Published online 2009/02/11 DOI: 10.1128/JVI.02028-08.

Borrego, F. (2006). The first molecular basis of the "missing self" hypothesis. J Immunol. 177(9), 5759-5760.

Bouziat, R., Hinterleitner, R., Brown, J.J., Stencel-Baerenwald, J.E., Ikizler, M., Mayassi, T., Meisel, M., Kim, S.M., Discepolo, V., Pruijssers, A.J., et al. (2017). Reovirus infection triggers inflammatory responses to dietary antigens and development of celiac disease. Science. 356(6333), 44-50. DOI: 10.1126/science.aah5298.

Brockhurst, M.A. (2011). Evolution. Sex, death, and the Red Queen. Science. 333(6039), 166-167. DOI: 10.1126/science.1209420.

Cann, G.M., Guignabert, C., Ying, L., Deshpande, N., Bekker, J.M., Wang, L., Zhou, B., and Rabinovitch, M. (2008). Developmental expression of LC3alpha and beta: absence of fibronectin or autophagy phenotype in LC3beta knockout mice. Dev Dyn. 237(1), 187-195. DOI: 10.1002/dvdy.21392.

Carlsson, S.R., and Simonsen, A. (2015). Membrane dynamics in autophagosome biogenesis. J Cell Sci. 128(2), 193-205. DOI: 10.1242/jcs.141036.

Chan, E.Y., Kir, S., and Tooze, S.A. (2007). siRNA screening of the kinome identifies ULK1 as a multidomain modulator of autophagy. J Biol Chem. 282(35), 25464-25474. Published online 2007/06/26 DOI: 10.1074/jbc.M703663200.

Changotra, H., Jia, Y., Moore, T.N., Liu, G., Kahan, S.M., Sosnovtsev, S.V., and Karst, S.M. (2009). Type I and type II interferons inhibit the translation of murine norovirus proteins. J Virol. 83(11), 5683-5692. Published online 2009/03/18 DOI: 10.1128/JVI.00231-09.

Chauhan, S., Mandell, M.A., and Deretic, V. (2015). IRGM Governs the Core Autophagy Machinery to Conduct Antimicrobial Defense. Mol Cell. 58(3), 507-521. DOI: 10.1016/j.molcel.2015.03.020.

Cheng, Y.S., Colonno, R.J., and Yin, F.H. (1983). Interferon induction of fibroblast proteins with guanylate binding activity. J Biol Chem. 258(12), 7746-7750.

Choi, J., Biering, S.B., and Hwang, S. (2016). Quo vadis? Interferon-inducible GTPases go to their target membranes via the LC3-conjugation system of autophagy. Small GTPases. 1-9. Published online 2016/07/18 DOI: 10.1080/21541248.2016.1213090.

Choi, J., Park, S., Biering, S.B., Selleck, E., Liu, C.Y., Zhang, X., Fujita, N., Saitoh, T., Akira, S., Yoshimori, T., et al. (2014). The parasitophorous vacuole membrane of Toxoplasma gondii is targeted for disruption by ubiquitin-like conjugation systems of autophagy. Immunity. 40(6), 924-935. DOI: 10.1016/j.immuni.2014.05.006.

Choi, Y., Bowman, J.W., and Jung, J.U. (2018). Autophagy during viral infection - a double-edged sword. Nat Rev Microbiol. Published online 2018/03/19 DOI: 10.1038/s41579-018-0003-6.

Chung, L., Bailey, D., Leen, E.N., Emmott, E.P., Chaudhry, Y., Roberts, L.O., Curry, S., Locker, N., and Goodfellow, I.G. (2014). Norovirus translation requires an interaction between the C Terminus of the genome-linked viral protein VPg and eukaryotic translation initiation factor 4G. J Biol Chem. 289(31), 21738-21750. Published online 2014/06/13 DOI: 10.1074/jbc.M114.550657.

Coers, J. (2013). Self and non-self discrimination of intracellular membranes by the innate immune system. PLoS Pathog. 9(9), e1003538. DOI: 10.1371/journal.ppat.1003538.

Coers, J., Bernstein-Hanley, I., Grotsky, D., Parvanova, I., Howard, J.C., Taylor, G.A., Dietrich, W.F., and Starnbach, M.N. (2008). Chlamydia muridarum evades growth restriction by the IFN-gamma-inducible host resistance factor Irgb10. J Immunol. 180(9), 6237-6245.

Collazo, C.M., Yap, G.S., Sempowski, G.D., Lusby, K.C., Tessarollo, L., Vande Woude, G.F., Sher, A., and Taylor, G.A. (2001). Inactivation of LRG-47 and IRG-47 reveals a family of interferon gamma-inducible genes with essential, pathogen-specific roles in resistance to infection. J Exp Med. 194(2), 181-188.

Coombes, J.L., Siddiqui, K.R., Arancibia-Cárcamo, C.V., Hall, J., Sun, C.M., Belkaid, Y., and Powrie, F. (2007). A functionally specialized population of mucosal CD103+ DCs induces Foxp3+ regulatory T cells via a TGF-beta and retinoic acid-dependent mechanism. J Exp Med. 204(8), 1757-1764. Published online 2007/07/09 DOI: 10.1084/jem.20070590.

Corona, A.K., Saulsbery, H.M., Corona Velazquez, A.F., and Jackson, W.T. (2018). Enteroviruses Remodel Autophagic Trafficking through Regulation of Host SNARE Proteins to Promote Virus Replication and Cell Exit. Cell Rep. 22(12), 3304-3314. DOI: 10.1016/j.celrep.2018.03.003.

Cotton, B.T., Hyde, J.L., Sarvestani, S.T., Sosnovtsev, S.V., Green, K.Y., White, P.A., and Mackenzie, J.M. (2017). The Norovirus NS3 Protein Is a Dynamic Lipid- and Microtubule-Associated Protein Involved in Viral RNA Replication. J Virol. 91(3). Published online 2017/01/18 DOI: 10.1128/JVI.02138-16.

Cox, C., Cao, S., and Lu, Y. (2009). Enhanced detection and study of murine norovirus-1 using a more efficient microglial cell line. Virol J. 6, 196. Published online 2009/11/10 DOI: 10.1186/1743-422X-6-196.

Daughenbaugh, K.F., Wobus, C.E., and Hardy, M.E. (2006). VPg of murine norovirus binds translation initiation factors in infected cells. Virol J. 3, 33. Published online 2006/05/23 DOI: 10.1186/1743-422X-3-33.

Daugherty, M.D., and Malik, H.S. (2012). Rules of engagement: molecular insights from host-virus arms races. Annu Rev Genet. 46, 677-700. DOI: 10.1146/annurev-genet-110711-155522.

Degrandi, D., Konermann, C., Beuter-Gunia, C., Kresse, A., Würthner, J., Kurig, S., Beer, S., and Pfeffer, K. (2007). Extensive characterization of IFN-induced GTPases mGBP1 to mGBP10 involved in host defense. J Immunol. 179(11), 7729-7740.

DeJesus, R., Moretti, F., McAllister, G., Wang, Z., Bergman, P., Liu, S., Frias, E., Alford, J., Reece-Hoyes, J.S., Lindeman, A., et al. (2016). Functional CRISPR screening identifies the ufmylation pathway as a regulator of SQSTM1/p62. Elife. 5. Published online 2016/06/28 DOI: 10.7554/eLife.17290.

den Boon, J.A., and Ahlquist, P. (2010). Organelle-like membrane compartmentalization of positive-strand RNA virus replication factories. Annu Rev Microbiol. 64, 241-256. DOI: 10.1146/annurev.micro.112408.134012.

den Boon, J.A., Diaz, A., and Ahlquist, P. (2010). Cytoplasmic viral replication complexes. Cell Host Microbe. 8(1), 77-85. DOI: 10.1016/j.chom.2010.06.010.

Deng, X., Hackbart, M., Mettelman, R.C., O'Brien, A., Mielech, A.M., Yi, G., Kao, C.C., and Baker, S.C. (2017). Coronavirus nonstructural protein 15 mediates evasion of dsRNA sensors and limits apoptosis in macrophages. Proc Natl Acad Sci U S A. 114(21), E4251-E4260. Published online 2017/05/08 DOI: 10.1073/pnas.1618310114.

DeSelm, C.J., Miller, B.C., Zou, W., Beatty, W.L., van Meel, E., Takahata, Y., Klumperman, J., Tooze, S.A., Teitelbaum, S.L., and Virgin, H.W. (2011). Autophagy proteins regulate the secretory component of osteoclastic bone resorption. Dev Cell. 21(5), 966-974. Published online 2011/11/04 DOI: 10.1016/j.devcel.2011.08.016.

Diao, J., Liu, R., Rong, Y., Zhao, M., Zhang, J., Lai, Y., Zhou, Q., Wilz, L.M., Li, J., Vivona, S., et al. (2015). ATG14 promotes membrane tethering and fusion of autophagosomes to endolysosomes. Nature. 520(7548), 563-566. Published online 2015/02/09 DOI: 10.1038/nature14147.

Doerflinger, S.Y., Cortese, M., Romero-Brey, I., Menne, Z., Tubiana, T., Schenk, C., White, P.A., Bartenschlager, R., Bressanelli, S., Hansman, G.S., et al. (2017). Membrane alterations induced by nonstructural proteins of human norovirus. PLoS Pathog. 13(10), e1006705. Published online 2017/10/27 DOI: 10.1371/journal.ppat.1006705.

Dong, X., and Levine, B. (2013). Autophagy and viruses: adversaries or allies? J Innate Immun. 5(5), 480-493. Published online 2013/01/31 DOI: 10.1159/000346388.

Dooley, H.C., Razi, M., Polson, H.E., Girardin, S.E., Wilson, M.I., and Tooze, S.A. (2014). WIPI2 links LC3 conjugation with PI3P, autophagosome formation, and pathogen clearance by recruiting Atg12-5-16L1. Mol Cell. 55(2), 238-252. DOI: 10.1016/j.molcel.2014.05.021.

Dreux, M., and Chisari, F.V. (2010). Viruses and the autophagy machinery. Cell Cycle. 9(7), 1295-1307. DOI: 10.4161/cc.9.7.11109.

Dreux, M., Gastaminza, P., Wieland, S.F., and Chisari, F.V. (2009). The autophagy machinery is required to initiate hepatitis C virus replication. Proc Natl Acad Sci U S A. 106(33), 14046-14051. Published online 2009/08/03 DOI: 10.1073/pnas.0907344106.

Duizer, E., Schwab, K.J., Neill, F.H., Atmar, R.L., Koopmans, M.P., and Estes, M.K. (2004). Laboratory efforts to cultivate noroviruses. J Gen Virol. 85(Pt 1), 79-87.

Engel, A.R., Vasconcelos, P.F., McArthur, M.A., and Barrett, A.D. (2006). Characterization of a viscerotropic yellow fever vaccine variant from a patient in Brazil. Vaccine. 24(15), 2803-2809. Published online 2006/01/18 DOI: 10.1016/j.vaccine.2006.01.009.

English, L., Chemali, M., Duron, J., Rondeau, C., Laplante, A., Gingras, D., Alexander, D., Leib, D., Norbury, C., Lippé, R., et al. (2009). Autophagy enhances the presentation of endogenous viral antigens on MHC class I molecules during HSV-1 infection. Nat Immunol. 10(5), 480-487. Published online 2009/03/22 DOI: 10.1038/ni.1720.

Esterházy, D., Loschko, J., London, M., Jove, V., Oliveira, T.Y., and Mucida, D. (2016). Classical dendritic cells are required for dietary antigen-mediated induction of peripheral T(reg) cells and tolerance. Nat Immunol. 17(5), 545-555. Published online 2016/03/28 DOI: 10.1038/ni.3408.

Ettayebi, K., Crawford, S.E., Murakami, K., Broughman, J.R., Karandikar, U., Tenge, V.R., Neill, F.H., Blutt, S.E., Zeng, X.L., Qu, L., et al. (2016). Replication of human noroviruses in stem cell-derived human enteroids. Science. 353(6306), 1387-1393. Published online 2016/08/25 DOI: 10.1126/science.aaf5211.

Feng, Y., He, D., Yao, Z., and Klionsky, D.J. (2014). The machinery of macroautophagy. Cell Res. 24(1), 24-41. DOI: 10.1038/cr.2013.168.

Fentress, S.J., Behnke, M.S., Dunay, I.R., Mashayekhi, M., Rommereim, L.M., Fox, B.A., Bzik, D.J., Taylor, G.A., Turk, B.E., Lichti, C.F., et al. (2010). Phosphorylation of immunity-related GTPases by a Toxoplasma gondii-secreted kinase promotes macrophage survival and virulence. Cell Host Microbe. 8(6), 484-495. DOI: 10.1016/j.chom.2010.11.005.

Ferreira-da-Silva, M.a.F., da Fonseca Ferreira-da-Silva, M., Springer-Frauenhoff, H.M., Bohne, W., and Howard, J.C. (2014). Identification of the microsporidian Encephalitozoon cuniculi as a new target of the IFNγ-inducible IRG resistance system. PLoS Pathog. 10(10), e1004449. DOI: 10.1371/journal.ppat.1004449.

Fleckenstein, M.C., Reese, M.L., Könen-Waisman, S., Boothroyd, J.C., Howard, J.C., and Steinfeldt, T. (2012). A Toxoplasma gondii pseudokinase inhibits host IRG resistance proteins. PLoS Biol. 10(7), e1001358. Published online 2012/07/10 DOI: 10.1371/journal.pbio.1001358.

Fleeton, M.N., Contractor, N., Leon, F., Wetzel, J.D., Dermody, T.S., and Kelsall, B.L. (2004). Peyer's patch dendritic cells process viral antigen from apoptotic epithelial cells in the intestine of reovirus-infected mice. J Exp Med. 200(2), 235-245. DOI: 10.1084/jem.20041132.

Fujita, N., Itoh, T., Omori, H., Fukuda, M., Noda, T., and Yoshimori, T. (2008). The Atg16L complex specifies the site of LC3 lipidation for membrane biogenesis in autophagy. Mol Biol Cell. 19(5), 2092-2100. DOI: 10.1091/mbc.E07-12-1257.

Fujita, N., Morita, E., Itoh, T., Tanaka, A., Nakaoka, M., Osada, Y., Umemoto, T., Saitoh, T., Nakatogawa, H., Kobayashi, S., et al. (2013). Recruitment of the autophagic machinery to endosomes during infection is mediated by ubiquitin. J Cell Biol. 203(1), 115-128. DOI: 10.1083/jcb.201304188.

Furman, L.M., Maaty, W.S., Petersen, L.K., Ettayebi, K., Hardy, M.E., and Bothner, B. (2009). Cysteine protease activation and apoptosis in Murine norovirus infection. Virol J. 6, 139. Published online 2009/09/10 DOI: 10.1186/1743-422X-6-139.

Gannagé, M., Dormann, D., Albrecht, R., Dengjel, J., Torossi, T., Rämer, P.C., Lee, M., Strowig, T., Arrey, F., Conenello, G., et al. (2009). Matrix protein 2 of influenza A virus blocks autophagosome fusion with lysosomes. Cell Host Microbe. 6(4), 367-380. DOI: 10.1016/j.chom.2009.09.005.

García-Sastre, A. (2017). Ten Strategies of Interferon Evasion by Viruses. Cell Host Microbe. 22(2), 176-184. DOI: 10.1016/j.chom.2017.07.012.

Gazzinelli, R.T., Mendonça-Neto, R., Lilue, J., Howard, J., and Sher, A. (2014). Innate resistance against Toxoplasma gondii: an evolutionary tale of mice, cats, and men. Cell Host Microbe. 15(2), 132-138. DOI: 10.1016/j.chom.2014.01.004.

Gerondopoulos, A., Jackson, T., Monaghan, P., Doyle, N., and Roberts, L.O. (2010). Murine norovirus-1 cell entry is mediated through a non-clathrin-, non-caveolae-, dynamin- and cholesterol-dependent pathway. J Gen Virol. 91(Pt 6), 1428-1438. Published online 2010/02/10 DOI: 10.1099/vir.0.016717-0.

Glass, R.I., Parashar, U.D., and Estes, M.K. (2009). Norovirus gastroenteritis. N Engl J Med. 361(18), 1776-1785. DOI: 10.1056/NEJMra0804575.

Goubau, D., Schlee, M., Deddouche, S., Pruijssers, A.J., Zillinger, T., Goldeck, M., Schuberth, C., Van der Veen, A.G., Fujimura, T., Rehwinkel, J., et al. (2014). Antiviral immunity via RIG-I-mediated recognition of RNA bearing 5'-diphosphates. Nature. 514(7522), 372-375. Published online 2014/08/10 DOI: 10.1038/nature13590.

Grau, K.R., Roth, A.N., Zhu, S., Hernandez, A., Colliou, N., DiVita, B.B., Philip, D.T., Riffe, C., Giasson, B., Wallet, S.M., et al. (2017). The major targets of acute norovirus infection are immune cells in the gut-associated lymphoid tissue. Nat Microbiol. 2(12), 1586-1591. Published online 2017/11/06 DOI: 10.1038/s41564-017-0057-7.

Grégoire, I.P., Richetta, C., Meyniel-Schicklin, L., Borel, S., Pradezynski, F., Diaz, O., Deloire, A., Azocar, O., Baguet, J., Le Breton, M., et al. (2011). IRGM is a common target of RNA viruses that subvert the autophagy network. PLoS Pathog. 7(12), e1002422. DOI: 10.1371/journal.ppat.1002422.

Guenzi, E., Töpolt, K., Cornali, E., Lubeseder-Martellato, C., Jörg, A., Matzen, K., Zietz, C., Kremmer, E., Nappi, F., Schwemmle, M., et al. (2001). The helical domain of GBP-1 mediates the inhibition of endothelial cell proliferation by inflammatory cytokines. EMBO J. 20(20), 5568-5577. DOI: 10.1093/emboj/20.20.5568.

Guenzi, E., Töpolt, K., Lubeseder-Martellato, C., Jörg, A., Naschberger, E., Benelli, R., Albini, A., and Stürzl, M. (2003). The guanylate binding protein-1 GTPase controls the invasive and angiogenic capability of endothelial cells through inhibition of MMP-1 expression. EMBO J. 22(15), 3772-3782. DOI: 10.1093/emboj/cdg382.

Guévin, C., Manna, D., Bélanger, C., Konan, K.V., Mak, P., and Labonté, P. (2010). Autophagy protein ATG5 interacts transiently with the hepatitis C virus RNA polymerase (NS5B) early during infection. Virology. 405(1), 1-7. Published online 2010/06/26 DOI: 10.1016/j.virol.2010.05.032.

Haga, K., Fujimoto, A., Takai-Todaka, R., Miki, M., Doan, Y.H., Murakami, K., Yokoyama, M., Murata, K., Nakanishi, A., and Katayama, K. (2016). Functional receptor molecules CD300lf and CD300ld within the CD300 family enable murine noroviruses to infect cells. Proc Natl Acad Sci U S A. 113(41), E6248-E6255. Published online 2016/09/28 DOI: 10.1073/pnas.1605575113.

Haldar, A.K., Foltz, C., Finethy, R., Piro, A.S., Feeley, E.M., Pilla-Moffett, D.M., Komatsu, M., Frickel, E.M., and Coers, J. (2015). Ubiquitin systems mark pathogen-containing vacuoles as targets for host defense by guanylate binding proteins. Proc Natl Acad Sci U S A. 112(41), E5628-5637. Published online 2015/09/28 DOI: 10.1073/pnas.1515966112.

Haldar, A.K., Piro, A.S., Finethy, R., Espenschied, S.T., Brown, H.E., Giebel, A.M., Frickel, E.M., Nelson, D.E., and Coers, J. (2016). Chlamydia trachomatis Is Resistant to Inclusion Ubiquitination and Associated Host Defense in Gamma Interferon-Primed Human Epithelial Cells. MBio. 7(6). Published online 2016/12/13 DOI: 10.1128/mBio.01417-16.

Haldar, A.K., Piro, A.S., Pilla, D.M., Yamamoto, M., and Coers, J. (2014). The E2-like conjugation enzyme Atg3 promotes binding of IRG and Gbp proteins to Chlamydia- and Toxoplasma-containing vacuoles and host resistance. PLoS One. 9(1), e86684. DOI: 10.1371/journal.pone.0086684.

Haldar, A.K., Saka, H.A., Piro, A.S., Dunn, J.D., Henry, S.C., Taylor, G.A., Frickel, E.M., Valdivia, R.H., and Coers, J. (2013). IRG and GBP host resistance factors target aberrant, "non-self" vacuoles characterized by the missing of "self" IRGM proteins. PLoS Pathog. 9(6), e1003414. DOI: 10.1371/journal.ppat.1003414.

Haller, O., Staeheli, P., Schwemmle, M., and Kochs, G. (2015). Mx GTPases: dynamin-like antiviral machines of innate immunity. Trends Microbiol. 23(3), 154-163. Published online 2015/01/06 DOI: 10.1016/j.tim.2014.12.003.

Harak, C., and Lohmann, V. (2015). Ultrastructure of the replication sites of positive-strand RNA viruses. Virology. 479-480, 418-433. Published online 2015/03/06 DOI: 10.1016/j.virol.2015.02.029.

He, C., and Klionsky, D.J. (2009). Regulation mechanisms and signaling pathways of autophagy. Annu Rev Genet. 43, 67-93. DOI: 10.1146/annurev-genet-102808-114910.

Heaton, N.S., and Randall, G. (2010). Dengue virus-induced autophagy regulates lipid metabolism. Cell Host Microbe. 8(5), 422-432. DOI: 10.1016/j.chom.2010.10.006.

Henry, S.C., Daniell, X.G., Burroughs, A.R., Indaram, M., Howell, D.N., Coers, J., Starnbach, M.N., Hunn, J.P., Howard, J.C., Feng, C.G., et al. (2009). Balance of Irgm protein activities determines IFN-gamma-induced host defense. J Leukoc Biol. 85(5), 877-885. DOI: 10.1189/jlb.1008599.

Hitomi, J., Christofferson, D.E., Ng, A., Yao, J., Degterev, A., Xavier, R.J., and Yuan, J. (2008). Identification of a molecular signaling network that regulates a cellular necrotic cell death pathway. Cell. 135(7), 1311-1323. DOI: 10.1016/j.cell.2008.10.044.

Howard, J.C., Hunn, J.P., and Steinfeldt, T. (2011). The IRG protein-based resistance mechanism in mice and its relation to virulence in Toxoplasma gondii. Curr Opin Microbiol. 14(4), 414-421. DOI: 10.1016/j.mib.2011.07.002.

Hunn, J.P., Koenen-Waisman, S., Papic, N., Schroeder, N., Pawlowski, N., Lange, R., Kaiser, F., Zerrahn, J., Martens, S., and Howard, J.C. (2008). Regulatory interactions

between IRG resistance GTPases in the cellular response to Toxoplasma gondii. EMBO J. 27(19), 2495-2509. DOI: 10.1038/emboj.2008.176.

Hunter, C.A., and Sibley, L.D. (2012). Modulation of innate immunity by Toxoplasma gondii virulence effectors. Nat Rev Microbiol. 10(11), 766-778. DOI: 10.1038/nrmicro2858.

Hwang, S., Alhatlani, B., Arias, A., Caddy, S.L., Christodoulou, C., Cunha, J.B., Emmott, E., Gonzalez-Hernandez, M., Kolawole, A., Lu, J., et al. (2014). Murine norovirus: propagation, quantification, and genetic manipulation. Curr Protoc Microbiol. 33, 15K.12.11-15K.12.61. DOI: 10.1002/9780471729259.mc15k02s33.

Hwang, S., Maloney, N.S., Bruinsma, M.W., Goel, G., Duan, E., Zhang, L., Shrestha, B., Diamond, M.S., Dani, A., Sosnovtsev, S.V., et al. (2012). Nondegradative role of Atg5-Atg12/ Atg16L1 autophagy protein complex in antiviral activity of interferon gamma. Cell Host Microbe. 11(4), 397-409. DOI: 10.1016/j.chom.2012.03.002.

Hyde, J.L., Gillespie, L.K., and Mackenzie, J.M. (2012). Mouse norovirus 1 utilizes the cytoskeleton network to establish localization of the replication complex proximal to the microtubule organizing center. J Virol. 86(8), 4110-4122. Published online 2012/02/01 DOI: 10.1128/JVI.05784-11.

Hyde, J.L., and Mackenzie, J.M. (2010). Subcellular localization of the MNV-1 ORF1 proteins and their potential roles in the formation of the MNV-1 replication complex. Virology. 406(1), 138-148. Published online 2010/08/01 DOI: 10.1016/j.virol.2010.06.047.

Hyde, J.L., Sosnovtsev, S.V., Green, K.Y., Wobus, C., Virgin, H.W., and Mackenzie, J.M. (2009). Mouse norovirus replication is associated with virus-induced vesicle clusters originating from membranes derived from the secretory pathway. J Virol. 83(19), 9709-9719. DOI: 10.1128/JVI.00600-09.

Itakura, E., Kishi-Itakura, C., and Mizushima, N. (2012). The hairpin-type tail-anchored SNARE syntaxin 17 targets to autophagosomes for fusion with endosomes/lysosomes. Cell. 151(6), 1256-1269. DOI: 10.1016/j.cell.2012.11.001.

Jabri, B., and Sollid, L.M. (2009). Tissue-mediated control of immunopathology in coeliac disease. Nat Rev Immunol. 9(12), 858-870. DOI: 10.1038/nri2670.

Jackson, W.T., Giddings, T.H., Taylor, M.P., Mulinyawe, S., Rabinovitch, M., Kopito, R.R., and Kirkegaard, K. (2005). Subversion of cellular autophagosomal machinery by RNA viruses. PLoS Biol. 3(5), e156. Published online 2005/04/26 DOI: 10.1371/journal.pbio.0030156.

Jensen, S., and Thomsen, A.R. (2012). Sensing of RNA viruses: a review of innate immune receptors involved in recognizing RNA virus invasion. J Virol. 86(6), 2900-2910. Published online 2012/01/18 DOI: 10.1128/JVI.05738-11.

Jia, W., and He, Y.W. (2011). Temporal regulation of intracellular organelle homeostasis in T lymphocytes by autophagy. J Immunol. 186(9), 5313-5322. DOI: 10.4049/jimmunol.1002404.

Johnston, A.C., Piro, A., Clough, B., Siew, M., Virreira Winter, S., Coers, J., and Frickel, E.M. (2016). Human GBP1 does not localize to pathogen vacuoles but restricts Toxoplasma gondii. Cell Microbiol. 18(8), 1056-1064. Published online 2016/03/10 DOI: 10.1111/cmi.12579.

Jones, J.L., Krueger, A., Schulkin, J., and Schantz, P.M. (2010). Toxoplasmosis prevention and testing in pregnancy, survey of obstetrician-gynaecologists. Zoonoses Public Health. 57(1), 27-33. Published online 2009/09/10 DOI: 10.1111/j.1863-2378.2009.01277.x.

Jones, M.K., Watanabe, M., Zhu, S., Graves, C.L., Keyes, L.R., Grau, K.R., Gonzalez-Hernandez, M.B., Iovine, N.M., Wobus, C.E., Vinjé, J., et al. (2014). Enteric bacteria promote human and mouse norovirus infection of B cells. Science. 346(6210), 755-759. DOI: 10.1126/science.1257147.

Jordan, T.X., and Randall, G. (2012). Manipulation or capitulation: virus interactions with autophagy. Microbes Infect. 14(2), 126-139. Published online 2011/10/24 DOI: 10.1016/j.micinf.2011.09.007.

Jordan, T.X., and Randall, G. (2017). Dengue Virus Activates the AMP Kinase-mTOR Axis To Stimulate a Proviral Lipophagy. J Virol. 91(11). Published online 2017/05/12 DOI: 10.1128/JVI.02020-16.

KALLMAN, F., WILLIAMS, R.C., DULBECCO, R., and VOGT, M. (1958). Fine structure of changes produced in cultured cells sampled at specified intervals during a single growth cycle of polio virus. J Biophys Biochem Cytol. 4(3), 301-308.

Karst, S.M., Wobus, C.E., Lay, M., Davidson, J., and Virgin, H.W. (2003). STAT1-dependent innate immunity to a Norwalk-like virus. Science. 299(5612), 1575-1578. DOI: 10.1126/science.1077905.

Kernbauer, E., Ding, Y., and Cadwell, K. (2014). An enteric virus can replace the beneficial function of commensal bacteria. Nature. 516(7529), 94-98. Published online 2014/11/19 DOI: 10.1038/nature13960.

Kim, B.H., Chee, J.D., Bradfield, C.J., Park, E.S., Kumar, P., and MacMicking, J.D. (2016). Interferon-induced guanylate-binding proteins in inflammasome activation and host defense. Nat Immunol. 17(5), 481-489. DOI: 10.1038/ni.3440.

Kim, B.H., Shenoy, A.R., Kumar, P., Bradfield, C.J., and MacMicking, J.D. (2012). IFN-inducible GTPases in host cell defense. Cell Host Microbe. 12(4), 432-444. DOI: 10.1016/j.chom.2012.09.007.

Kim, B.H., Shenoy, A.R., Kumar, P., Das, R., Tiwari, S., and MacMicking, J.D. (2011). A family of IFN-γ-inducible 65-kD GTPases protects against bacterial infection. Science. 332(6030), 717-721. DOI: 10.1126/science.1201711.

Kim, D., Pertea, G., Trapnell, C., Pimentel, H., Kelley, R., and Salzberg, S.L. (2013). TopHat2: accurate alignment of transcriptomes in the presence of insertions, deletions and gene fusions. Genome Biol. 14(4), R36. Published online 2013/04/25 DOI: 10.1186/gb-2013-14-4-r36.

Kim, M., Lee, H., Chang, K.O., and Ko, G. (2010). Molecular characterization of murine norovirus isolates from South Korea. Virus Res. 147(1), 1-6. Published online 2009/09/30 DOI: 10.1016/j.virusres.2009.08.013.

Kimura, T., Nakayama, K., Penninger, J., Kitagawa, M., Harada, H., Matsuyama, T., Tanaka, N., Kamijo, R., Vilcek, J., and Mak, T.W. (1994). Involvement of the IRF-1 transcription factor in antiviral responses to interferons. Science. 264(5167), 1921-1924.

Knoops, K., Kikkert, M., Worm, S.H., Zevenhoven-Dobbe, J.C., van der Meer, Y., Koster, A.J., Mommaas, A.M., and Snijder, E.J. (2008). SARS-coronavirus replication is supported by a reticulovesicular network of modified endoplasmic reticulum. PLoS Biol. 6(9), e226. DOI: 10.1371/journal.pbio.0060226.

Kodama, Y., and Hu, C.D. (2012). Bimolecular fluorescence complementation (BiFC): a 5-year update and future perspectives. Biotechniques. 53(5), 285-298. DOI: 10.2144/000113943.

Kolawole, A.O., Gonzalez-Hernandez, M.B., Turula, H., Yu, C., Elftman, M.D., and Wobus, C.E. (2016). Oral Norovirus Infection Is Blocked in Mice Lacking Peyer's Patches and Mature M Cells. J Virol. 90(3), 1499-1506. Published online 2015/11/18 DOI: 10.1128/JVI.02872-15.

Koonin, E.V., and Dolja, V.V. (1993). Evolution and taxonomy of positive-strand RNA viruses: implications of comparative analysis of amino acid sequences. Crit Rev Biochem Mol Biol. 28(5), 375-430. DOI: 10.3109/10409239309078440.

Kopek, B.G., Perkins, G., Miller, D.J., Ellisman, M.H., and Ahlquist, P. (2007). Three-dimensional analysis of a viral RNA replication complex reveals a virus-induced mini-organelle. PLoS Biol. 5(9), e220. DOI: 10.1371/journal.pbio.0050220.

Krapp, C., Hotter, D., Gawanbacht, A., McLaren, P.J., Kluge, S.F., Stürzel, C.M., Mack, K., Reith, E., Engelhart, S., Ciuffi, A., et al. (2016). Guanylate Binding Protein (GBP) 5

Is an Interferon-Inducible Inhibitor of HIV-1 Infectivity. Cell Host Microbe. 19(4), 504-514. Published online 2016/03/17 DOI: 10.1016/j.chom.2016.02.019.

Kravets, E., Degrandi, D., Ma, Q., Peulen, T.O., Klümpers, V., Felekyan, S., Kühnemuth, R., Weidtkamp-Peters, S., Seidel, C.A., and Pfeffer, K. (2016). Guanylate binding proteins directly attack Toxoplasma gondii via supramolecular complexes. Elife. 5. Published online 2016/01/27 DOI: 10.7554/eLife.11479.

Kravets, E., Degrandi, D., Weidtkamp-Peters, S., Ries, B., Konermann, C., Felekyan, S., Dargazanli, J.M., Praefcke, G.J., Seidel, C.A., Schmitt, L., et al. (2012). The GTPase activity of murine guanylate-binding protein 2 (mGBP2) controls the intracellular localization and recruitment to the parasitophorous vacuole of Toxoplasma gondii. J Biol Chem. 287(33), 27452-27466. Published online 2012/06/22 DOI: 10.1074/jbc.M112.379636.

Kresse, A., Konermann, C., Degrandi, D., Beuter-Gunia, C., Wuerthner, J., Pfeffer, K., and Beer, S. (2008). Analyses of murine GBP homology clusters based on in silico, in vitro and in vivo studies. BMC Genomics. 9, 158. Published online 2008/04/10 DOI: 10.1186/1471-2164-9-158.

Kumar, Y., and Valdivia, R.H. (2009). Leading a sheltered life: intracellular pathogens and maintenance of vacuolar compartments. Cell Host Microbe. 5(6), 593-601. DOI: 10.1016/j.chom.2009.05.014.

Lam, L.K.M., Watson, A.M., Ryman, K.D., and Klimstra, W.B. (2018). Gamma-interferon exerts a critical early restriction on replication and dissemination of yellow fever virus vaccine strain 17D-204. NPJ Vaccines. 3, 5. Published online 2018/01/23 DOI: 10.1038/s41541-017-0039-z.

Lau, L., Gray, E.E., Brunette, R.L., and Stetson, D.B. (2015). DNA tumor virus oncogenes antagonize the cGAS-STING DNA-sensing pathway. Science. 350(6260), 568-571. Published online 2015/09/24 DOI: 10.1126/science.aab3291.

Lee, H.K., Lund, J.M., Ramanathan, B., Mizushima, N., and Iwasaki, A. (2007). Autophagy-dependent viral recognition by plasmacytoid dendritic cells. Science. 315(5817), 1398-1401. Published online 2007/02/01 DOI: 10.1126/science.1136880.

Lee, H.K., Mattei, L.M., Steinberg, B.E., Alberts, P., Lee, Y.H., Chervonsky, A., Mizushima, N., Grinstein, S., and Iwasaki, A. (2010). In vivo requirement for Atg5 in antigen presentation by dendritic cells. Immunity. 32(2), 227-239. Published online 2010/02/18 DOI: 10.1016/j.immuni.2009.12.006.

Lee, S., Wilen, C.B., Orvedahl, A., McCune, B.T., Kim, K.W., Orchard, R.C., Peterson, S.T., Nice, T.J., Baldridge, M.T., and Virgin, H.W. (2017). Norovirus Cell Tropism Is Determined by Combinatorial Action of a Viral Non-structural Protein and Host Cytokine.

Cell Host Microbe. 22(4), 449-459.e444. Published online 2017/09/28 DOI: 10.1016/j.chom.2017.08.021.

Levine, B., Mizushima, N., and Virgin, H.W. (2011). Autophagy in immunity and inflammation. Nature. 469(7330), 323-335. DOI: 10.1038/nature09782.

Li, B., and Dewey, C.N. (2011). RSEM: accurate transcript quantification from RNA-Seq data with or without a reference genome. BMC Bioinformatics. 12, 323. DOI: 10.1186/1471-2105-12-323.

Li, G., Zhang, J., Sun, Y., Wang, H., and Wang, Y. (2009). The evolutionarily dynamic IFN-inducible GTPase proteins play conserved immune functions in vertebrates and cephalochordates. Mol Biol Evol. 26(7), 1619-1630. Published online 2009/04/15 DOI: 10.1093/molbev/msp074.

Liang, X.H., Kleeman, L.K., Jiang, H.H., Gordon, G., Goldman, J.E., Berry, G., Herman, B., and Levine, B. (1998). Protection against fatal Sindbis virus encephalitis by beclin, a novel Bcl-2-interacting protein. J Virol. 72(11), 8586-8596.

Liu, J., Cao, S., Herman, L.M., and Ma, X. (2003). Differential regulation of interleukin (IL)-12 p35 and p40 gene expression and interferon (IFN)-gamma-primed IL-12 production by IFN regulatory factor 1. J Exp Med. 198(8), 1265-1276. DOI: 10.1084/jem.20030026.

Liu, J., Guan, X., and Ma, X. (2005). Interferon regulatory factor 1 is an essential and direct transcriptional activator for interferon {gamma}-induced RANTES/CCl5 expression in macrophages. J Biol Chem. 280(26), 24347-24355. Published online 2005/04/27 DOI: 10.1074/jbc.M500973200.

Loo, Y.M., Fornek, J., Crochet, N., Bajwa, G., Perwitasari, O., Martinez-Sobrido, L., Akira, S., Gill, M.A., García-Sastre, A., Katze, M.G., et al. (2008). Distinct RIG-I and MDA5 signaling by RNA viruses in innate immunity. J Virol. 82(1), 335-345. Published online 2007/10/17 DOI: 10.1128/JVI.01080-07.

Lord, P.W., Stevens, R.D., Brass, A., and Goble, C.A. (2003). Investigating semantic similarity measures across the Gene Ontology: the relationship between sequence and annotation. Bioinformatics. 19(10), 1275-1283.

MacMicking, J.D., Taylor, G.A., and McKinney, J.D. (2003). Immune control of tuberculosis by IFN-gamma-inducible LRG-47. Science. 302(5645), 654-659. DOI: 10.1126/science.1088063.

Macpherson, A.J., and Smith, K. (2006). Mesenteric lymph nodes at the center of immune anatomy. J Exp Med. 203(3), 497-500. Published online 2006/03/13 DOI: 10.1084/jem.20060227.

Maloney, N.S., Thackray, L.B., Goel, G., Hwang, S., Duan, E., Vachharajani, P., Xavier, R., and Virgin, H.W. (2012). Essential cell-autonomous role for interferon (IFN) regulatory factor 1 in IFN-γ-mediated inhibition of norovirus replication in macrophages. J Virol. 86(23), 12655-12664. DOI: 10.1128/JVI.01564-12.

Maric-Biresev, J., Hunn, J.P., Krut, O., Helms, J.B., Martens, S., and Howard, J.C. (2016). Loss of the interferon-γ-inducible regulatory immunity-related GTPase (IRG), Irgm1, causes activation of effector IRG proteins on lysosomes, damaging lysosomal function and predicting the dramatic susceptibility of Irgm1-deficient mice to infection. BMC Biol. 14, 33. Published online 2016/04/20 DOI: 10.1186/s12915-016-0255-4.

Martens, S., Parvanova, I., Zerrahn, J., Griffiths, G., Schell, G., Reichmann, G., and Howard, J.C. (2005). Disruption of Toxoplasma gondii parasitophorous vacuoles by the mouse p47-resistance GTPases. PLoS Pathog. 1(3), e24. DOI: 10.1371/journal.ppat.0010024.

Martens, S., Sabel, K., Lange, R., Uthaiah, R., Wolf, E., and Howard, J.C. (2004). Mechanisms regulating the positioning of mouse p47 resistance GTPases LRG-47 and IIGP1 on cellular membranes: retargeting to plasma membrane induced by phagocytosis. J Immunol. 173(4), 2594-2606.

Matzinger, S.R., Carroll, T.D., Dutra, J.C., Ma, Z.M., and Miller, C.J. (2013). Myxovirus resistance gene A (MxA) expression suppresses influenza A virus replication in alpha interferon-treated primate cells. J Virol. 87(2), 1150-1158. Published online 2012/11/14 DOI: 10.1128/JVI.02271-12.

McAlpine, F., Williamson, L.E., Tooze, S.A., and Chan, E.Y. (2013). Regulation of nutrient-sensitive autophagy by uncoordinated 51-like kinases 1 and 2. Autophagy. 9(3), 361-373. DOI: 10.4161/auto.23066.

McCarthy, D.J., Chen, Y., and Smyth, G.K. (2012). Differential expression analysis of multifactor RNA-Seq experiments with respect to biological variation. Nucleic Acids Res. 40(10), 4288-4297. Published online 2012/01/28 DOI: 10.1093/nar/gks042.

McCartney, S.A., Thackray, L.B., Gitlin, L., Gilfillan, S., Virgin, H.W., Virgin Iv, H.W., and Colonna, M. (2008). MDA-5 recognition of a murine norovirus. PLoS Pathog. 4(7), e1000108. Published online 2008/07/18 DOI: 10.1371/journal.ppat.1000108.

McFadden, N., Bailey, D., Carrara, G., Benson, A., Chaudhry, Y., Shortland, A., Heeney, J., Yarovinsky, F., Simmonds, P., Macdonald, A., et al. (2011). Norovirus regulation of the innate immune response and apoptosis occurs via the product of the alternative open reading frame 4. PLoS Pathog. 7(12), e1002413. Published online 2011/12/08 DOI: 10.1371/journal.ppat.1002413.

Miyanari, Y., Hijikata, M., Yamaji, M., Hosaka, M., Takahashi, H., and Shimotohno, K. (2003). Hepatitis C virus non-structural proteins in the probable membranous

compartment function in viral genome replication. J Biol Chem. 278(50), 50301-50308. Published online 2003/09/08 DOI: 10.1074/jbc.M305684200.

Neufeldt, C.J., Joyce, M.A., Levin, A., Steenbergen, R.H., Pang, D., Shields, J., Tyrrell, D.L., and Wozniak, R.W. (2013). Hepatitis C virus-induced cytoplasmic organelles use the nuclear transport machinery to establish an environment conducive to virus replication. PLoS Pathog. 9(10), e1003744. Published online 2013/10/31 DOI: 10.1371/journal.ppat.1003744.

Neufeldt, C.J., Joyce, M.A., Van Buuren, N., Levin, A., Kirkegaard, K., Gale, M., Tyrrell, D.L., and Wozniak, R.W. (2016). The Hepatitis C Virus-Induced Membranous Web and Associated Nuclear Transport Machinery Limit Access of Pattern Recognition Receptors to Viral Replication Sites. PLoS Pathog. 12(2), e1005428. Published online 2016/02/10 DOI: 10.1371/journal.ppat.1005428.

Nice, T.J., Baldridge, M.T., McCune, B.T., Norman, J.M., Lazear, H.M., Artyomov, M., Diamond, M.S., and Virgin, H.W. (2015). Interferon-λ cures persistent murine norovirus infection in the absence of adaptive immunity. Science. 347(6219), 269-273. Published online 2014/11/27 DOI: 10.1126/science.1258100.

Nice, T.J., Strong, D.W., McCune, B.T., Pohl, C.S., and Virgin, H.W. (2013). A single-amino-acid change in murine norovirus NS1/2 is sufficient for colonic tropism and persistence. J Virol. 87(1), 327-334. Published online 2012/10/17 DOI: 10.1128/JVI.01864-12.

Niedelman, W., Sprokholt, J.K., Clough, B., Frickel, E.M., and Saeij, J.P. (2013). Cell death of gamma interferon-stimulated human fibroblasts upon Toxoplasma gondii infection induces early parasite egress and limits parasite replication. Infect Immun. 81(12), 4341-4349. Published online 2013/09/16 DOI: 10.1128/IAI.00416-13.

Niewiesk, S. (2014). Maternal antibodies: clinical significance, mechanism of interference with immune responses, and possible vaccination strategies. Front Immunol. 5, 446. Published online 2014/09/16 DOI: 10.3389/fimmu.2014.00446.

Nikonov, A., Mölder, T., Sikut, R., Kiiver, K., Männik, A., Toots, U., Lulla, A., Lulla, V., Utt, A., Merits, A., et al. (2013). RIG-I and MDA-5 detection of viral RNA-dependent RNA polymerase activity restricts positive-strand RNA virus replication. PLoS Pathog. 9(9), e1003610. Published online 2013/09/05 DOI: 10.1371/journal.ppat.1003610.

Ning, S., Pagano, J.S., and Barber, G.N. (2011). IRF7: activation, regulation, modification and function. Genes Immun. 12(6), 399-414. Published online 2011/04/14 DOI: 10.1038/gene.2011.21.

Nishimura, T., Kaizuka, T., Cadwell, K., Sahani, M.H., Saitoh, T., Akira, S., Virgin, H.W., and Mizushima, N. (2013). FIP200 regulates targeting of Atg16L1 to the isolation membrane. EMBO Rep. 14(3), 284-291. DOI: 10.1038/embor.2013.6.

Noda, N.N., and Inagaki, F. (2015). Mechanisms of Autophagy. Annu Rev Biophys. 44, 101-122. Published online 2015/02/26 DOI: 10.1146/annurev-biophys-060414-034248.

Nordmann, A., Wixler, L., Boergeling, Y., Wixler, V., and Ludwig, S. (2012). A new splice variant of the human guanylate-binding protein 3 mediates anti-influenza activity through inhibition of viral transcription and replication. FASEB J. 26(3), 1290-1300. DOI: 10.1096/fj.11-189886.

Novoa, R.R., Calderita, G., Arranz, R., Fontana, J., Granzow, H., and Risco, C. (2005). Virus factories: associations of cell organelles for viral replication and morphogenesis. Biol Cell. 97(2), 147-172. DOI: 10.1042/BC20040058.

O'Donnell, T.B., Hyde, J.L., Mintern, J.D., and Mackenzie, J.M. (2016). Mouse Norovirus infection promotes autophagy induction to facilitate replication but prevents final autophagosome maturation. Virology. 492, 130-139. Published online 2016/03/21 DOI: 10.1016/j.virol.2016.02.018.

Ohshima, J., Lee, Y., Sasai, M., Saitoh, T., Su Ma, J., Kamiyama, N., Matsuura, Y., Pann-Ghill, S., Hayashi, M., Ebisu, S., et al. (2014). Role of mouse and human autophagy proteins in IFN-γ-induced cell-autonomous responses against Toxoplasma gondii. J Immunol. 192(7), 3328-3335. DOI: 10.4049/jimmunol.1302822.

Olszewski, M.A., Gray, J., and Vestal, D.J. (2006). In silico genomic analysis of the human and murine guanylate-binding protein (GBP) gene clusters. J Interferon Cytokine Res. 26(5), 328-352. DOI: 10.1089/jir.2006.26.328.

Orchard, R.C., Wilen, C.B., Doench, J.G., Baldridge, M.T., McCune, B.T., Lee, Y.C., Lee, S., Pruett-Miller, S.M., Nelson, C.A., Fremont, D.H., et al. (2016). Discovery of a proteinaceous cellular receptor for a norovirus. Science. 353(6302), 933-936. Published online 2016/08/18 DOI: 10.1126/science.aaf1220.

Orvedahl, A., and Levine, B. (2008). Viral evasion of autophagy. Autophagy. 4(3), 280-285. Published online 2007/11/13.

Orvedahl, A., MacPherson, S., Sumpter, R., Tallóczy, Z., Zou, Z., and Levine, B. (2010). Autophagy protects against Sindbis virus infection of the central nervous system. Cell Host Microbe. 7(2), 115-127. DOI: 10.1016/j.chom.2010.01.007.

Oudshoorn, D., van der Hoeven, B., Limpens, R.W., Beugeling, C., Snijder, E.J., Bárcena, M., and Kikkert, M. (2016). Antiviral Innate Immune Response Interferes with the Formation of Replication-Associated Membrane Structures Induced by a Positive-Strand RNA Virus. MBio. 7(6). Published online 2016/12/06 DOI: 10.1128/mBio.01991-16.

Overby, A.K., Popov, V.L., Niedrig, M., and Weber, F. (2010). Tick-borne encephalitis virus delays interferon induction and hides its double-stranded RNA in intracellular membrane vesicles. J Virol. 84(17), 8470-8483. Published online 2010/06/16 DOI: 10.1128/JVI.00176-10.

Paludan, C., Schmid, D., Landthaler, M., Vockerodt, M., Kube, D., Tuschl, T., and Münz, C. (2005). Endogenous MHC class II processing of a viral nuclear antigen after autophagy. Science. 307(5709), 593-596. Published online 2004/12/09 DOI: 10.1126/science.1104904.

Pan, W., Zuo, X., Feng, T., Shi, X., and Dai, J. (2012). Guanylate-binding protein 1 participates in cellular antiviral response to dengue virus. Virol J. 9, 292. DOI: 10.1186/1743-422X-9-292.

Panyasrivanit, M., Khakpoor, A., Wikan, N., and Smith, D.R. (2009). Co-localization of constituents of the dengue virus translation and replication machinery with amphisomes. J Gen Virol. 90(Pt 2), 448-456. DOI: 10.1099/vir.0.005355-0.

Pappas, G., Roussos, N., and Falagas, M.E. (2009). Toxoplasmosis snapshots: global status of Toxoplasma gondii seroprevalence and implications for pregnancy and congenital toxoplasmosis. Int J Parasitol. 39(12), 1385-1394. Published online 2009/05/09 DOI: 10.1016/j.ijpara.2009.04.003.

Park, S., Choi, J., Biering, S.B., Dominici, E., Williams, L.E., and Hwang, S. (2016). Targeting by AutophaGy proteins (TAG): Targeting of IFNG-inducible GTPases to membranes by the LC3 conjugation system of autophagy. Autophagy. 12(7), 1153-1167. Published online 2016/05/12 DOI: 10.1080/15548627.2016.1178447.

Paul, D., Hoppe, S., Saher, G., Krijnse-Locker, J., and Bartenschlager, R. (2013). Morphological and biochemical characterization of the membranous hepatitis C virus replication compartment. J Virol. 87(19), 10612-10627. Published online 2013/07/24 DOI: 10.1128/JVI.01370-13.

Perry, J.W., and Wobus, C.E. (2010). Endocytosis of murine norovirus 1 into murine macrophages is dependent on dynamin II and cholesterol. J Virol. 84(12), 6163-6176. Published online 2010/04/07 DOI: 10.1128/JVI.00331-10.

Pfefferkorn, E.R. (1984). Interferon gamma blocks the growth of Toxoplasma gondii in human fibroblasts by inducing the host cells to degrade tryptophan. Proc Natl Acad Sci U S A. 81(3), 908-912.

Pilla-Moffett, D., Barber, M.F., Taylor, G.A., and Coers, J. (2016). Interferon-Inducible GTPases in Host Resistance, Inflammation and Disease. J Mol Biol. 428(17), 3495-3513. Published online 2016/05/12 DOI: 10.1016/j.jmb.2016.04.032.

Plot, L., and Amital, H. (2009). Infectious associations of Celiac disease. Autoimmun Rev. 8(4), 316-319. Published online 2008/10/29 DOI: 10.1016/j.autrev.2008.10.001.

Prentice, E., Jerome, W.G., Yoshimori, T., Mizushima, N., and Denison, M.R. (2004). Coronavirus replication complex formation utilizes components of cellular autophagy. J Biol Chem. 279(11), 10136-10141. DOI: 10.1074/jbc.M306124200.

Quinkert, D., Bartenschlager, R., and Lohmann, V. (2005). Quantitative analysis of the hepatitis C virus replication complex. J Virol. 79(21), 13594-13605. DOI: 10.1128/JVI.79.21.13594-13605.2005.

Radoshevich, L., and Dussurget, O. (2016). Cytosolic Innate Immune Sensing and Signaling upon Infection. Front Microbiol. 7, 313. Published online 2016/03/14 DOI: 10.3389/fmicb.2016.00313.

Rajsbaum, R., García-Sastre, A., and Versteeg, G.A. (2014). TRIMmunity: the roles of the TRIM E3-ubiquitin ligase family in innate antiviral immunity. J Mol Biol. 426(6), 1265-1284. Published online 2013/12/12 DOI: 10.1016/j.jmb.2013.12.005.

Ran, F.A., Hsu, P.D., Wright, J., Agarwala, V., Scott, D.A., and Zhang, F. (2013). Genome engineering using the CRISPR-Cas9 system. Nat Protoc. 8(11), 2281-2308. DOI: 10.1038/nprot.2013.143.

Randow, F., MacMicking, J.D., and James, L.C. (2013). Cellular self-defense: how cell-autonomous immunity protects against pathogens. Science. 340(6133), 701-706. DOI: 10.1126/science.1233028.

Reggiori, F., Monastyrska, I., Verheije, M.H., Calì, T., Ulasli, M., Bianchi, S., Bernasconi, R., de Haan, C.A., and Molinari, M. (2010). Coronaviruses Hijack the LC3-I-positive EDEMosomes, ER-derived vesicles exporting short-lived ERAD regulators, for replication. Cell Host Microbe. 7(6), 500-508. DOI: 10.1016/j.chom.2010.05.013.

Rodríguez-Acebes, S., de la Cueva, P., Fernández-Hernando, C., Ferruelo, A.J., Lasunción, M.A., Rawson, R.B., Martínez-Botas, J., and Gómez-Coronado, D. (2009). Desmosterol can replace cholesterol in sustaining cell proliferation and regulating the SREBP pathway in a sterol-Delta24-reductase-deficient cell line. Biochem J. 420(2), 305-315. Published online 2009/05/13 DOI: 10.1042/BJ20081909.

Romero-Brey, I., and Bartenschlager, R. (2014). Membranous replication factories induced by plus-strand RNA viruses. Viruses. 6(7), 2826-2857. Published online 2014/07/22 DOI: 10.3390/v6072826.

Roux, A., Uyhazi, K., Frost, A., and De Camilli, P. (2006). GTP-dependent twisting of dynamin implicates constriction and tension in membrane fission. Nature. 441(7092), 528-531. Published online 2006/04/30 DOI: 10.1038/nature04718.

Rubin, D.H. (1987). Reovirus serotype 1 binds to the basolateral membrane of intestinal epithelial cells. Microb Pathog. 3(3), 215-219.

Sasai, M., Sakaguchi, N., Ma, J.S., Nakamura, S., Kawabata, T., Bando, H., Lee, Y., Saitoh, T., Akira, S., Iwasaki, A., et al. (2017). Essential role for GABARAP autophagy proteins in interferon-inducible GTPase-mediated host defense. Nat Immunol. 18(8), 899-910. Published online 2017/06/12 DOI: 10.1038/ni.3767.

Schlegel, A., Giddings, T.H., Ladinsky, M.S., and Kirkegaard, K. (1996). Cellular origin and ultrastructure of membranes induced during poliovirus infection. J Virol. 70(10), 6576-6588.

Schlicker, A., Domingues, F.S., Rahnenführer, J., and Lengauer, T. (2006). A new measure for functional similarity of gene products based on Gene Ontology. BMC Bioinformatics. 7, 302. Published online 2006/06/15 DOI: 10.1186/1471-2105-7-302.

Schmid, D., Pypaert, M., and Münz, C. (2007). Antigen-loading compartments for major histocompatibility complex class II molecules continuously receive input from autophagosomes. Immunity. 26(1), 79-92. Published online 2006/12/21 DOI: 10.1016/j.immuni.2006.10.018.

Schneider, W.M., Chevillotte, M.D., and Rice, C.M. (2014). Interferon-stimulated genes: a complex web of host defenses. Annu Rev Immunol. 32, 513-545. Published online 2014/02/06 DOI: 10.1146/annurev-immunol-032713-120231.

Schoggins, J.W., and Rice, C.M. (2011). Interferon-stimulated genes and their antiviral effector functions. Curr Opin Virol. 1(6), 519-525. DOI: 10.1016/j.coviro.2011.10.008.

Scutigliani, E.M., and Kikkert, M. (2017). Interaction of the innate immune system with positive-strand RNA virus replication organelles. Cytokine Growth Factor Rev. Published online 2017/06/27 DOI: 10.1016/j.cytogfr.2017.05.007.

Selleck, E.M., Fentress, S.J., Beatty, W.L., Degrandi, D., Pfeffer, K., Virgin, H.W., Macmicking, J.D., and Sibley, L.D. (2013). Guanylate-binding protein 1 (Gbp1) contributes to cell-autonomous immunity against Toxoplasma gondii. PLoS Pathog. 9(4), e1003320. DOI: 10.1371/journal.ppat.1003320.

Selleck, E.M., Orchard, R.C., Lassen, K.G., Beatty, W.L., Xavier, R.J., Levine, B., Virgin, H.W., and Sibley, L.D. (2015). A Noncanonical Autophagy Pathway Restricts Toxoplasma gondii Growth in a Strain-Specific Manner in IFN-γ-Activated Human Cells. MBio. 6(5), e01157-01115. Published online 2015/09/08 DOI: 10.1128/mBio.01157-15.

Sharma, M., Bhattacharyya, S., Nain, M., Kaur, M., Sood, V., Gupta, V., Khasa, R., Abdin, M.Z., Vrati, S., and Kalia, M. (2014). Japanese encephalitis virus replication is negatively regulated by autophagy and occurs on LC3-I- and EDEM1-containing membranes. Autophagy. 10(9), 1637-1651. DOI: 10.4161/auto.29455.

Shulla, A., and Randall, G. (2016). (+) RNA virus replication compartments: a safe home for (most) viral replication. Curr Opin Microbiol. 32, 82-88. Published online 2016/05/30 DOI: 10.1016/j.mib.2016.05.003.

Sibley, L.D. (2011). Invasion and intracellular survival by protozoan parasites. Immunol Rev. 240(1), 72-91. DOI: 10.1111/j.1600-065X.2010.00990.x.

Singh, S.B., Davis, A.S., Taylor, G.A., and Deretic, V. (2006). Human IRGM induces autophagy to eliminate intracellular mycobacteria. Science. 313(5792), 1438-1441. DOI: 10.1126/science.1129577.

Singh, S.B., Ornatowski, W., Vergne, I., Naylor, J., Delgado, M., Roberts, E., Ponpuak, M., Master, S., Pilli, M., White, E., et al. (2010). Human IRGM regulates autophagy and cell-autonomous immunity functions through mitochondria. Nat Cell Biol. 12(12), 1154-1165. Published online 2010/11/21 DOI: 10.1038/ncb2119.

Sir, D., Kuo, C.F., Tian, Y., Liu, H.M., Huang, E.J., Jung, J.U., Machida, K., and Ou, J.H. (2012). Replication of hepatitis C virus RNA on autophagosomal membranes. J Biol Chem. 287(22), 18036-18043. Published online 2012/04/10 DOI: 10.1074/jbc.M111.320085.

Smeekens, S.P., Ng, A., Kumar, V., Johnson, M.D., Plantinga, T.S., van Diemen, C., Arts, P., Verwiel, E.T., Gresnigt, M.S., Fransen, K., et al. (2013). Functional genomics identifies type I interferon pathway as central for host defense against Candida albicans. Nat Commun. 4, 1342. DOI: 10.1038/ncomms2343.

Smith, D.B., McFadden, N., Blundell, R.J., Meredith, A., and Simmonds, P. (2012). Diversity of murine norovirus in wild-rodent populations: species-specific associations suggest an ancient divergence. J Gen Virol. 93(Pt 2), 259-266. Published online 2011/11/09 DOI: 10.1099/vir.0.036392-0.

Sorace, J.M., Johnson, R.J., Howard, D.L., and Drysdale, B.E. (1995). Identification of an endotoxin and IFN-inducible cDNA: possible identification of a novel protein family. J Leukoc Biol. 58(4), 477-484.

Sosnovtsev, S.V., Belliot, G., Chang, K.O., Onwudiwe, O., and Green, K.Y. (2005). Feline calicivirus VP2 is essential for the production of infectious virions. J Virol. 79(7), 4012-4024. DOI: 10.1128/JVI.79.7.4012-4024.2005.

Sosnovtsev, S.V., Belliot, G., Chang, K.O., Prikhodko, V.G., Thackray, L.B., Wobus, C.E., Karst, S.M., Virgin, H.W., and Green, K.Y. (2006). Cleavage map and proteolytic processing of the murine norovirus nonstructural polyprotein in infected cells. J Virol. 80(16), 7816-7831. DOI: 10.1128/JVI.00532-06.

Sou, Y.S., Waguri, S., Iwata, J., Ueno, T., Fujimura, T., Hara, T., Sawada, N., Yamada, A., Mizushima, N., Uchiyama, Y., et al. (2008). The Atg8 conjugation system is indispensable for proper development of autophagic isolation membranes in mice. Mol Biol Cell. 19(11), 4762-4775. Published online 2008/09/03 DOI: 10.1091/mbc.E08-03-0309.

Springer, H.M., Schramm, M., Taylor, G.A., and Howard, J.C. (2013). Irgm1 (LRG-47), a regulator of cell-autonomous immunity, does not localize to mycobacterial or listerial phagosomes in IFN-γ-induced mouse cells. J Immunol. 191(4), 1765-1774. DOI: 10.4049/jimmunol.1300641.

Staeheli, P., Haller, O., Boll, W., Lindenmann, J., and Weissmann, C. (1986). Mx protein: constitutive expression in 3T3 cells transformed with cloned Mx cDNA confers selective resistance to influenza virus. Cell. 44(1), 147-158.

Stanley, E.R., and Heard, P.M. (1977). Factors regulating macrophage production and growth. Purification and some properties of the colony stimulating factor from medium conditioned by mouse L cells. J Biol Chem. 252(12), 4305-4312.

Stene, L.C., Honeyman, M.C., Hoffenberg, E.J., Haas, J.E., Sokol, R.J., Emery, L., Taki, I., Norris, J.M., Erlich, H.A., Eisenbarth, G.S., et al. (2006). Rotavirus infection frequency and risk of celiac disease autoimmunity in early childhood: a longitudinal study. Am J Gastroenterol. 101(10), 2333-2340. DOI: 10.1111/j.1572-0241.2006.00741.x.

Strong, D.W., Thackray, L.B., Smith, T.J., and Virgin, H.W. (2012). Protruding domain of capsid protein is necessary and sufficient to determine murine norovirus replication and pathogenesis in vivo. J Virol. 86(6), 2950-2958. Published online 2012/01/18 DOI: 10.1128/JVI.07038-11.

Subba-Reddy, C.V., Goodfellow, I., and Kao, C.C. (2011). VPg-primed RNA synthesis of norovirus RNA-dependent RNA polymerases by using a novel cell-based assay. J Virol. 85(24), 13027-13037. Published online 2011/10/12 DOI: 10.1128/JVI.06191-11.

Subba-Reddy, C.V., Goodfellow, I., and Kao, C.C. (2018). Correction for Subba-Reddy et al., "VPg-Primed RNA Synthesis of Norovirus RNA-Dependent RNA Polymerases by Using a Novel Cell-Based Assay". J Virol. 92(1). Published online 2017/12/14 DOI: 10.1128/JVI.01706-17.

Suhy, D.A., Giddings, T.H., and Kirkegaard, K. (2000). Remodeling the endoplasmic reticulum by poliovirus infection and by individual viral proteins: an autophagy-like origin for virus-induced vesicles. J Virol. 74(19), 8953-8965.

Takeshige, K., Baba, M., Tsuboi, S., Noda, T., and Ohsumi, Y. (1992). Autophagy in yeast demonstrated with proteinase-deficient mutants and conditions for its induction. J Cell Biol. 119(2), 301-311.

Takeshita, S., Kaji, K., and Kudo, A. (2000). Identification and characterization of the new osteoclast progenitor with macrophage phenotypes being able to differentiate into mature osteoclasts. J Bone Miner Res. 15(8), 1477-1488. DOI: 10.1359/jbmr.2000.15.8.1477.

Takeuchi, O., and Akira, S. (2007). Recognition of viruses by innate immunity. Immunol Rev. 220, 214-224. DOI: 10.1111/j.1600-065X.2007.00562.x.

Takeuchi, O., and Akira, S. (2009). Innate immunity to virus infection. Immunol Rev. 227(1), 75-86. DOI: 10.1111/j.1600-065X.2008.00737.x.

Taube, S., Perry, J.W., Yetming, K., Patel, S.P., Auble, H., Shu, L., Nawar, H.F., Lee, C.H., Connell, T.D., Shayman, J.A., et al. (2009). Ganglioside-linked terminal sialic acid moieties on murine macrophages function as attachment receptors for murine noroviruses. J Virol. 83(9), 4092-4101. Published online 2009/02/25 DOI: 10.1128/JVI.02245-08.

Taylor, G.A., Collazo, C.M., Yap, G.S., Nguyen, K., Gregorio, T.A., Taylor, L.S., Eagleson, B., Secrest, L., Southon, E.A., Reid, S.W., et al. (2000). Pathogen-specific loss of host resistance in mice lacking the IFN-gamma-inducible gene IGTP. Proc Natl Acad Sci U S A. 97(2), 751-755.

te Velthuis, A.J. (2014). Common and unique features of viral RNA-dependent polymerases. Cell Mol Life Sci. 71(22), 4403-4420. Published online 2014/08/01 DOI: 10.1007/s00018-014-1695-z.

Thackray, L.B., Wobus, C.E., Chachu, K.A., Liu, B., Alegre, E.R., Henderson, K.S., Kelley, S.T., and Virgin, H.W. (2007). Murine noroviruses comprising a single genogroup exhibit biological diversity despite limited sequence divergence. J Virol. 81(19), 10460-10473. Published online 2007/07/25 DOI: 10.1128/JVI.00783-07.

Theiler, M., and Smith, H.H. (1937). THE EFFECT OF PROLONGED CULTIVATION IN VITRO UPON THE PATHOGENICITY OF YELLOW FEVER VIRUS. J Exp Med. 65(6), 767-786.

Thorne, L.G., and Goodfellow, I.G. (2014). Norovirus gene expression and replication. J Gen Virol. 95(Pt 2), 278-291. Published online 2013/11/16 DOI: 10.1099/vir.0.059634-0.

Tiwari, S., Choi, H.P., Matsuzawa, T., Pypaert, M., and MacMicking, J.D. (2009). Targeting of the GTPase Irgm1 to the phagosomal membrane via PtdIns(3,4)P(2) and PtdIns(3,4,5)P(3) promotes immunity to mycobacteria. Nat Immunol. 10(8), 907-917. DOI: 10.1038/ni.1759.

Tjon, J.M., van Bergen, J., and Koning, F. (2010). Celiac disease: how complicated can it get? Immunogenetics. 62(10), 641-651. Published online 2010/07/27 DOI: 10.1007/s00251-010-0465-9.

Traver, M.K., Henry, S.C., Cantillana, V., Oliver, T., Hunn, J.P., Howard, J.C., Beer, S., Pfeffer, K., Coers, J., and Taylor, G.A. (2011). Immunity-related GTPase M (IRGM) proteins influence the localization of guanylate-binding protein 2 (GBP2) by modulating macroautophagy. J Biol Chem. 286(35), 30471-30480. DOI: 10.1074/jbc.M111.251967.

Tsukada, M., and Ohsumi, Y. (1993). Isolation and characterization of autophagy-defective mutants of Saccharomyces cerevisiae. FEBS Lett. 333(1-2), 169-174.

Uchida, L., Espada-Murao, L.A., Takamatsu, Y., Okamoto, K., Hayasaka, D., Yu, F., Nabeshima, T., Buerano, C.C., and Morita, K. (2014). The dengue virus conceals double-stranded RNA in the intracellular membrane to escape from an interferon response. Sci Rep. 4, 7395. Published online 2014/12/10 DOI: 10.1038/srep07395.

Urrutia, R., Henley, J.R., Cook, T., and McNiven, M.A. (1997). The dynamins: redundant or distinct functions for an expanding family of related GTPases? Proc Natl Acad Sci U S A. 94(2), 377-384.

Vongpunsawad, S., Venkataram Prasad, B.V., and Estes, M.K. (2013). Norwalk Virus Minor Capsid Protein VP2 Associates within the VP1 Shell Domain. J Virol. 87(9), 4818-4825. Published online 2013/02/13 DOI: 10.1128/JVI.03508-12.

Wandel, M.P., Pathe, C., Werner, E.I., Ellison, C.J., Boyle, K.B., von der Malsburg, A., Rohde, J., and Randow, F. (2017). GBPs Inhibit Motility of Shigella flexneri but Are Targeted for Degradation by the Bacterial Ubiquitin Ligase IpaH9.8. Cell Host Microbe. 22(4), 507-518.e505. DOI: 10.1016/j.chom.2017.09.007.

Wang, W., Xiao, F., Wan, P., Pan, P., Zhang, Y., Liu, F., Wu, K., Liu, Y., and Wu, J. (2017). EV71 3D Protein Binds with NLRP3 and Enhances the Assembly of Inflammasome Complex. PLoS Pathog. 13(1), e1006123. Published online 2017/01/06 DOI: 10.1371/journal.ppat.1006123.

Wang, W., Xiao, F., Wan, P., Pan, P., Zhang, Y., Liu, F., Wu, K., Liu, Y., and Wu, J. (2018). Correction: EV71 3D Protein Binds with NLRP3 and Enhances the Assembly of Inflammasome Complex. PLoS Pathog. 14(3), e1006921. Published online 2018/03/12 DOI: 10.1371/journal.ppat.1006921.

Weber, F., Wagner, V., Rasmussen, S.B., Hartmann, R., and Paludan, S.R. (2006). Double-stranded RNA is produced by positive-strand RNA viruses and DNA viruses but not in detectable amounts by negative-strand RNA viruses. J Virol. 80(10), 5059-5064. DOI: 10.1128/JVI.80.10.5059-5064.2006.

Weidberg, H., Shvets, E., Shpilka, T., Shimron, F., Shinder, V., and Elazar, Z. (2010). LC3 and GATE-16/GABARAP subfamilies are both essential yet act differently in autophagosome biogenesis. EMBO J. 29(11), 1792-1802. Published online 2010/04/23 DOI: 10.1038/emboj.2010.74.

Welsch, S., Miller, S., Romero-Brey, I., Merz, A., Bleck, C.K., Walther, P., Fuller, S.D., Antony, C., Krijnse-Locker, J., and Bartenschlager, R. (2009). Composition and three-dimensional architecture of the dengue virus replication and assembly sites. Cell Host Microbe. 5(4), 365-375. DOI: 10.1016/j.chom.2009.03.007.

Wobus, C.E., Karst, S.M., Thackray, L.B., Chang, K.O., Sosnovtsev, S.V., Belliot, G., Krug, A., Mackenzie, J.M., Green, K.Y., and Virgin, H.W. (2004). Replication of Norovirus in cell culture reveals a tropism for dendritic cells and macrophages. PLoS Biol. 2(12), e432. Published online 2004/11/30 DOI: 10.1371/journal.pbio.0020432.

Wobus, C.E., Thackray, L.B., and Virgin, H.W. (2006). Murine norovirus: a model system to study norovirus biology and pathogenesis. J Virol. 80(11), 5104-5112. DOI: 10.1128/JVI.02346-05.

Yamamoto, M., Okuyama, M., Ma, J.S., Kimura, T., Kamiyama, N., Saiga, H., Ohshima, J., Sasai, M., Kayama, H., Okamoto, T., et al. (2012). A cluster of interferon-γ-inducible p65 GTPases plays a critical role in host defense against Toxoplasma gondii. Immunity. 37(2), 302-313. DOI: 10.1016/j.immuni.2012.06.009.

Ye, J., Zhu, B., Fu, Z.F., Chen, H., and Cao, S. (2013). Immune evasion strategies of flaviviruses. Vaccine. 31(3), 461-471. Published online 2012/11/13 DOI: 10.1016/j.vaccine.2012.11.015.

Yoneyama, M., Onomoto, K., Jogi, M., Akaboshi, T., and Fujita, T. (2015). Viral RNA detection by RIG-I-like receptors. Curr Opin Immunol. 32, 48-53. Published online 2015/01/14 DOI: 10.1016/j.coi.2014.12.012.

Zhang, Y., Li, Z., Ge, X., Guo, X., and Yang, H. (2011). Autophagy promotes the replication of encephalomyocarditis virus in host cells. Autophagy. 7(6), 613-628. Published online 2011/06/01.

Zhao, Z., Fux, B., Goodwin, M., Dunay, I.R., Strong, D., Miller, B.C., Cadwell, K., Delgado, M.A., Ponpuak, M., Green, K.G., et al. (2008). Autophagosome-independent essential function for the autophagy protein Atg5 in cellular immunity to intracellular pathogens. Cell Host Microbe. 4(5), 458-469. DOI: 10.1016/j.chom.2008.10.003.

Appendix A

Figures

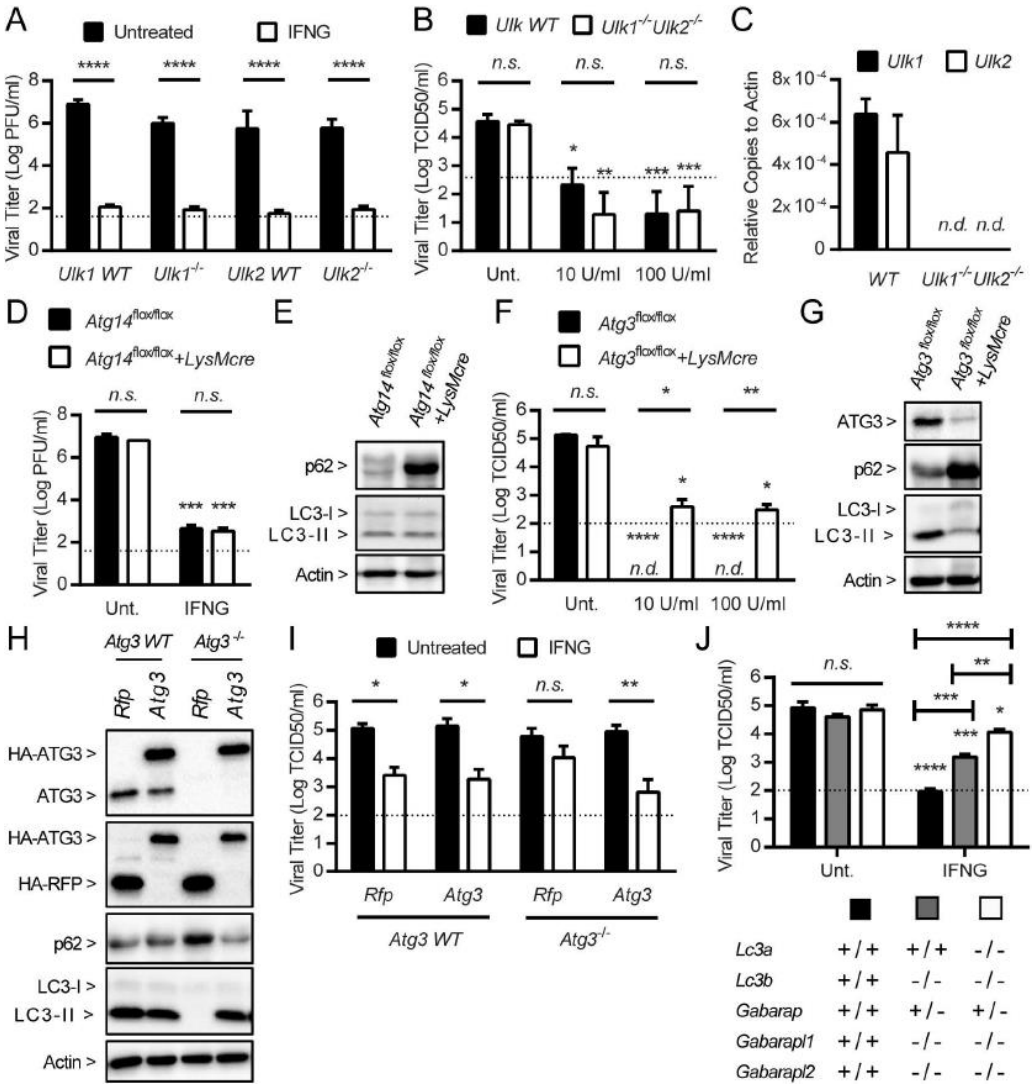

Figure 2.1. IFNG Inhibits MNV Replication via the LC3-Conjugation System of Autophagy. (A) Growth analysis of MNV in *Ulk1*$^{-/-}$, *Ulk2*$^{-/-}$ and WT BMDMs. Cells were untreated or treated with 100 U/ml IFNG for 12 hours and then infected with MNV at the multiplicity of infection (MOI) of 0.05. At 24 hour-post-infection (hpi), cells were harvested to titer infectious virus. N=5 replicates using 2 *Ulk1*$^{+/+}$ mice, 4 *Ulk1*$^{-/-}$ mice, 1 *Ulk2*$^{+/+}$ mouse, and 3 *Ulk2*$^{-/-}$ mouse. (B) Growth analysis of MNV in *Ulk1*$^{-/-}$*Ulk2*$^{-/-}$ and WT MEFs. Cells were treated with none (Unt.) or the indicated dose of IFNG for 24 hours and then transfected with 50 ng of MNV vRNA. At 24 hour-post-transfection (hpt), cells were harvested to titer infectious virus. N=5 replicates. (C) Quantitative PCR analysis for the transcript levels of *Ulk1* and *Ulk2* in *Ulk1*$^{-/-}$*Ulk2*$^{-/-}$ and WT MEFs. N=3 replicates.

Figure 2.1. (continued)
(D) Growth analysis of MNV in *Atg14*$^{flox/flox}$+*LysMcre* and littermate control *Atg14*$^{flox/flox}$ BMDMs as described in (A). N=3 replicates using 2 mice from each genotype. (E) A representative western blot of cells described in (D) on the level of p62 and the lipidation of LC3. Actin as loading control. N=3 replicates. (F) Growth analysis of MNV in *Atg3*$^{flox/flox}$+*LysMcre* and *Atg3*$^{flox/flox}$ BMDMs as described in (A). N=3 replicates using 2 mice from each genotype. (G) A representative western blot of cells described in (F), as described in (E). N=3 replicates. (H) A representative western blot of *Atg3*$^{-/-}$ and WT MEFs transduced with lentiviruses expressing *Atg3* WT or red fluorescent protein (RFP), as described in (E). N=3 replicates. (I) Growth analysis of MNV in the cells described in (H), as described in (B). N=3 replicates. (J) Growth analysis of MNV in the cells with deletions of *Lc3* homologs as indicated on the bottom, as described in (B). N=3 replicates. For all experiments with quantitative analysis, data are shown as mean ± SEM. One-way ANOVA with Tukey's multiple comparisons test; n.d., not detected. n.s., not significant; *, $p<0.05$; **, $p<0.01$; ***, $p<0.001$; ****, $p<0.0001$. Dashed line indicates the limit of detection.

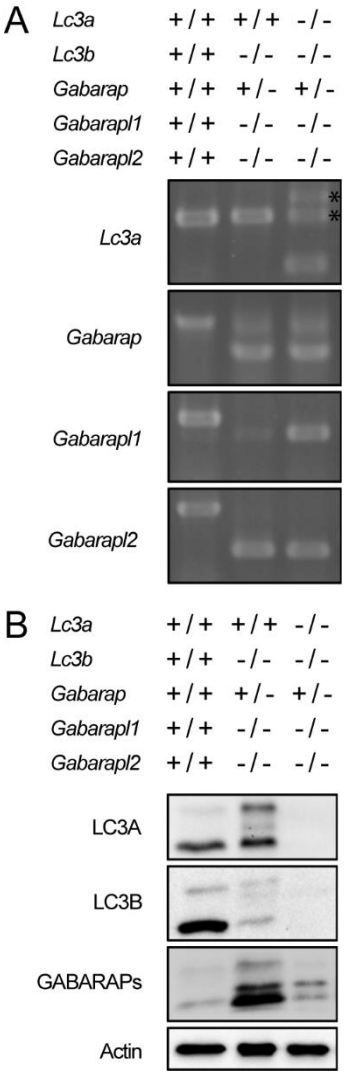

Figure 2.2. LC3 Homologs Are Knocked-out. (A and B) Genotyping PCR (A) and representative western blots (B) demonstrating the knocking-out of the indicated LC3 homologs in MEFs. * indicates PCR products from frameshift mutants with nonsense mutations (instead of deletion). N=3 replicates.

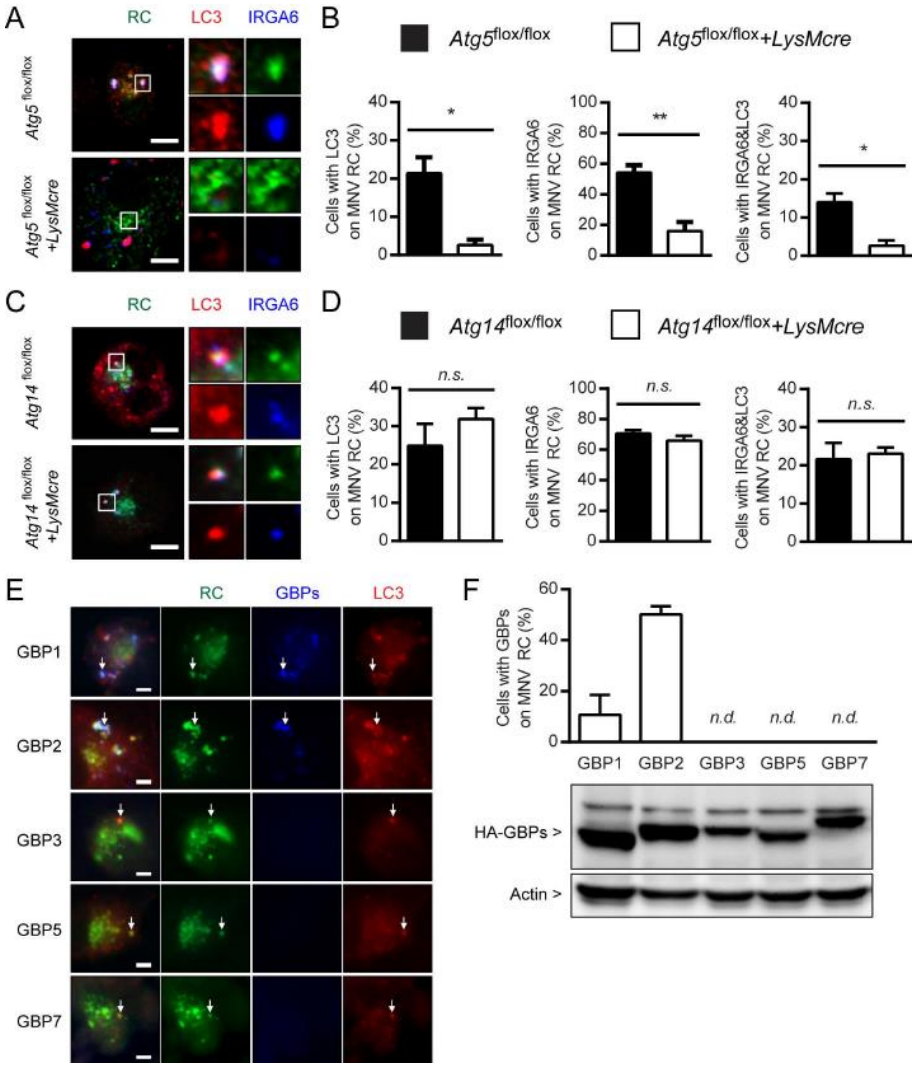

Figure 2.3. IFN-Inducible GTPases Are Targeted to the MNV RC via the LC3-Conjugation System. (A and B) Immunofluorescence assay for the localization of LC3 and IRGA6 with regard to the MNV RC (via anti-ProPol detecting both protease and polymerase of MNV) at 10 hpi in *Atg5*$^{flox/flox}$*+LysMcre* and *Atg5*$^{flox/flox}$ BMDMs upon MNV infection at MOI=5 and simultaneous 100 U/ml IFNG treatment. Representative images (A) and quantitation (B). Data as mean±SEM. N=3 replicates using 2 mice from each genotype. Student's t-test. *, $p<0.05$; **, $p<0.01$. Scale bars, 5 μm. (C and D) The same assays as described for (A) and (B) in *Atg14*$^{flox/flox}$*+LysMcre* and *Atg14*$^{flox/flox}$ BMDMs. Data as mean±SEM. N=3 replicates using 2 mice from each genotype. Student's t-test. n.s., not significant. (E and F) The same assays as described for (A) and (B) in WT BMDMs transduced with lentiviruses expressing the indicated GBPs. Individual FLAG/HA-tagged GBP was detected by anti-FLAG (E) or anti-HA (F, bottom panel) antibodies. White arrows in (E) indicate colocalization. n.d., not detected. A representative western blot in F for the expression of individual GBPs. N=3 replicates using 2 mice.

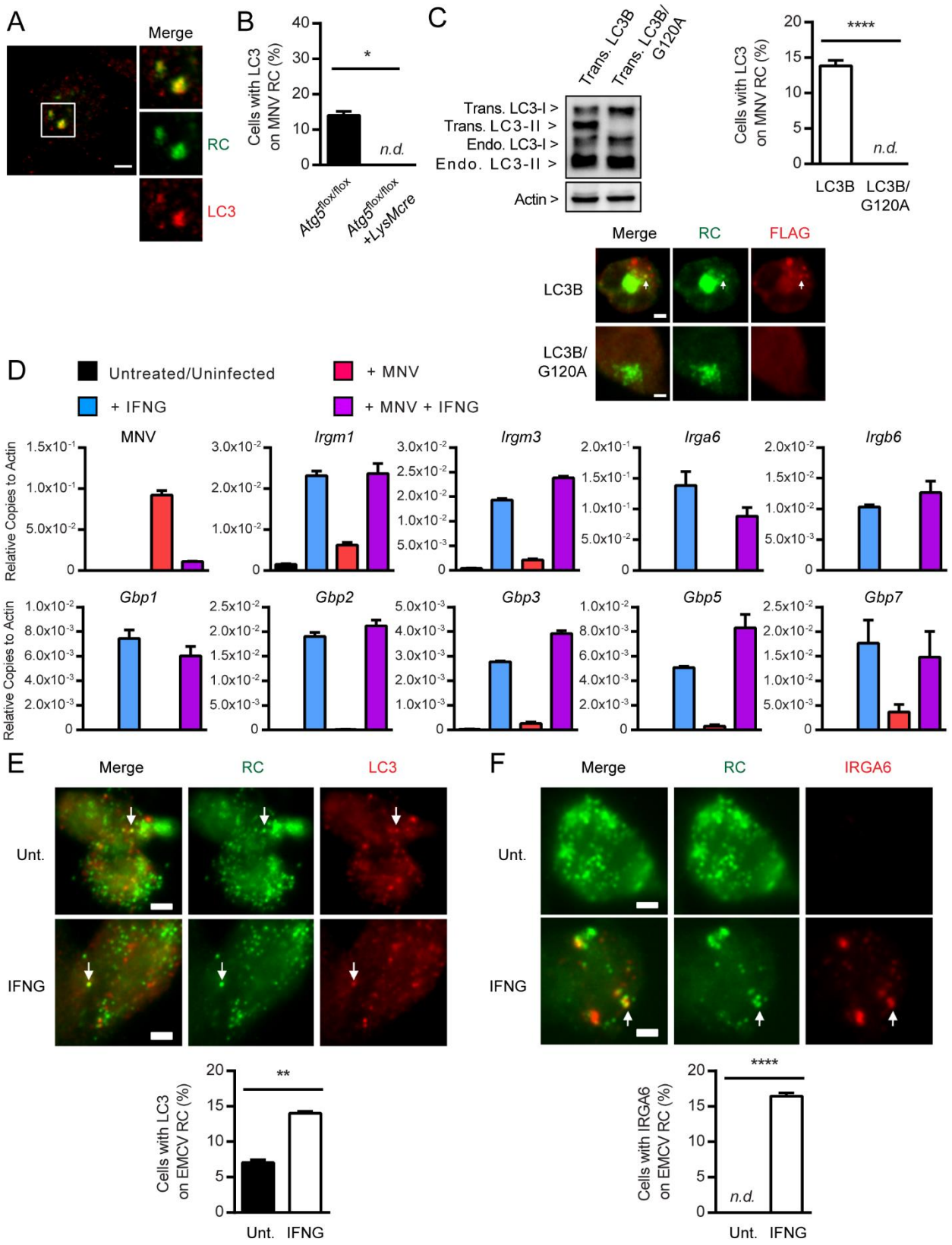

Figure 2.4. IFN-Inducible GTPases Are Targeted to Viral RCs via the LC3-Conjugation System. (A and B) Immunofluorescence assay for the localization of LC3

Figure 2.4. (continued)
with regard to the MNV RC in *Atg5*$^{flox/flox}$*+LysMcre* or control *Atg5*$^{flox/flox}$ BMDMs at 10 hour-post-infection (hpi) of MNV at the multiplicity of infection at 5 (MOI=5). Representative images in *Atg5*$^{flox/flox}$ BMDMs (A) and quantitation (B). Scale bar, 2 μm. Data as mean±SEM. N=3 replicates. n.d., not detected. Student's t-test. *, $p<0.05$. (C) Immunofluorescence assay for the localization of wild type (WT) LC3B or non-conjugatable mutant of LC3B (G120A) with regard to the MNV RC at 10 hpi of MNV at MOI=5 and simultaneous treatment of 100 U/ml IFNG in BV-2 cells transduced with lentiviruses expressing FLAG/HA-tagged WT LC3B and LC3B/G120A. A representative western blot of the transduced cells (top, left), representative images (bottom), and quantitation (top, right). White arrows indicate representative colocalization. Scale bar, 5 μm. Data as mean±SEM. N=3 replicates. n.d., not detected. Student's t-test. ****, $p<0.0001$. (D) Quantitative PCR analysis for the transcript levels of the indicated genes in WT BMDMs with or without 10 hrs infection of MNV at MOI=5 and/or 100 U/ml IFNG treatment. N=3 replicates. (E and F) Immunofluorescence assay for the localization of LC3 (E) and IRGA6 (F) with regard to the EMCV RC (via anti-dsRNA antibody) in WT BMDMs at 6 hpi of EMCV at MOI=500 with or without 8 hrs treatment of 100 U/ml IFNG. Representative images (top) and quantitation (bottom). White arrows indicate representative colocalization. Scale bars, 5 μm. Data as mean±SEM. N=3 replicates. n.d., not detected. Student's t-test. **, $p<0.01$; ****, $p<0.0001$. BMDMs for (A), (B), (D), (E), and (F) were from 2 mice for each genotype.

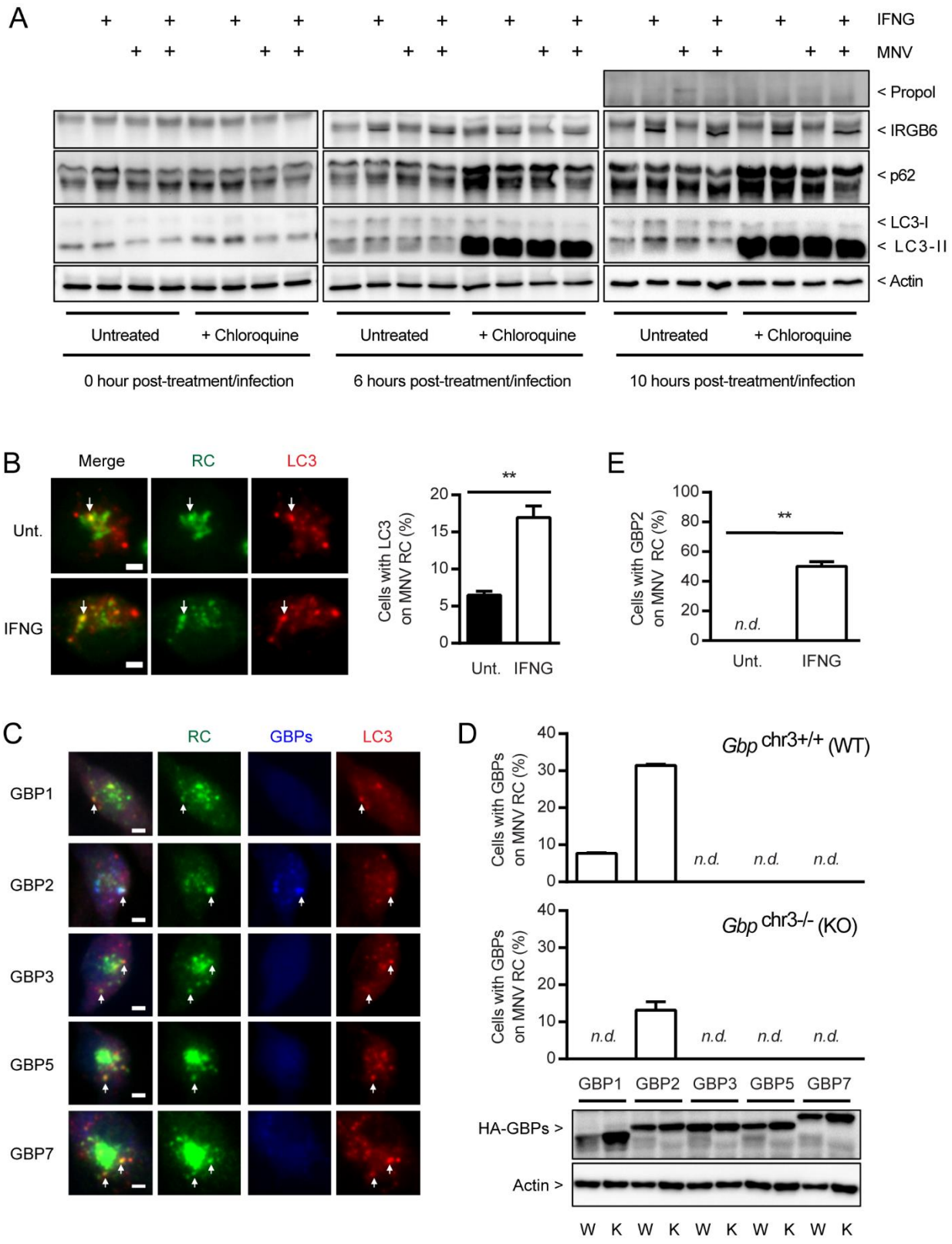

Figure 2.5. IFN-Inducible GTPases Are Targeted to the MNV RC. (A) A representative western blot of LC3 lipidation in WT BMDMs with or without 50 μM

Figure 2.5. (continued)
chloroquine treatment (to inhibit lysosomal degradation), upon infection of MNV at MOI=5 and/or treatment of 100 U/ml IFNG for 0, 6, 10 hours. Propol for MNV infection, IRGB6 for IFNG treatment, p62 for autophagy status, and Actin as loading control. N=3 replicates. (B) Immunofluorescence assay for the localization of LC3 with regard to the MNV RC in WT BMDMs at 10 hpi of MNV at MOI=5 with simultaneous treatment of none (Unt.) or 100 U/ml IFNG. Representative images (left) and quantitation (right). White arrows indicate representative colocalization. Scale bar, 5 μm. Data as mean±SEM. N=3 replicates. Student's t-test. **, $p<0.01$. (C and D) immunofluorescence analysis of GBPs with regard to the MNV RC in *Gbp*$^{chr3+/+}$ (W) and *Gbp*$^{chr3-/-}$ (K) BMDMs transduced with lentiviruses expressing the indicated GBPs at 10 hpi of MNV at MOI=5 and simultaneous treatment of 100 U/ml IFNG. Individual FLAG/HA-tagged GBP was detected by anti-FLAG (C) or anti-HA (D, bottom panel) antibodies. Representative images from the transduced *Gbp*$^{chr3-/-}$ BMDMs (C) and quantitation from both BMDMs (D). White arrows in (C) indicate representative colocalization. Scale bars, 5 μm. Data as mean±SEM. N=3 replicates. n.d., not detected. A representative western blot in D for the expression of individual GBPs. (E) Quantitation of immunofluorescence analysis of GBP2 localization to the MNV RC in WT BMDMs transduced with lentivirus expressing GBP2 at 10 hpi of MNV at MOI=5 with simultaneous treatment of none (Unt.) or 100 U/ml IFNG. Data as mean±SEM. N=3 replicates. n.d., not detected. Student's t-test. **, $p<0.01$. BMDMs were from 2 mice for each genotype.

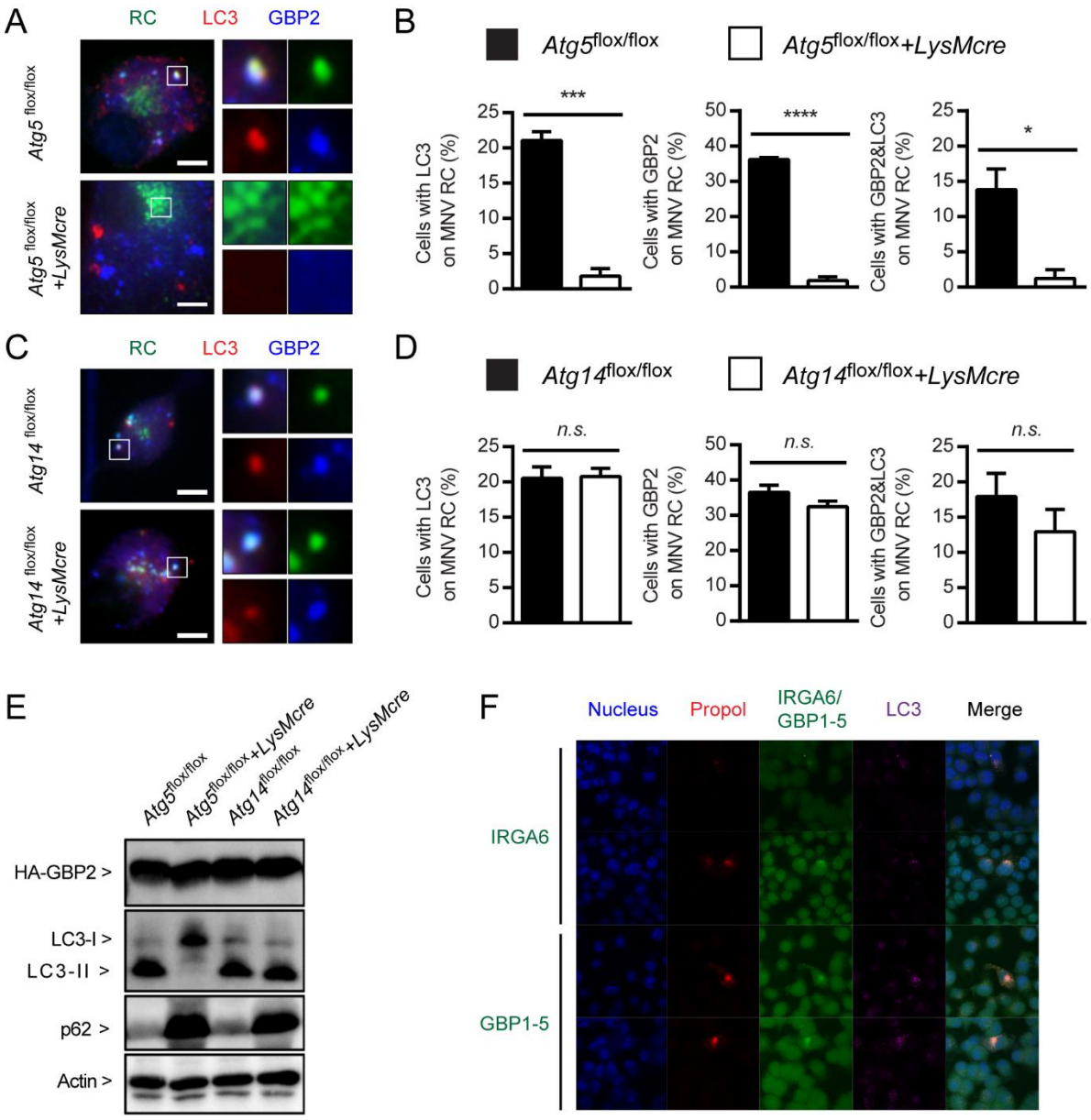

Figure 2.6. GBP2 is Targeted to the MNV RC via the LC3-Conjugation System. (A and B) Immunofluorescence assay for the localization of LC3 and GBP2 with regard to the MNV RC in *Atg5*$^{flox/flox}$+*LysMcre* and *Atg5*$^{flox/flox}$ BMDMs transduced with lentiviruses expressing FLAG/HA-tagged GBP2 at 10 hpi of MNV at MOI=5 and simultaneous treatment of 100 U/ml IFNG. Representative images (A) and quantitation (B). Scale bars, 10 μm. Data as mean±SEM. N=3 replicates. Student's t-test. *, $p<0.05$; ***, $p<0.001$; ****, $p<0.0001$. (C and D) The same assays as described for (A) and (B) in *Atg14*$^{flox/flox}$+*LysMcre* and *Atg14*$^{flox/flox}$ BMDMs. n.s., not significant. N=3 replicates. (E) A representative western blot for the cells described in (A) and (C). N=3 replicates. (F) Representative immunofluorescence images for the localization of endogenous IRGA6

Figure 2.6. (continued)
and GBP1-5 with regard to the MNV RC. BV-2 cells were infected with MNV at MOI=25 and simultaneously treated with 100 U/ml IFNG. At 10 hpi, cells were fixed and stained for MNV Propol (RC), LC3, and IRGA6 or GBP1-5. N=2 replicates. BMDMs for (A) to (E) were from 2 mice for each genotype.

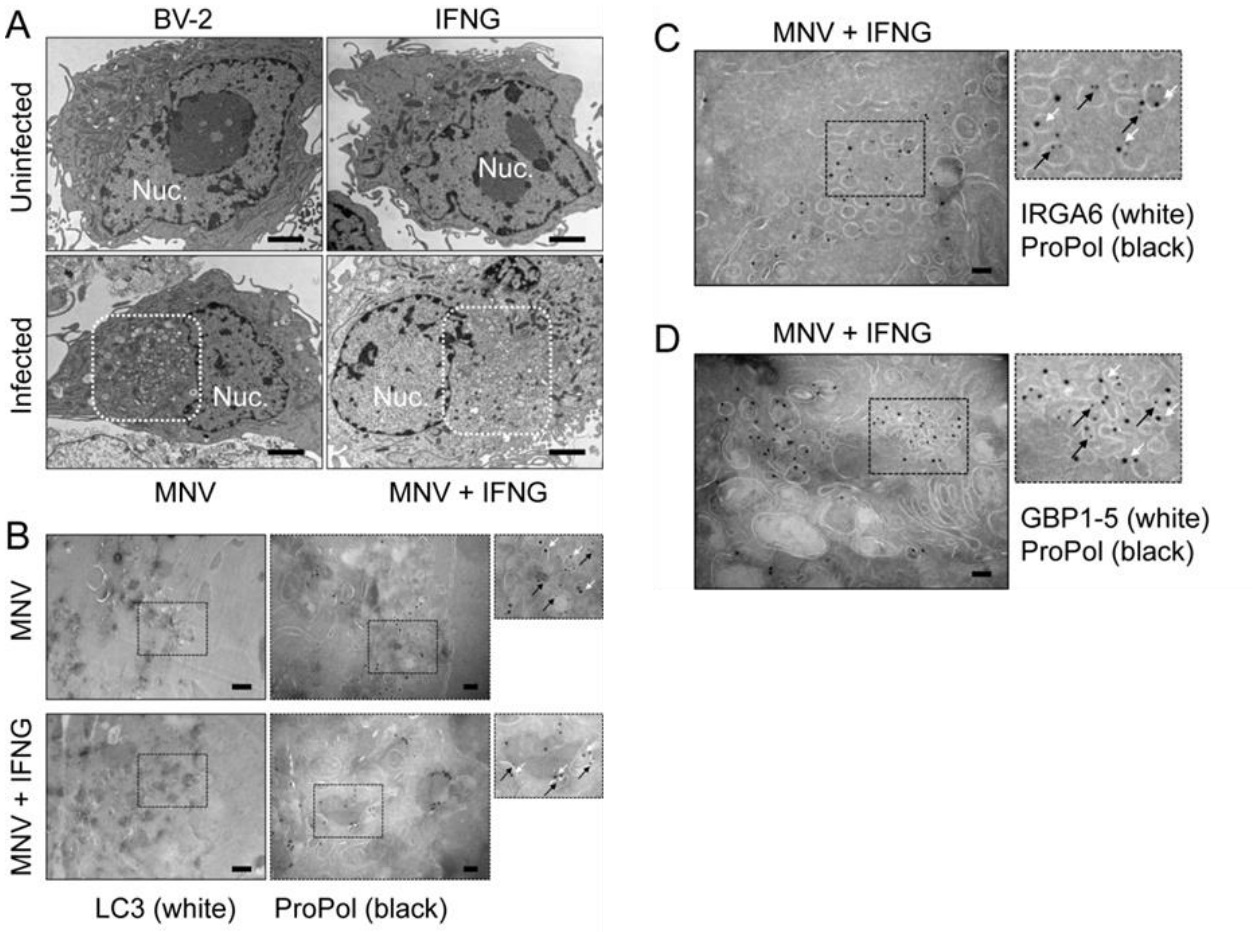

Figure 2.7. LC3 and IFN-Inducible GTPases Localize on the Membrane of the MNV RC. (A) Transmission electron microscopy of BV-2 cells: uninfected (BV-2), activated with 100 U/ml IFNG for 12 hours (IFNG), at 12 hpi of MNV infection at the MOI of 25 (MNV), and at 12 hpi of MNV infection after 12 hour activation with IFNG (MNV + IFNG). Scale bars, 2 μm. Dotted rectangles show the area of vacuole structures. N=2 replicates. (B) Cryo-immuno-EM localization of LC3 and ProPol in (MNV) and (MNV + IFNG) condition as described in (A). Scale bars, 500 nm (left) and 100 nm (center). (C and D) The same analysis as described in (B) for IRGA6 and ProPol (C) and GBP1-5 and ProPol (D). Scale bars, 100 nm. White arrows indicate LC3 (B), IRGA6 (C), and GBP1-5 (D). Black arrows indicate ProPol. N=2 replicates.

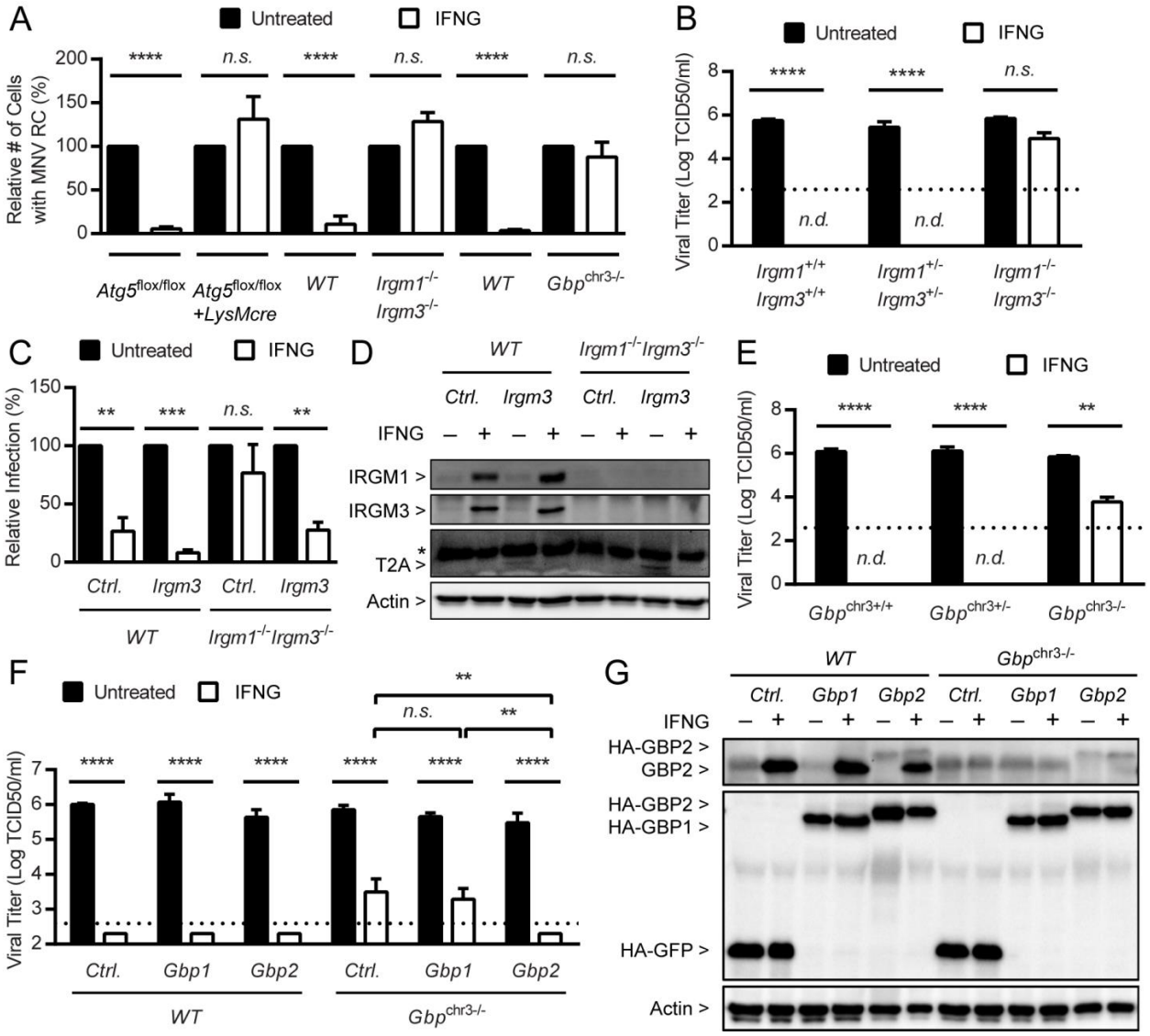

Figure 2.8. IFNG Requires the IFN-Inducible GTPases to Inhibit MNV Replication *in vitro.* (A) Quantitation of MNV RCs in BMDMs from *Atg5*$^{flox/flox}$+*LysMcre*, *Irgm1*$^{-/-}$ *Irgm3*$^{-/-}$, *Gbp*$^{chr3-/-}$, and respective littermate control mice. Cells were either untreated or treated with 100 U/ml IFNG for 12 hours before infection with MNV at MOI=5 and harvested and analyzed at 12 hpi with anti-ProPol immunofluorescence. Data as mean±SEM. N=3 replicates using 2 mice for each genotype. Student's t-test. n.s., not significant; p<0.001; ****. (B) Growth analysis of MNV in *Irgm1*$^{-/-}$*Irgm3*$^{-/-}$ or control BMDMs. Cells were untreated or treated with 100 U/ml IFNG for 24 hours and then infected with MNV at MOI=0.05. At 24 hpi, cells were harvested to titer infectious virus. N=3 replicates using 2 mice for each genotype. (C) Growth analysis of MNV in *Irgm1*$^{-/-}$ *Irgm3*$^{-/-}$ and control BMDMs transduced with lentiviruses expressing green fluorescent protein (GFP) (Ctrl.) or IRGM3. Cells were untreated or treated with 100 U/ml IFNG for 12 hours and then infected with MNV at MOI=5. At 12 hpi, cells were harvested to analyze viral replication with anti-ProPol flow cytometry. N=3 replicates using 2 mice for each genotype. (D) Representative western blot data of cells described in (C) for the

Figure 2.8. (continued)
expression of IRGM1, IRGM3, and transduced IRGM3 (detected with anti-T2A antibody against remaining T2A at the C-term of IRGM3 expressed from lentivirus). * indicates non-specific signal. Actin as loading control. N=3 replicates. (E) Growth analysis of MNV in *Gbp*$^{chr3-/-}$ or control BMDMs as described in (B). N=5 replicates using 2 mice for each genotype. (F) Growth analysis of MNV in *Gbp*$^{chr3-/-}$ or control BMDMs transduced with lentiviruses expressing GFP (Ctrl.), GBP1 or GBP2 as described in (B). N=3 replicates using 2 mice for each genotype. (G) A representative western blot of cells described in (F) for the expression of IFN-induced endogenous GBP2 (as a representative) and transduced genes (HA-tagged). Actin as loading control. N=3 replicates. For (B), (C), (E), and (F), data as mean±SEM. One-way ANOVA with Tukey's multiple comparisons test; n.d., not detected. n.s., not significant; *, $p<0.05$; **, $p<0.01$; ***, $p<0.001$; ****, $p<0.0001$. Dashed line indicates the limit of detection.

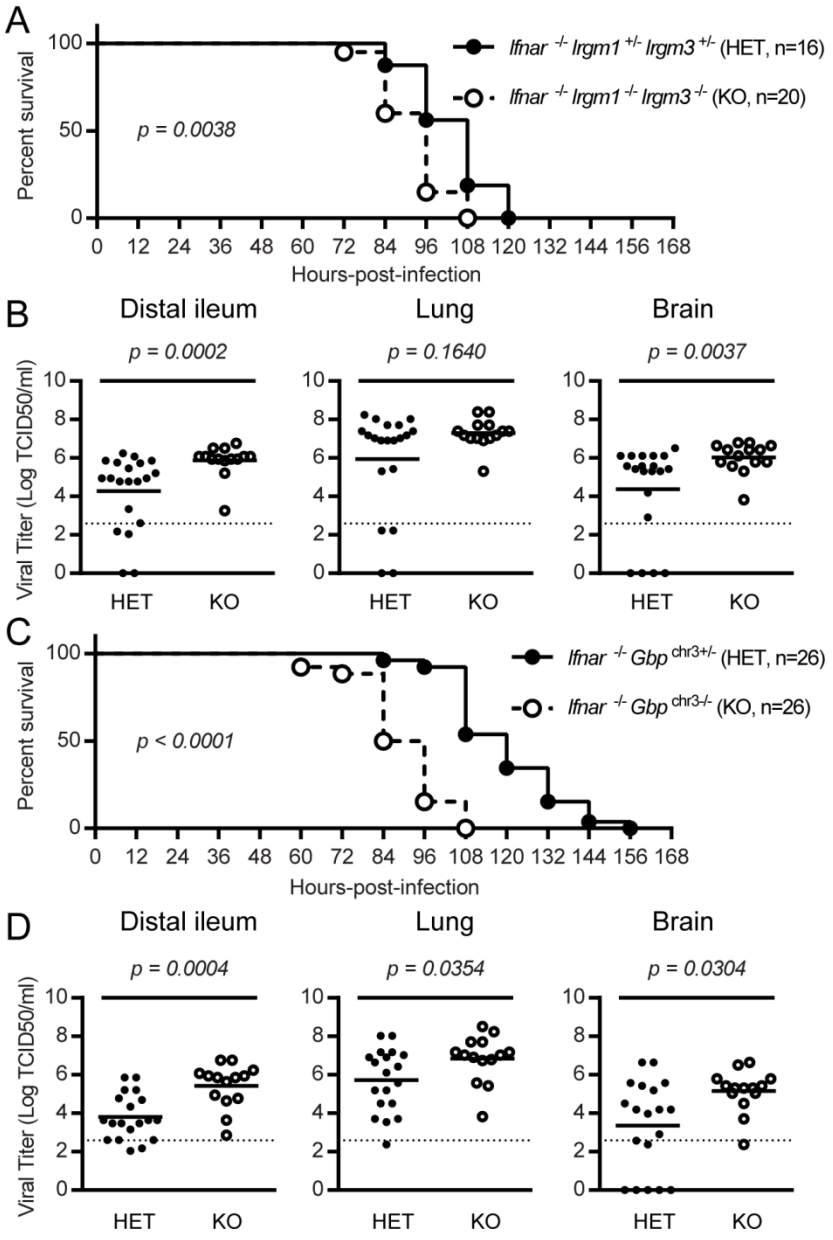

Figure 2.9. IFN-Inducible GTPases Are Required to Control MNV *in vivo*. (A) Survival of *Ifnar*$^{-/-}$*Irgm1*$^{+/-}$*Irgm3*$^{+/-}$ (HET) and *Ifnar*$^{-/-}$*Irgm1*$^{-/-}$*Irgm3*$^{-/-}$ (KO) mice after peroral infection with 1x10^5 plaque forming unit (PFU) of MNV. Numbers in parentheses indicate the number of mice used. (B) Tissue viral burden in the indicated organs of mice at 3 days-post-infection as described in (A). (C and D) The same analysis as described in (A) and (B) with *Ifnar*$^{-/-}$*Gbp*$^{chr3+/-}$ (HET) and *Ifnar*$^{-/-}$*Gbp*$^{chr3-/-}$ (KO) mice. (A) and (C) were analyzed using a Log-rank (Mantel-Cox) test and (B) and (D) were analyzed using a Student's t-test. p-values are indicated in the figure.

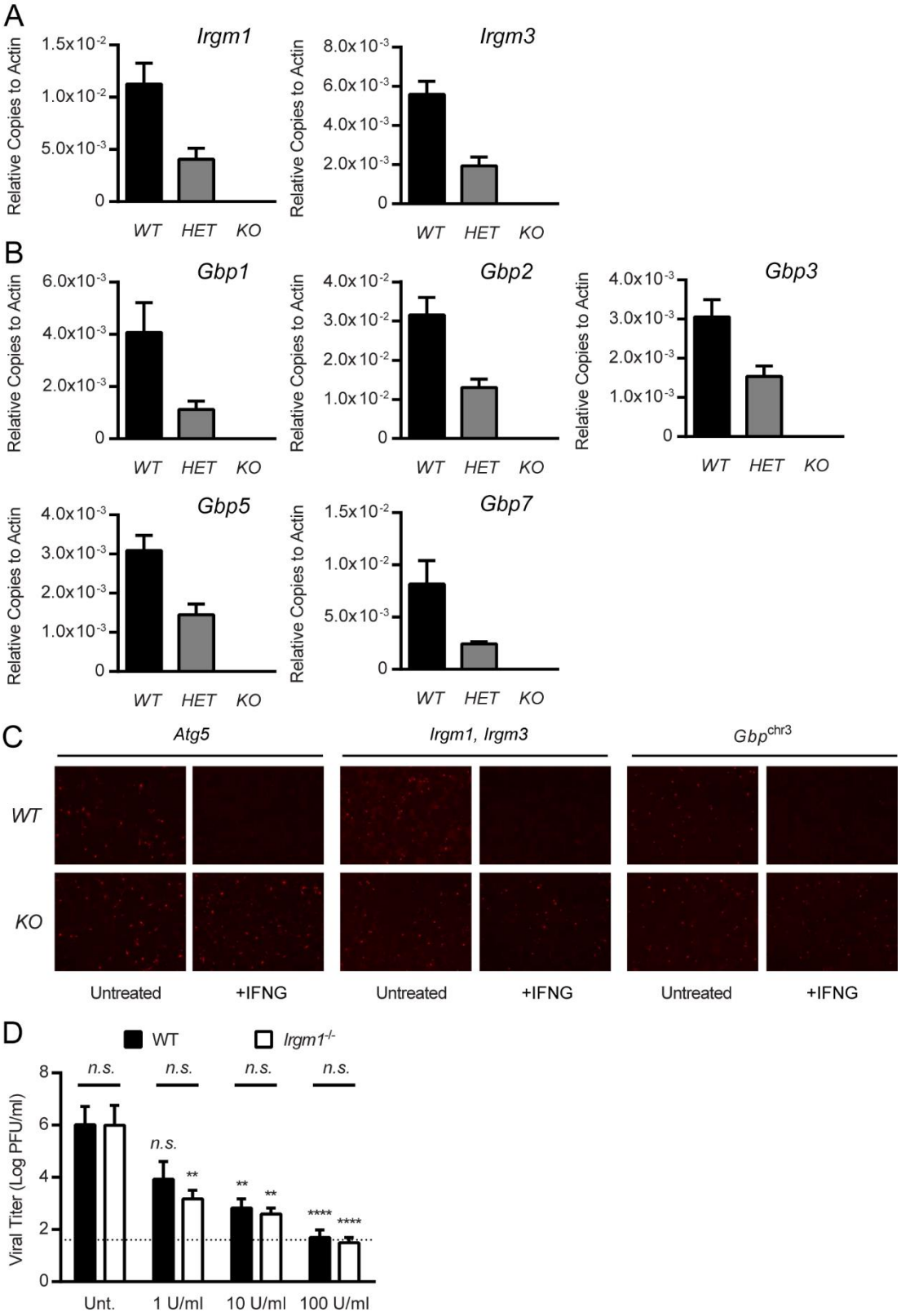

Figure 2.10. Analysis of IFN-inducible GTPase Defective cells. (A) Quantitative PCR analysis for the transcript levels of *Irgm1* and *Irgm3* in BMDMs from *Irgm1*$^{-/-}$*Irgm3*$^{-/-}$mice (KO), compared to wild type (WT) and heterozygote (HET) control mice at 12 hour-post-

Figure 2.10. (continued)
treatment (hpt) of 100 U/ml IFNG. N=3 replicates. (B) Quantitative PCR analysis for the transcript levels of *Gbp1, Gbp2, Gbp3, Gbp5, and Gbp7* in BMDMs from *Gbp*$^{chr3-/-}$ mice (KO) compared to wild type (WT) and heterozygote (HET) control mice at 12 hpt of 100 U/ml IFNG. N=3 replicates. (C) Representative images of MNV RCs in BMDMs from *Atg5*$^{flox/flox}$+*LysMcre*, *Irgm1*$^{-/-}$*Irgm3*$^{-/-}$, *GBP*$^{chr3-/-}$, and their respective littermate control mice. Cells were either untreated or treated with 100 U/ml IFNG for 12 hours before infection with MNV at MOI=5 and harvested and analyzed at 12 hpi with anti-Propol immunofluorescence. N=3 replicates. (D) Growth analysis of MNV in BMDMs from *Irgm1*$^{-/-}$ and littermate control mice. Cells were treated with none (Unt.) or indicated doses of IFNG for 12 hours and then infected with MNV at MOI=0.05. At 24 hpi, cells were harvested to titer infectious virus. Data as mean±SEM. N=3 replicates. One-way ANOVA with Tukey's multiple comparisons test; n.s., not significant; **, $p<0.01$; ****, $p<0.0001$. Dashed line indicates the limit of detection. BMDMs were from 2 mice of each genotype.

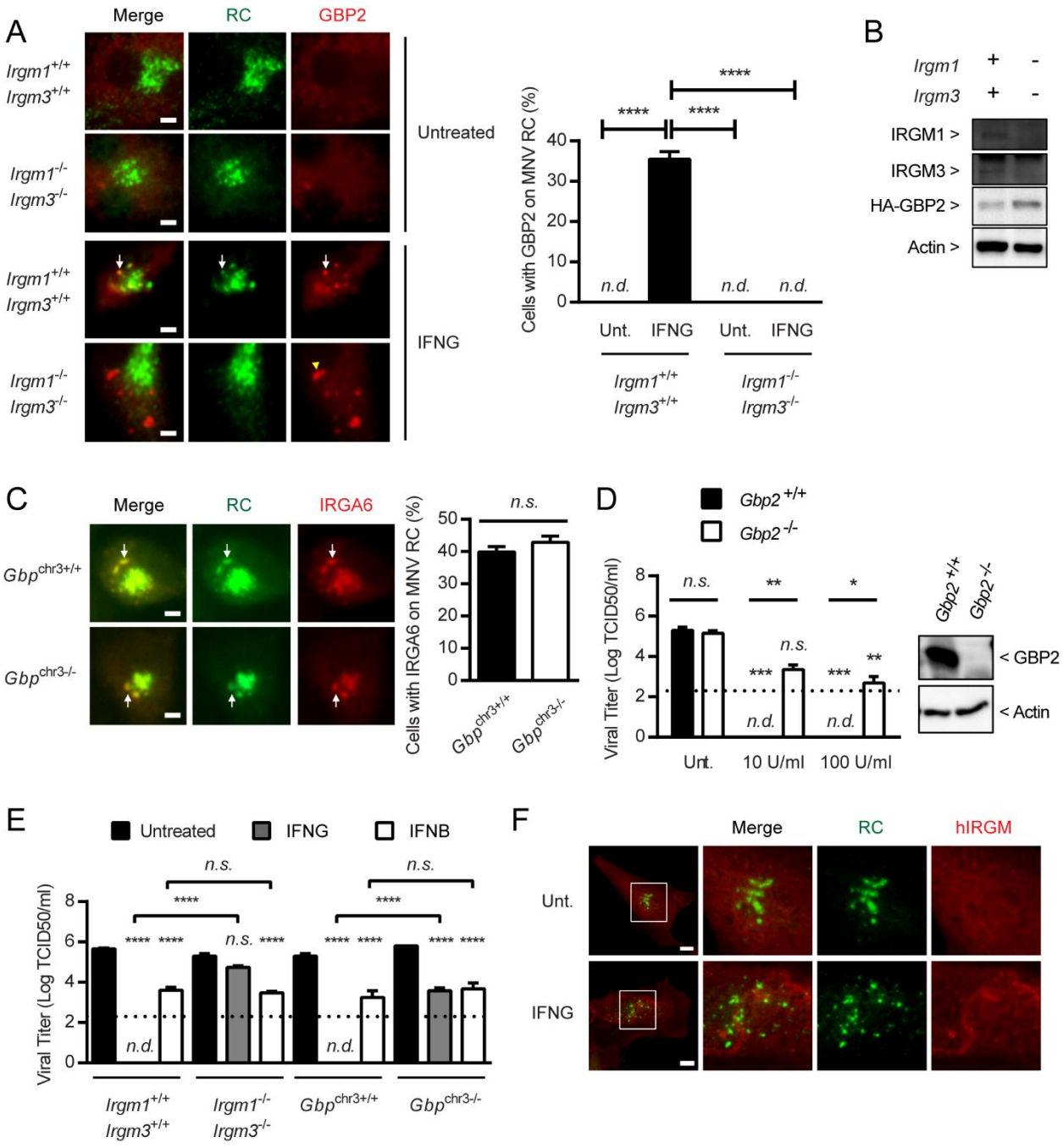

Figure 2.11. IFNG Requires the IFN-Inducible GTPases to Inhibit MNV Replication *in vitro* and *in vivo*. (A) Immunofluorescence analysis of GBP2 in *Irgm1*$^{+/+}$*Irgm3*$^{+/+}$ and *Irgm1*$^{-/-}$*Irgm3*$^{-/-}$ BMDMs transduced with lentiviruses expressing FLAG/HA-tagged GBP2 at 10 hpi of MNV at MOI=5 with simultaneous treatment of none (Untreated) or 100 U/ml IFNG. Representative images (left) and quantitation (right). White arrows indicate representative colocalization and yellow arrowhead indicates a representative aggregate of GBP2. Scale bars, 5 μm. Data as mean±SEM. N=3 replicates. Student's t-test.; ****, p<0.0001. n.d., not detected. (B) A representative western blot of cells

Figure 2.11. (continued)
described in (A). N=3 replicates. (C) The same analysis described in (A) for endogenous IRGA6 in *Gbp*$^{chr3+/+}$ and *Gbp*$^{chr3-/-}$ BMDMs. Data as mean±SEM. N=3 replicates. Student's t-test. n.s., not significant. (D) Growth analysis of MNV in WT and *Gbp2*$^{-/-}$ BMDMs. Cells were treated with none (Unt.), 10 U/ml or 100 U/ml IFNG for 24 hours and then infected with MNV at MOI=0.05. At 24 hpi, cells were harvested to titer infectious virus. Data as mean±SEM. N=4 replicates. n.d., not detected. One-way ANOVA with Tukey's multiple comparisons test; n.s., not significant; *, p<0.05; **, p<0.01; ***, p<0.001. Dashed line indicates the limit of detection. A representative western blot shown (right). (E) Growth analysis of MNV in BMDMs from *Irgm1*$^{-/-}$*Irgm3*$^{-/-}$, *GBP*$^{chr3-/-}$, and their respective littermate control mice. Cells were treated with none (Untreated), 100 U/ml of IFNG, or 100 U/ml of IFN-beta (IFNB) for 24 hours and then infected with MNV at MOI=0.05. At 24 hpi, cells were harvested to titer infectious virus. Data as mean±SEM. N=3 replicates. n.d., not detected. One-way ANOVA with Tukey's multiple comparisons test; n.s., not significant; ****, p<0.0001. Dashed line indicates the limit of detection. (F) Immunofluorescence assay for the localization of endogenous human IRGM (Red) with regard to the MNV RC (Green) in HeLa cells transfected with a plasmid expressing MNV ORF1 for 6 hours followed by treatment with 100 U/ml IFNG for an additional 18 hours. Representative images shown here. Scale bars, 20 μm. N=3 replicates. BMDMs for (A) to (E) were from 2 mice for each genotype.

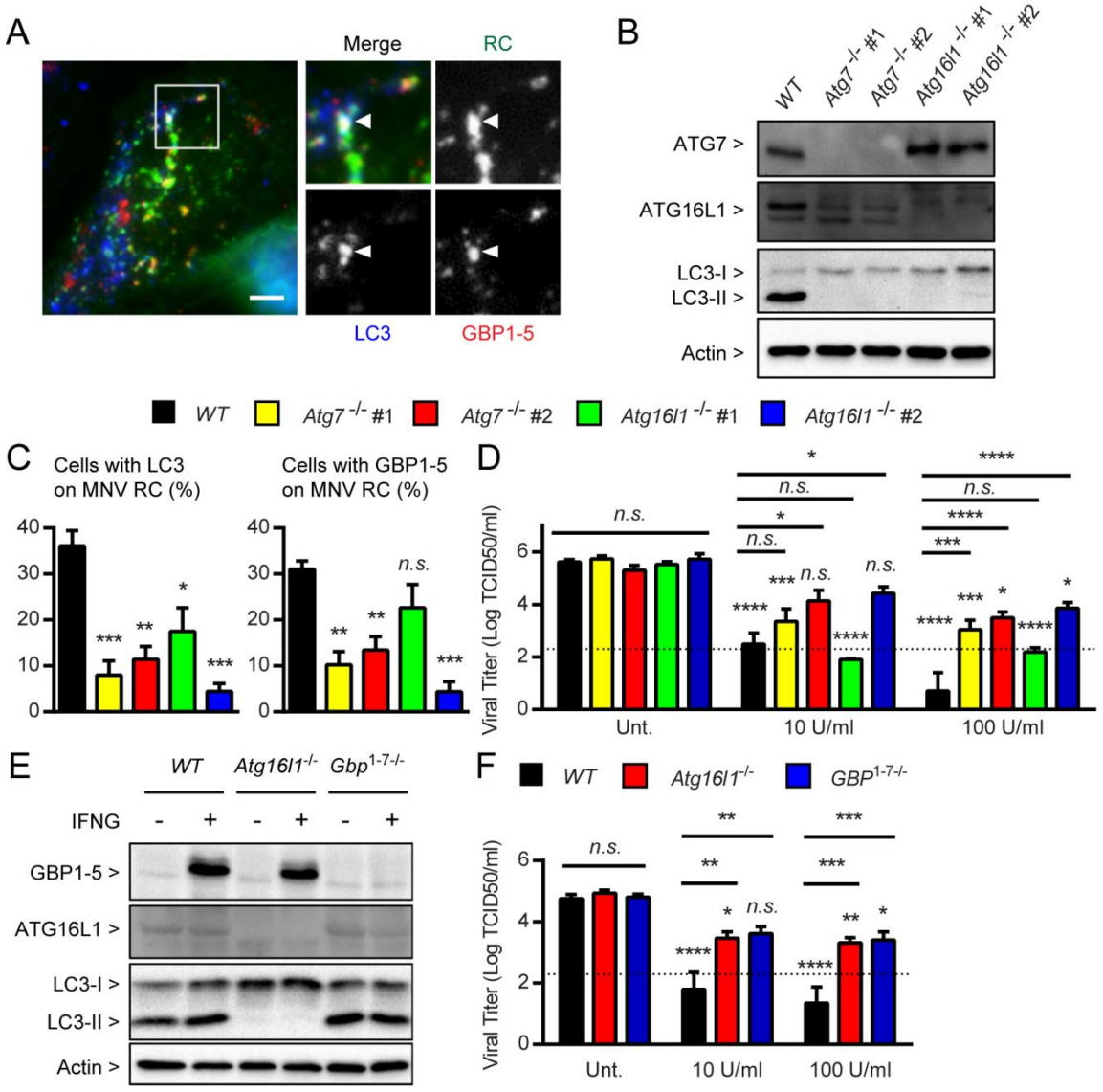

Figure 2.12. The LC3 Conjugation System and IFN-Inducible GTPases Are Required for IFNG to Inhibit MNV Replication in the Human System. (A) Immunofluorescence assay for the localization of LC3 (Blue) and GBP1-5 (Red) with regard to the MNV RC (Green) in HeLa cells transfected with a plasmid expressing MNV ORF1 for 6 hours followed by treatment with 100 U/ml IFNG for an additional 18 hours. Representative images shown here. White arrowheads indicate representative colocalization. Scale bar, 10 μm. N=3 replicates. (B) Representative western blot of HeLa cells; WT, two clones of *Atg7*$^{-/-}$, and two clones of *Atg16l1*$^{-/-}$. N=3 replicates. (C) Quantitation of immunofluorescence assay for the localization of LC3 (left) and GBP1-5 (right) with regard to the MNV RC as described in (A) for the cells described in (B). Data as mean±SEM. N=3 replicates. One-way ANOVA with Dunnett's multiple comparisons test; n.s., not significant; *, p<0.05; **, p<0.01; ***, p<0.001. (D) Growth analysis of MNV in the cells described in (B). The cells were treated with none (Unt.) or the indicated dose of IFNG for 24 hours and then transfected with 50 ng MNV viral RNA. At 24 hpt,

Figure 2.12. (continued)
cells were harvested to titer infectious virus. N=3 replicates. (E) Representative western blot of HAP1 cells; WT, *Atg16l1*$^{-/-}$, and *Gbp*$^{1\text{-}7\text{-}/\text{-}}$. Cells were treated with none or 100 U/ml IFNG for 24 hours. N=3 replicates. (F) Growth analysis of MNV as described in (D) for the cells described in (E). N=3 replicates. Data as mean±SEM. (D) and (F) were analyzed using a One-way ANOVA with Tukey's multiple comparisons test; n.s., not significant; *, $p<0.05$; **, $p<0.01$; ***, $p<0.001$; ****, $p<0.0001$. Dashed line indicates the limit of detection.

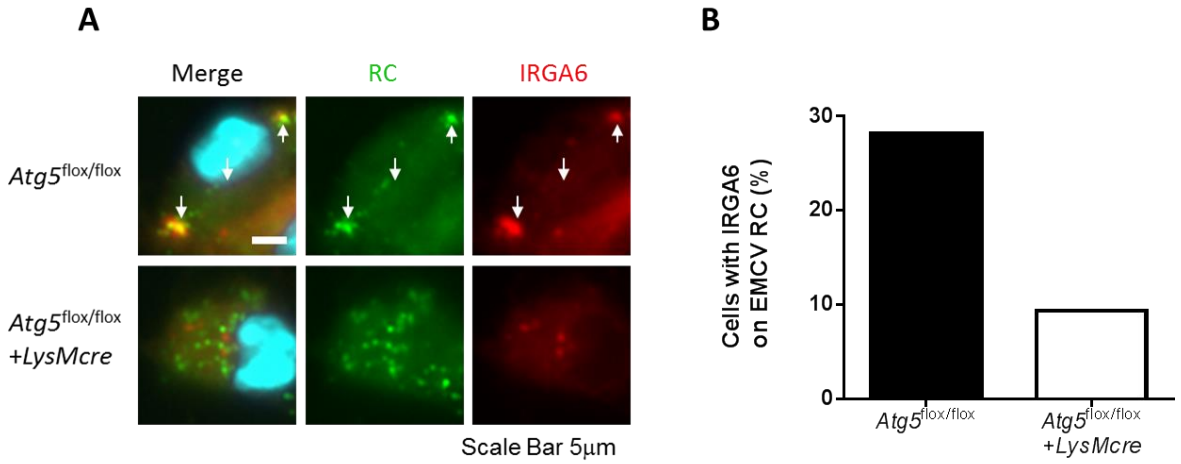

Figure 3.1. The LC3 Conjugation System is Required for Targeting the IFN-inducible GTPases to the EMCV Replication Complex. (A and B) Immunofluorescence assay for the localization IRGA6 with regard to the EMCV RC (via a anti-dsRNA antibody) in *Atg5*$^{flox/flox}$ or *Atg5*$^{flox/flox}$ + *LysMcre* BMDMs at 6 HPI of EMCV at an MOI of 500 with 8 hrs treatment of 100 U/ml IFNG. Representative images (A) and quantitation (B). White arrows indicate representative colocalization. Scale bars, 5 μm. N=1 replicate.

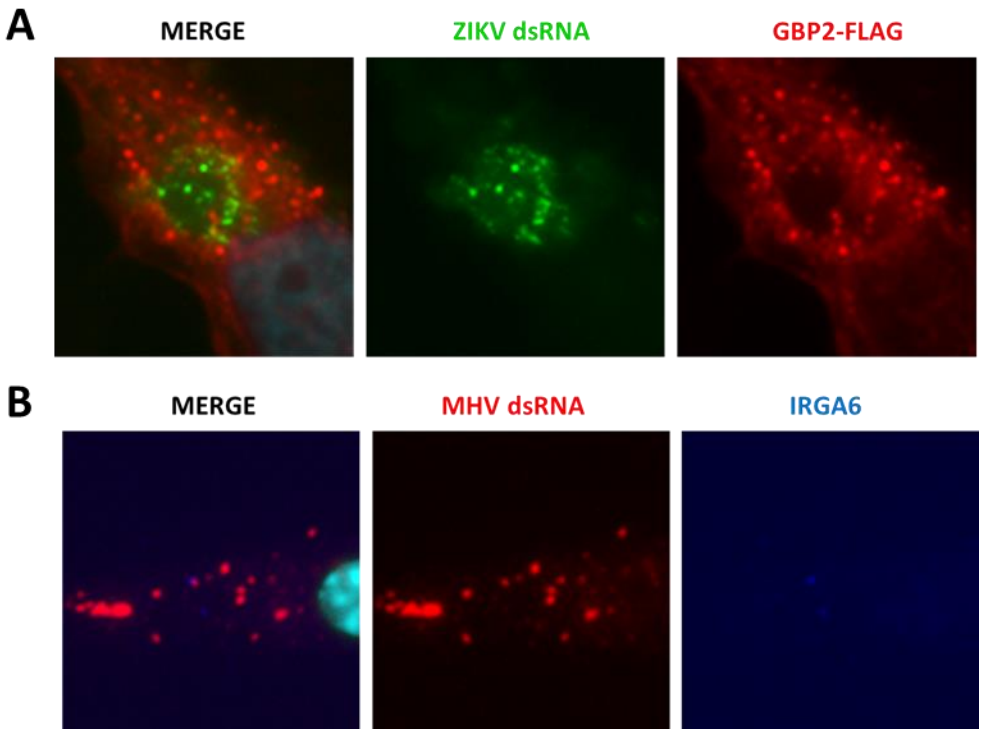

Figure 3.2. The Replication Complexes of Zika Virus and Murine Hepatitis Virus are not Major Targets for the IFN-inducible GTPases. (A and B) Immunofluorescence assay for the localization of FLAG-tagged human GBP2 (A) or IRGA6 (B) with regard to the ZIKV (A) or MHV (B) RC (via a anti-dsRNA antibody). (A) HeLa cells, stably expressing FLAG-tagged human GBP2, were treated with 100 U/ml human IFNG and infected with ZIKV at an MOI of 0.5, simultaneously, cells were fixed 18 hours post infection and IFNG treatment. (B) WT 10% L929-BMDMs were treated with 100 U/ml murine IFNG for 2 hours then infected with MHV at an MOI of 0.05. Cells were fixed 8 hours post infection (10 hours post IFNG treatement). N=3 replicates.

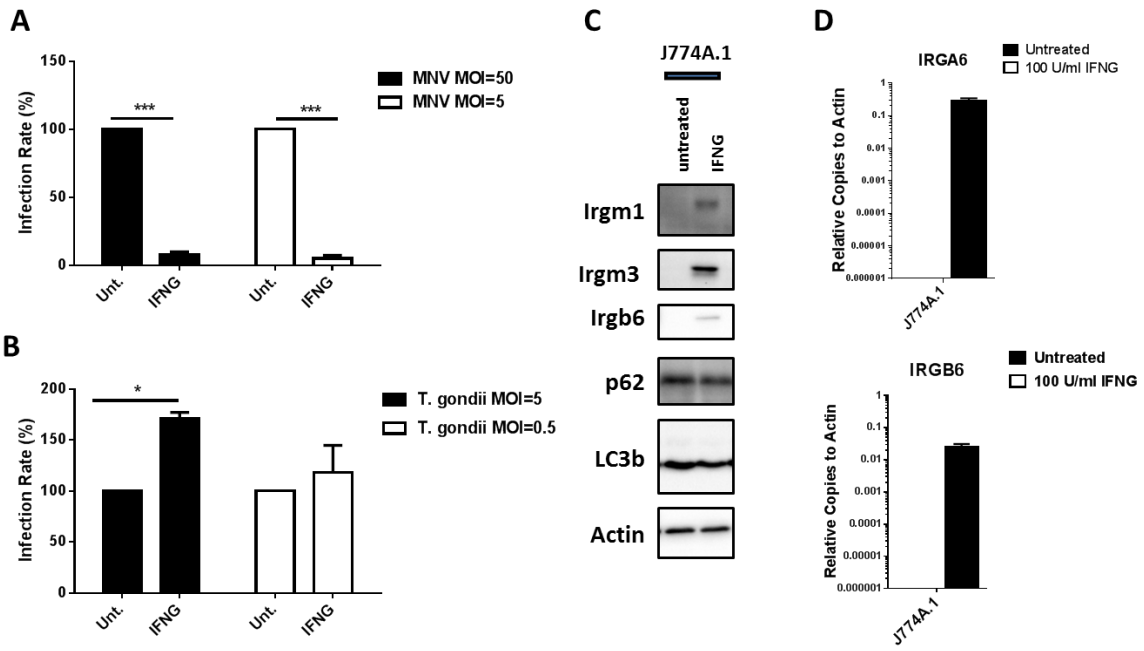

Figure 3.3. Distinct Host Sensing Mechanisms of the *T. gondii* PV and MNV RC. (A) J774A.1 MNV flow-cytometry infection analysis. J774A. cells were pre-treated or not with 100 U/ml IFNG 24 hours and then infected with MNV at the indicated MOIs. Cells were fixed 12 hours post infection. (B) J774A.1 *T. gondii* flow-cytometry infection analysis. J774A. cells were pretreated or not with 100 U/ml IFNG 24 hours pre-infection and then infected with *T. gondii* at the indicated MOIs. Cell were fixed 24 hours post infection. (C) WB analysis of J774A.1 cells treated or not with IFNG for 24 hours. (D) qPCR analysis for the indicated transcripts from J774A.1 cells pretreated or not for 24 hours with IFNG. N=3 replicates.

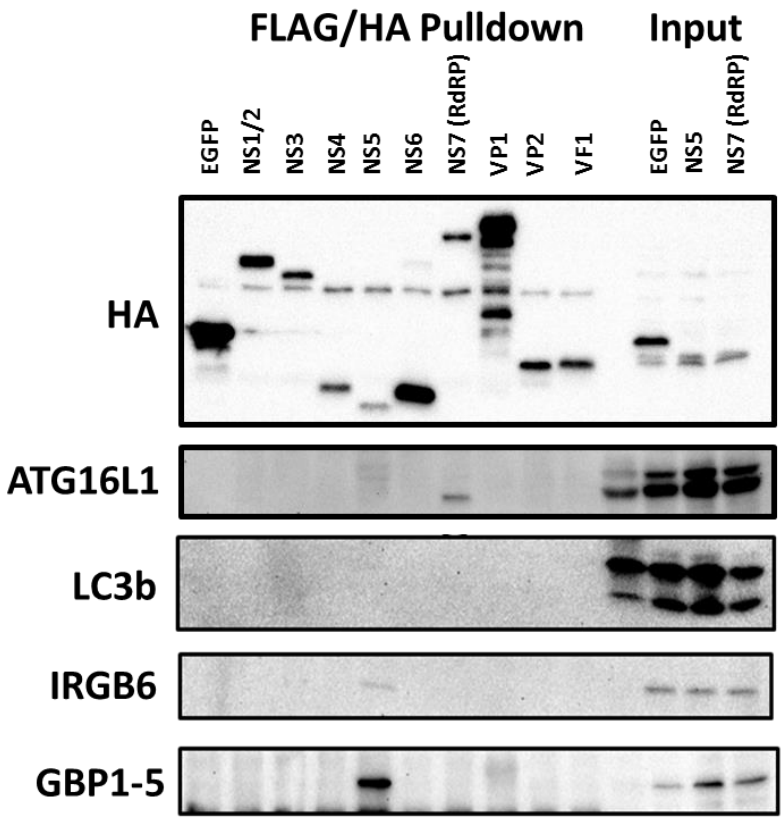

Figure 3.4. Co-Immunoprecipitation Analysis of MNV Proteins with Autophagy Proteins and IFN-inducible GTPases. BV-2 cells stably expressing a FLAG/HA-tagged version of the proteins indicated above were treated with 100 U/ml IFNG for 24 hours then lysed in a 1% Triton-X 100 lysis buffer containing protease inhibitors. Lysates were mixed with anti-FLAG M2 beads for 12 hours, washed 4x in lysis buffer, eluted in 2x sample buffer, then subjected to WB analysis. N=3 replicates.

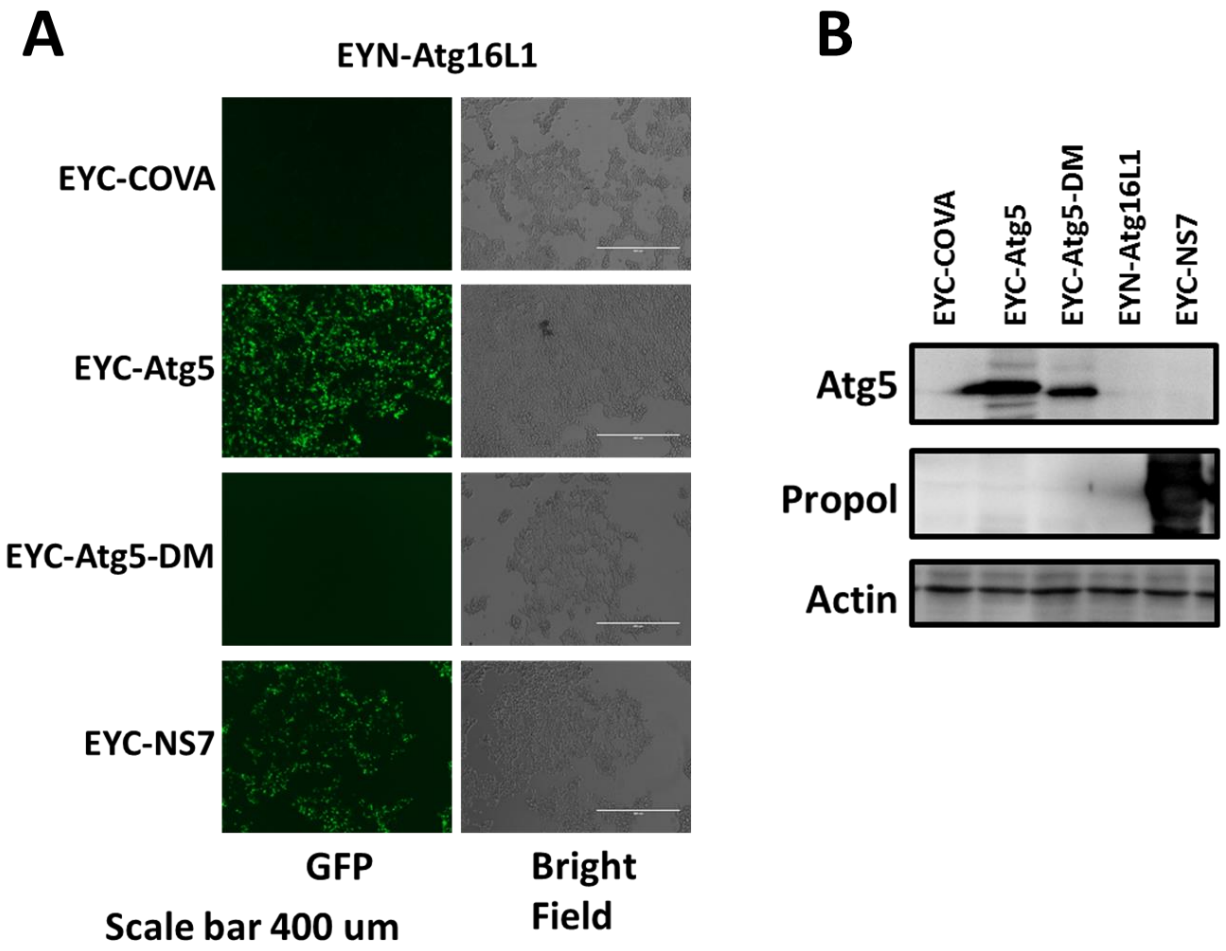

Figure 3.5. Bimolecular Fluorescence Complementation Assay Reveals an Interaction Between Atg16L1 and NS7. (A) 1x10^5 293T cells were seeded in a 24-well plate. The following day cells were co-transfected with 250 ng of EYN-Atg16L1 in addition to the indicated plasmids using lipofectamine 3000 reagents. Cells were incubated at 37° C for 36 hours and then moved to 30° C for 12 hours to allow the complemented YFP to mature. 48 hours post transfection cell were fixed with 2% FA and imaged with a fluorescent microscope on the GFP channel. (B) WB analysis for select samples from A probed with antibodies detecting the indicated proteins. N=3 replicates.

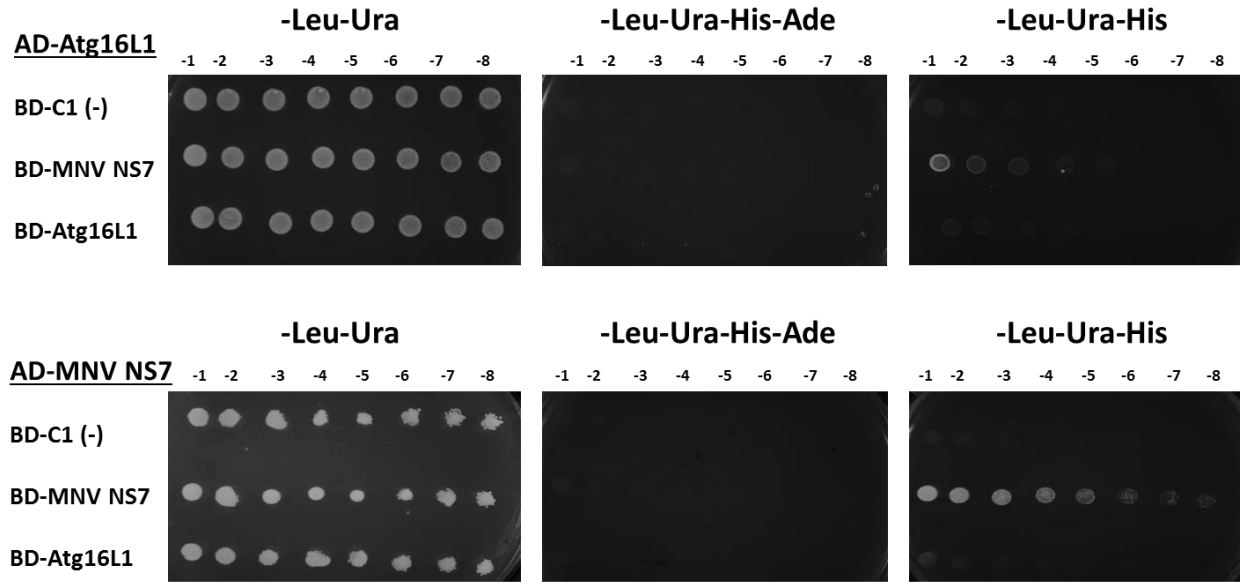

Figure 3.6. Yeast-Two-Hybrid Assay Reveals an Interaction Between Atg16L1 and NS7. (A) The *Saccharomyces cerevisiae* yeast strain PJ69-4A was co-transformed with the indicated plasmid combinations using a lithium acetate transformation strategy then spotted on solid-agar dishes containing the indicated selective medias using 2-fold serial dilutions. Colonies growth was examined 3 days post plating. N=2 replicates.

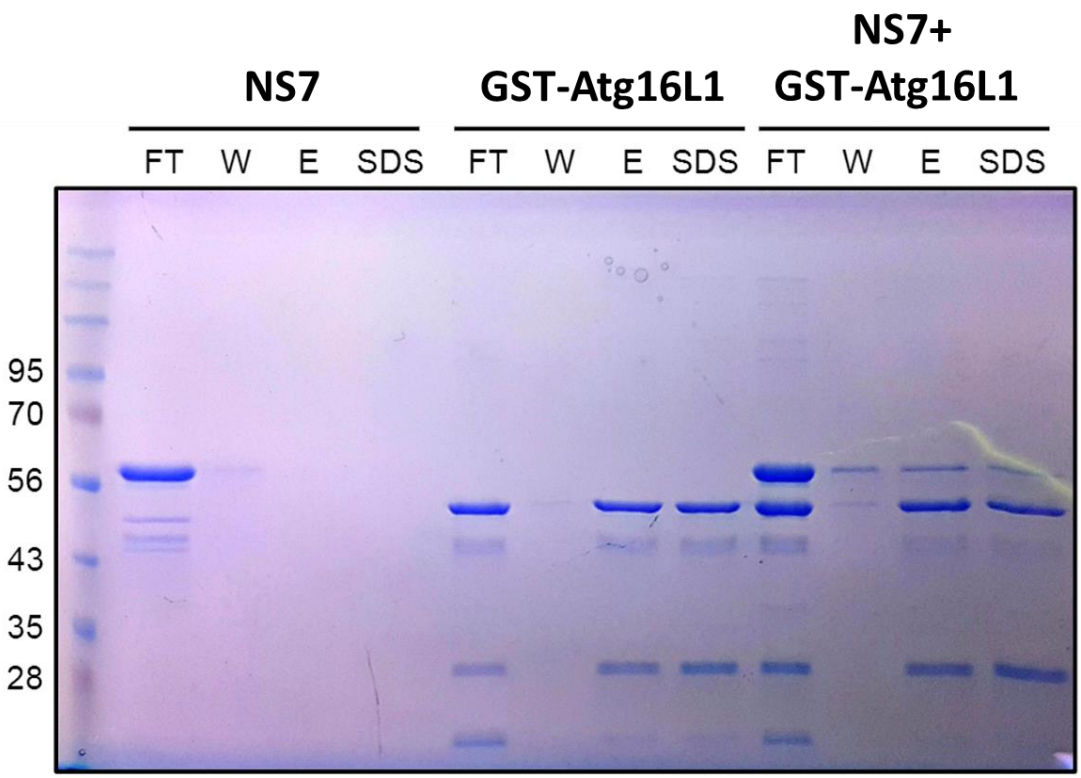

Figure 3.7. GST-Pulldown Analysis Reveals a Direct Interaction Between Atg16L1 and NS7. (A) NS7 and Atg16L1-dN79-249 recombinant proteins were obtained using a bacterial expression system and subjected to a GST-pulldown assay. Proteins in solution were flowed through a column containing glutathione immoblized beads either individually or in combination, washed, eluted with elution buffer, then the remaining proteins bound to the beads was eluted in SDS buffer. The sample fractions were collected and subjected to SDS-PAGE followed by coomassie blue staining. FT= flow through, W= wash, E= elution, SDS= post-eluted beads mixed with SDS buffer.

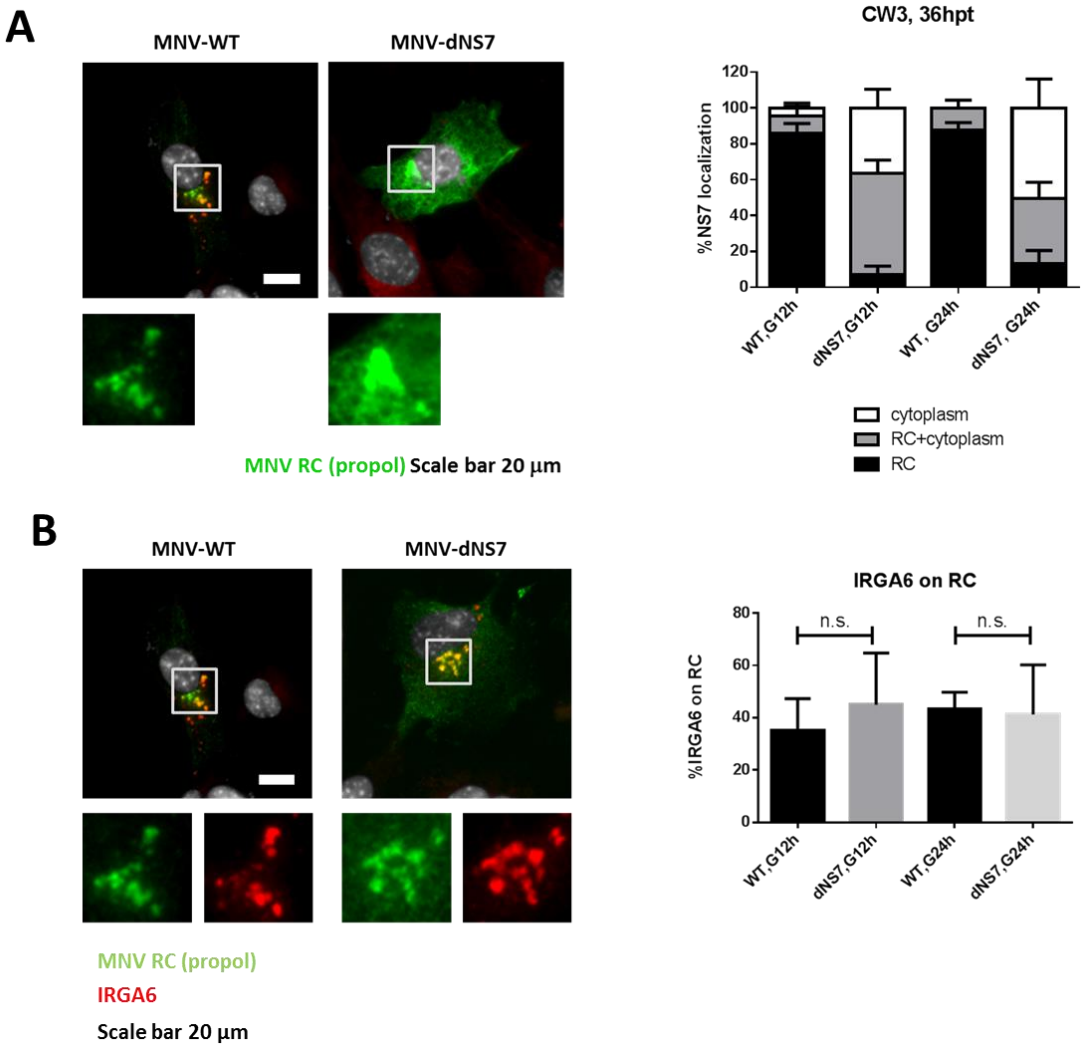

Figure 3.8. IFN-inducible GTPases can Target the MNV Replication Complex in the Absence of MNV NS7. (A) MEFs were transfected with WT MNV ORF1 or MNV ORF1 with an NS7 deletion (dNS7) using lipofectamine 3000. Cells were then treated with 100 U/ml IFNG (or not) 12 or 24 hours later. Cells were fixed 36 hours post transfection for immunofluorecence assay comparing the ability of the two contructs to form a visible RC by propol staining. The left pannel is a representative image and the right pannel is the quantitation of the different staining patterns observed. (B) Same experimental set up as A but stained for IRGA6 (red) in addition to propol (green) to determine the ability of the IFN-inducible GTPases to target to the MNV RC without NS7. The left pannels are representative images while the right is the quantitation of IRGA6 targeting to the RC. G12h= treated with IFNG for 12 hours, G24h= treated with IFNG for 24 hours. All scale bars are 20 µm. N=3 replicates.

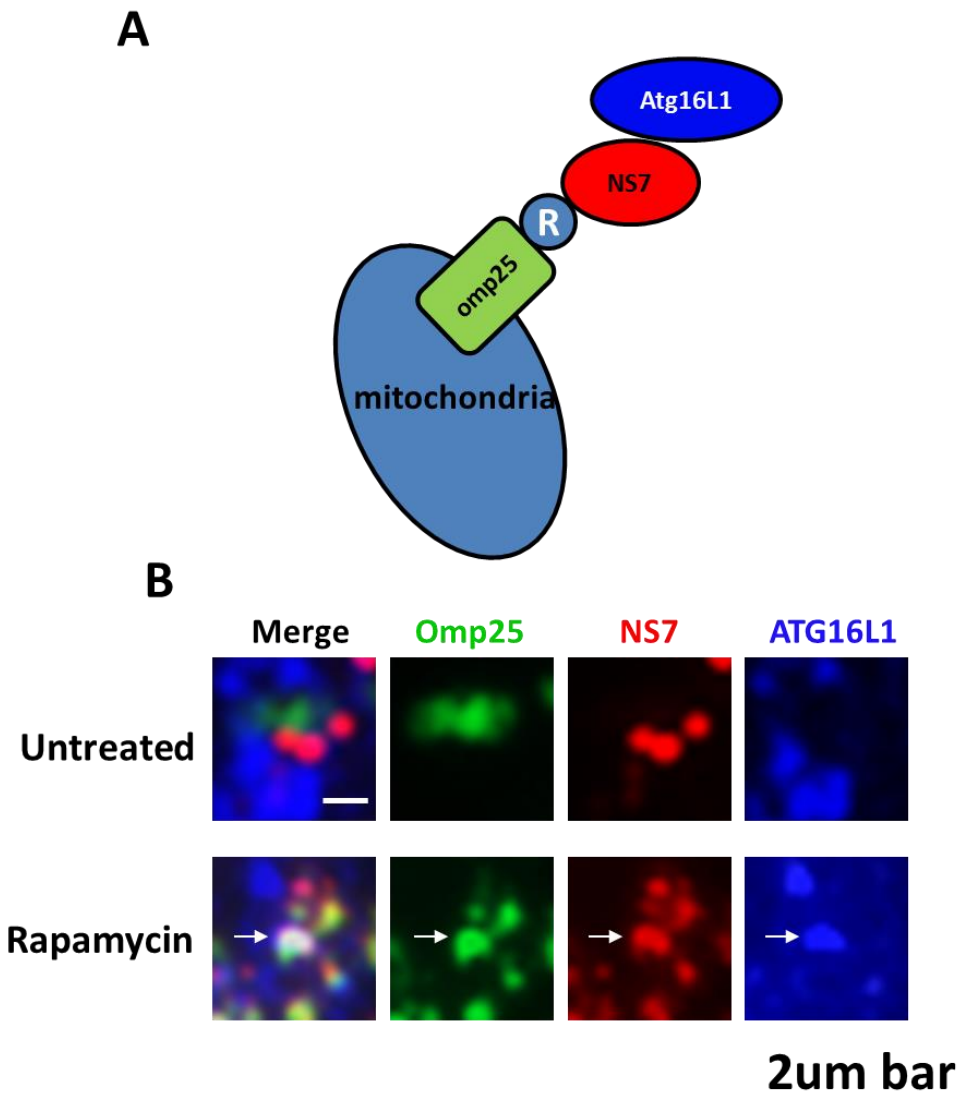

Figure 3.9. NS7 is Sufficient to Designate a Target Membrane for Atg16L1. (A and B) WT MEFs were transfected, using lipofectamine 3000, with two constructs encoding a mitochondrial anchor (pEGFP-N1-TOMM20-2xFRB) and a bait construct (pDRFP-MNV-NS7-4xFKBP). 24 hours after transfection cells, were treated with 100 U/ml IFNG. 48 hours post transfection and 24 hours post IFNG treatment, cells were treated with 50 nM of rapamycin or a DMSO vehicle control for 2 h and fixed for immunofluorescence analysis. (A) is a schematic diagram of the anchor away process and (B) are representative images. R = rapamycin. N=1 replicate.

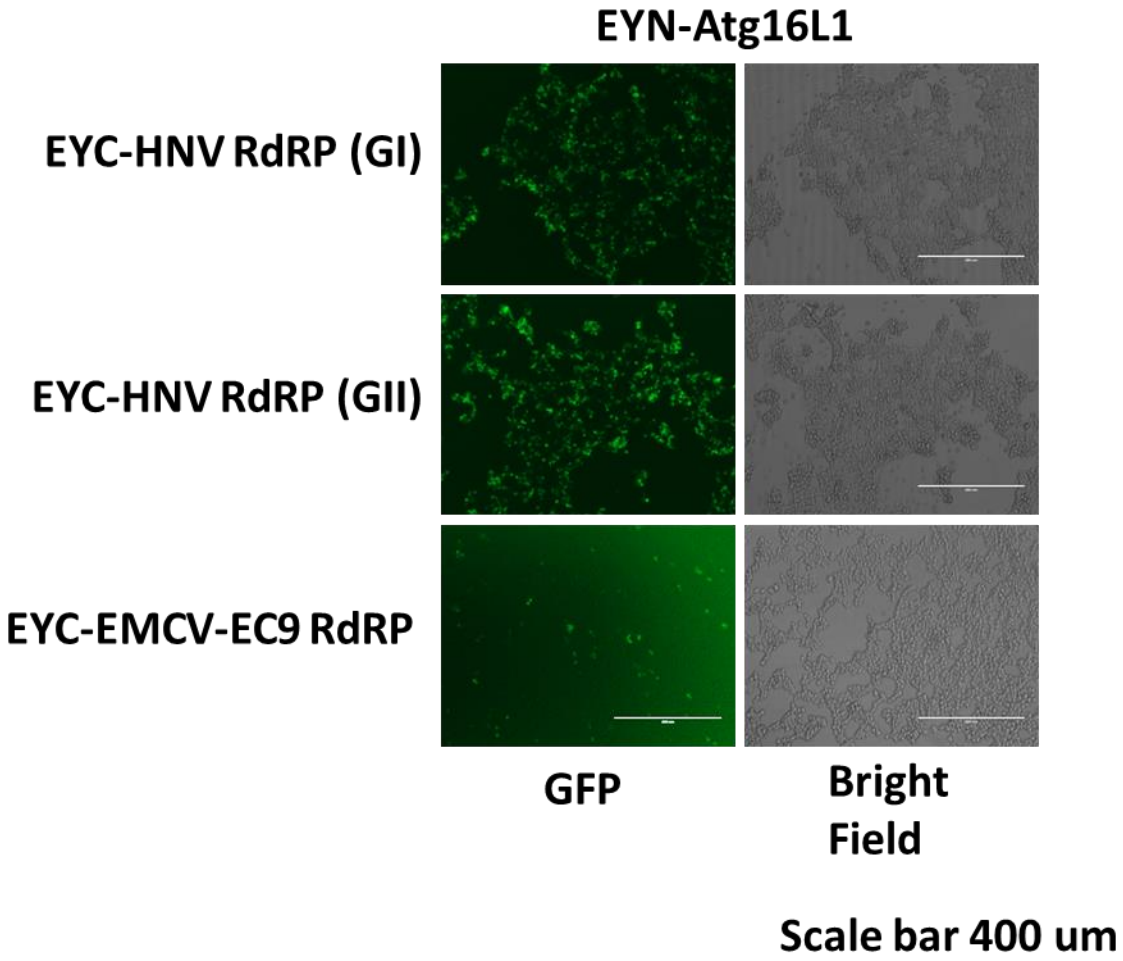

Figure 3.10. Bimolecular Fluorescence Complementation Assay Reveals an Interaction Between Atg16L1 and the RdRPs of Other (+)RNA Viruses. (A) $1x10^5$ 293T cells were seeded in a 24-well plate. The following day cells were co-transfected with 250 ng of EYN-Atg16L1 in addition to the indicated plasmids using lipofectamine 3000 reagents. Cells were incubated at 37° C for 36 hours and then moved to 30° C for 12 hours to allow the complemented YFP to mature. 48 hours post transfection cell were fixed with 2% FA and imaged with a fluorescent microscope on the GFP channel. N=3 replicates.

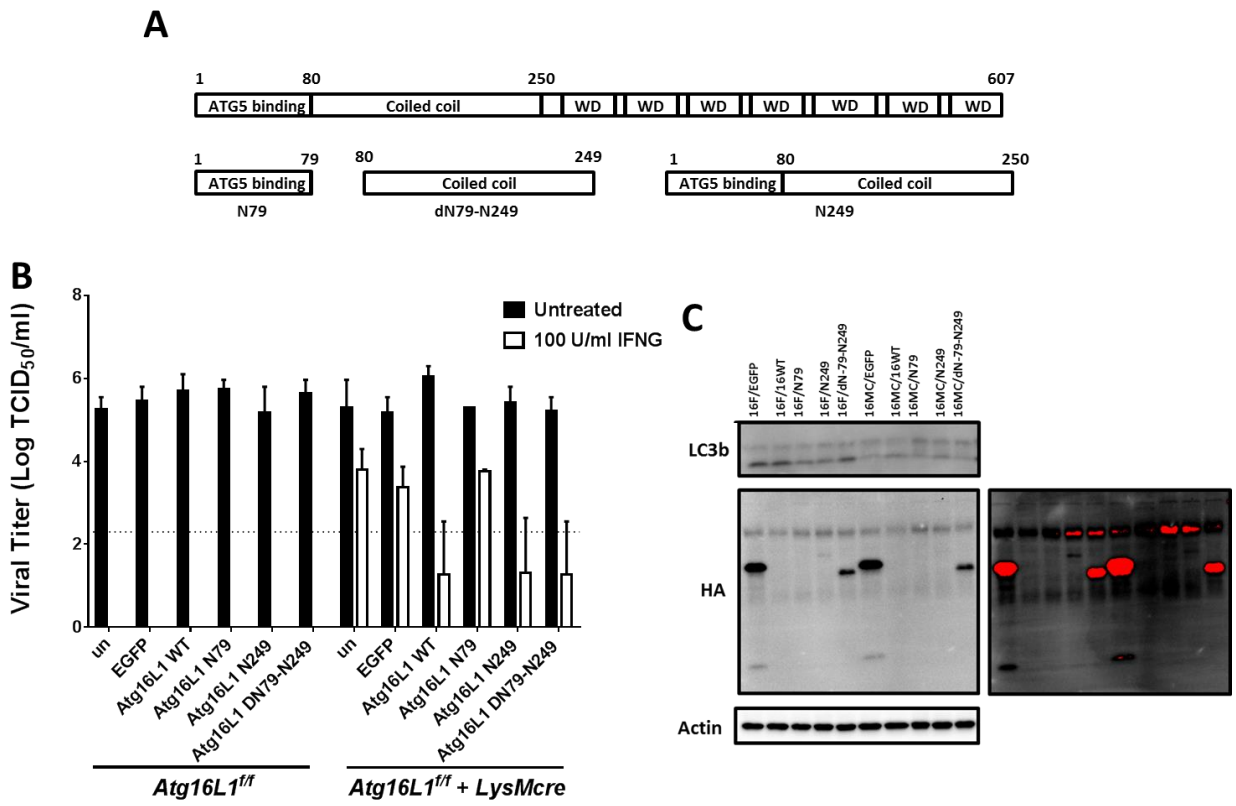

Figure 3.11. The Coiled-coil domain of Atg16L1 is Essential for the IFNG Mediated Antiviral Activity Against MNV. (A) A schematic diagram of the domains of Atg16L1. (B) TCID50 analysis of MNV viral infection of *Atg16L1*$^{flox/flox}$ (16F) or *Atg16L1*$^{flox/flox}$ + *LysMcre* (16MC) D21 BMDMs grown in 10% CMG14-12 media as a source of M-CSF, reconstituted with the indicated HA tagged-Atg16L1 truncation mutants. BMDMs were treated (or not) with 100 U/ml IFNG for 24 hours then infected with MNV at an MOI of 0.05 and the entire plate was frozen in a negative 80° C freezer before being tittered by TCID50. (C) WB analyis of the samples from B. N=2 replicates.

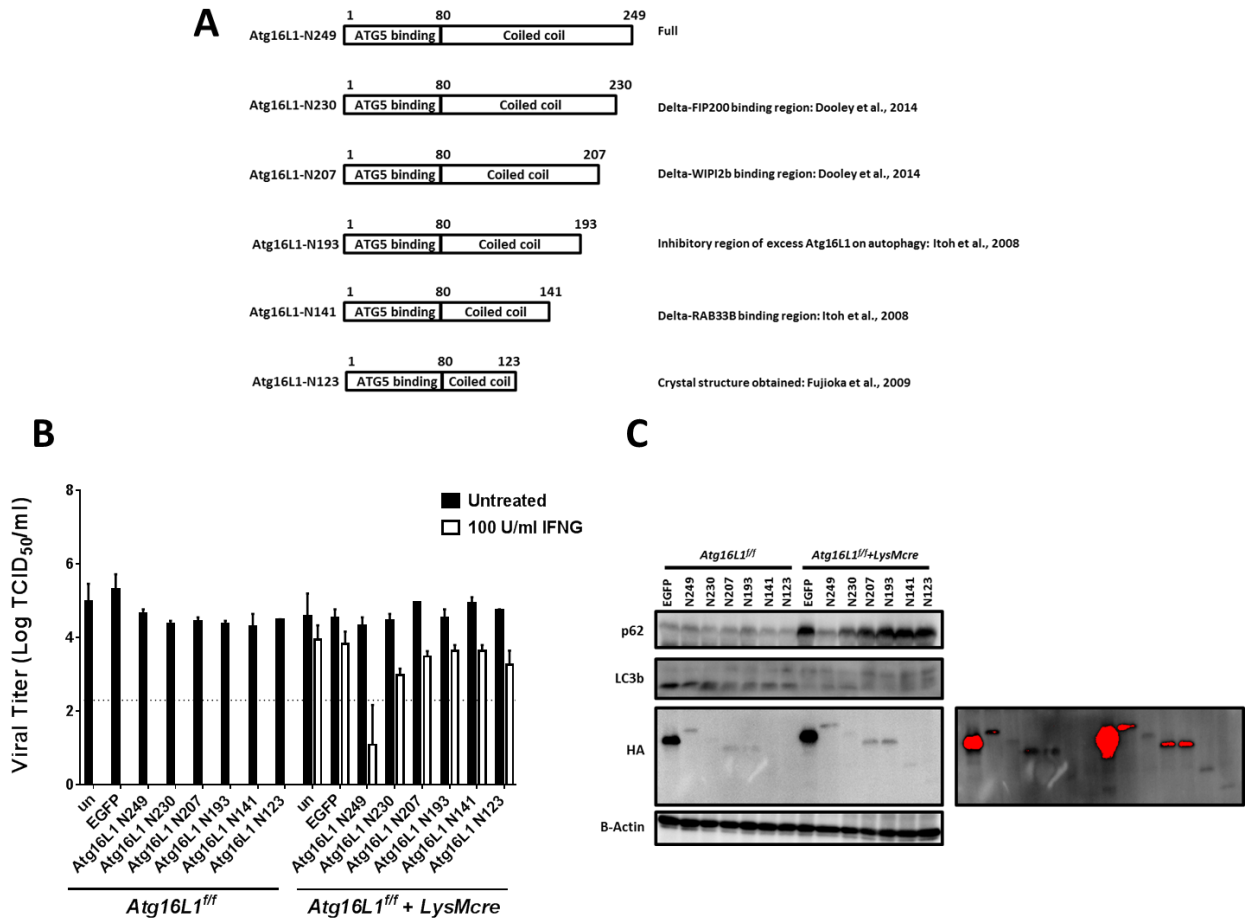

Figure 3.12. A 19 Amino Acid Region in the Coiled-coil domain of Atg16L1 is Essential for the IFNG Mediated Antiviral Activity Against MNV. (A) A schematic diagram of the Coiled-coil region truncation mutants of Atg16L1 utilized. (B) TCID50 analysis of MNV viral infection of *Atg16L1*$^{flox/flox}$ (16F) or *Atg16L1*$^{flox/flox}$ + *LysMcre* (16MC) D21 BMDMs grown in 10% CMG14-12 media as a source of M-CSF, reconstituted with HA tagged-Atg16L1 truncation mutants. BMDMs were treated (or not) with 100 U/ml IFNG for 24 hours then infected with MNV at an MOI of 0.05 and the entire plate was frozen in a negative 80° C freezer before being tittered by TCID50. (C) WB analyis of the samples from B. N=2 replicates.

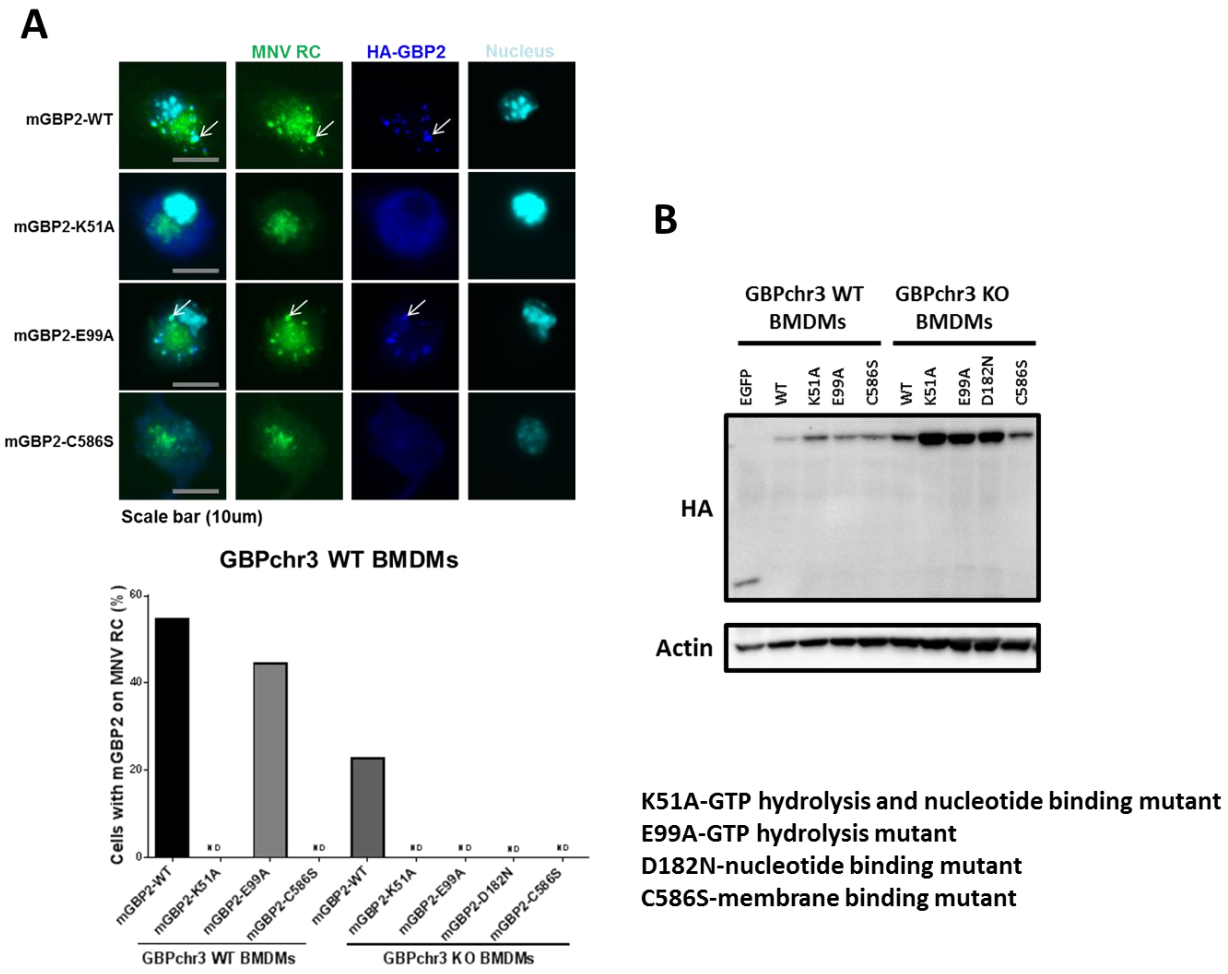

Figure 3.13. The GTPase Domain and the Membrane Binding Domain of Murine GBP2 are Required to Target to the MNV Replication Complex. (A) Immunofluorescence analysis of BMDMs from *GBPchr3* WT and KO mice reconstituted with HA-tagged WT or mutants of murine GBP2. D14 BMDMs are infected with MNV at an MOI of 5 and simultaneously treated with 100 U/ml of IFNG and fixed 10 hours post infection/treatment for staining and quantitation. Top pannel shows representative images from *GBPchr3* WT BMDMs while the bottom pannel shows the quantitation of HA stained GBPs targeted to the MNV RC in both *GBPchr3* WT and KO BMDMs. (B) WB analysis of the cells in A. N=1 replicate.

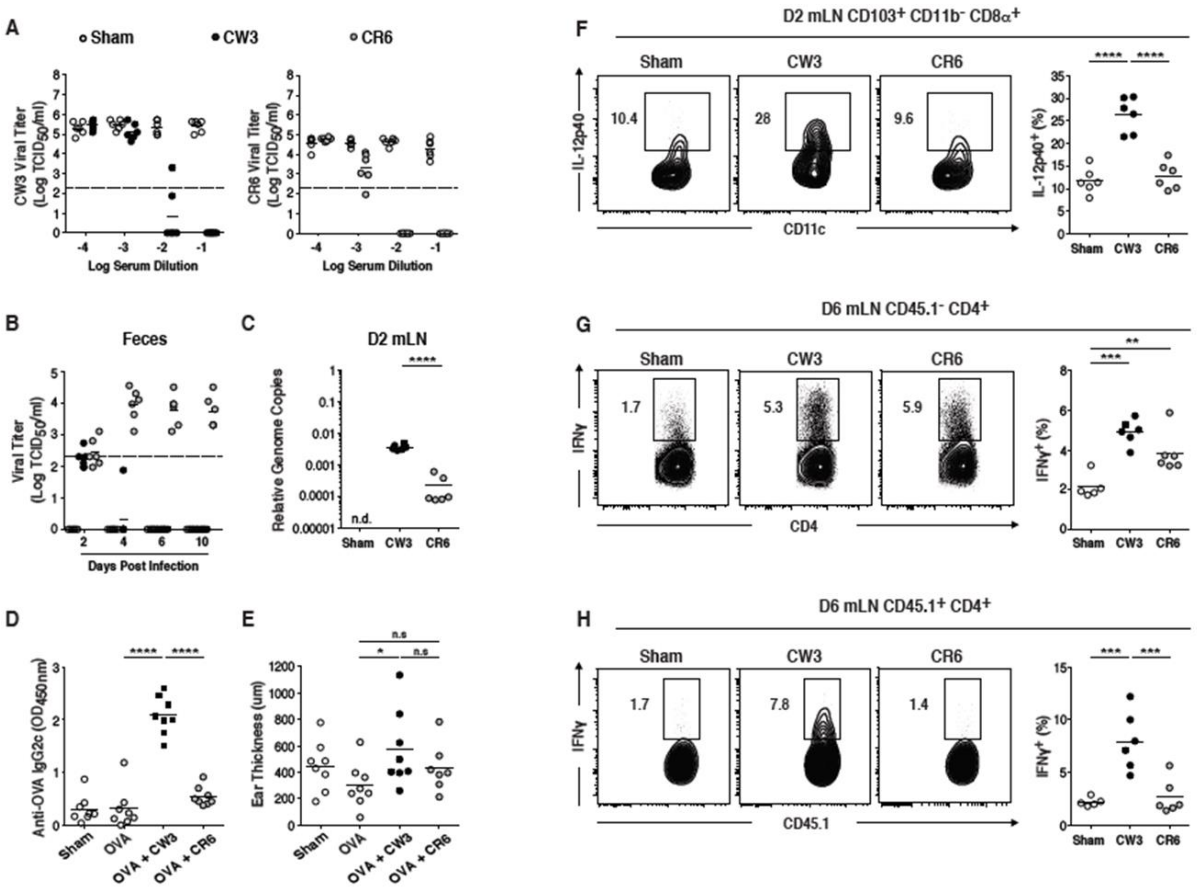

Figure C.1. MNV-CW3 induces the loss of tolerance to dietary antigen. (A and B) C57BL/6 mice were inoculated with medium (n = 6 mice), CW3 5e7 (n = 6 mice), or CR6 5e7 (n = 6 mice) and sera were harvested 18 days post infection. **(A)** Sera were incubated with CW3 or CR6 prior to cell infection. CW3 or CR6 titers were then evaluated. **(B)** Titers in the feces were evaluated at the indicated time points. For A and B, dashed lines indicate the limit of detection. **(C and F)** C57BL/6 mice were inoculated with medium (n = 6 mice), CW3 5e7 (n = 6 mice), or CR6 5e7 (n = 6 mice) and mLNs were harvested 48 hpi. **(C)** Quantification of genome copies in the mLN was evaluated by RT-PCR. **(F)** Expression of IL-12p40 on the $CD103^+$ $CD11b^-$ $CD8\alpha^+$ DC subset in the mLN was evaluated by FACS. Graphs depict 2 independent experiments. **(D and E)** C57BL/6 mice were inoculated perorally with 5e7 PFU of CW3 or CR6 at the initiation of an oral tolerance/delayed type hypersensitivity protocol. Mice were fed orally with ovalbumin (OVA) for 2 days and then immunized subcutaneously with a CFA-OVA emulsion. Levels of OVA-specific IgG2c antibodies **(D)** in the serum were quantified at day 16 by means of enzyme-linked immunosorbent assay (ELISA). On day 28, mice were challenged subcutaneously with OVA, and the degree of ear swelling **(D)** was determined 48 hours after challenge. Sham (n = 8 mice), OVA (n = 8 mice), OVA + CW3 (n = 8 mice) and OVA + CR6 (n = 7 or 8 mice). Graphs depict 2 independent experiments. **(G and H)** $OT\text{-}II^+$ $CD45.1^+$ $CD4^+$ T cells were transferred into C57BL/6 $CD45.2^+$ mice. One day after transfer, mice were inoculated perorally with medium (sham, n = 5), CW3 5e7 (n = 6 mice) or CR6 5e7 (n = 6 mice) and fed an OVA

Figure C.1. (continued)
containing diet for 6 days. Expression of IFNγ in recipient $CD4^+$ T cells **(G)** and transferred OT-II^+ $CD45.1^+$ $CD4^+$ T cells **(H)** in the mLN was evaluated by FACS. Graphs depict 2 independent experiments. For all experiments with quantitative analysis, data are shown as mean. One-way ANOVA with Tukey's multiple comparisons test; n.d., not detected. n.s., not significant; *$p < 0.05$; **$p < 0.01$; ***$p < 0.001$; ****$p < 0.0001$.

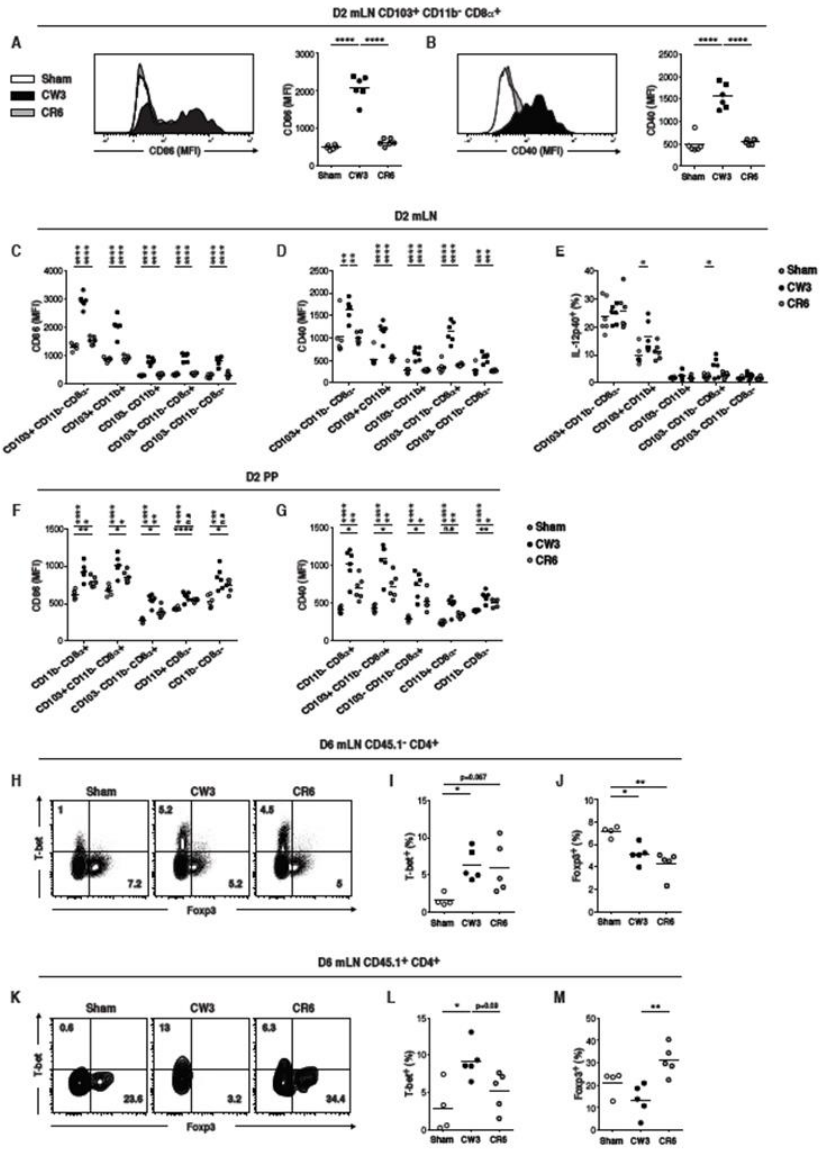

Figure C.2. MNV-CW3 induces the loss of tolerance to dietary antigen, part 2. (A to G) C57BL/6 mice were inoculated with medium (n = 6 mice), CW3 5e7 (n = 6 mice) or CR6 5e7 (n = 6 mice) and mLN were harvested 48 hpi. (A and B) Expression of the DC activation markers CD86 **(A)** and CD40 **(B)** on $CD103^+$ $CD11b^-$ $CD8\alpha^+$ DC subset in the mLN was evaluated by FACS. Expression of the DC activation markers CD86 **(C)** and CD40 **(D)**, and IL-12p40 **(E)** on the other DC subsets in the mLN was evaluated by FACS. **(F and G)** Expression of the DC activation markers CD86 **(F)** and CD40 **(G)** in the PP DC subsets were evaluated 48hpi. Graphs depict 2 independent experiments. **(H to M)** OT-II^+ $CD45.1^+$ $CD4^+$ T cells were transferred into C57BL/6 $CD45.2^+$ mice. One day after transfer, mice were inoculated perorally with medium (sham, n = 4), CW3 5e7 (n = 5 mice) or CR6 5e7 (n = 5 mice) and fed an OVA containing diet for 6 days. Expression of T-bet and Foxp3 in recipient CD4+ T cells **(H to J)** and transferred OT-II^+ $CD45.1^+$ $CD4^+$ T cells **(K to M)** in the mLN were evaluated by FACS. Graphs depict 2 independent experiments. For all experiments with quantitative analysis, data are

Figure C.2. (continued)
shown as mean. One-way ANOVA with Tukey's multiple comparisons test; n.s., not significant; *p < 0.05; **p < 0.01; ***p < 0.001; ****p < 0.0001.

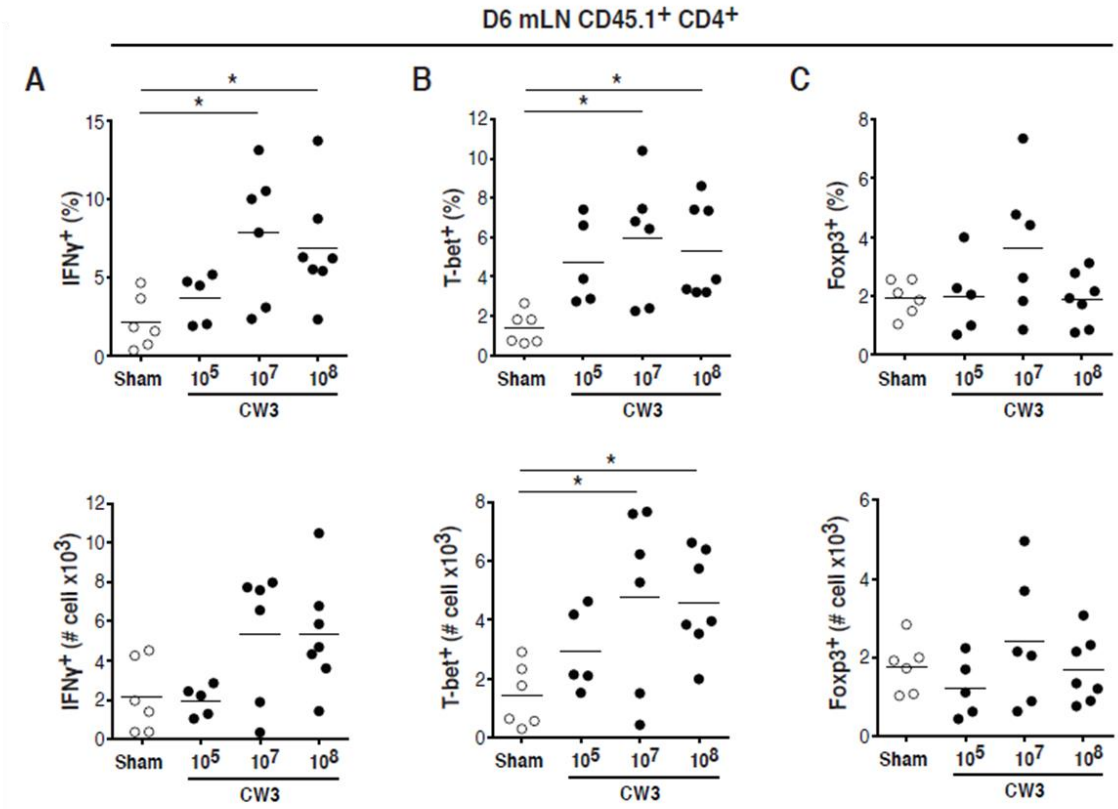

Figure C.3. MNV-CW3 induces the loss of tolerance to dietary antigen, part 3. OT-II$^+$ CD45.1$^+$ CD4$^+$ T cells were transferred into C57BL/6 CD45.2$^+$ mice. One day after transfer, mice were inoculated perorally with medium (sham, n = 6), CW3 1e5 (n = 5 mice), CW3 1e7 (n = 6 mice) or CW3 1e8 (n = 7 mice) and fed 1.5% OVA in the drinking water for 6 days. Expression of IFNγ **(A)**, T-bet **(B)** and Foxp3 **(C)** in transferred OT-II$^+$ CD45.1$^+$ CD4$^+$ T cells in the mLN were evaluated by FACS. Percentages and cells number are shown. Graphs depict 2 independent experiments. For all experiments with quantitative analysis, data are shown as mean. One-way ANOVA with Tukey's multiple comparisons test; *p < 0.05; **p < 0.01; ***p < 0.001; ****p < 0.0001.

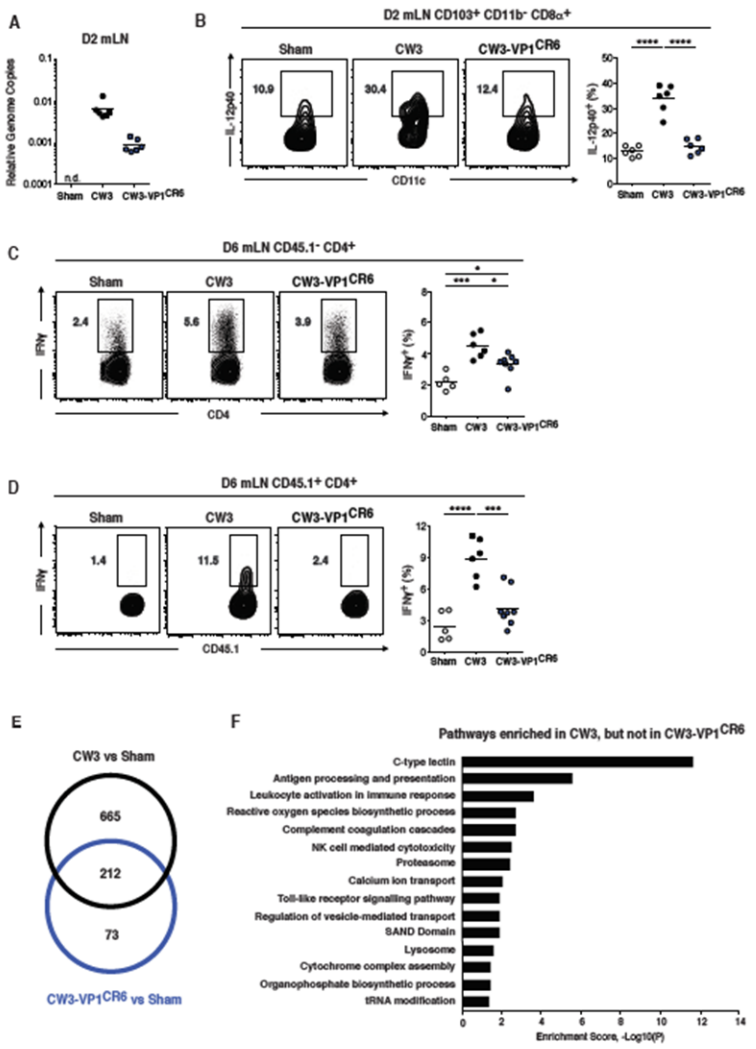

Figure C.4. VP1 gene from CW3 is the viral genetic determinant of MNV induced inflammatory response to dietary antigen. (A and B) C57BL/6 mice were inoculated with medium (n = 6 mice), CW3 5e7 (n = 6 mice), or CW3-VP1^{CR6} 5e7 (n = 6 mice) and mLNs were harvested 48 hpi. **(A)** Quantification of genome copies in the mLN was evaluated by RT-PCR. **(B)** Expression of IL-12p40 on the CD103^{+} CD11b^{-} CD8α^{+} DC subset in the mLN was evaluated by FACS. Graphs depict 2 independent experiments. **(C and D)** OT-II^{+} CD45.1^{+} CD4^{+} T cells were transferred into C57BL/6 CD45.2^{+} mice. One day after transfer, mice were inoculated perorally with medium (sham, n = 6), CW3 5e7 (n = 6 mice) or CW3-VP1^{CR6} 5e7 (n = 6 mice) and fed an OVA containing diet for 6 days. Expression of IFNγ in recipient CD4^{+} T cells **(C)** and transferred OT-II^{+} CD45.1^{+} CD4^{+} T cells **(D)** in the mLN were evaluated by FACS. Graphs depict 2 independent experiments. **(E and F)** C57BL/6 mice were inoculated with medium (n = 5 mice), CW3 5e7 (n = 5 mice), or CW3-VP1^{CR6} 5e7 (n = 5 mice) and mLNs were harvested 48 hpi. Transcriptional responses to each of the viruses indicated were analyzed by RNAseq. **(E)** Venn diagram showing the number virus-specific and shared response genes that were differentially induced relative to Sham. Enriched pathways and processes of differentially induced genes that were **(F)** enriched for CW3 but distinct from CW3-

Figure C.4. (continued)
$VP1^{CR6}$. Graphs depict 2 independent experiments. For all experiments with quantitative analysis, data are shown as mean. One-way ANOVA with Tukey's multiple comparisons test; *p < 0.05; **p < 0.01; ***p < 0.001; ****p < 0.0001.

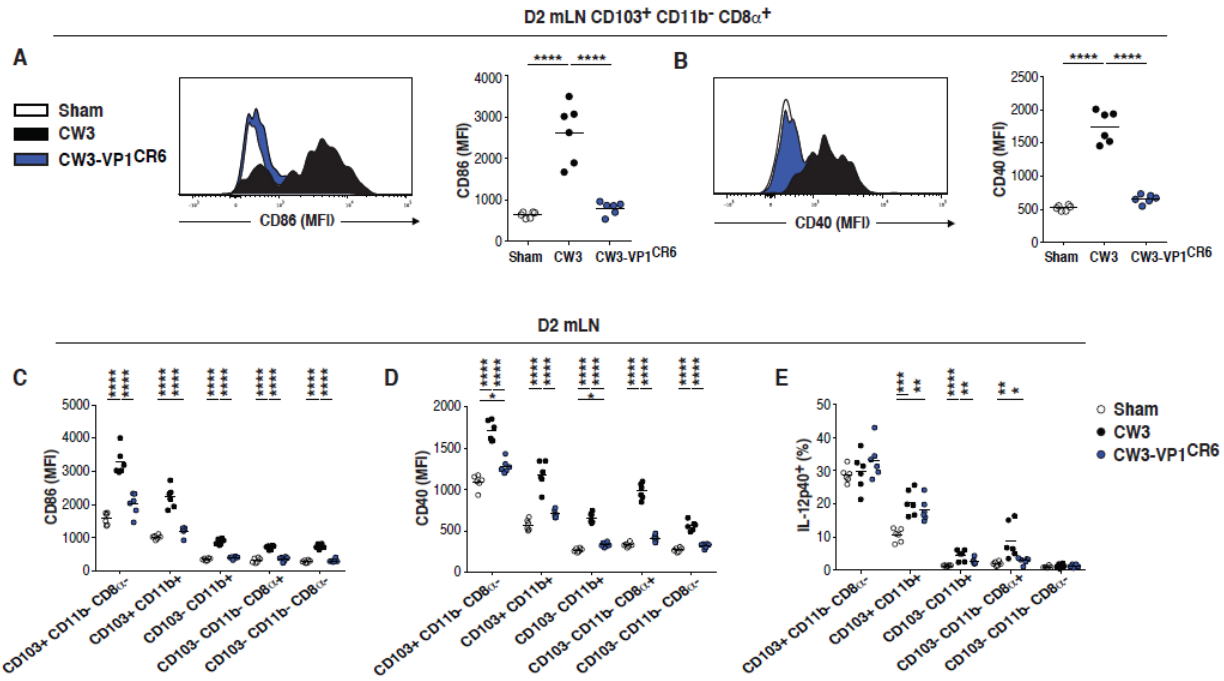

Figure C.5. VP1 gene from CW3 is the viral genetic determinant of MNV induced inflammatory response to dietary antigen, part 2. (A to E) C57BL/6 mice were inoculated with medium (n = 6 mice), CW3 5e7 (n = 6 mice) or CW3-VP1^{CR6} 5e7 (n = 6 mice) and mLNs were harvested 48 hpi. (A) Expression of the DC activation markers CD86 **(A)** and. CD40 **(B)** on CD103^{+} CD11b^{-} CD8α^{+} DC subset and expression of the DC activation markers CD86 **(C)** and CD40 **(D)** and IL-12p40 **(E)** on the other DC subsets in the mLN were evaluated by FACS. Graphs depict 2 independent experiments. For all experiments with quantitative analysis, data are shown as mean. One-way ANOVA with Tukey's multiple comparisons test; *p < 0.05; **p < 0.01; ***p < 0.001; ****p < 0.0001.

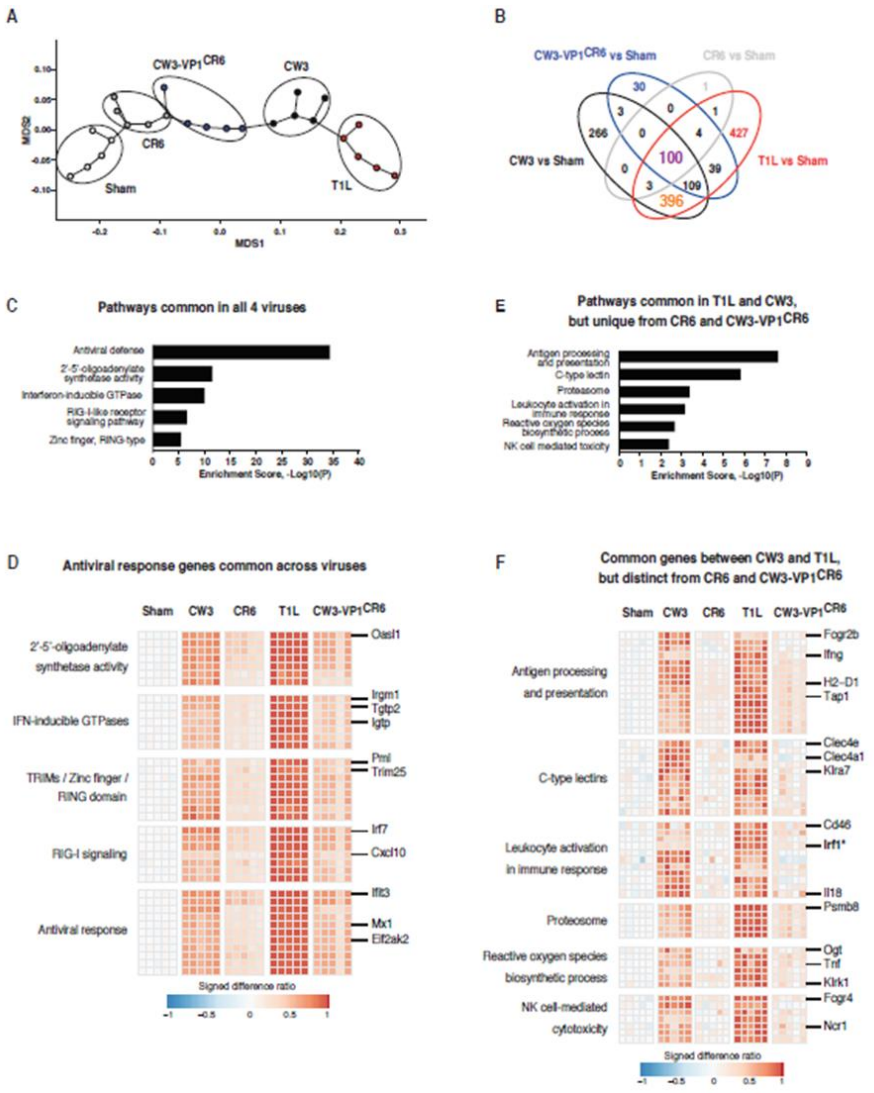

Figure C.6. Norovirus CW3 and Reovirus T1L have different infection kinetics but induce an overlapping inflammatory signature in the oral tolerance inductive site. (A to F) C57BL/6 mice were inoculated with medium (n = 5 mice), CW3 5e7 (n = 5 mice), CW3-VP1^{CR6} 5e7 (n = 5 mice), CR6 5e7 (n = 5 mice) or T1L 10e8 pfu (n = 5 mice) and mLN were harvested 48 hpi. Transcriptional responses to each of the viruses indicated were analyzed by RNAseq. **(A)** A minimum spanning tree (MST) was constructed and represented on multidimensional scaling (MDS) ordination. The MST traced a path of minimum weight through each vertex or node that represents the expression profile of differentially expressed genes across viral response states shown, relative to Sham. The lengths of edges (or connecting paths) indicate the level of dissimilarity between samples. Each state and the distances between them were represented in the two-dimensional MDS plot. The coordinates of each state along each dimension are indicated by the two axes of the MDS plot. **(B)** Venn diagram showing the number virus-specific and shared response genes that were differentially induced relative to Sham. **(C and E)** Enriched pathways and processes of differentially induced genes that were **(C)** common across CW3, T1L, CR6 and CW3-VP1^{CR6} viruses, and **(E)**

Figure C.6. (continued)
those common to CW3 and T1L but distinct from CR6 and CW3-VP1^{CR6}. **(D and F)** Heatmaps showing expression profiles of genes associated with key pathways and processes that were **(D)** common across CW3, T1L, CR6 and CW3-VP1^{CR6} viruses, and **(F)** those common to CW3 and T1L but distinct from CR6 and CW3-VP1^{CR6}.
Heatmaps show Log_2-transformed expression values expressed as signed difference ratios relative to the sham state and scaled by normalizing to the maximum absolute deviation of each gene's expression level from the sham control, so that all values lie between −1 and +1.

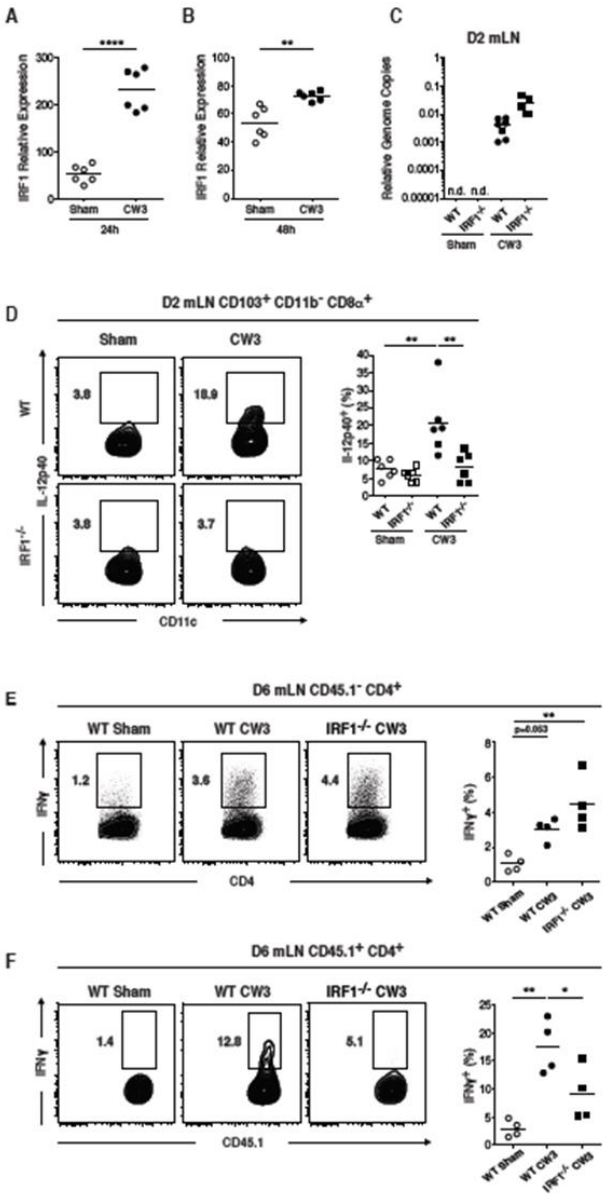

Figure C.7. A central role for IRF1 in norovirus mediated T_H1 immunity to dietary antigens. (A) DC activation assay. Mice were infected with $5x10^7$ TCID50 units of CW3 or T1L for 48 HPI and the mLNs were collected and DCs analyzed for DC activation marker CD86 by flow cytometry for the $CD103^+CD11b^-CD8a^+$ DC subset. (B) Same analysis as A except for the DC marker CD40. (C) T cell conversion assay. Naïve CD4+ OT-II T cells were transferred to WT or IRF1 KO mice by retro orbital injection and then mice were infected with $5x10^7$ TCID50 units of CW3 or T1L. 2 days post infection OT-II CD4+ T cells from the mLN were analyzed for the T_H1 marker IFNG by flow cytometry.

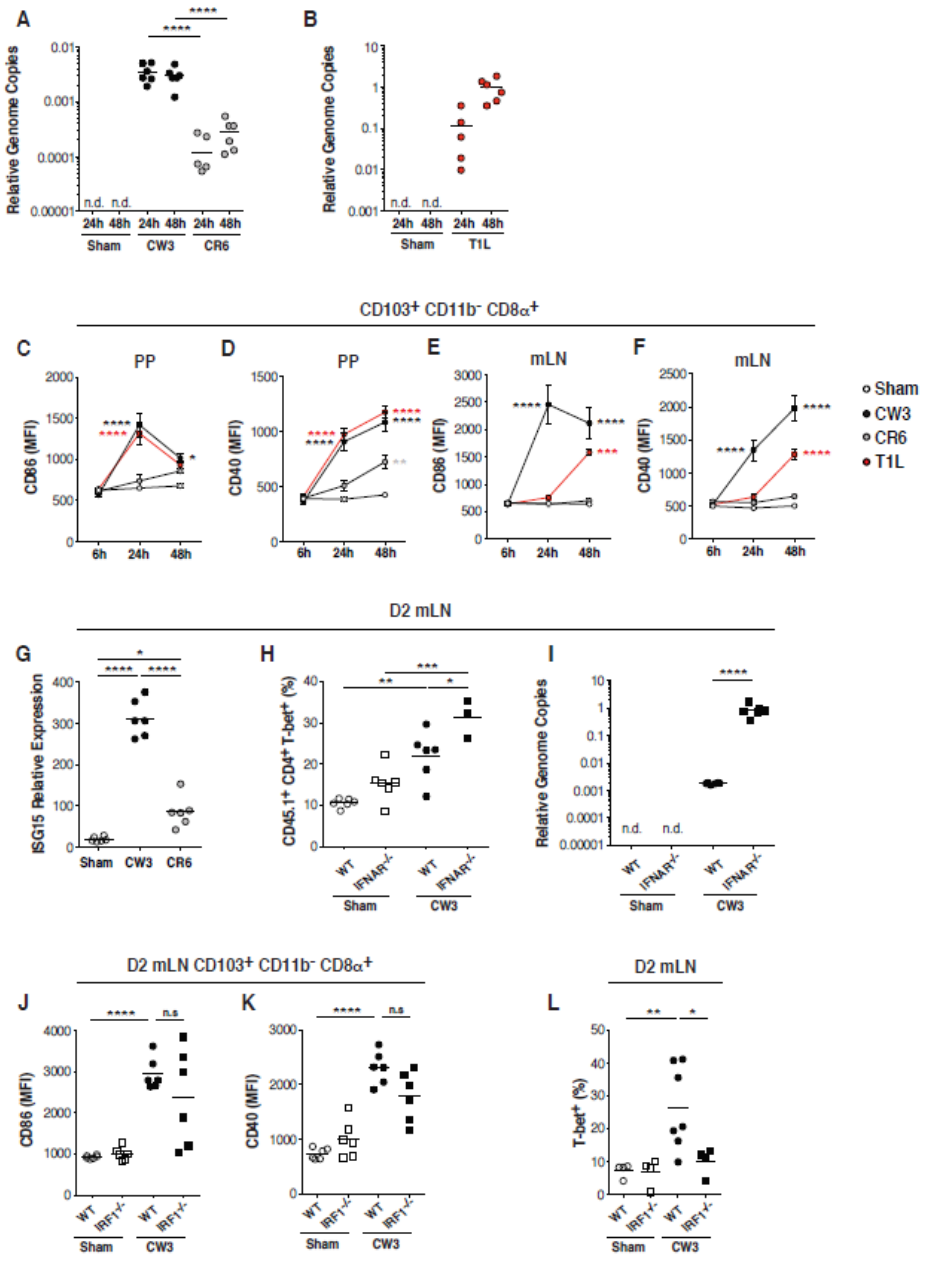

Figure C.8. A central role for IRF1 in norovirus mediated T_H1 immunity to dietary antigens, part 2. (A to F) C57BL/6 mice were inoculated with medium (n = 6 mice), CW3 5e7 (n = 6 mice), CR6 5e7 (n = 6 mice) or T1L 5e8 pfu (n = 6 mice) and PP and mLNs were harvested 6h, 24h or 48h post infection. Quantification of genome copies of MNV CW3 and CR6 **(A)** or T1L **(B)** in the mLN was evaluated by RT-PCR 24 and 48 hpi. Expression of the DC activation markers CD86 and CD40 on $CD103^+$ $CD11b^-$ $CD8\alpha^+$ DC subset in the PP **(C and D)** and mLN **(E and F)** were evaluated by FACS. **(C to F)** Statistical differences for each virus compared to the respective sham group are shown. Graphs depict 2 independent experiments. **(G)** C57BL/6 mice were inoculated with medium (n = 6 mice), CW3 5e7 (n = 6 mice), or CR6 5e7 (n = 6 mice) and mLN were harvested 48 hpi. Quantification of ISG15 expression in the mLN was evaluated by

Figure C.8. (continued)
RT-PCR. Graphs depict 3 independent experiments. **(H and I)** OT-II^{+} CD45.1^{+} CD4^{+} T cells were transferred into C57BL/6 or IFNAR$^{-/-}$ CD45.2^{+} mice. One day after transfer, mice were inoculated perorally with medium (sham, n = 6 mice / genoptype) or CW3 5e7 (n = 6 mice / genotype) and fed an OVA containing diet for 2 days. **(H)** Expression of T-bet in transferred OT-II^{+} CD45.1^{+} CD4^{+} T cells in the mLN was evaluated by FACS. **(I)** Quantification of genome copies in the mLN was evaluated by RT-PCR. Graphs depict 2 independent experiments. **(J and K)** C57BL/6 WT or IRF1$^{-/-}$ mice were inoculated with medium (n = 6 mice / genotype), or CW3 5e7 (n = 6 mice / genotype) and mLN were harvested 48 hpi. Expression of the DC activation markers CD86 **(J)** and CD40 **(K)** on CD103^{+} CD11b^{-} CD8α^{+} DC subset in the mLN were evaluated by FACS. Graphs depict 2 independent experiments. **(L)** OT-II^{+} CD45.1^{+} CD4^{+} T cells were transferred into C57BL/6 WT or IRF1$^{-/-}$ CD45.2^{+} mice. One day after transfer, WT mice were inoculated perorally with medium (sham, n = 4) or CW3 5e7 (n = 7 mice) and IRF1$^{-/-}$ mice were inoculated perorally with medium (sham, n = 4) or CW3 5e7 (n = 4 mice) and fed an OVA containing diet for 2 days. Expression of T-bet in transferred OT-II^{+} CD45.1^{+} CD4^{+} T cells in the mLN were evaluated by FACS. Graphs depict 2 independent experiments. For all experiments with quantitative analysis, data are shown as mean. One-way ANOVA with Tukey's multiple comparisons test; n.d., not detected. n.s., not significant; *$p < 0.05$; **$p < 0.01$; ***$p < 0.001$; ****$p < 0.0001$.

Appendix B

Tables

Table 1: A compilation of all major resources and reagents utilized for this dissertation.

KEY RESOURCES TABLE

REAGENT or RESOURCE	SOURCE	IDENTIFIER
Antibodies		
Rabbit polyclonal anti-PROPOL	Dr. Kim Green (Hwang et al., 2012)	N/A
Guinea Pig polyclonal anti-PROPOL	Dr. Kim Green (Hwang et al., 2012)	N/A
Mouse monoclonal anti-IRGA6	Dr. Jonathan Howard (Martens et al., 2004)	Clone 10D7
Rabbit polyclonal anti-IRGA6	Dr. Jonathan Howard (Martens et al., 2004)	Batch #165/4
Rabbit polyclonal anti-IRGB6	Dr. Jonathan Howard (Martens et al., 2004)	Batch #141/3
Rabbit polyclonal anti-IRGM1	Dr. Gregory Taylor (Henry et al., 2009)	N/A
Rabbit polyclonal anti-IRGM3	Dr. Gregory Taylor (Henry et al., 2009)	N/A
Rabbit polyclonal anti-ATG7	Sigma-Aldrich	Cat# A2856; RRID:AB_1078239
Rabbit polyclonal anti-ATG16L1	Sigma-Aldrich	Cat# A7356; RRID:AB_1840706
Rabbit polyclonal anti-FLAG	Sigma-Aldrich	Cat# F7425; RRID:AB_439687
Mouse monoclonal anti-FLAG M2	Sigma-Aldrich	Cat# F1804; RRID:AB_262044
Rabbit polyclonal anti-LC3B	Sigma-Aldrich	Cat# L7543; RRID: AB_796155
Rabbit polyclonal anti-p62	Sigma-Aldrich	Cat# P0067; RRID:AB_1841064
Rabbit polyclonal anti-ATG5	Novus Biologicals	Cat# NB110-53818 AB_828587
Rabbit polyclonal anti-LC3B	MBL International	Cat# PM036; RRID:AB_2274121
Mouse monoclonal anti-ATG3	MBL International	Cat# M133-3; RRID:AB_1278759
Mouse monoclonal anti-GBP1-5	Santa Cruz Biotechnology	Cat# sc-166960; RRID:AB_10611378
Goat polyclonal anti-GBP2	Santa Cruz Biotechnology	Cat# sc-10588; RRID:AB_2109344
Mouse monoclonal anti-β-ACTIN HRP Conjugated	Santa Cruz Biotechnology	Cat# sc-47778; RRID:AB_626632

Table 1 (continued)

Mouse monoclonal anti-HA	The Frank W. Fitch Monoclonal Antibody Facility, The University of Chicago	Clone 12CA5
Rabbit polyclonal anti-2A	Millipore	Cat# ABS31; RRID:AB_11214282
Rabbit monoclonal anti-LC3A	Cell Signaling Technology	Cat# 4599S; RRID:AB_10548192
Rabbit monoclonal anti-GABARAP	Abcam	Cat# ab109364; RRID:AB_10861928
Mouse monoclonal anti-dsRNA, J2	SCICONS, Hungary	Cat# 10010200
Rabbit polyclonal anti-IRGM	Abcam	Cat# ab69494; RRID:AB_1209373
HRP Goat polyclonal anti-Mouse	BioLegend	Cat# 405306; RRID:AB_315009
HRP Donkey polyclonal anti-Rabbit	BioLegend	Cat# 406401; RRID:AB_2099368
HRP Donkey polyclonal anti-Goat	Jackson ImmunoResearch	Cat# 705-035-147; RRID:AB_2313587
Dylight 649 Donkey polyclonal anti-Rabbit	BioLegend	Cat# 406406; RRID:AB_1575135
Alexa Fluor 555 Donkey polyclonal anti-Rabbit	BioLegend	Cat# 406412; RRID:AB_2563181
Alexa Fluor 488 Donkey polyclonal anti-Rabbit	Jackson ImmunoResearch	Cat# 711-545-152; RRID:AB_2313584
DyLight 649 Goat polyclonal anti-Mouse	BioLegend	Cat# 405312; RRID:AB_1575128
Alexa Fluor 555 Goat polyclonal anti-Mouse	BioLegend	Cat# 405324; RRID:AB_2563179
DyLight 488 Goat polyclonal anti-Mouse	BioLegend	Cat# 405310; RRID:AB_1575124
Alexa Fluor 488 Donkey polyclonal anti-Guinea Pig	Jackson ImmunoResearch	Cat# 706-545-148; RRID:AB_2340472
Alexa Fluor 647 Donkey polyclonal anti-Guinea Pig	Jackson ImmunoResearch	Cat# 706-606-148; RRID:AB_2340477
12 nm, Colloidal Gold- Donkey polyclonal anti-Guinea Pig	Jackson ImmunoResearch	Cat# 706-205-148; RRID:AB_2340465
18 nm, Colloidal Gold- Goat polyclonal anti-Rabbit	Jackson ImmunoResearch	Cat# 111-215-144; RRID:AB_2338017
18 nm, Colloidal Gold- Donkey polyclonal anti-Mouse	Jackson ImmunoResearch	Cat# 715-215-150; RRID:AB_2340823
Viruses, Protozoan Parasites, and Yeast		
MNV-1.CW3	Herbert W. Virgin (Thackray et al., 2007)	N/A
EMCV Strain K	Dr. Marco Colonna	N/A
ZIKV-Zika-Fortaleza/2015	Dr. Michaela Gack	N/A
MHV-A59	Dr. Susan Baker (Deng et al., 2017)	N/A
Toxoplasma gondii Type II PTG Strain	Dr. Herbert Virgin (Choi et al., 2014)	N/A
Saccharomyces cerevisiae yeast strain PJ69-4A	Dr. Benjamin Glick	N/A

Table 1 (continued)		
Chemicals, Peptides, and Recombinant Proteins		
Recombinant Murine IFN-γ	Peprotech	Cat# 315-05
Recombinant Human IFN-γ	Peprotech	Cat# 300-02
Mouse IFN Beta	PBL Assay Science	Cat# 12410-1
Chloroquine	Sigma-Aldrich	Cat# C6628
Rapamycin	LC laboratories	R5000
Experimental Models: Cell Lines		
Human: 293T	Dr. Herbert W. Virgin (Hwang et al., 2012)	N/A
Mouse: BV-2	Dr. Yuanan Lu (Cox et al., 2009)	N/A
Mouse: RAW264.7	Dr. Herbert W. Virgin (Hwang et al., 2012)	N/A
Mouse: MEF *Lc3b*$^{+/+}$	Dr. Marlene Rabinovitch (Cann et al., 2007)	N/A
Mouse: MEF *Lc3b*$^{-/-}$	Dr. Marlene Rabinovitch (Cann et al., 2007)	N/A
Mouse: MEF *Lc3a*$^{+/+}$, *Lc3b*$^{-/-}$, *Gabarap*$^{+/-}$, *Gabarapl1*$^{-/-}$, *Gabarapl2*$^{-/-}$	This study	N/A
Mouse: MEF *Lc3a*$^{-/-}$, *Lc3b*$^{-/-}$, *Gabarap*$^{+/-}$, *Gabarapl1*$^{-/-}$, *Gabarapl2*$^{-/-}$	This study	N/A
Mouse: MEF *Atg3*$^{+/+}$	Dr. Masaaki Komatsu (Sou et al., 2008)	N/A
Mouse: MEF *Atg3*$^{-/-}$	Dr. Masaaki Komatsu (Sou et al., 2008)	N/A
Mouse: MEF *Ulk1*$^{+/+}$*Ulk2*$^{+/+}$	Dr. Sharon Tooze (McAlpine et al., 2013)	N/A
Mouse: MEF *Ulk1*$^{-/-}$*Ulk2*$^{-/-}$	Dr. Sharon Tooze (McAlpine et al., 2013)	N/A
Mouse: J774A.1	Dr. Herbert W. Virgin (Rodríguez-Acebes et al., 2009)	N/A
Human: HAP1	Dr. Masahiro Yamamoto (Ohshima et al., 2014)	N/A
Human: HAP1 *Atg16l1*$^{-/-}$	Dr. Masahiro Yamamoto (Ohshima et al., 2014)	N/A
Human: HAP1 *Gbp*$^{1-/-/-}$	Dr. Masahiro Yamamoto (Ohshima et al., 2014)	N/A
Human: HeLa	ATCC	Cat# CCL-2; RRID:CVCL_0030
Human: HeLa *Atg7*$^{-/-}$ #1	Dr. Herbert W. Virgin (Selleck et al., 2015)	Clone 1A11
Human: HeLa *Atg7*$^{-/-}$ #2	Dr. Herbert W. Virgin (Selleck et al., 2015)	Clone 1A6
Human: HeLa *Atg16l1*$^{-/-}$ #1	Dr. Ramnik Xavier (Selleck et al., 2015)	Clone G9

Table 1 (continued)		
Human: HeLa *Atg16l1*$^{-/-}$ #2	Dr. Ramnik Xavier (Selleck et al., 2015)	Clone E6
Experimental Models: Organisms/Strains		
Mouse: C57BL/6: *Atg3*$^{flox/flox}$*+/-LysMcre*	Dr. You-Wen He (Jia et al., 2011)	N/A
Mouse: C57BL/6: *Atg5*$^{flox/flox}$*+/-LysMcre*	Dr. Herbert W. Virgin (Hwang et al., 2012)	N/A
Mouse: C57BL/6: *Atg16L1*$^{flox/flox}$*+/-LysMcre*	Dr. Herbert W. Virgin (Hwang et al., 2012)	N/A
Mouse: C57BL/6: *Atg14*$^{flox/flox}$*+/-LysMcre*	Dr. Shizuo Akira	N/A
Mouse: C57BL/6: *Irgm1*$^{-/-}$*Irgm3*$^{-/-}$	Dr. Gregory Taylor (Henry et al., 2009)	N/A
Mouse: C57BL/6: *Gbp*$^{chr3-/-}$	Dr. Masahiro Yamamoto (Yamamoto et al., 2012)	N/A
Mouse: C57BL/6: *Irgm1*$^{+/-}$*Irgm3*$^{+/-}$*Ifnar*$^{-/-}$	This study	N/A
Mouse: C57BL/6: *Irgm1*$^{-/-}$*Irgm3*$^{-/-}$*Ifnar*$^{-/-}$	This study	N/A
Mouse: C57BL/6: *Gbp*$^{chr3+/-}$*Ifnar*$^{-/-}$	This study	N/A
Mouse: C57BL/6: *Gbp*$^{chr3-/-}$*Ifnar*$^{-/-}$	This study	N/A
Mouse: C57BL/6: *Ifnar*$^{-/-}$	Dr. Herbert W. Virgin (Hwang et al., 2012)	N/A
Mouse bone marrow: C57BL/6: *Irgm1*$^{-/-}$	Dr. Gregory Taylor (Henry et al., 2009)	N/A
Mouse bone marrow: C57BL/6: *Ulk1*$^{-/-}$	Dr. Sharon Tooze (McAlpine et al., 2013)	N/A
Mouse bone marrow: C57BL/6: *Ulk2*$^{-/-}$	Dr. Sharon Tooze (McAlpine et al., 2013)	N/A
Oligonucleotides		
See table 2 for qPCR primers used to analyze the transcription of genes	This study	N/A
See table 3 for sequence of guide RNAs to delete DNA and primers to screen the deletion	This study	N/A
Recombinant DNA: Plasmids		
Plasmid: C274-empty	Hwang et al., 2012	N/A
Plasmid: C274-IRMG1	This study	N/A
Plasmid: C274-IRMG3	This study	N/A
Plasmid: pCDNA3-MNV.1-CW3-ORF1	Dr. Herbert W. Virgin (Hwang et al., 2012)	N/A
Plasmid: pCDNA3-MNV.1-CW3-ORF1-dNS7	This study	N/A
Plasmid: pSpCas9(BB)-2A-GFP (PX458)	Ran et al., 2013	Addgene plasmid #48138
Plasmid: pSpCas9(BB)-2A-GFP (PX459)	Ran et al., 2013	Addgene plasmid #48139
Plasmid: psPAX2	Dr. Herbert W. Virgin (Hwang et al., 2012)	N/A
Plasmid: pMD2.G	Dr. Herbert W. Virgin (Hwang et al., 2012)	N/A
Plasmid: pGAD-C1	Dr. Benjamin Glick	N/A
Plasmid: pGAD-CW3-NS7	This study	N/A
Plasmid: pGAD-Atg16L1	This study	N/A

Table 1 (continued)		
Plasmid: pGBDU-C1	Dr. Benjamin Glick	N/A
Plasmid: pGBDU-CW3-NS7	This study	N/A
Plasmid: pGBDU-Atg16L1	This study	N/A
Plasmid: pCAGGS-EYC-COVA	This study	N/A
Plasmid: pCAGGS-EYC-Atg5	This study	N/A
Plasmid: pCAGGS-EYC-Atg5-DM	This study	N/A
Plasmid: pCAGGS-EYC-CW3-NS7	This study	N/A
Plasmid: pCAGGS-EYN-Atg16L1	This study	N/A
Plasmid: pCAGGS-EYC-RdRP HNV GI_South Hampton	This study	N/A
Plasmid: pCAGGS-EYC-RdRP HNV GII.4_Sydney	This study	N/A
Plasmid: pCAGGS-EYC-EMCV-3Dpol	This study	N/A
Plasmid: pEGFP-N1-TOMM20-2xFRP	Park et al., 2016	N/A
Plasmid: pDRFP-MNV-NS7-4xFKBP	This study	N/A
Plasmid: pENTR-mGBP1	This study	N/A
Plasmid: pENTR-mGBP2	This study	N/A
Plasmid: pENTR-mGBP2-K51A	(Kravets et al., 2012)	N/A
Plasmid: pENTR-mGBP2-E99A	(Kravets et al., 2012)	N/A
Plasmid: pENTR-mGBP2-D182N	(Kravets et al., 2012)	N/A
Plasmid: pENTR-mGBP2-C586S	(Kravets et al., 2012)	N/A
Plasmid: pENTR-mGBP3	This study	N/A
Plasmid: pENTR-mGBP5	This study	N/A
Plasmid: pENTR-mGBP7	This study	N/A
Plasmid: pENTR-ATG3	This study	N/A
Plasmid: pENTR-LC3B	This study	N/A
Plasmid: pENTR-LC3B-G120A	This study	N/A
Plasmid: pENTR-EGFP	This study	N/A
Plasmid: pENTR-RFP	This study	N/A
Plasmid: pENTR-CW3-NS1/2	This study	N/A
Plasmid: pENTR-CW3-NS3	This study	N/A
Plasmid: pENTR-CW3-NS4	This study	N/A
Plasmid: pENTR-CW3-NS5	This study	N/A
Plasmid: pENTR-CW3-NS6	This study	N/A
Plasmid: pENTR-CW3-NS7	This study	N/A
Plasmid: pENTR-CW3-VP1	This study	N/A
Plasmid: pENTR-CW3-VP2	This study	N/A
Plasmid: pENTR-CW3-VF1	This study	N/A
Plasmid: pENTR-Atg16L1-WT	Park et al., 2016	N/A
Plasmid: pENTR-Atg16L1-N79	Park et al., 2016	N/A
Plasmid: pENTR-Atg16L1-N249	Park et al., 2016	N/A
Plasmid: pENTR-Atg16L1-dN79-N249	Park et al., 2016	N/A
Plasmid: pENTR-Atg16L1-N230	This study	N/A
Plasmid: pENTR-Atg16L1-N207	This study	N/A
Plasmid: pENTR-Atg16L1-N193	This study	N/A
Plasmid: pENTR-Atg16L1-N141	This study	N/A
Plasmid: pENTR-Atg16L1-N123	This study	N/A
Plasmids: All pENTR above transferred into the destination vector pHNHF (described in Materials and Methods)	This study	N/A

Table 1 (continued)		
Software and Algorithms		
GraphPad Prism Version 6	GraphPad Software	URL: https://www.graphpad.com/ RRID:SCR_002798
FlowJo Version 10	FlowJo, LLC	URL: https://www.flowjo.com/ RRID:SCR_008520
Image Lab Version 4.1	BIO-RAD	URL: http://www.bio-rad.com/en-us/product/image-lab-software
ImageJ/Fiji Version 1.49m	NIH	URL: https://imagej.nih.gov/ij/ RRID:SCR_003070

Table 2: Quantitative PCR primers used to analyze the transcription of genes.

Genes	Forward Primer	Reverse Primer
MNV	agctcaggatggtctcggat	tcaagagcaaggtcgaaggg
Irgm1	tgctccactactccccaacat	gctcctactgacctcaggtaac
Irgm3	ctcatcagcccgtggtctaaa	caccgccttaccaatatcttcaa
Irga6	caggacatccgccttaactgt	aggaagtaagtacccattagcca
Irgb6	aggcatgtaagcacctccac	ggacagagaggcaggttcac
Gbp1	acctggagacttcactggct	tttattcagctggtcctcctgtatcc
Gbp2	acctggaacattccctgacc	acagctcctcctcccgcagag
Gbp3	ccagaaaaccaactggaacggaa	tctccagacaaggcacagtc
Gbp5	cactcagcaacgaggagctgaact	tgttctctatggaaggcagagcc
Gbp7	ttgaggaaatgccagaggaccagt	gtctccactattgatagcatccacg
Ulk1	tgcccttgatgagatgttcc	agtctcctctcaatgcacagc
Ulk2	tcgtttatcgctaccacaagg	gcctgctactcacacagttgc
Actin	gccttccttcttgggtatgg	gcactgtgttggcatagagg

Table 3: Sequence of guide RNAs to delete DNA and primers to screen the deletion.

Gene	Guide RNA	Primers for Screening		Expected Size of Product from WT Genome
Lc3a	gtgatcatcgagcgctacaa	Forward	gaccgctgtaaggaggtgc	678
	tgagttgcaggcggcgcctg	Reverse	tcagaagccgaaggtttcttg	
Gabarap	cggggccggtccgatggtcg	Forward	gtctgcctttccccaacgta	854
	agcgtcagcgacgctagcct	Reverse	gatcctagaacggcgcatca	
Gabarapl1	tagtgcggcgactggcgcgt	Forward	ccagctcttgggaaaagcca	696
	tcgaaagcgcagcgtgcgcg	Reverse	atgggcacaaggctcatctc	
Gabarapl2	gcgacgactactccacaggc	Forward	acagcgcttggaacaggtta	867
	cggacccgtgtcgccctacg	Reverse	gaactcggtcggggtacttc	

Appendix C

Norovirus infection induces inflammatory responses to dietary antigens

Romain Bouziat[1,2,11], Scott B. Biering[3,11], Reinhard Hinterleitner[1,2], Elaine Kouame[1,2], Kishan A. Sangani[1,2], Jordan D. Ernest[1,2], Mukund Varma[4,5], Judy J. Brown[6], Kelly Urbanek[7], Terence S. Dermody[7,8], Aylwin Ng[4,5], Seungmin Hwang[2,3,9]*, and Bana Jabri[1,2,9,10,12]*

[1]Department of Medicine; [2]Committee on Immunology; [3]Committee on Microbiology, University of Chicago, Chicago, IL, USA.

[4]Division of Gastroenterology, Department of Medicine, Gastrointestinal Unit and Center for the Study of Inflammatory Bowel Disease, Massachusetts General Hospital and Harvard Medical School, Boston, MA, USA.

[5]Broad Institute of MIT and Harvard University, Cambridge, MA, USA.

[6]Department of Pathology, Microbiology, and Immunology, Vanderbilt University Medical Center, Nashville, TN, USA.

[7]Department of Pediatrics; [8]Department of Microbiology and Molecular Genetics, University of Pittsburgh School of Medicine, Pittsburgh, PA, USA.

[9]Department of Pathology; [10]Section of Gastroenterology, Hepatology, and Nutrition, Department of Pediatrics; University of Chicago, Chicago, IL, USA.

[11]These authors contributed equally

[12]Lead Contact

*Correspondence: bjabri@bsd.uchicago.edu (B.J.); shwang@bsd.uchicago.edu (S.H.)

Summary

Reovirus infection has been implicated in loss of oral tolerance, T helper 1 (T_H1) immunity to dietary antigen, and celiac disease. Here we found that T_H1 immunity to dietary antigen was promoted by infection with the acute CW3 strain of murine norovirus, but not by the persistent CR6 strain. This property of CW3 was dependent on its major capsid protein, a virulence determinant. Furthermore, transcriptional profiling of mesenteric lymph nodes following infection with various viral strains revealed a signature that segregated with break of tolerance to dietary antigen and included the upregulation of interferon regulatory factor 1 (IRF1). Indeed, initiation of T_H1 immunity to dietary antigen in response to CW3, similar to reovirus infection, required IRF1. These data reveal common features of virus-host interactions in the induction of T_H1 immunity to dietary antigens and provide a foundation for the development of therapeutic strategies against T_H1-mediated complex immune disorders triggered by viral infections.

Keywords

Celiac Disease, norovirus, reovirus, T helper 1, T_H1, major capsid protein, VP1, oral tolerance, inflammation, interferon regulatory factor 1, IRF1

Introduction

Celiac Disease (CeD) is a complex immune disorder characterized by an inflammatory T helper 1 (T_H1) response against dietary gluten present in wheat, preceding onset of enteropathy and villous atrophy (Abadie et al., 2011; Jabri and Sollid, 2009). CeD has a genetic component in which susceptible individuals harbor the human leukocyte antigens DQ2 or DQ8. However, these genetic risk factors alone are not sufficient to explain the onset of pathology, and environmental factors are thought to play a role in the development of CeD (Abadie et al., 2011; Tjon et al., 2010). Furthermore, it is unclear why CeD patients exhibit a T_H1 response instead of a canonical regulatory immune response to dietary gluten. Previous studies have implicated adenovirus, enteroviruses, hepatitis C virus, and rotavirus as potential environmental triggers of CeD; however, these studies showed only correlation and lacked direct experimental evidence supporting this possibility (Plot and Amital, 2009; Stene et al., 2006).

We recently discovered that the type 1 Lang (T1L) strain of the segmented double-stranded RNA (dsRNA) reovirus (RV), a member of the *Reoviridae* family like rotavirus, can trigger inflammatory responses to dietary antigens (Ag) and development of CeD (Bouziat et al., 2017). This study provided the first experimental evidence of a virus-induced pro-inflammatory T_H1 immune response against dietary Ag, which is dependent on interferon regulatory factor 1 (IRF1) (Bouziat et al., 2017). Intriguingly, the type 3 Dearing reassortant strain T3D-RV, which is capable of infecting the intestine, induced protective immunity similarly to T1L but failed to induce loss of oral tolerance (LOT) (Bouziat et al., 2017), suggesting that protective immunity could be dissociated

from immunopathology. More specifically, T1L and T3D-RV induced similar responses in Peyer's patches (PP), the site where protective immunity to reovirus takes place (Fleeton et al., 2004). However, only T1L disrupted intestinal immune homeostasis at the inductive sites of oral tolerance. In particular, T1L, but not T3D-RV, conferred an inflammatory phenotype to dendritic cells (DC) in mesenteric lymph nodes (mLN) that promote T cell immunity to dietary Ag (Bouziat et al., 2017). Based on these findings, we hypothesized that any enteric virus capable of creating an inflammatory environment at sites where DCs prime T cell responses to dietary Ag, has the potential to trigger loss of tolerance to dietary Ag.

To test this hypothesis, we used murine norovirus (MNV), a positive-sense RNA (+RNA) virus from the *Caliciviridae* family and a model for human norovirus that causes the majority of acute gastroenteritis world-wide (Glass et al., 2009). Many strains of MNV have been isolated with two of the best studied *in vivo* being the acute strain CW3 and the persistent strain CR6. CW3 and CR6 have similar growth kinetics *in vitro* but differ in their tissue tropism and capacity to persist in mice (Nice et al., 2013). When inoculated orally, CW3 replicates in the small intestine, spreads systemically, and is cleared from the host in about 7 days (Nice et al., 2013). On the other hand, CR6 remains at the mesenteric lymph node (mLN), intestine, and colon and is shed persistently in the feces for the life of the mouse (Nice et al., 2013). We tested the capacity of CW3 and CR6 to trigger an inflammatory response to dietary ovalbumin (OVA) and identified a viral determinant of norovirus-induced inflammatory immunity to dietary Ag. We found that the acute CW3 strain, but not the persistent CR6 strain, can induce inflammatory responses and loss of oral tolerance (LOT) to OVA. Furthermore,

our study identifies the viral major capsid protein of CW3 as a critical driver of norovirus-induced T_H1 immunity to dietary Ag. Finally, our data support the hypothesis that multiple viruses can act as external inflammatory stimuli mediating a T_H1 response to dietary antigens and identifies a common signaling pathway by which viruses disrupt immune homeostasis at inductive sites of oral tolerance.

Results

An acute strain of norovirus induces an inflammatory response and loss of oral tolerance to a dietary antigen

To examine the effect of MNV infection on immune responses to dietary antigens, C57BL/6 mice were orally inoculated with the CW3 or CR6 strains of MNV (Fig. C1). While both CW3 and CR6 triggered neutralizing antibody responses in C57BL/6 mice (Fig. C.1A), CW3 was cleared from the mouse around 4 days post infection (dpi) whereas, in agreement with previous studies (Nice et al., 2013), CR6 persisted (Fig. C.1B). Despite these differences, both CW3 and CR6 were readily detectable in the mesenteric lymph node (mLN) at 2 dpi (Fig. C.1C), a time and location relevant to induction of oral tolerance (Bouziat et al., 2017; Macpherson and Smith, 2006). CW3 viral genome copy numbers were significantly higher compared to CR6 at 2 dpi (Fig. C.1C). To compare their effect on the immune response to dietary OVA, we performed an oral tolerance assay (Bouziat et al., 2017; Esterházy et al., 2016); to assess whether mice can mount an immune response against antigen after establishing peripheral immune tolerance through oral administration of the same antigen. Mice were given a dose of OVA by oral gavage, while simultaneously receiving either strain of MNV or a sham infection. Two days later, mice were immunized subcutaneously with OVA in complete Freund's adjuvant (CFA). As expected, the sham-infected mice failed to produce a robust IgG2c antibody response to OVA at 16 dpi (Fig. C.1D). Similarly, mice infected with CR6 also failed to produce a robust antibody response to OVA, indicating that CR6 infection did not break oral tolerance (Fig. C.1D). Interestingly, CW3 infection in mice resulted in a robust IgG2c antibody response to OVA at 16 dpi,

indicating LOT to OVA and a T-helper 1 (T_H1) immune response (Fig. C.1D). Furthermore, when these mice were subjected to a delayed-type hypersensitivity assay (DTH) via subcutaneous injection of OVA into the ear, mice previously infected with CW3, but not CR6, exhibited significantly greater ear swelling than mice infected with OVA alone (Fig. C.1E). These data suggest that infection with the acute CW3 strain but not the persistent CR6 strain of MNV perturbed immune homeostasis and triggered LOT to the dietary OVA.

Induction of oral tolerance as well as T_H1 mediated LOT to dietary antigens is mediated by dendritic cell (DC) populations in the mLN (Coombes et al., 2007; Esterházy et al., 2016), especially the $CD103^+$ $CD11b^-$ $CD8\alpha^+$ subset that takes up the majority of dietary OVA (Bouziat et al., 2017). Thus, we compared the capacity of CW3 and CR6 to activate various DC subsets in the mLN by measuring surface expression levels of CD86 and CD40. While CR6 did not significantly activate the DC subsets tested, CW3 activated all DC subsets including the $CD103^+$ $CD11b^-$ $CD8\alpha^+$ subset (Fig. C.2A-D). This result is consistent with the finding that CW3 was present at higher levels in the mLN compared to CR6 (Fig. C.1C). We next determined the capacity of the two norovirus strains to induce the T_H1 promoting cytokine, IL-12p40, in mLN DCs, using intracellular flow cytometry. Like induction of DC activation markers, CW3 but not CR6 triggered IL-12p40 production in several DC subsets (Fig. C.1F and C.2E), with the strongest induction in the $CD103^+$ $CD11b^-$ $CD8\alpha^+$ subset. Though CR6 did not significantly activate DC subsets in the mLN at 2 dpi, both CW3 and CR6 activated DC subsets in the Peyer's patches (PPs) at 2 dpi compared with sham infection, although CW3 activated these DCs to a greater extent (Fig. C.2F-G). This finding suggests that

CR6 elicits an immune response at the MNV portal of entry (PPs), (Kolawole et al., 2016), resulting in protective immunity, but not in the mLN at 2 dpi. Additionally, these data suggest that CW3, but not CR6, activates DC subsets required for induction of oral tolerance in the mLN, thereby driving pro-inflammatory T_H1 responses to dietary OVA.

To determine whether CW3 infection is indeed capable of triggering conversion of naïve T cells into a T_H1 lineage rather than T-regulatory cells (T_{regs}), we transferred naïve OVA-specific CD45.1$^+$ CD4$^+$ T cells (OT-II T cells) by retro-orbital injection into naïve C57BL/6 mice. The mice were subsequently infected with CW3 or CR6 by oral gavage and given OVA with food; the fates of the transferred naïve OT-II T cells were examined at 6 dpi. Infection with both viruses induced a robust and similar host T_H1 response, as assessed by the analysis of T-bet and interferon gamma (IFNγ) expression in mLN CD45.1$^-$ CD4$^+$ host T cells (Fig. C.1G, C.2H-I), while also reducing the number pT_{regs} as compared to sham infected mice (Fig. C.2H and J). In contrast to the host response but in accordance with the DC data, CW3 but not CR6, converted the transferred CD45.1$^+$ OT-II T cells into the high IFNγ and T-bet expressing T_H1 lineage (Fig. C.1H, C.2K-L). Furthermore, CR6 infection did not interfere with the capacity of CD45.1$^+$ OT-II T cells to differentiate into pT_{regs}, and significantly promoted higher levels of pT_{reg} conversion than CW3 (Fig. C.2K and M). However, while CW3-mediated T_H1 responses to dietary Ag were consistently observed (Fig.C.1H, C.2K-L, and C.3A-B) the capacity of CW3 to block T cell conversion into pT_{regs} expressing forkhead box P3 (Foxp3) was inconsistent and not significant compared with sham-infected mice (Fig. C.2K, C.2M and C.3C), even at high viral doses (Fig. C.3C). This is in line with previous

observations suggesting that T_H1 immunity to dietary Ag can be dissociated from pT_{reg} conversion (Bouziat et al., 2017).

Collectively, these data demonstrate that, similarly to reovirus T1L, the CW3 strain of norovirus can trigger a broad inflammatory pathway capable of disrupting immune homeostasis and triggering LOT and T_H1 immunity to oral antigens. Further, this phenotype can be dissociated from protective immunity to viruses (Bouziat et al., 2017).

The major capsid protein of norovirus is the viral determinant that triggers an inflammatory response to dietary antigen

We next investigated the genetic determinant of CW3 required for the inflammatory response to OVA. Previous studies identified two major genetic determinants of MNV responsible for the phenotypic differences between the CW3 and CR6 strains. The non-structural protein NS1/2 of CR6 confers the capacity of this strain to persist in mice; a D94E mutation in the NS1/2 of CW3 allows this mutant virus to persist in mice at low inoculum doses, which is not relevant to our phenotype (Nice et al., 2013). Another phenotypic difference was attributed to the major capsid protein, viral protein 1 (VP1), of CW3. The VP1 of CW3, but not of CR6, renders the virus virulent in immunocompromised mice; swapping the VP1 of CW3 with that of CR6 (CW3-$VP1^{CR6}$) results in an acute but non-pathogenic mutant of CW3 in immunocompromised mice (Strong et al., 2012). The VP1 of CW3 also has been implicated in recruiting inflammatory monocytes and neutrophils to sites of infection (Van Winkle *et al.*,

submitted). Thus, we compared the capacity of wild-type (WT) CW3 and the CW3-VP1^{CR6} mutant to trigger inflammatory responses to OVA.

While both viruses were detectable in the mLN at 2 dpi (Fig. C.4A), CW3, but not CW3-VP1^{CR6}, activated all mLN DC subsets tested, as determined by surface expression of CD86 and CD40 (Fig. C.5A-D). In addition, only CW3 induced production of the proinflammatory cytokine IL-12p40 in the CD103^{+} CD11b^{-} CD8α^{+} DC subset (Fig. C.4B). Consistent phenotypes were observed for all the other DC subsets tested, except the CD103^{+} CD11b^{+} subset in which CW3 and CW3-VP1^{CR6} induced comparable levels of IL-12p40 (Fig. C.5E). We further examined the capacity of this mutant virus to convert transferred naïve CD45.1^{+} CD4^{+} OT-II T cells into a T_H1 lineage. Similar to the comparison between CW3 and CR6, both WT CW3 and CW3-VP1^{CR6} induced a T_H1 host response compared to the sham infection (Fig. C.4C). In contrast, only CW3-infection induced IFNγ expression in the transferred CD45.1^{+} OT-II cells (Fig. C.4D), indicating that VP1 is the MNV genetic determinant required for the induction of this T_H1 response to dietary OVA.

To identify the potential signaling pathways that underlie the distinct immunopathological properties of CW3 and CW3-VP1^{CR6}, we examined the transcriptional profiles of the mLN via RNA-seq at 48 hours post infection (hpi) of mice with sham, CW3, or CW3-VP1^{CR6}. Both viruses altered the transcriptional profile of the mLN, triggering a robust antiviral response characterized by the induction of 212 genes that were common to both CW3 and CW3-VP1^{CR6} (Fig. C.4E). However, CW3 elicited a more extensive transcriptional response in the number and level of genes induced (Fig. C.4E). The differential response to CW3 was characterized by an overrepresentation of

genes encoding C-type lectins, genes associated with antigen processing/presentation, and leukocyte activation pathways (Fig. C.4F), which were not seen for CW3-VP1^{CR6}. Of note, VP1 of CW3 significantly induced *Ccr2, Ccrl2* and *Csf3r* that encode proteins regulating granulocyte migration and function. This is in line with a report by Van Winkle *et al.*, demonstrating the capacity of VP1 from CW3 to recruit inflammatory monocytes and neutrophils to sites of infection (Van Winkle *et al.*, submitted). These data suggest that CW3 triggered DC activation and T_H1 T cell conversion to dietary antigen in a manner dependent on the inflammation-prone major viral capsid protein, VP1.

Norovirus and reovirus have different infection kinetics but induce overlapping inflammatory gene expression profiles at the inductive site of oral tolerance

Since both norovirus CW3 and reovirus T1L triggered a similar inflammatory response to dietary OVA, we compared the host immune signaling pathways activated by these viruses to identify common and distinct pathways associated with LOT. Both enteric viruses were detected within the mLN (Fig. C.8A-B), the site of inductive immunity to oral antigens (Bouziat et al., 2017; Macpherson and Smith, 2006; Nice et al., 2013). To determine the optimal time-point to examine the activated immune pathway, we compared the temporal kinetics of infection and immune activation of these two viruses; expression of DC activation markers at 6, 24, and 48 hpi were examined, since these time points are relevant to induction of oral tolerance (Bouziat et al., 2017). CR6 and CW3-VP1^{CR6} were included as negative controls to exclude pathways activated by viruses that do not trigger inflammatory responses to OVA. While the activation kinetics of the CD103$^+$ CD11b$^-$ CD8α$^+$ DCs were nearly identical in the

Peyer's patches for both CW3 and T1L (Fig. C.8C-D), CW3 but not T1L induced DC activation in the mLN at 24 hpi (Fig. C.8E-F). However, both viruses significantly activated DCs in mLN at 48h (Fig. C.8E-F).

To identify the potential signaling pathways leading to T_H1 T cell conversion and LOT, we examined the transcriptional profiles of the mLN via RNA-seq at 48 hpi of sham, CW3, CR6, CW3-VP1^{CR6}, or T1L infected mice, as both CW3 and T1L activated DCs at this time point. We incorporated the RNA-seq data into minimum spanning trees (MSTs) using multidimensional scaling (MDS) ordination, which revealed that our experimental groups were separated in a manner consistent with our previous results comparing CW3 and CW3-VP1^{CR6}. The CW3- and T1L-infected groups clustered together closely and were distant from the cluster of sham- and CR6-infected groups. CW3-VP1^{CR6}-infected groups clustered in-between but closer to the CR6-infected groups than the CW3-infected groups, concordant with the capacity of T1L and CW3, but not CR6 and CW3-VP1^{CR6}, to induce T_H1 immunity to dietary Ag (Fig. C.6A). Interestingly, the RNA-seq analysis revealed a core set of 100 genes commonly induced by all viruses that primarily constitute pathways involved in anti-viral responses, 2'-5'-oligoadenylate synthetase activity, interferon-inducible GTPases, RLRs and RIG-I signaling (Fig. C.6B-D). Many of these genes play direct antiviral roles against viruses and are up regulated by interferon signaling or are important for interferon signaling (Schoggins and Rice, 2011). In fact, the IFN-inducible GTPases (e.g., IGTP) block replication of MNV (Biering et al., 2017b). Furthermore, the tripartite motif-containing (TRIM) and myxovirus resistance (MX) proteins possess potent antiviral activity and are induced by interferon signaling, which is controlled by IRF7 expression (Haller et al.,

2015; Ning et al., 2011; Rajsbaum et al., 2014). Importantly, beyond this core set, we also observed 396 genes that were selectively induced by both CW3 and T1L (Fig. C.6B). These genes include numerous C-type lectins and genes involved in pathways and processes associated with antigen presentation, chemotaxis, and NK-cell mediated cytotoxicity (Fig. C.6E-F). Many of these genes encode proteins important for T_H1 inflammatory immune responses, such as IFNγ, H2-D1, and IRF1. Of note, when comparing T1L and CW3, T1L promoted an overall more extensive transcriptional change in the mLN, both in the number of genes and expression level of the genes induced. An example of this is the type I IFN-associated response. This difference can potentially be explained by our observation that CW3-triggered DC activation peaks at 24 hpi, while T1L-triggered DC activation peaks at 48 hpi (Fig. C.8E-F). The identification of specific signals overlapping between T1L and CW3 provides a framework to determine pathways used by these viruses to trigger T_H1 immunity to dietary Ag. Furthermore, IRF1 was identified by our transcriptome analysis as an overlapping factor induced by both CW3 and T1L, but not by CR6 or CW3-VP1^{CR6}, an intriguing finding considering that IRF1 is essential for T1L to trigger inflammatory responses to OVA (Bouziat et al., 2017). Taken together, these data demonstrate that, while CW3 and T1L activated pro-inflammatory pathways to different degrees at different time points, they ultimately triggered an overlapping pro-inflammatory signaling pathway in the mLN, which may be a common feature of inflammatory responses to dietary antigens.

CW3 triggers inflammatory responses to dietary antigen in an IRF1 dependent manner

Our previous study showed that T1L-induced T_H1 immunity to dietary Ag was type-I IFN independent but required IRF1 (Bouziat et al., 2017). Because MNV infection induces a robust type I interferon response, which modulates the host immune response (Kernbauer et al., 2014) (Fig. C.8G), we first tested whether, like T1L, CW3 promoted T_H1 immunity to dietary Ag in a type I interferon-independent manner. In agreement with our previous findings with T1L, CW3 still triggered T_H1 conversion of transferred OT-II $CD4^+$ T cells in the absence of type I interferon receptor ($IFNAR^{-/-}$) (Fig. C.8H). A caveat is that CW3 replication was not well controlled in $IFNAR^{-/-}$ mice, resulting in much higher viral loads in the mLN at 2 dpi compared to WT mice (Fig. C.8I).

We next assessed the role of IRF1, given that it was previously found to be critical for T1L induced LOT (Bouziat et al., 2017) and specifically up regulated by CW3 and T1L (Fig. C.6F). To validate the RNA-seq data, we quantified transcript levels of IRF1 in the mLN of CW3-infected mice at 24 and 48 hpi. As anticipated, compared with sham infection, CW3 infection strongly induced IRF1 expression (Fig. C.7A-B). In agreement with the DC activation kinetics data (Fig. C.8E-F), CW3-induced IRF1 expression peaked at 24 hpi and waned at 48 hpi (Fig. C.7A-B). To determine whether IRF1 is a common factor for the CW3- and T1L-induced inflammatory responses to OVA, we examined the CW3-induced activation of mLN DCs and conversion of naïve OT-II T cells into a T_H1 lineage in $IRF1^{-/-}$ mice. CW3 infected the mLNs of WT and $IRF1^{-/-}$ mice to comparable levels (Fig. C.7C). However, in $IRF1^{-/-}$ mice CW3 failed to

consistently induce activation markers (Fig. C.8J-K) or IL-12p40 production (Fig. C.7D) in $CD103^+$ $CD11b^-$ $CD8\alpha^+$ DCs. Finally, while CW3 could trigger a robust T_H1 host response in both WT and $IRF1^{-/-}$ mice (Fig. C.7E), it failed to induce significant conversion of naïve $CD45.1^+$ $CD4^+$ OT-II T cells into T_H1 cells at 6 dpi in $IRF1^{-/-}$ mice (Fig. C.7F). Consistently, CW3 failed to induce T-bet expression upon OVA feeding in naïve $CD45.1^+$ $CD4^+$ OT-II T cells at 2 dpi in $IRF1^{-/-}$ mice (Fig. C.8L). These data establish a critical role for IRF1 in the CW3-triggered inflammatory response to the model oral antigen OVA. Taken together, these data suggest that, despite the differences in biology between norovirus and reovirus, the capacity to activate a common inflammatory signaling pathway (Fig. C.6E-F), involving IRF1, results in virus-triggered inflammatory responses to oral antigens.

Discussion

Development of a HLA-DQ2– or HLA-DQ8–restricted T_H1 response to dietary gluten is a critical event required for the development of CeD, a complex immune disorder that affects genetically susceptible individuals (Jabri and Sollid, 2009; Tjon et al., 2010). HLA genes are required but not sufficient for the development of CeD, and many people harbor these risk alleles but never exhibit symptoms of CeD, suggesting that environmental factors trigger the onset of a T_H1 response and LOT to gluten (Abadie et al., 2011; Jabri and Sollid, 2009). Because the host induces an inflammatory response instead of a regulatory response to dietary antigens, inflammatory events are likely to occur at the inductive site of oral tolerance (Jabri and Sollid, 2009). We previously discovered that reovirus T1L induces loss of tolerance to gluten and triggers the onset of CeD (Bouziat et al., 2017), posing the question of whether other enteric viruses could also induce inflammatory responses to dietary Ag. Our current study supports this hypothesis by showing that enteric MNV infection is capable of breaking intestinal homeostasis and triggering LOT to the oral antigen OVA.

Intriguingly, this study suggests that despite differences in cellular tropism and infection kinetics, both CW3 and T1L promote T_H1 immunity to dietary Ag by triggering a similar pathway in the mLN, in which IRF1 is central. How do two viruses from distant families, with distinct cellular tropisms and replication kinetics, activate the same immune pathway that promotes inflammatory immunity to dietary Ag? CW3 is a positive-sense RNA virus of the *Caliciviridae* family while T1L is a double-stranded RNA virus of the *Reoviridae*. Despite belonging to different viral families, they are both RNA viruses that trigger antiviral host responses through the RIG-I like signaling pathway;

CW3 activates MDA5 while T1L activates RIG-I (Goubau et al., 2014; McCartney et al., 2008), providing a basis for common signaling pathways induced by these two viruses. Whether other enteric viruses that do not activate the RIG-I like signaling pathway, such as adenovirus, a DNA virus that activates the cGAS/STING signaling pathway, induce LOT remains to be determined (Lau et al., 2015). We hypothesize that any virus capable of inducing a T_H1 skewing phenotype in the DC subset that takes up dietary Ag, regardless of the antiviral signaling pathway triggered, will have the capacity to induce inflammatory responses to dietary Ag. The present study implicates IRF1 as a transcription factor that is generally required for virus-triggered Th1 immunity to dietary Ag, but additional virus studies are needed to further establish the role of IRF1.

While both T1L and CW3 promote inflammatory immune responses to dietary Ag, it is unclear why T1L but not CW3 can consistently block pT_{reg} conversion. We previously showed that type-I IFN are required for blockade of p_{Treg} conversion but not induction of T_H1 immunity to dietary Ag, suggesting that these two events can be dissociated. The differential capacity of CW3 and T1L to block pT_{reg} conversion may be linked to differences in the type I IFN-associated response triggered by these two viruses in the mLN (Fig. 3), the kinetics of infection (Fig S4E-F), or their cellular tropism; CW3 primarily infects macrophages and dendritic cells (Wobus et al., 2004), and T1L primarily infects epithelial cells (Rubin, 1987; Wobus et al., 2004). Regardless of the differential capacity of these two viruses to block p_{Treg} conversion, they both robustly trigger LOT to Ag, suggesting differences between the pathways activated by these viruses.

Another important question is why CW3 triggers an inflammatory response to dietary Ag while CR6 does not. Because both CW3 and CR6 can infect DCs (Wobus et al., 2004) and both can activate DCs in the PPs (Fig. S1F-G), the tropism of MNV for DCs is not sufficient to explain why CW3, but not CR6, can trigger LOT to Ag. Our data suggest that the major viral capsid protein, VP1, is responsible for this difference in phenotype, but mechanistically the explanation is unclear. One possibility is that the CW3-VP1^{CR6} mutant virus has altered tissue tropism and cannot migrate efficiently to the mLN. Alternatively, this CW3 mutant may migrate to the mLN, but may not have the capacity to replicate at high enough levels to disrupt immune homeostasis and promote T_H1 immunity to dietary Ag. This is supported by our observation that CW3, but not CW3-VP1^{CR6}, upregulated chemokine receptors, such as CCR2, that were shown by Van Winkle *et al.*, to regulate the recruitment of inflammatory monocytes and neutrophils to the site of infection (Van Winkle *et al.*, submitted). These cells not only induce inflammation, but they are also susceptible to infection by CW3, promoting viral replication (Van Winkle *et al.*, submitted). Furthermore, infection of mice with CW3 but not CW3-VP1^{CR6}, resulted in elevated levels of CD300lf, the MNV receptor, in the mLN (Table S1) (Haga et al., 2016; Orchard et al., 2016). The capacity of CW3 to up regulate levels of its own receptor, in a manner dependent on VP1, may further explain why CW3 replicates to higher copy numbers than CR6 and CW3-VP1^{CR6}, and thus drive stronger inflammatory transcriptional changes in mLN, the site of oral tolerance induction (Macpherson and Smith, 2006).

A critical translational question is how to use this information to develop preventative measures against CeD. It is possible that CeD might be prevented through

vaccination against key viral triggers. To test this possibility, it is essential to know which viruses can trigger CeD, when an infection must happen in a person's life, and the severity or frequency of infection required to trigger an inflammatory response to oral antigens. This gives rise to two possibilities of how viruses may trigger an inflammatory response to oral antigens. First, infection with reovirus or norovirus at a young age, when people first begin consuming gluten at the age of 6-9 months and protective maternal antibodies have significantly declined (Niewiesk, 2014), may prevent proper oral tolerance of gluten from taking place by converting DCs essential for establishing tolerance into T_H1 skewing DCs. Alternatively, severe or repeated infections with reovirus or norovirus throughout life may break oral tolerance to gluten and eventually skew resident tolerizing DCs into inflammatory DCs. These possibilities are not mutually exclusive and certainly other viruses and even other undiscovered factors may contribute to the eventual onset of CeD. Gaining a better understanding of the pathways and spatiotemporal context by which reovirus and norovirus trigger LOT may lead to a method to screen for other viruses or factors able to trigger inflammatory responses to dietary antigens. Identifying and comparing how other viruses can mediate these effects will be essential for developing therapeutic measures to block virally triggered CeD.

Acknowledgements

We are grateful to Timothy J. Nice for critical reading of this manuscript and helpful discussion. Library generation and sequencing was performed by the University of Chicago Genomics Facility (http://genomics.bsd. uchicago.edu). This work was supported by the following grants from the NIH: R01DK098435 to B.J and T.S.D.; NIH R01AI127518 and NIH DP2CA225208 to S.H.; Investigator Fund from the Department of Medicine, MGH to A.N.. Additional support includes a Cancer Center Support Grant P30CA014599 and Digestive Diseases Research Core Center P30 DK42086 at the University of Chicago to B.J.; an award from the Bettencourt Schueller Foundation to R.B.; NIH T32 GM007183 to S.B.B.; and the Austrian Science Fund (FWF) J3408-B13 to R.H..

Author Contributions

Conceptualization, R.B., S.B.B., S.H., B.J.; Validation, R.B., S.B.B.; Formal Analysis, M.V., A.N.; Investigation, R.B., S.B.B., R.H., E.K., K.A.S., J.D.E.; Resources, J.J.B., K.U., T.S.D.; Writing – Original Draft, S.B.B., B.J., S.H.; Writing – Review & Editing, R.B., S.B.B., R.H., T.S.D., A.N., S.H., B.J.; Visualization, R.B., K.A.S., M.V., A.N.; Supervision, S.H., B.J.; Funding Acquisition, S.H, B.J.

Declaration of Interests

We declare no competing interests.

STAR METHODS

CONTACT FOR REAGENT AND RESOURSE SHARING

Further information and requests for resources and reagents should be directed to and will be fulfilled by the Lead Contact, Bana Jabri (bjabri@bsd.uchicago.edu).

EXPERIMENTAL MODEL AND SUBJECT DETAILS

Mice

All mice used in this study were from a C57BL/6 background with WT, IFNAR$^{-/-}$ (B6.129S2-*Ifnar1*^{tm1Agt}/Mmjax), IRF1$^{-/-}$ (B6.129S2-*Irf1*^{tm1Mak}/J), or RAG$^{-/-}$ OT-II$^{+/-}$ CD45.1$^{+/+}$ genotypes. In all experiments mice were 6-12 week old littermates of both genders. Mice were housed by sex and genotype. Mice were either bred at the University of Chicago or purchased from the Jackson Laboratories. All mice were housed under specific pathogen free conditions in a BSL2 barrier facility in accordance with federal and university guidelines. All experimental methods and procedures were approved by the Animal Care and Use Committee at the University of Chicago. Mice were assigned to experimental groups randomly after being transferred to the infection facility. Mice were infected one week after transfer to the infection facility. Mice that were noticeably sick, smaller, or weighed less than littermate controls on the day of infection were removed from the study. All *in vivo* experiments were conducted at least twice.

Cell Lines

Female 293Ts cells were obtained previously from Dr. Herbert W. Virgin and used in this study for MNV viral stock production. Female BV-2 cells were provided by Dr. Yuanan Lu, University of Hawaii at Manoa, USA (Cox et al., 2009) and used in this study for MNV viral stock production and MNV TCID50 titration assays. All cell lines were cultured at 37°C with 5% CO2 with standard media: Dulbeco's Modified Eagle Medium (Mediatech, 10–013), 10% fetal bovine serum (Biowest, US1520), 1x MEM nonessential amino acids (Mediatech, 25-025-CI), 10 mM HEPES (Mediatech, 25-060-CI), and 100 U/ml of both penicillin and streptomycin (Mediatech, 30-002-CI).

Viruses

The MNV strains and mutants MNV-1.CW3, CR6, and MNV-1.CW3-VP1^{CR6} (Nice et al., 2013; Thackray et al., 2007) were used in this study. All reovirus (RV) infections were conducted with the T1L strain obtained from Dr. Terence Dermody at the University of Pittsburgh, USA. MNV viral stocks were prepared from a plasmid containing a cDNA clone with the genome of MNV-1.CW3, CR6, or MNV-1.CW3-VP1^{CR6}. 6-well plates seeded with 1x10^{6} 293T cells were transfected with 4 µg of the MNV plasmid for 48 hours to produce infectious virus. These MNV stocks were amplified further in BV-2 cells. These infected BV-2 cells were incubated until they showed ~ 90% cytopathic effect around 48 hours later. Infected cells were lysed by freezing and thawing once, and the cell lysates were centrifuged for 20 minutes at 3000 rpm to pellet and remove the cell debris. Supernatants were further centrifuged for 3 hours at 26,250 rpm at 4° C to produce experimental concentrated viral stocks. These viral stocks were aliquoted

and frozen. One aliquot was then thawed and the virus titer was determined by TCID50. All MNV infections in this study were conducted using a viral stock aliquot having undergone one freeze/thaw cycle.

METHOD DETAILS

Mouse Infection

For MNV and RV mouse infections, mice were infected by oral gavage using a 22-gauge round-tipped needle (Cadence Science), with the dose and virus strain indicated in the figures, in 200 µl of standard media. Mouse weight was recorded before infection and monitored every 48 hours. For feces viral shedding analysis, a pellet of feces was collected from live infected mice and processed/analyzed as previously described (Biering et al., 2017b; Hwang et al., 2014). In brief, pellets of feces were collected in standard media, subjected to a freeze-and-thaw cycle, and then homogenized in a bead beater using 1.0 mm zirconia/silica beads (BioSpec Products, 11079110z). After debris was removed by centrifugation, viral titers in the homogenates were measured by $TCID_{50}$ as described below. For tissue viral burden analysis, mice were sacrificed and organs were harvested at the indicated time point post infection and processed/analyzed as described below and as described previously (Bouziat et al., 2017).

Mouse Submandibular Bleeding

Peripheral blood was collected by cheek bleeding into EDTA-coated 1.5ml tubes (ThermoFisher Scientific, MT-46034CI).

Preparing Single Cell Tissue Suspensions

Peyer's patches (PP) and mesenteric lymph nodes (mLNs) were removed and treated with collagenase VIII (Sigma) for 35 min at 37º C. To obtain single cell suspensions, the PPs and mLNs were processed through a 70-µm cell strainer by mechanical disruption. Following quantitation, cells were utilized for the below *ex vivo* analyses.

***In vivo* T Cell Conversion Assay**

T cell conversion *in vivo* was performed as previously described (Bouziat et al., 2017). In detail, naïve $CD4^+$ T cells were purified from the spleen and lymph nodes of $RAG^{-/-}$ $OT\text{-}II^{+/-}$ $CD45.1^{+/+}$ mice using the $CD4^+$ T cell isolation Kit (Miltenyi) or sorted on a FACS Aria Fusion (BD Biosciences). $1x10^5$ to $4x10^5$ cells were transferred retro-orbitally into congenic naïve C57BL/6 WT, $IFNAR^{-/-}$ or $IRF1^{-/-}$ mice. Mice received ovalbumin (OVA) (grade V, Sigma) dissolved in the drinking water (1.5%) for 2 or 6 days, as indicated, or were fed an OVA-containing diet (Harlan Envigo TD 130362 10mg/kg) for 6 days, as indicated. One day after transfer, mice were infected by oral gavage with the dose and virus strain indicated in the figures. Mice were euthanized and intranuclear levels of Foxp3, T-bet, or cytokine IFNγ were evaluated by flow cytometry in transferred $CD45.1^+$ and recipient T cells from mLN incubated in the presence of 50 ng/ml phorbol 12-myristate 13-acetate (PMA), 500 ng/ml ionomycin (Sigma) and 1.3 µl/ml Golgi Stop (BD Biosciences) for 2 hours at 37 ºC, 5% CO_2.

Loss of Tolerance (LOT) / Delayed-Type Hypersensitivity (DTH) Assay

C57BL/6 mice received a dose of 50 mg of OVA orally for 2 days. At the start of the experiment, mice were inoculated perorally with $5x10^7$ TCID50 units of CW3 or CR6. Two days after OVA administration and infection, a mixture of complete Freund's adjuvant and OVA (CFA-OVA) was administered subcutaneously between the shoulder blades as an emulsion of 100 µl CFA and 100 µl PBS containing 300 µg OVA, under isofluorane gas anesthesia. At day 16, mouse sera were obtained by submandibular bleeding for anti-OVA IgG2c ELISA quantification. Ear challenges were performed 14 and 24 days after immunization. A volume of 20 µl of 100 µg OVA / PBS was injected under isofluorane gas anesthesia. Ear thickness was measured 1, 2, and 3 days after second OVA challenge using a digital precision caliper (Fisher Scientific). Swelling was determined by subtracting pre-challenge from post-challenge ear thickness.

ELISA

Anti-OVA IgG2c ELISA was performed as previously described (Bouziat et al., 2017). In detail, high-binding ELISA 96-well plates (Corning) were coated with 50 µl of 10 µg/ml OVA in PBS overnight at 4 °C. Plates were washed three times with PBS 0.05% Tween 20 and blocked with 200 µl of PBS 10% FBS for 2 hours at room temperature. Unlabeled IgG2c (SouthernBiotech) was used as a positive control. Serum was assessed in duplicate and at two dilutions, typically 1/1000 and 1/5000. Sera were incubated overnight at 4° C and plates were washed three times with PBS 0.05% Tween 20. Anti-mouse IgG2c-horseradish peroxidase (HRP) (SouthernBiotech) in blocking buffer (50 µl at 1/500 dilution) was added to plates and incubated for 1 hour at room temperature. Plates were washed five times with PBS containing 0.05% Tween 20. HRP substrate TMB (50 µl) was added and the reaction stopped by the addition of

50 µl 2 N H_2SO_4. Absorbance was read at 450 nm. Levels of anti-OVA IgG2c were expressed in OD values.

DC Activation Assay

To assess DC activation, mice were inoculated with the dose and virus strain indicated in the figures, and PP and mLNs were harvested 24 and 48 hpi. Activation markers CD86 and CD40 were analyzed by flow cytometry and expressed as mean fluorescence intensity (MFI). For IL-12p40 staining, cells were incubated in RPMI (Corning) for 6 hours at 37º C, 5% CO_2 in the presence of 1 µl/ml Golgi Plug (BD Biosciences) and analyzed by flow cytometry.

Flow Cytometry

The following fluorophore conjugated antibodies were purchased from eBioscience: T-bet (4B10), Foxp3 (FJK-16s), MHCII (M5/114.15.2), CD11b (M1/70), IL-12p40 (C17.8), CD62L (MEL-14), CD25 (PC61.5), Rat IgG1, Rat IgG2a, Rat IgG2b and Mouse IgG1. The following antibodies were purchased from BD Biosciences: IFNγ (XMG1.2), CD103 (M290), CD45 (30-F11), and Fc Block™ (2.4G2). The following antibodies were purchased from Biolegend: CD4 (GK1.5), TCRb (H57-597), CD45.1 (A20), CD11c (N418), CD8a (53-6.7), CD86 (GL-1), and CD44 (IM7). Aqua LIVE/DEAD® Fixable Aqua Dead Cell Stain Kit was purchased from Life Technologies. Cells were permeabilized with the Foxp3 fixation/permeabilization kit for transcription factor (eBioscience) or Cytofix/Cytoperm (BD Biosciences) for cytokine staining. Flow cytometry was performed with a 9-color BD FACSCanto (BD Biosciences) and data

were analyzed using FlowJo software (Treestar). Sorting experiments were performed with an Aria Fusion (BD Biosciences).

Antibody Neutralization Assay

Mice were infected with the indicated MNV strain, as described above, and blood was collected through submandibular bleeding 18 days post infection. Serum samples were prepared by spinning down and removing red blood cells and frozen at -80° C. Serum was thawed on ice and mixed with $5x10^4$ $TCID_{50}$ units of either CW3 or CR6, 10-fold serial dilutions of the serum were conducted in these fixed viral aliquots. The Viral aliquots mixed with diluted serum were then incubated for 30 minutes at 37° C. Remaining infectious virus from these virus/serum mixes were quantified by $TCID_{50}$ as described below.

$TCID_{50}$

To quantify infectious MNV using the tissue culture infectious dose 50% assay, the cells or fecal pellet with media were harvested by freezing at -80° C and lysed through a freeze/thaw cycle. The viral lysates were then 10-fold serially diluted using standard media and then added to BV-2 cells seeded in 96-well plates. 8-wells were infected/ dilution and incubated for 5 days at 37°C with 5% CO2. The TCID50 was calculated by determining the dilution factor needed to show cytopathic effect (CPE) in 4 out of 8 wells or 50% of wells. The limit of detection is defined and calculated as the number of infectious units that cause CPE in 4 out of 8 wells at the lowest dilution tested.

Quantitative PCR (qPCR)

Cells lysates were obtained from single cell suspensions from mouse tissues and RNA was prepared using the RNeasy Mini Kit (Qiagen, 74136) according to the manufacturer's instruction. To determine *Irf1, Isg15 and S4 Reovirus* gene expression, cDNA synthesis was performed using GoScript (Promega, A5004) according to the manufacturer's instructions. To determine MNV genome copies, cDNA was reverse transcribed using IMPROM-II reverse transcriptase (Promega, A3803) with random hexamer according to the manufacturer's instruction, using 1 µg of total RNA. qPCR was conducted using SYBR Green reagents (Clontech, 639265), a QuantStudio 3 Real-Time PCR system from Applied Biosystems, and a Roche LightCycler 480.

RNA-sequencing processing, data analysis, and minimum spanning tree

RNA-seq libraries were prepared using the Illumina TruSeq protocol and sequenced with single-end 50bp reads on an Illumina HiSeq4000. Reads were mapped to the mouse genome (mm10) using Tophat2 (Kim et al., 2013). To improve mapping, a GTF-file containing exon boundaries of all known RefSeq genes was supplied to Tophat. Quality control was performed using the RSEM-based quantification approach (Li and Dewey, 2011). HTSeq was used to count features from the alignment files. The count data was normalized by the trimmed mean of M-values normalization (TMM) method, followed by variance estimation and applying generalized linear models (GLMs), utilizing functions from empirical analysis of digital gene expression (McCarthy et al., 2012) to identify differentially expressed genes. The associated p-values were adjusted to control the false discovery rate in multiple testing, using the Benjamini and Hochberg's (BH) method (BH-adjusted $p<0.05$). Multiple dimensional scaling (MDS) was applied to visualize profiles assembled from genes that were identified as

differentially expressed in each sham or virus response state. MDS facilitates the representation of distances between pairs of samples in lower dimensional space and samples are assigned 'coordinates' in each dimension. By applying Prim's algorithm implemented as priority-first search for graphs, a Minimum Spanning Tree, MST (for dissimilarities) that connected all vertices or nodes (denoting the profile vector for each sample) was found by minimizing the total weighting for its edges.

Enrichment analysis of pathway / biological processes and semantic similarity clustering

Pathway and biological process enrichment analysis were performed as previously described (DeJesus et al., 2016; Hitomi et al., 2008; Smeekens et al., 2013). Briefly, data were interrogated from KEGG pathways and gene ontology biological processes. Each module or category was assessed for statistical enrichment or over-representation among differentially expressed genes relative to their representation in the global set of genes in the genome. P-values were computed using the hypergeometric test. Semantic similarity analysis was applied to pathways and biological processes identified as over-represented to establish similarity or ‘relatedness’ between pathway/process categories, utilizing node-based measures of information content (IC), i.e. how informative or specific each pathway/process category, *c* is. IC is defined as the negative log likelihood for the occurrence of *c* in the pathway/process knowledgebase or in the most informative common ancestor in the ontology hierarchy, c_{MICA} (Lord et al., 2003). We utilized the relevance similarity measure (Schlicker et al., 2006), sim_{Rel} :

$$sim_{Rel}(c_1, c_2) = \frac{2IC(c_{MICA})}{IC(c_1) + IC(c_2)} \times (1 - p(c_A))$$

QUANTITATION AND STATISTICAL ANALYSIS

Mice were allocated to experimental groups on the basis of their genotype and randomized within the given sex- and age-matched group. Given that our mice were inbred and matched for age and sex, we always assumed similar variance between the different experimental groups. We did not perform an a priori sample size estimation but always used as many mice per group as possible in an attempt to minimize type I and type II errors. Investigators were not blinded during experiments and outcome assessment. The number of mice per group is described in the corresponding figure legends as n and all quantitative data are presented as mean (horizontal bar) unless otherwise indicated. Data were first analyzed for normal distribution using D'Agostino and Pearson omnibus normality tests. Normally distributed data was analyzed using unpaired two-tailed Student's *t*-test for single comparisons, and one-way ANOVA for multiple comparisons. ANOVA analysis was followed by a Tukey's post-hoc test. The statistical test used and *P* values are indicated in each figure legend. Figures and statistical analysis were generated using GraphPad Prism 6 (GraphPad Software). P values of < 0.05 were considered to be statistically significant. *$P < 0.05$, **$P < 0.01$, ***$P < 0.001$ and ****$P < 0.0001$. ns = not significant.